Specifics of Forced-Convective Heat Transfer to Supercritical CO_2 Flowing Upward in Vertical Bare Tubes

by

Eugene Saltanov

A Thesis Submitted in Partial Fulfillment of the Requirements for the Degree of Doctor of Philosophy in Nuclear Engineering

The Faculty of Energy Systems and Nuclear Science
University of Ontario Institute of Technology

April, 2015

Abstract

Heat transfer in the forced convection regime of fluids at supercritical conditions has been studied extensively for the past 60 years. The dominant approach to summarize the experimental results was by proposing empirical correlations for the data within the investigated range of parameters. It was soon realized by researchers worldwide that heat transfer coefficients become non-linear functions of wall and bulk-fluid temperatures at certain combinations of experimental parameters within the region of the peak of specific heat at supercritical pressures. Thus, it has become a standard approach to remove non-linear experimental heat transfer coefficient values treating them as a sign of a deteriorated (as opposed to normal) heat transfer regime. There were recent attempts to address this shortcoming and extend the applicability of conventional empirical correlations to the deteriorated heat transfer regime. However, these attempts were not satisfactory.

In this thesis, a new methodology has been developed that allows the use conventional empirical correlations without distinguishing entrance effects or deteriorated heat transfer regime. The methodology is based on binning experimental data according to the parameter $\mathbf{X} = \frac{h_b - h_{pc}}{q / G}$ and then combining correlations based on wall and bulk-fluid temperature on each bin to minimize RMS and maximal overprediction of heat transfer coefficients within each of the bins.

Using this methodology, 95% of normal heat transfer data were predicted with a spread of ±19%, which is 1.74 times narrower compared to the prediction by the empirical correlations developed based on the conventional methodology and on the same data; while all the data (2786 points, including entrance effects and deteriorated heat transfer) were predicted with a spread of ±20% (based on 2σ-level). The data correlated based on the new methodology where obtained within the following range of experimental parameters: P = 7.58 – 8.91 MPa, T_b = 20 – 142 °C, T_w = 32 – 231 °C, G = 885 – 3048 kg/m^{2}s, q = 26 – 616 kW/m^{2}K, D = 8.1 mm.

The experimental data were obtained based on a series of tests on supercritical CO_2 flowing upwards in a bare tube at the MR-1 loop (located in Chalk River) of the former Atomic Energy of Canada Limited (AECL). Normal, deteriorated, and improved heat transfer regimes were covered in the experiments.

Keywords: supercritical CO_2, heat transfer correlation, deteriorated heat transfer, new methodology

Acknowledgments

I would like express my deep gratitude to my thesis supervisors Dr. Pioro and Dr. Harvel who pushed me beyond my limits, pushed me to think, and taught me to follow high standards. Without Dr. Pioro's encouragement and support I would never have been able to even start PhD studies.

I would like to express sincere gratitude to Dr. Machrafi for insights and moral support when I faced predicaments in research and communication.

Thank you: Sarah Mokry, Amjad Farah, and Alexey Dragunov for allowing me to include some of your figures in my thesis.

Thank you: Margarita Tzivaki, Nicholas Chornoboy, Sourena Golesorkhi, Jordan Gilbert, Adam Lipchitz, Jeffrey Samuel, Amjad Farah, and Terry Price for teaching me irony and helping to me learn to see people from alternative perspectives.

Wargha Peiman, Sahil Gupta, and Alexey Dragunov: I deeply appreciate your validating me at the last stages of my struggle with my PhD.

May 2014 – May 2015 dwellers and friends of 1769 McGill house in Oshawa: thank you for your acceptance, jokes, wine, and food. You allowed me to relieve a lot of stress.

I would also like to thank my friend Adam Caly who never found an excuse not to mentor me through my graduate studies.

No words would be enough to express my endless gratitude to my parents. Their encouragement, love, and faith in me carried and protected me through my studies.

I am also thankful to a brave reader who decided to open the physical copy of this thesis. I hope that you will find it useful for something, even if you decide to start a fire with it.

Table of Contents

List of Tables

List of Figures

List of Appendices

List of Nomenclature

Symbols

A	area, m^2
c_p	specific heat (at constant pressure), J/kg·K
$\overline{c_p}$	average specific heat, $\left(\frac{h_w - h_b}{T_w - T_b}\right)$, J/kg·K
D	diameter, m
g	acceleration due to gravity, 9.81 m/s^2
G	mass flux, kg/m^2s
h	specific enthalpy, J/kg
HTC	heat transfer coefficient, $W/m^2·K$
k	thermal conductivity, W/m·K
L, l	length of the test section, m
P	pressure, Pa
q	heat flux, W/m^2
T, t	temperature, K or °C
u	velocity, m/s
y	radial distance from the wall, m
y^+	dimensionless wall distance $\left(y\frac{\sqrt{\tau_w \rho}}{\mu}\right)$
x	axial location, m
z	location along a test-section, m

Greek Letters

β	volumetric thermal expansion coefficient $\left(-\frac{1}{\rho}\left(\frac{\partial \rho}{\partial T}\right)_P\right)$, 1/K

μ viscosity, Pa·s

ξ friction factor

ρ density, kg/m^3

$\overline{\rho}$ average density $\left(\frac{1}{T_w - T_b} \int_{T_b}^{T_w} \rho dT \right)$, kg/m^3

τ_w wall shear stress, Pa

Dimensionless Numbers

$\mathbf{Ac_b^*}$ acceleration parameter $\left(\frac{\mathbf{Q_b^*}}{\mathbf{Re_b^{1.625} Pr_b}} \right)$

$\mathbf{Bo_b^*}$ buoyancy parameter $\left(\frac{\mathbf{Gr_b^*}}{\mathbf{Re_b^{3.425} Pr_b^{0.8}}} \right)$

$\overline{\mathbf{Gr}}$ average Grashof number $\left(\frac{\left(\rho_b - \overline{\rho} \right) D^3 g \rho_b}{\mu_b^2} \right)$

$\mathbf{Gr_b^*}$ modified Grashof number $\left(\frac{g \beta q D^4 \rho^2}{k \mu^2} \right)$

$\mathbf{Nu}$ Nusselt number $\left(\frac{HTC \cdot D}{k} \right)$

$\mathbf{Q_b^*}$ thermal expansion parameter $\left(\frac{\beta q D}{k} \right)$

$\mathbf{Pr}$ Prandtl number $\left(\frac{\mu c_p}{k} \right)$

$\overline{\mathbf{Pr}}$ average Prandtl number $\left(\frac{\mu \overline{c_p}}{k} \right)$

$\mathbf{Re}$ Reynolds number $\left(\frac{GD}{\mu} \right)$

X proposed non-dimensional number $\left(\frac{h_b - h_{pc}}{q / G} \right)$

Subscripts

b (calculated at) bulk-fluid (temperature)

calc calculated $\left(\frac{q\beta D}{k_b} \right)$

cr critical

exp experimental

f film

fl flow

h heated

in inlet

min minimal

P at constant pressure

pc (calculated at) pseudocritical (temperature)

TS Test Section

vol volumetric

w (calculated at) wall (temperature)

Abbreviations and acronyms

ABTR	Advanced Burner Test Reactor
AECL	Atomic Energy of Canada Limited
CFD	Computational Fluid Dynamics
CRP	Coordinated Research Project
DAS	Data Acquisition System
DHT	Deteriorated Heat Transfer
FCT	Fuel Channel Thermalhydraulics
FM	Flow Meter
GIF	Generation IV International Forum
GFR	Gas-cooled Fast Reactor

HEC	High Efficiency Channel
HP	High Pressure
HPLWR	High Pressure Light Water Reactor
HTC	Heat Transfer Coefficient
H	Heater
IAEA	International Atomic Energy Agency
ID	Internal Diameter
IHT	Improved Heat Transfer
IP	Intermediate Pressure
KAERI	Korea Atomic Energy Research Institute
LFR	Lead-cooled Fast Reactor
LP	Low Pressure
MSR	Molten Salt Reactor
NHT	Normal Heat Transfer
NPP	Nuclear Power Plant
OD	Outer Diameter
PDT	Pressure Differential Transducer
POW	Test-section POWer
R&D	Research and Development
RANS	Reynolds number Averaged Navier-Stokes
RMS	Root Mean Square
SC	SuperCritical
SCF	SuperCritical Fluid
SCW	SuperCritical Water
SCWR	SuperCritical Water-cooled Reactor
SFR	Sodium-cooled Fast Reactor
SJTU	Shanghai Jiao Taong University
SPHINX	Supercritical Pressure Heat transfer Investigation for NeXt generation
SST	Shear Stress Transport (model)
TC	ThermoCouple
UOIT	University of Ontario Institute of Technology

US	The United States
VHTR	Very-High-Temperature Reactor

List of Special Definitions

Terms related to a narrow topic of forced-convective heat transfer are used frequently throughout this thesis. Please refer to the diagrams in the end of this list that illustrate these terms.

Compressed fluid is a fluid at a pressure above the critical pressure, but at a temperature below the critical temperature.

Critical point (also called a *critical state*) is a point in which the distinction between the liquid and gas (or vapor) phases disappears, i.e., both phases have the same temperature, pressure, and density. The *critical point* is, therefore, characterized by these phase state which have unique values for each pure substance.

Deteriorated Heat Transfer is characterized with lower values of the wall heat transfer coefficient compared to those at the normal heat transfer; and hence has higher values of wall temperature within some part of a test section or within the entire test section.

Improved Heat Transfer is characterized with higher values of the wall heat transfer coefficient compared to those at the normal heat transfer; and hence lower values of wall temperature within some part of a test section or within the entire test section.

Normal Heat Transfer can be characterized in general with wall heat transfer coefficients similar to those of subcritical convective heat transfer far from the critical or pseudocritical regions.

Overheated vapor is vapor at a temperature above the satureation temperature and below the critical temperature.

Pseudo-boiling is a physical phenomenon similar to subcritical pressure nucleate boiling, which may appear at supercritical pressures. Due to heating of the supercritical fluid with a bulk-fluid temperature below the pseudocritical temperature (high-density fluid, i.e., "liquid"), some layers near a heating surface may attain temperatures above the pseudocritical temperature (low-density fluid, i.e., "gas"). This low-density "gas" leaves the heating surface in the form of variable density (bubble) volumes. During the pseudo-

boiling, the wall heat transfer coefficient usually increases (improved heat-transfer regime).

Pseudocritical point is a point at a pressure above the critical pressure and at a temperature above the critical temperature that corresponds to the maximum value of the specific heat for this particular pressure.

Pseudo-film boiling is a physical phenomenon similar to subcritical pressure film boiling, which may appear at supercritical pressures. At pseudo-film boiling, a low-density fluid (a fluid at temperatures above the pseudocritical temperature, i.e., "gas") prevents a high-density fluid (a fluid at temperatures below the pseudocritical temperature, i.e., "liquid") from contacting ("rewetting") a heated surface. Pseudo-film boiling leads to the deteriorated heat transfer regime.

Subcooled liquid is a liquid at a pressure below the critical pressure.

Supercritical fluid is a fluid at pressures and temperatures that are higher than the critical pressure and critical temperature.

Superheated steam is steam at a pressure below the critical pressure and at a temperature above the critical temperature.

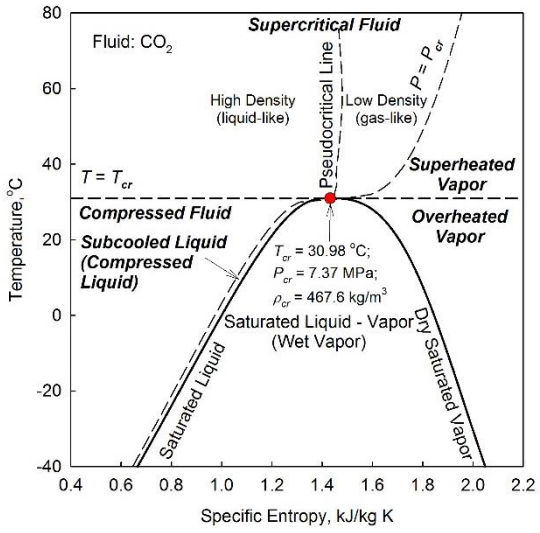

T-s diagram for CO_2

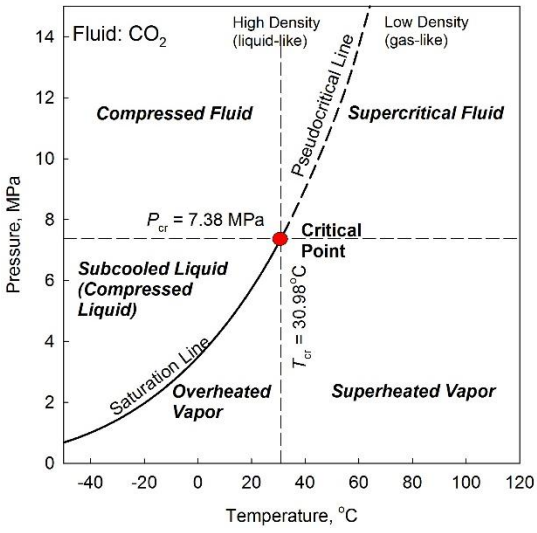

P-T diagram for CO_2

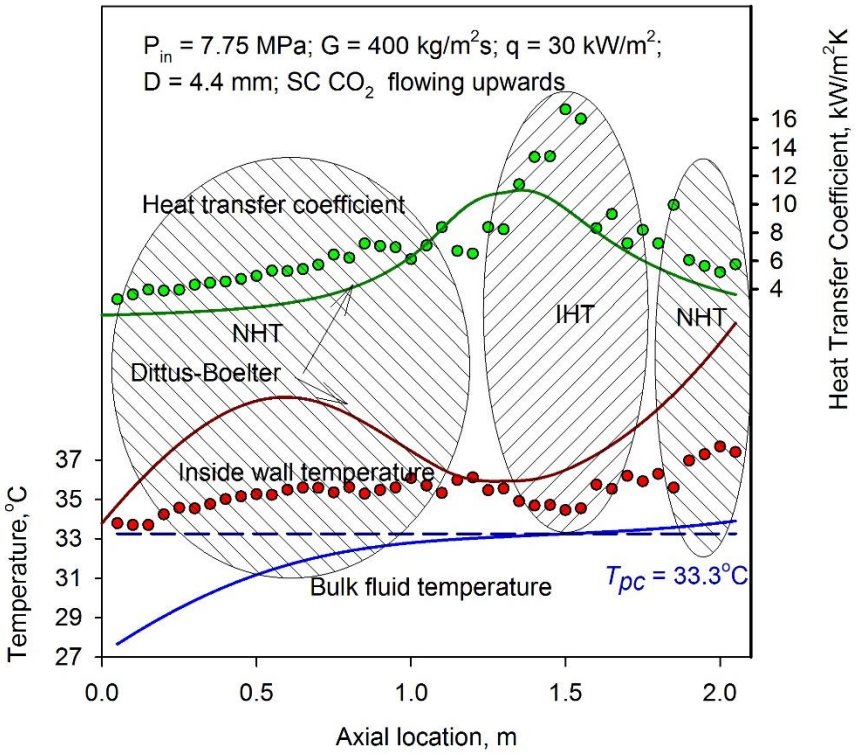

Normal and improved heat transfer regimes (IAEA, 2011)

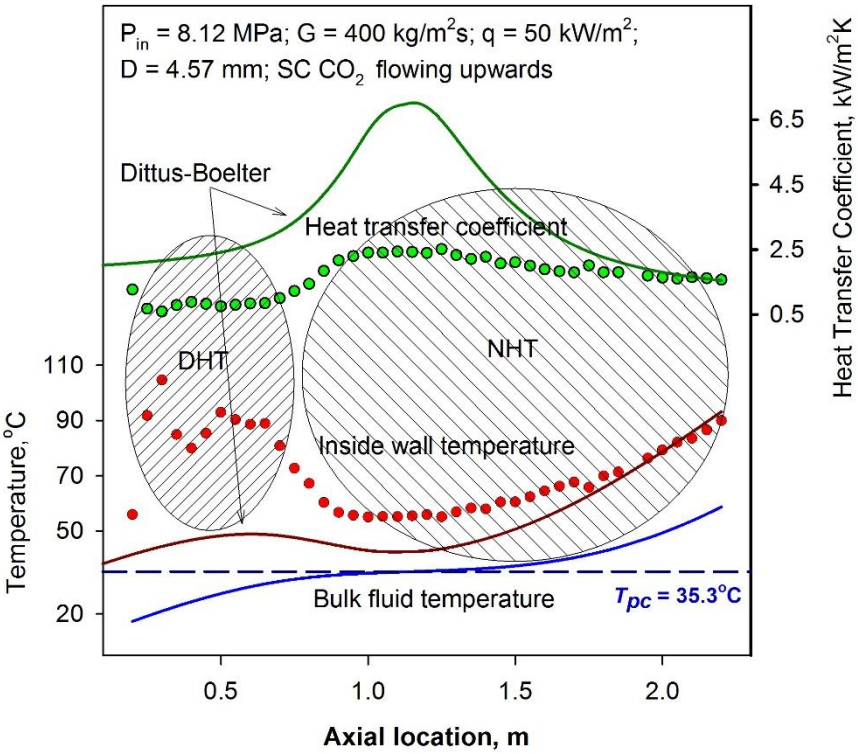

Deteriorated and normal heat transfer regimes (IAEA, 2011)

CHAPTER 1. INTRODUCTION

Electrical-power generation is considered an indispensable commodity for advances and intensification of industries, agriculture, and improvement to the standard of living. International energy statistics (*US Energy Information Administration*, 2014) show that a net of 21,080.88 TWh of electricity was generated in 2011 worldwide. Fractions of the electricity produced by various sources are presented in Figure 1.1.

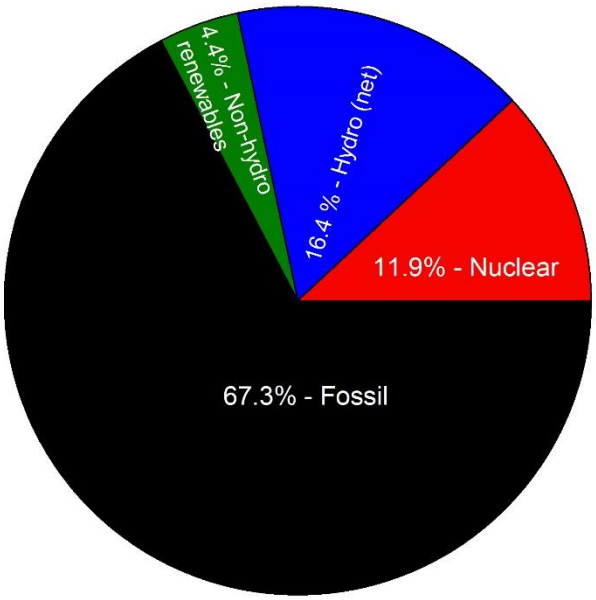

Figure 1.1. Net electricity generation in the world by source (based on the data from *US Energy Information Administration*, 2014).

Although nuclear power amounts to only 11.9%, it has the huge advantage of producing no carbon dioxide during operation, which is a major concern with using fossil fuels. However, currently operating Nuclear Power Plants (NPPs) belong to Generation II and III and have much lower thermal efficiencies than the modern combined-cycle and supercritical-pressure coal-fired power plants (Pioro, 2014). With the purpose of enhancing efficiency and supporting the future role of the next generation nuclear energy systems, the Generation IV International Forum (GIF) was created in January 2000. The research and development was outlined in the *Technology Roadmap for Generation IV Nuclear Energy Systems* (2002) (briefly: *Technology Roadmap*).

The *Technology Roadmap* was updated by the *Technology Roadmap Update for Generation IV Nuclear Energy Systems* (2014) (briefly: *Technology Roadmap Update*). The *Technology Roadmap Update* confirmed the choice made in the *Technology Roadmap* of the following six systems:

1) Gas-cooled Fast Reactor (GFR);
2) Lead-cooled Fast Reactor (LFR);
3) Molten Salt Reactor (MSR);
4) Sodium-cooled Fast Reactor (SFR);
5) SuperCritical-Water-cooled Reactor (SCWR); and
6) Very-High-Temperature Reactor (VHTR).

The GFR is considered to be operated with a SuperCritical (SC) carbon dioxide (onwards: CO_2) Brayton gas-turbine cycle (Hejzlar et al., 2005; Kato et al., 2005; and *Technology Roadmap Update*), with the ingress of helium into the gas-turbine bearings being a major issue for the helium Brayton cycle.

Liquid-metal and molten-salt reactors are also proposed to be connected through heat exchangers with an SC CO_2 Brayton gas-turbine cycle (Zvorykina et al., 2012; Li et al., 2011; Moisseytsev and Sienicki, 2009; Simon et al., 2007; Sohn et al., 2005; and *Technology Roadmap Update*). Such an arrangement of thermodynamic cycle has safety benefits compared to those of the Rankine steam cycle. At any practical temperatures, a sodium – water reaction results in exothermic energy release and the formation of hydrogen gas; therefore, any leaks in a sodium-water heat exchanger may lead to serious damage. A sodium – CO_2 reaction results in energy release as well, however, at temperatures exceeding 250 °C (Miyahara et al., 2011) and becomes a fast global reaction, which can be interpreted as auto-combustion of CO_2 in sodium, at temperatures exceeding 500 °C (Simon et al., 2007).

In addition to the Generation IV reactor systems applications, SC CO_2 was proposed to be used in heat pumps for long-distance district heat supply systems (Kalnin et al. 2013), enhanced geothermal power conversion systems (Wan et al., 2011), solar power conversion systems (Chapman and Arias, 2009), and advanced air-conditioning systems (Lorentzen,

1994). The main reason for these proposals are: 1) thermal properties of SC CO_2 allow for compact size of heat exchangers; and 2) SC CO_2 is a more environmentally friendly working fluid compared to conventional refrigerants (R-12, R-22, R-134a and others).

Recognizing the benefits of using SC CO_2 in fossil, renewable, and NPPs, the SC CO_2 Power Cycle Symposium was established in the United States several years ago (in 2007).

The application of SC CO_2 for power-conversion cycles will require designing appropriate heat exchangers (intermediate heat exchangers, recuperators, intercoolers, etc.). Thermal hydraulic calculations at the preliminary stage of the design of the heat exchangers will require a reliable heat transfer correlation for SC CO_2.

Having a much lower thermodynamic critical point than water, CO_2 (7.38 MPa and 30.98 °C for CO_2 vs 22.06 MPa and 373.95 °C for water) is also being used as a modelling fluid.

The majority of the data on heat transfer to SuperCritical Fluids (SCFs) was obtained for SuperCritical Water (SCW) in the 1960's-1980's. Unfortunately, at least half of the experimental data on SCW was lost; other data are proprietary; and the bulk of the remaining data comes in the form of graphs (Kurganov et al., 2009; Groeneveld et al., 2007). Additionally, thermal properties of water were updated several times; thus, correlations for forced-convective heat transfer developed prior to 1997 are based on obsolete properties (IAPWS, 2008; IAPWS, 2005; IAPWS, 1998), and, thus the performance of the correlations based on the outdated properties is questionable (Kurganov et al., 2012). Moreover, reduced properties of water and CO_2 at the SC state are dissimilar enough; thus, the direct application of an SCW correlation will most likely produce unreliable results in CO_2. Therefore, a separate forced-convective heat-transfer correlation is needed for SC CO_2.

Despite current unreliability of transferring heat transfer data from SC CO_2 to SCW, and in the absence of the experimental heat transfer data from a full-scale mock-up of an SCWR fuel channel, any improvement in understanding of physics of heat transfer or increasing

the numerical accuracy of predictions at similar-to-the-SCWR-scaled-conditions will be a valuable input.

Therefore, an in-depth investigation of specifics of heat transfer to SC CO_2 at forced convection conditions is very important and needs to be performed. In view of the discussed prospective power and engineering applications of SC CO_2, this investigation should be carried in two steps: 1) understanding the reasoning behind the limitations of the existing prediction methods for Heat Transfer Coefficient (HTC) in the forced convective regime; and 2) if possible, proposing an improved method for predicting HTC in the forced convective regime.

Chapter 2 will present a literature review on the power and engineering applications for SC CO_2 and developed detailed power-conversion options for SFRs. Chapter 3 will present a detailed literature review on specifics of heat transfer to SCFs, current methods of describing heat transfer to SCFs, and methods of scaling heat transfer data. Chapter 4 will present the available datasets on heat transfer to SC CO_2 (including instrumentation, uncertainties of the measured and calculated parameters, and observed effects of experimental parameters on heat transfer). Chapter 5 will present detailed analysis of thermal and transport properties of SC CO_2. Chapter 6 will present the conventional methodology for developing heat transfer correlations, the conventional methodology for the onset of DHT, and a new methodology for developing heat transfer correlations. Chapter 7 will present developed correlations and their assessment. Chapter 8 will present verification of the obtained correlations. Chapter 9 will present the summary and conclusions of the thesis.

CHAPTER 2. LITERATURE REVIEW – POWER AND ENGINEERING APPLICATIONS OF SC CO_2

Electrical-power generation is universally acknowledged as a key factor and indispensable commodity for advances and intensification of industries, agriculture, and improvement to the standard of living. International energy statistics (*US Energy Information Administration*, 2014) show that a net of 21,080.88 TWh of electricity was generated in 2011 worldwide. The main sources for global electrical-energy generation are (*US Energy Information Administration*, 2014)):

1) Thermal power (mainly coal and natural gas, 67.3%);
2) Hydro power from dams and rivers (16.4%); and
3) Nuclear power (11.9%).

The remaining 4.4% of the electrical energy is generated by a mixture of sources, being mainly comprised of wind, geothermal, and solar energy.

Unfortunately, renewable "green" sources are intermittent and cannot be used for baseload electricity generation. To illustrate this, power generated by source and capacity factors of various power sources in Ontario are plotted in Figures 2.1 – 2.2.

According to Pioro (2014), the highest thermal efficiencies are currently achieved at combined power plants (gross efficiencies up to 62%), supercritical-pressure coal-fired power plants (gross efficiencies up to 55%), internal-combustion-engine generators (gross efficiencies up to 50%), subcritical-pressure coal-fired power plant (gross efficiencies up to 40%), and NPPs (gross efficiencies up to 40%). Thermal power plants produce a lot of CO_2 emissions during normal operation, which is a major global concern. NPPs do not emit CO_2 during normal operation, however, they have much lower thermal efficiencies compared to thermal power plants.

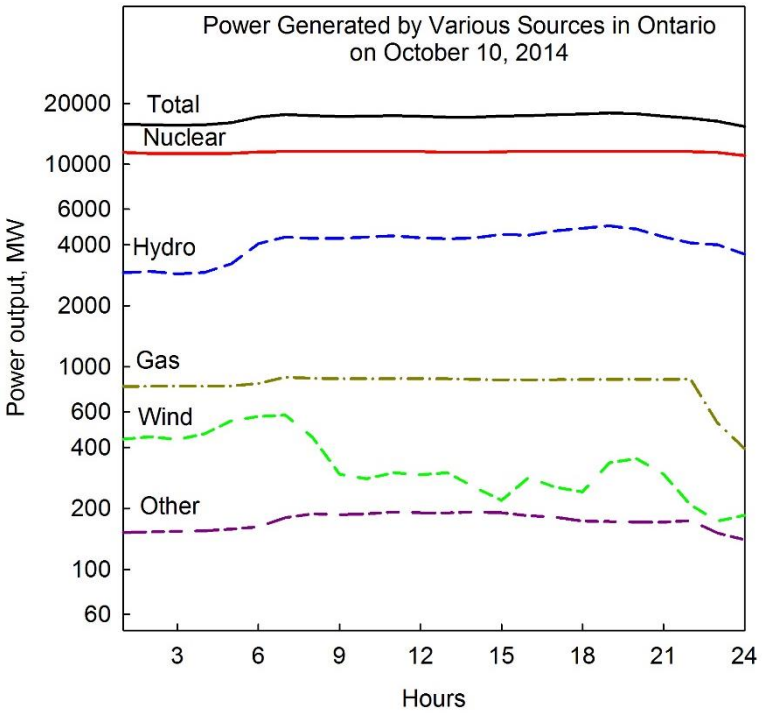

Figure 2.1. Power generated by various sources in Ontario on October 10, 2014 (Generators Output and Capability Report, 2014).

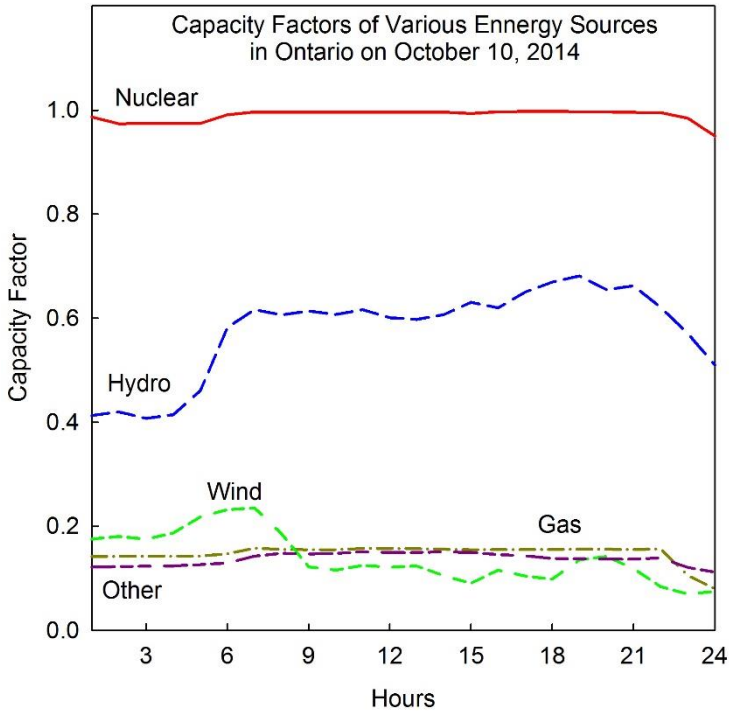

Figure 2.2. Capacity factors of various energy sources in Ontario on October 10, 2014 (Generators Output and Capability Report, 2014).

One of the attempts to increase efficiencies of current NPPs is to use waste heat for district heating with the use of high-capacity heat pumps with SC CO_2 as a working fluid (Kalnin et al., 2003). Another long-term effort to increase efficiencies of NPPs is to develop next generation nuclear reactor systems.

2.1. Application of SC CO_2 in the turbine side of the Generation IV reactor systems

With the purpose of enhancing and supporting the future role of the next generation nuclear energy systems, the Generation IV International Forum (GIF) was created in January 2000. The research and development was outlined in the *Technology Roadmap for Generation IV Nuclear Energy Systems* (2002) (briefly: *Technology Roadmap*). The following key characteristics of the Generation IV reactor systems were outlined: 1) sustainability; 2) economic competitiveness; 3) safety and reliability; and 4) proliferation resistance and physical protection.

The *Technology Roadmap* was updated by the *Technology Roadmap Update for Generation IV Nuclear Energy Systems* (2014) (briefly: *Technology Roadmap Update*). The *Technology Roadmap Update* confirmed the choice made in the *Technology Roadmap* of the following six systems[1]:

1) Gas-cooled Fast Reactor (GFR) (see Figure 2.3);
2) Lead-cooled Fast Reactor (LFR) (see Figure 2.4);
3) Molten Salt Reactor (MSR) (see Figure 2.5);
4) Sodium-cooled Fast Reactor (SFR) (see Figure 2.6);
5) SuperCritical-Water-cooled Reactor (SCWR) (see Figure 2.7); and
6) Very-High-Temperature Reactor (VHTR) (see Figure 2.8).

The ingress of helium into the gas-turbine bearings is a major issue for the helium Brayton cycle. Therefore, GFR is proposed to be operated with the SC CO_2 Brayton gas-turbine cycle (Hejzlar et al., 2005; Kato et al., 2005; and *Technology Roadmap Update*).

[1] A brief summary of thermal and transport properties of prospective coolants for the Generation IV nuclear reactors is presented in Appendix G.

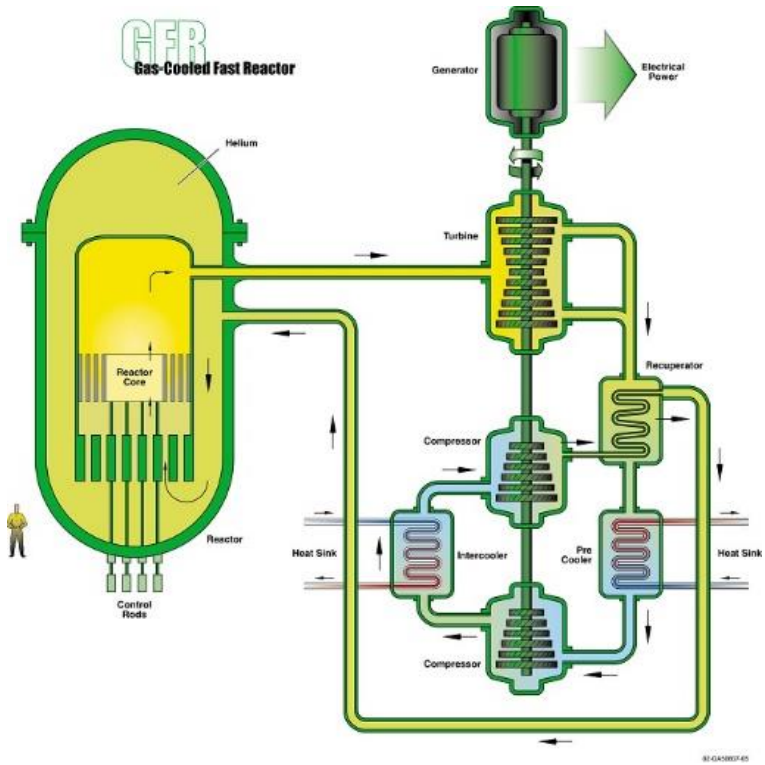

Figure 2.3. Schematic of a Gas-cooled Fast Reactor (GFR, source: Generation IV International Forum https://www.gen-4.org).

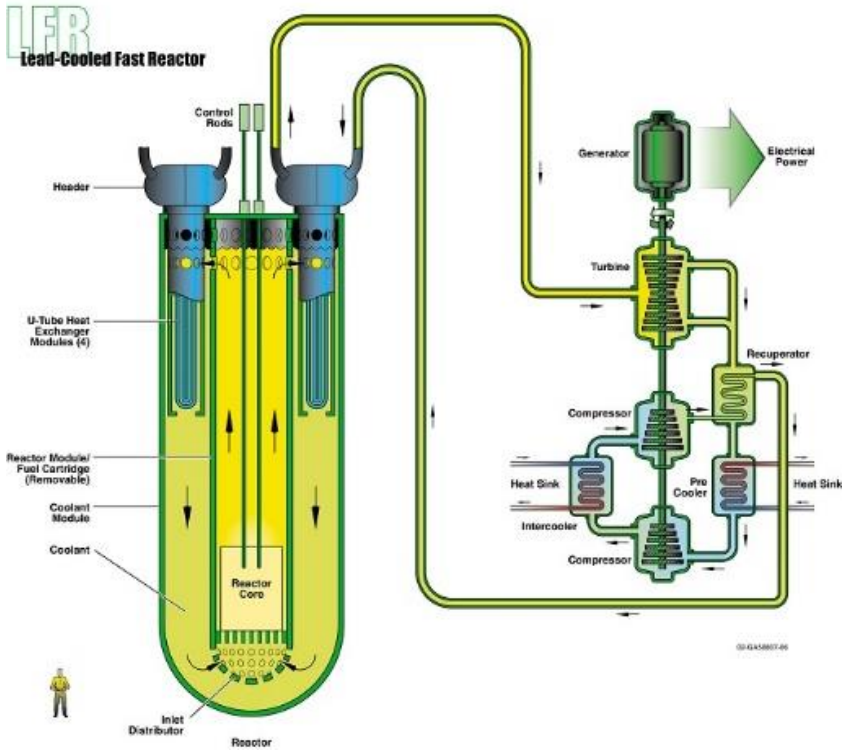

Figure 2.4. Schematic of a Lead-cooled Fast Reactor (LFR, source: Generation IV International Forum https://www.gen-4.org).

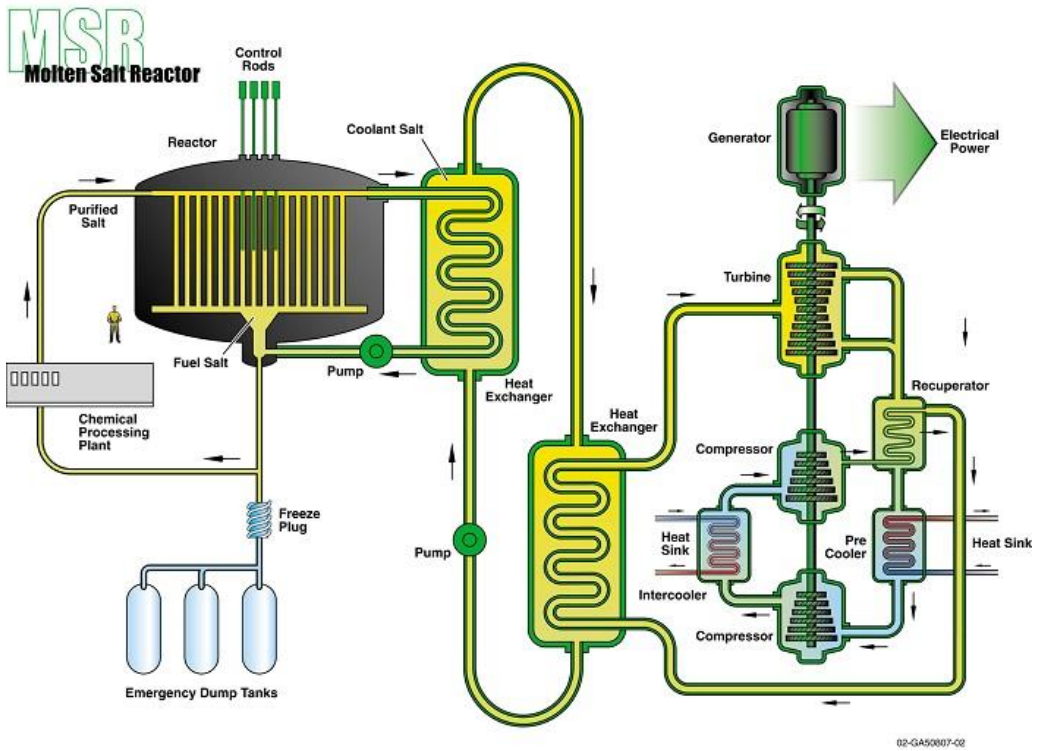

Figure 2.5. Schematic of a Molten Salt Reactor (MSR, source: Generation IV International Forum https://www.gen-4.org).

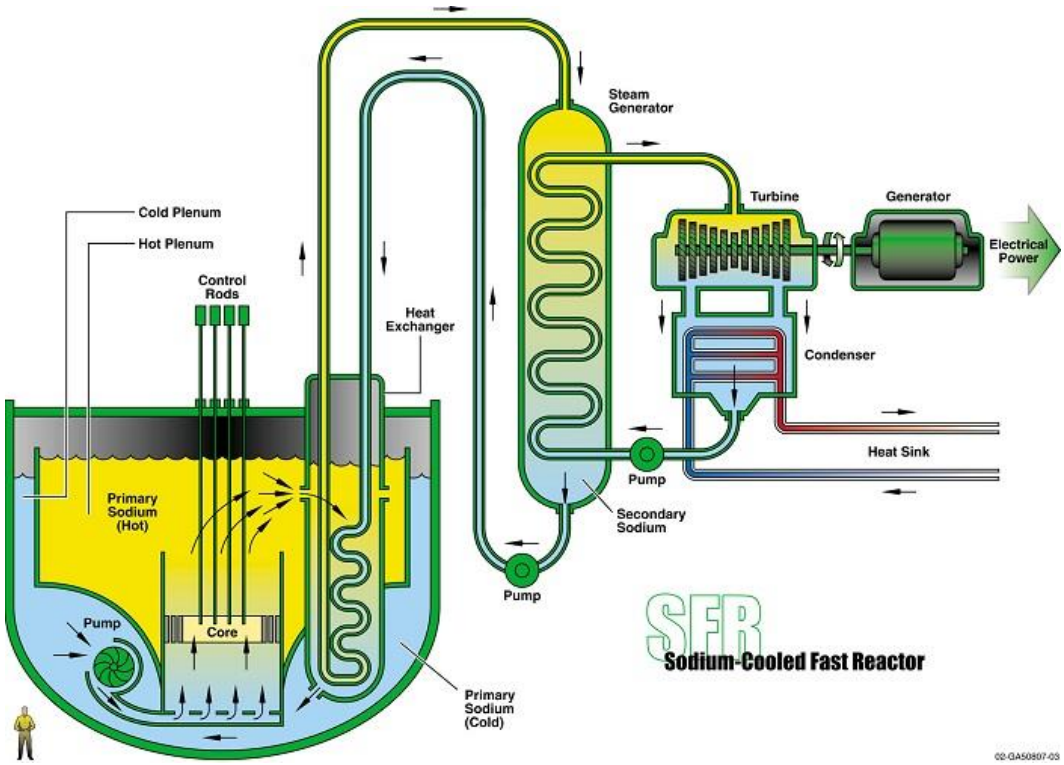

Figure 2.6. Schematic of a Sodium-cooled Fast Reactor (SFR, source: Generation IV International Forum https://www.gen-4.org).

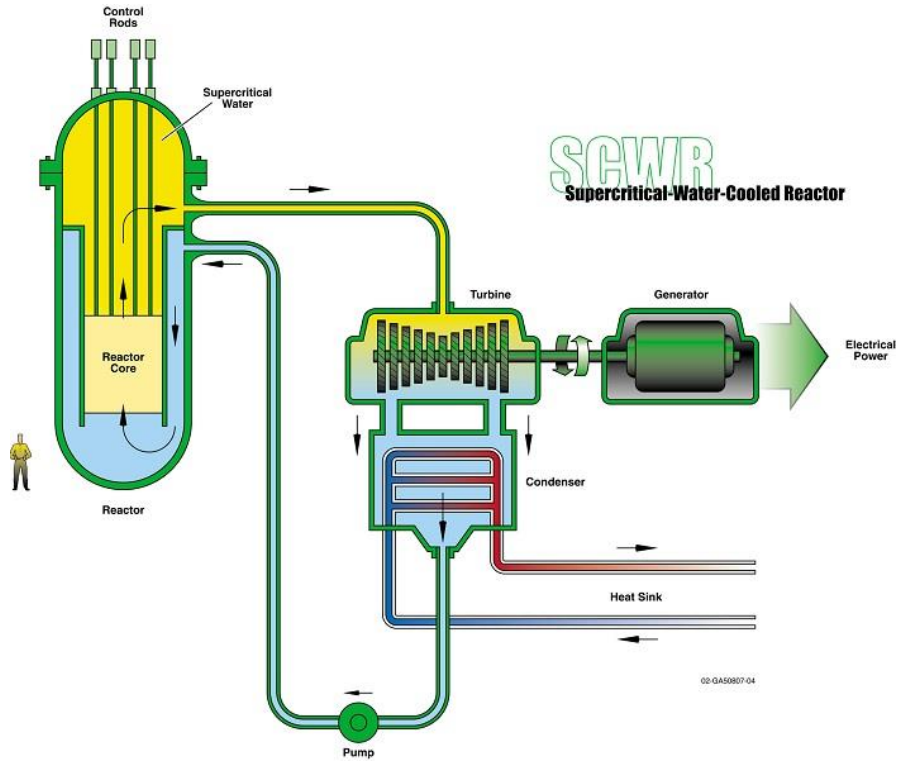

Figure 2.7. Schematic of a SuperCritical-Water-cooled Reactor (SCWR, source: Generation IV International Forum https://www.gen-4.org).

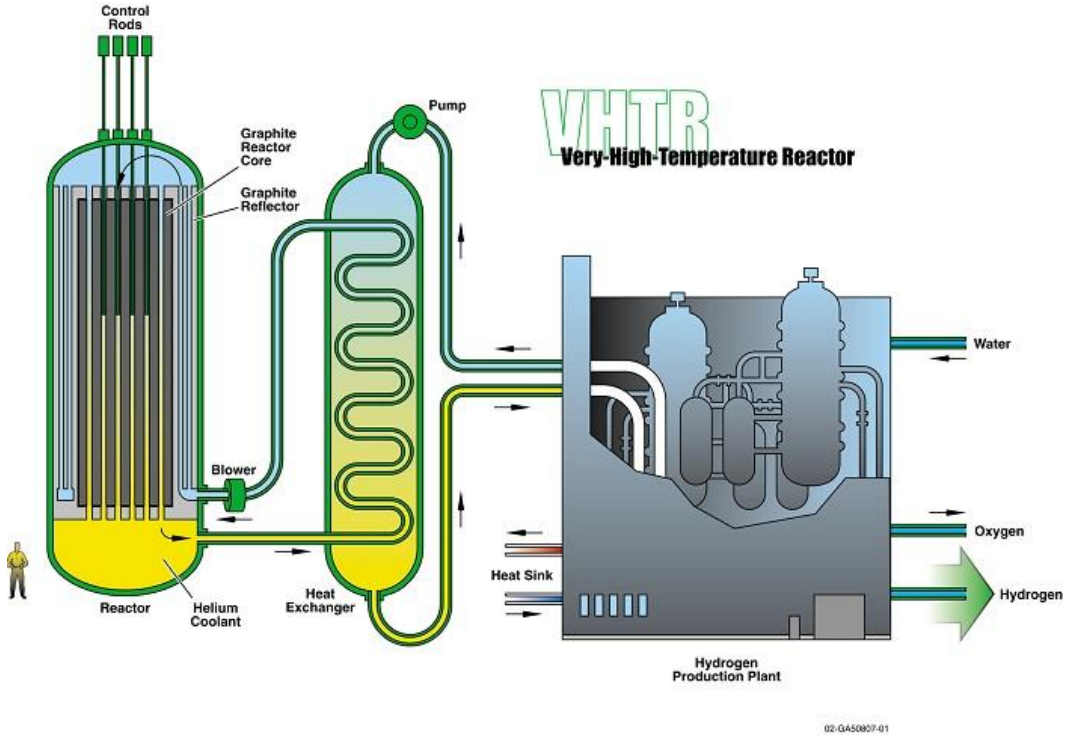

Figure 2.8. Schematic of a Very-High-Temperature Reactor (VHTR, source: Generation IV International Forum https://www.gen-4.org).

Liquid-metal and molten-salt reactors are also proposed to be connected through heat exchangers with the SC CO_2 Brayton gas-turbine cycle (*Technology Roadmap Update*; Zvorykina et al., 2012; Li et al., 2011; Moisseytsev and Sienicki, 2009; Simon et al., 2007; and Sohn et al., 2005). The SC CO_2 Brayton gas-turbine cycle is considered to be a promising choice for the liquid-metal and molten-salt-cooled reactors, because of the reduced capital costs. The reduction is possible due to: 1) minimized sizes of heat exchangers, because of the high specific heat near the pseudocritical point; and 2) reduced compressor work because of the high density value.

Employment of the SC CO_2 Brayton gas-turbine cycle has safety benefits compared to that of the Rankine steam cycle if used for the SFR. Sodium (Na) reacts exothermally with water at any temperature, therefore, any leaks in a sodium-water heat exchanger may lead to its serious damage. Therefore, Na – CO_2 reaction was investigated recently.

Simon et al. (2007) conducted calorimetric studies to investigate the kinetics of a Na – CO_2 reaction. They found that the Na – CO_2 reaction occurred at temperatures below 500°C and was characterized by an induction time, which reduced with the increase in temperature. A fast global reaction, which could be interpreted as auto-combustion of CO_2 in sodium, started at temperatures higher than 500°C.

Miyahara et al. (2011) conducted a number of experiments to study the reaction behavior between Na and CO_2. Some of their experiments were simulating a leak of CO_2 to Na in different points of a Na – CO_2 heat exchanger. Several combinations of temperatures of Na and CO_2 were investigated. Miyahara et al. (2011) came to a conclusion that Na – CO_2 was an exothermal reaction that became continuous beyond a threshold temperature, which lied in the range of 250 – 300°C.

Therefore, CO_2 reacts exothermally with sodium, however, at higher temperatures than water.

Moisseytsev and Sienicki (2009) performed a rigorous analysis of an SC CO_2 Brayton gas-turbine cycle applied to the preliminary conceptual design of an Advanced Burner Test Reactor (ABTR), which is of SFR-type. Realistic considerations of pressure drops and

efficiencies of HXs were made. Moisseytsev and Sienicki (2009) compared double recompression cycles with and without reheat and intercooling. They found that there was no appreciable increase in thermodynamic efficiency of the cycle compared to the recompression, or so-called Feher, cycle. For the maximum temperature of 470°C corresponding to the ABTR design, Moisseytsev and Sienicki (2009) obtained about 39.1% efficiency.

Possible power-conversion options for SFRs are discussed in the following section.

2.2. Possible Power-Converstion Options for SFRs[2]

As discussed in the previous section, CO_2 recently gained wide attention as an alternative to water as a working fluid in power conversion cycles of SFRs. The current operating reactors are represented by BN-600 in Beloyarsk, Russia and Monju in Tsuruga, Japan. Both reactors employ two sodium loops (to prevent possible leakage of radioactive sodium to power conversion cycle, and to have a buffer loop between low pressure sodium (0.1 – 0.3 MPa) from high pressure water (12 – 16 MPa)). Still, since the basic method of increasing the thermal efficiency of power plants is by increasing the operating pressure and temperature, the turbine side can employ water at SC parameters. Indeed, with the advent of modern super alloys, the Rankine-"steam"-cycle technology has advanced to be employed within the SC region of the coolant. As discussed in Chapter 1, conventional fossil-fired plants have thermal efficiencies in the mid 40% range.

Thus, there are three general possibilities for an SFR in terms of the secondary cycle:

1. Subcritical-pressure Rankine-"steam"-cycle through a heat exchanger (current approach).
2. Supercritical-pressure Rankine-"steam"-cycle through a heat exchange (new approach).
3. Supercritical-pressure CO_2 Brayton-gas-turbine-cycle through a heat exchanger (US approach).

[2] Section 2.3 – 2.6 are based on author's common papers with Alexey Dragunov (Dragunov et al., 2012; and Dragunov et al. 2013a), as well as on the author's paper (Saltanov et al., 2013a).

Results of thermodynamic efficiency calculations for the first option are presented below in Section 2.3. Calculations of thermal efficiency of a secondary SC Rankine-"steam"-cycle with heat regeneration is presented in Section 2.4. Calculations of thermal efficiencies of a secondary SC CO_2 Brayton cycles are presented in Sections 2.5 and 2.6.

2.3. Current thermodynamic cycle of BN-600 reactor

Thermodynamic layout of BN-600 NPP consists of three loops, with liquid sodium being the coolant in the primary and intermediate loop, and water being the coolant in the secondary loop. The secondary loop of the plant operates on subcritical-pressure Rankine-"steam"-cycle with heat regeneration. Steam extractions are taken from High-Pressure (HP), Intermediate-Pressure (IP), and Low-Pressure (LP) turbines. The 600-MW_{el} unit at Beloyarsk is the largest power reactor of its type in the world. The BN-600 has inherent built-in safety features. Sodium as the reactor coolant has the advantage that it can be heated to 560°C without being pressurized, so the reactor does not need a massive pressure vessel. The reactor also has a very attractive safety feature in that it can maintain cooling by natural convection, should cooling pumps fail. Major parameters of this reactor are listed in Table 2.1.

Table 2.1. Major Parameters of BN-600 Sodium-cooled Fast Breeder Reactor (Grigoryev and Zorin, 1989).

Parameters	**BN-600**
Thermal power, MW_{th}	1470
Electrical power, MW_{el}	600
Thermal efficiency, %	40
Steam pressure, MPa	14.2
Sodium volume in primary circuit, m^3	820
Sodium volume in secondary circuit, m^3	960
Coolant inlet/outlet temperature, °C	370/550
Inlet/outlet temperature of secondary circuit sodium, °C	320/520

Three conventional K-210-130 turbines are connected to the reactor. The turbines were designed with a steam-reheat option in order to increase the thermal efficiency of the cycle and to reduce the amount of moisture in the last stages of the turbine. Major parameters of this turbine are shown in Table 2.2.

Table 2.2. Parameters of K-210-130 Russian Turbine (Grigoryev and Zorin, 1989).

Parameters	K-210-130
Power/Max Power, MW	210/215
Main Steam Pressure, MPa	14.2
Main Steam Temperature, °C	505
Reheat Steam Pressure, MPa	2.45
Reheat Steam Temperature, °C	505
Max Flow Rate through HP Turbine, t/h	670
Number of Steam Extractions	7
Outlet Pressure, kPa	5
Cooling-Water Temperature, °C	10
Cooling-Water Flow Rate, m^3/h	25,000
Feedwater Temperature, °C	240
Total Mass, t	560
Total Length, m	20
Total Length with generator, m	33

The turbine K-210-130 has 7 steam extractions from HP, LP, and IP turbines for regeneration. Parameters of these steam extractions are presented in Table 2.3. It should be noted that the relative steam consumptions were calculated as solutions of heat-balance equations for HP and LP Heaters (HPHs and LPHs).

Table 2.3. Parameters of Steam Extractions for K-210-130 Turbine (Kostyuk and Frolov, 2001).

Steam Extractions	*P*, MPa	*T*,°C	Enthalpy, kJ/kg	Relative steam consumption α, %
1	3.855	403	3224	4.9
2	2.520	347	3119	7.4
3	1.187	477	3427	3.5
4	0.627	393	3255	3.7
5	0.270	289	3048	4.1
6	0.125	207	2888	3.0
7	0.026	78	2643	3.4

Calculations of thermodynamic efficiency were based on a reversible thermodynamic cycle and did not account for any major irreversibilities that would occur in an actual cycle. The thermal-cycle efficiencies calculated for the subcritical Rankine-"steam"-cycle were based on the following simplifying assumptions:

- No mechanical losses (e.g., bearing losses);
- No steam turbine packing leakage or gland steam-system losses;
- No turbine exhaust losses;
- No generator losses;
- No piping heat losses;
- No steam-generator heat losses.

The layout of the power-conversion side of the BN-600 SFR in Russia corresponds to the subcritical-pressure Rankine-"steam"-cycle configuration.

A simplified cycle for the BN-600 reactor is presented in Figure 2.9. Steam is reheated once after passing through the HP turbine in order to achieve a higher efficiency. The regenerative feedwater-heating system consists of four LPHs, three HPHs, and one deaerator.

The subcritical water flows through the steam generator, being heated from 240°C to 505°C, and enters the HP turbine at pressure 14.2 MPa. Steam is extracted twice from the HP turbine in order to heat the feedwater flowing through HPH2 and HPH3. After passing through the HP turbine, steam is reheated once in an intermediate reheater with an output pressure of 2.45 MPa and temperature of 505°C in order to achieve a higher efficiency. The IP turbine supplies extraction steam for the HPH1 and a fraction of the steam is diverted to heat the water in the deaerator. The IP and LP turbines also supply steam extractions for the LPH1, LPH1, LPH3 and LPH4. The condensate from the LPH1 is fed back to the condenser. The condensate from the HPH1 is fed back to the deaerator.

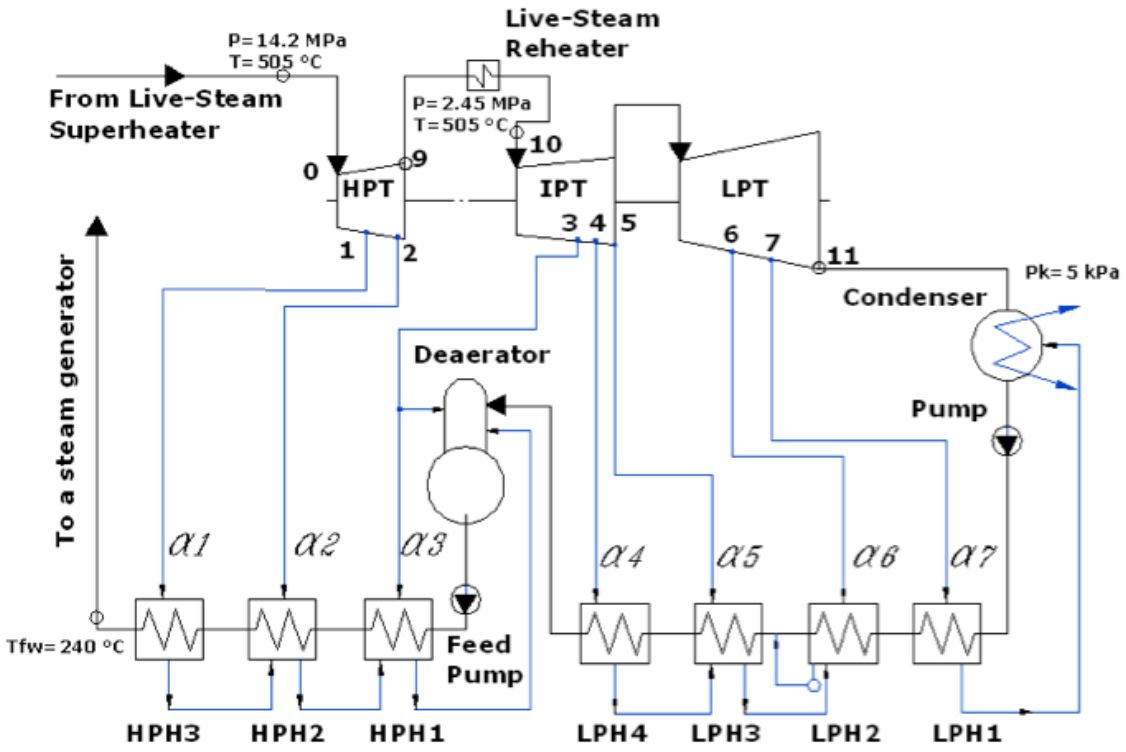

Figure 2.9. Single-Reheat Subcritical-Pressure Rankine-"Steam"-Cycle with Heat Regeneration: T – Turbine, T_{fw} – feedwater temperature, P_k – condenser pressure (Courtesy of A. Dragunov (UOIT), Dragunov et al., 2012).

The efficiency of current thermodynamic layout of BN-600 can be calculated straightforwardly using basic heat balance equations (Cengel and Boles, 2006). The efficiency of the discussed thermodynamic layout was calculated to be 49.1%.

2.4. Supercritical-pressure Rankine-"steam"-cycle with heat regeneration

The efficiency of the Rankine cycle, such as the one presented in the previous section, can be greatly improved by operating it within the SC region of the coolant. Most modern thermal power plants employ the SC Rankine-"steam"-cycle, which raises the thermal efficiency of the plant (Grigoryev and Zorin, 1989). The steam-cycle configuration of the SC cycle is very similar to that of the subcritical cycle in a modern fossil-fueled power plant. Steam is usually reheated once in a boiler after passing through the HP turbine, in order to achieve a higher efficiency. The regenerative feedwater-heating system consists

of LP and HP feedwater heaters and a deaerator. Typically, SC "steam" cycles involve 8 to 10 stages of feedwater heating, while subcritical-steam cycles usually involve 6-8 stages.

Following the previous discussion of on subcritical Rankine cycle, it is reasonable to match SFR outlet conditions to the existing modern SC turbines. For consistency with the previous section it was decided to consider power-conversion side with a single-reheat option and the same temperature of the working fluid at the heat exchanger outlet (505ºC).

The thermodynamic layout considered in this section corresponds to the conventional SC-pressure Rankine-"steam"-regenerative-cycles used in thermal power stations in Russia. Steam extractions are taken from HP, IP and LP turbines.

One conventional K-1200-240 turbine was considered to be connected to the reactor. The turbines were designed with a steam-reheat option in order to increase the thermal efficiency of the cycle and to reduce the amount of moisture in the last stages of the turbine. Major parameters of this turbine are listed in Table 2.4.

Table 2.4. Parameters of K-1200-240 Russian Turbine (Grigoryev and Zorin, 1989).

Parameters	K-1200-240
Power/Max Power, MW	1200/1380
Main Steam Pressure, MPa	23.54
Main Steam Temperature, °C	505
Reheat Steam Pressure, MPa	3.51
Reheat Steam Temperature, °C	505
Max Flow Rate Through HP Turbine, t/h	3950
Number of Steam Extractions	9
Outlet Pressure, kPa	3.58
Cooling Water Temperature, °C	12
Cooling Water Flow Rate, m^3/h	108,000
Feedwater Temperature, °C	274
Total Mass, t	1900
Total Length, m	47.9
Total Length with Generator, m	78.1

As shown in Table 2.4, the K-1200-240 turbine has 9 steam extractions from HP, IP and LP turbines for heat regeneration. Parameters of these steam extractions are listed in Table 2.5.

Table 2.5. Parameters of Steam Extractions for K-1200-240 Turbine (Kostyuk and Frolov, 2001).

Steam Extractions	*P*, MPa	*T*,°C	Specific enthalpy, kJ/kg	Relative steam consumption α, %
1	6.29	354	3047	9.0
2	3.90	295	2951	6.4
3	1.82	450	3360	5.0
4	0.90	355	3170	0.4
5	0.49	280	3023	2.3
6	0.26	218	2904	2.1
7	0.13	150	2774	1.9
8	0.05	80	2643	1.8
9	0.02	60	2505	2.1

A simplified SC Rankine cycle for an SFR is shown in Figure 2.10. Steam is reheated once after passing through the HP turbine to achieve a higher efficiency. The regenerative feedwater-heating system consists of five LP HTRs and three HP HTRs and one deaerator.

In the proposed layout, SCW flows through the steam generator, being heated from 274 °C to 505 °C and enters the HP turbine at pressure of 23.54 MPa. Steam is extracted twice from the HP turbine in order to heat the feedwater flowing through HPH2 and HPH3. After passing through the HP turbine, steam, in order to achieve a higher efficiency, is reheated once in an intermediate reheater at the output pressure of 3.51 MPa and the same temperature of 505 °C.

The IP turbine supplies extraction steam for the HP HTR1, deaerator and LHP5. In addition to it, a fraction of the steam is diverted to heat the water in the deaerator. The condensate from the HP HTR1 is fed back to the deaerator. The LP turbine also supplies steam extractions for the low-pressure heaters LP HTR 1 – 4. The condensate from the LP HTR1 is fed back to the condenser.

Thermal efficiency of the SC-pressure Rankine-“steam”-cycle was calculated to be 52.7%.

Thus, the thermal efficiency of the SC-pressure Rankine-“steam”-cycle is higher than that of subcritical pressure for the BN-600 SFR by 7.3%.

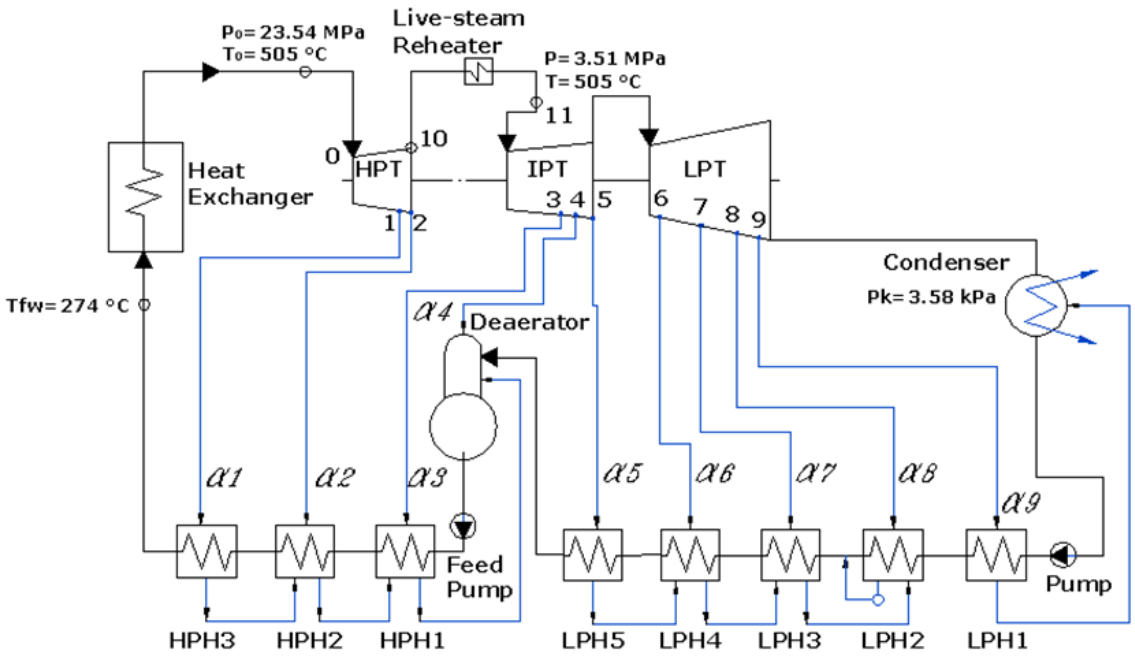

Figure 2.10. Single-Reheat Supercritical-Pressure Rankine-Steam-Cycle with Heat Regeneration: T – Turbine, T_{fw} – feedwater temperature, P_k – condenser pressure (courtesy of A. Dragunov (UOIT), Dragunov et al., 2012).

However, sodium reacts chemically with air and water, and thus the design of a heat exchanger should prevent the possibility for such reactions and their results. To improve safety, a secondary sodium system acts as a buffer between the radioactive sodium in the first loop and the steam (or water) in the third loop. As an alternative, SC CO_2 may be used as a working fluid in the NPP with a SFR.

2.5. Supercritical CO_2 Brayton cycle with heat regeneration

As was mentioned, conventionally subcritical Rankine-steam cycle is used as a power-conversion cycle at SFRs. Recently, research on the power cycle for the next generation reactors showed, that the SC CO_2 Brayton cycle is a promising alternative to the current Rankine cycle. SC CO_2 cycle is a new approach in the Brayton-gas-turbine cycle. CO_2 is becoming an important working fluid due to its low toxicity and environmental impact. It is well known that liquid sodium is more compatible with SC CO_2 than with water. In addition, the high fluid density of supercritical CO_2 greatly reduces the size of a turbine

and compressors, resulting in significant reductions in the size and capital cost of the turbomachinery. Therefore, a study of the ideal and SC CO_2 cycle with heat regeneration was performed.

For the analysis of the ideal SC CO_2 Brayton cycle the following assumptions were made:

- Gas turbine efficiency is 100%;
- Compressor efficiency is 100%;
- No mechanical losses;
- No heat losses to the surroundings; and
- All heat exchangers have 100% effectiveness.

The layout of a simple ideal SC CO_2 Brayton-gas-turbine closed-cycle is shown in Figure 2.11 and consists of a compressor, a recuperator, a heater, a gas turbine, and a cooler. CO_2 leaves the cooler in SC state.

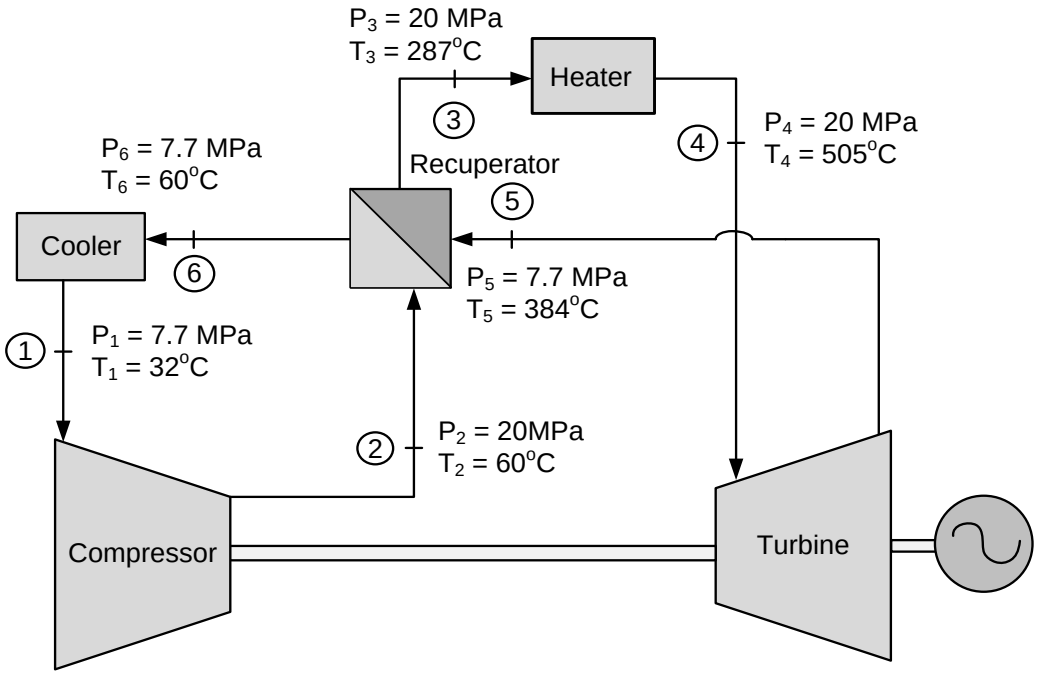

Figure 2.11. Ideal supercritical-pressure CO_2 Brayton-gas-turbine cycle (Courtesy of A. Dragunov (UOIT), Dragunov et al., 2013a).

In the compressor a fraction of the SC fluid is compressed from 7.7 MPa to 20 MPa (point 2). Then the fluid enters recuperator where waste heat from the turbine exhaust steam heats the compressed CO_2. Use of heat regeneration greatly improves the thermal efficiency of the cycle. A brief overview of the simple ideal Brayton cycle performed by Dragunov et al. (2012) showed that only 17% of thermal efficiency could be attained with no regeneration. After the recuperators, the fluid then enters the Na-to-CO_2 heat exchanger (point 3) at the temperature of 287 °C, where it is then heated, and heat addition to the cycle takes place. The fluid leaves the heater (point 4) at the highest temperature of 505 °C (the same as the inlet temperature for the steam in actual BN-600 SFR NPP). The SC CO_2 turbine operating conditions are: P_3 = 20 MPa, T_3 = 505 °C. The SC fluid expansion takes place in the turbine. After leaving the turbine (point 5), fluid with parameters P_4 = 7.7 MPa, T_5 = 384 °C is going into a recuperator. After that, fluid enters the cooler at the temperature of 60 °C. Finally, fluid entering compressor with temperature 32 °C and returns to the initial state.

Parameters of state points of the cycle are listed in Table 2.6.

Table 2.6. State points of the ideal SC CO_2 Brayton-gas-turbine cycle.

Point	*P*, MPa	*T*, °C	Specific Enthalpy, kJ/kg	Specific Entropy, kJ/kg·K
1	7.7	32	306.2	1.346
2	20	60	324.5	1.346
3	20	287	711.5	2.267
4	20	505	979.5	2.671
5	7.7	384	849.3	2.671
6	7.7	60	462.3	1.840

Major parameters of the cycle are listed in Table 2.7.

Table 2.7. Major parameters of the SC CO_2 Brayton-gas-turbine cycle.

Parameters	SC CO_2 Brayton cycle
Pressure ratio	2.6
Heat addition to the cycle, kJ/kg	268
Turbine work, kJ/kg	130.1
Compressor work, kJ/kg	18.3
Thermal efficiency, %	42
Highest pressure, MPa	20
Highest temperature, °C	505
Lowest pressure, MPa	7.7
Lowest temperature, °C	32

The overall thermal efficiency of the ideal SC CO_2 Brayton-gas-turbine cycle was calculated to be 42%.

The values discussed above, of the highest and the lowest pressures and temperatures, can be considered as those corresponding to the reference layout. It is reasonable to investigate the effect of variation of the highest pressure and temperature on the efficiency of the cycle. For this reason, inlet pressure to the turbine was varies from 16 to 24 MPa with a step of 2 MPa, and inlet temperature was varied from 505 °C to 550 °C. The lowest pressure and temperature were held unchanged. The results of calculations are presented in the Table 2.8.

The values presented in Table 2.8 show that the higher thermal efficiency is achieved at higher operating temperatures. The highest thermal efficiency achieved for the turbine inlet temperature of 550 °C is 45.5%, which is competitive with the traditional Rankine-steam cycle currently utilized in BN-600. Moreover, assuming that this Rankine-steam cycle is based on about 8 stages of regeneration and 1 stage of reheat, while the ideal SC CO_2 Brayton-gas-turbine cycle has just one recuperator, it can be stated that Brayton layout appears to be a prospective option.

Even further improvement in the thermal efficiency of the cycle can be achieved by adding one stage of reheat as well as an additional stage of compression.

Table 2.8. Parameters of various ideal SC CO_2 Brayton-gas-turbine cycles by temperature and pressure.

Turbine inlet temperature, °C	Turbine inlet pressure, MPa	Pressure ratio	Heat addition to the cycle, kJ/kg	Turbine work, kJ/kg	Compressor work, kJ/kg	Thermal efficiency, %
505	**16**	2.17	231.62	101.73	12.64	38.5
505	**18**	2.33	251.29	116.94	15.48	40.4
505	**20**	2.60	267.96	130.13	18.27	41.8
505	**22**	2.86	282.66	142.06	21.01	42.8
505	**24**	3.12	295.50	152.65	23.71	43.6
520	**16**	2.17	233.85	103.96	12.64	39.1
520	**18**	2.33	253.82	119.47	15.48	40.9
520	**20**	2.60	270.91	133.08	18.27	42.4
520	**22**	2.86	285.82	145.22	21.01	43.5
520	**24**	3.12	298.93	156.08	23.71	44.3
535	**16**	2.17	236.09	106.20	12.64	39.6
535	**18**	2.33	256.43	122.08	15.48	41.6
535	**20**	2.60	273.72	135.89	18.27	42.9
535	**22**	2.86	288.99	148.39	21.01	44.1
535	**24**	3.12	302.37	159.52	23.71	44.9
550	**16**	2.17	238.23	108.34	12.64	40.2
550	**18**	2.33	258.95	124.60	15.48	42.1
550	**20**	2.60	276.56	138.73	18.27	43.6
550	**22**	2.86	292.14	151.54	21.01	44.7
550	**24**	3.12	305.71	162.86	23.71	45.5

2.6. Two-stage compression with intercooling cycle

Since the maximum temperatures of the second loop sodium are relatively low, it is important to optimize the corresponding power conversion cycle. Therefore, the effects of intercooling and recompression on the thermodynamic efficiency of the cycle are discussed here on the example of Monju reactor conditions (which has lower secondary sodium temperature than that of BN-600).

To simplify the analysis, 100% efficiencies of all equipment components were assumed, as follows:

1) 100% isentropic efficiency of the expansion process in a turbine;
2) 100% isentropic efficiency of the compression process in a compressor;

3) 100% efficiency of the heat exchangers; and
4) negligible changes in potential and kinetic energy of CO_2 in the piping.

These assumptions allows estimation of the maximal attainable efficiency. Two-stage compression with intercooling cycle is shown in Figure 2.12. Parameters of CO_2 at each of the points of the cycle are given in Table 2.9.

Parameters of CO_2 entering first stage of compression were chosen to be slightly above the critical point. Pressure at the turbine inlet was chosen somewhat arbitrarily to be 20 MPa. Mass-flow rate of CO_2 for this cycle 886.7 kg/s. Thermodynamic efficiency of the cycle was found to be 41.5%. This values is almost identical to the one that was obtained for a single regeneration SC Brayton cycle corresponding to the BN-600 conditions (where temperature of CO_2 at the outlet of the primary heat exchanger was considered to be 20 °C higher than in the considered case).

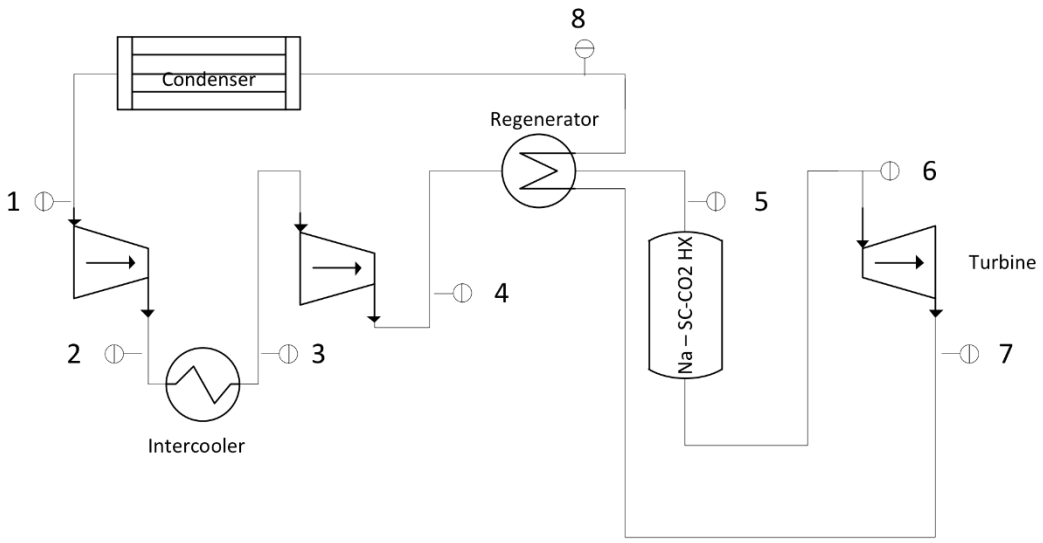

Figure 2.12. Two-stage compression with intercooling cycle, where: 1 – inlet to the first compressor, 2 – inlet to the intercooler, 3 – inlet to the second compressor, 4 – inlet to the heat regenerator (heat gain), 5 – inlet to the main Na – SC CO_2 heat exchanger, 6 – inlet to the turbine, 7 – inlet to the heat regenerator (heat rejection), 8 – inlet to the condenser; HX – Heat eXchanger.

Table 2.9. Parameters of CO_2 at different points of cycle shown in Figure 2.12.

Point	*T*, °C	*P*, MPa
1 (inlet to the 1st compressor)	32	7.8
2 (inlet to the intercooler)	45	12.5
3 (inlet to the 2nd compressor)	32	12.5
4 (inlet to the heat regenerator (heat gain))	41	20.0
5 (inlet to the main Na – SC CO_2 heat exchanger)	268	20.0
6 (inlet to the turbine)	480	20.0
7 (inlet to the heat regenerator (heat rejection))	362	7.8
8 (inlet to the condenser)	41	7.8

An alternative layout which includes reheat is shown in Figure 2.13. Parameters of CO_2 at each of the points of the alternative layour are given in Table 2.10.

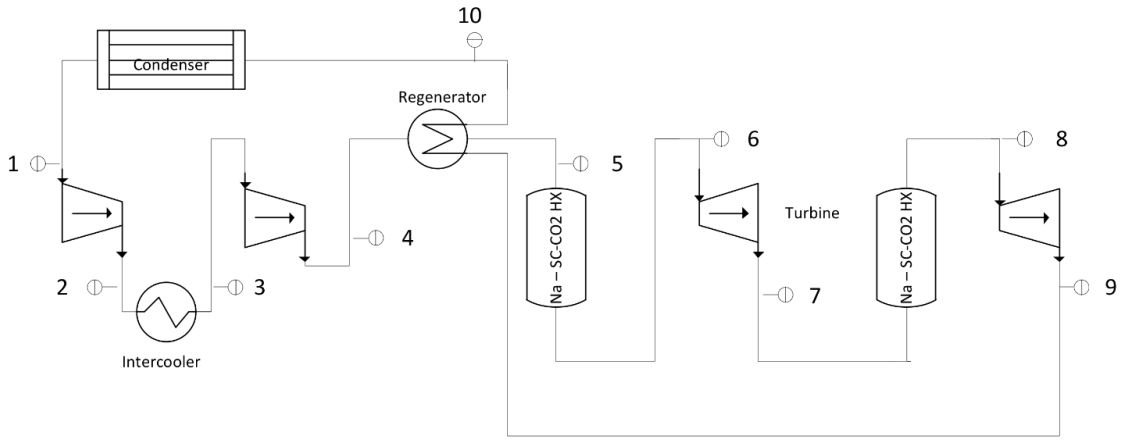

Figure 2.13. Two-stage compression with intercooling and reheat cycle, where: 1 – inlet to the first compressor, 2 – inlet to the intercooler, 3 – inlet to the second compressor, 4 – inlet to the heat regenerator (heat gain), 5 – inlet to the main Na – SC CO_2 heat exchanger, 6 – inlet to the high pressure turbine, 7 – inlet to the Na – SC CO_2 reheater, 8 – inlet to the low pressure turbine, 9 – heat regenerator (heat rejection), 10 – inlet to the condenser; HX – Heat eXchanger.

Table 2.10. Parameters of CO_2 at different points of cycle shown in Figure 2.13.

Point	*T*, °C	*P*, MPa
1 (inlet to the first compressor)	32	7.8
2 (inlet to the intercooler)	45	12.5
3 (inlet to the second compressor)	32	12.5
4 (inlet to the heat regenerator (heat gain))	41	20.0
5 (inlet to the main Na – SC CO_2 heat exchanger)	303	20.0
6 (inlet to the high pressure turbine)	480	20.0
7 (inlet to the Na – SC CO_2 reheater)	417	12.5
8 (inlet to the low pressure turbine)	480	12.5
9 (heat regenerator (heat rejection))	422	7.8
10 (inlet to the condenser)	41	7.8

Parameters of CO_2 entering first stage of compression were chosen to be the same as in the previous case. Mass-flow rate of CO_2 was found to be 867.2 kg/s, which slightly less than that of the previous cycle. Thermodynamic efficiency of the cycle was found to be: 42.7% (3% increase in efficiency compared to the previous case). The comparison of T-s diagrams for both cycles is presented in Figure 2.14. It is easy to see the amount of work added by implementing reheat and using an additional stage of turbine from this figure.

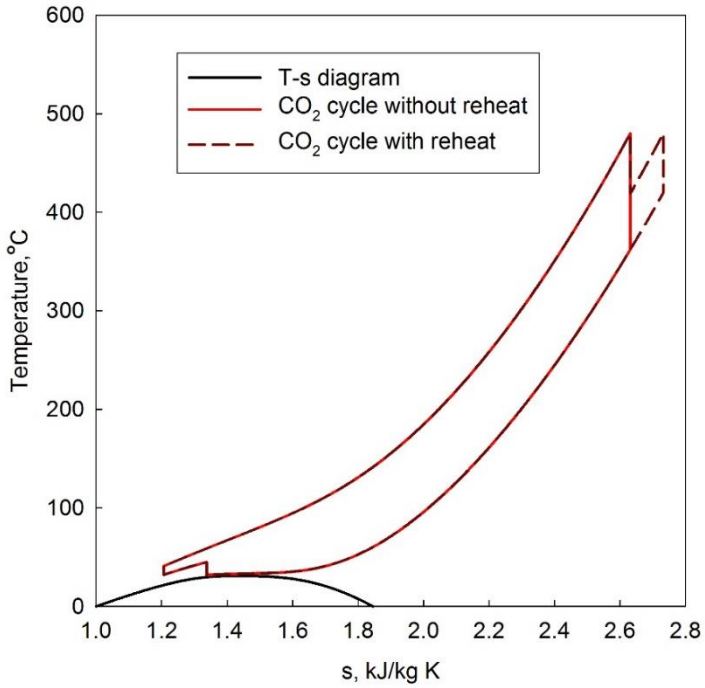

Figure 2.14. T-s diagram for the considered SC CO_2 cycles.

Thus, addition of stage of reheat leads to a 3% increase in thermal efficiency. High thermodynamic efficiency of 43% of the ideal two-stage compression with intercooling and single reheat was found for the SC CO_2 power conversion cycle with as low as 480 °C turbine inlet temperature, which corresponds to the Monju reactor.

Although a more rigorous analysis of the cycle is needed with accounting for the costs and inefficiencies of equipment components, SC CO_2 Brayton cycles appears as a promising option for power-conversion side of SFRs.

2.7. Other applications of SC CO_2

Since the thermodynamic critical point of CO_2 (7.38 MPa and 30.98 °C)[3] is much lower than that of water (22.06 MPa and 373.95), CO_2 has been widely used as a modelling fluid for water (e.g., Zahlan et al., 2013; Bae and Kim, 2009; Kurganov et al., 2009; Pioro and Duffey, 2007; Fewster and Jackson, 2004; Kurganov and Kaptil'ny, 1992; Jackson and Hall, 1979a; and Kransoshchekov and Protopopov, 1966) to study specifics of heat transfer at the SC state.

The increased worldwide concern of global warming and ozone depletion called for studying prospective fluids to replace conventional refrigerants. According to Environment Canada (2014), the global warming potential of: R-12 is 2400 times, R-22 is 1700 times, and R-134a is 1300 times that of CO_2. Thus, SC CO_2 attracted attention in this domain due to being a non-toxic and non-flammable fluid with lower global warming potential. It was considered as a working fluid for many power/engineering applications, such as: innovative air-conditioning and refrigeration systems (Mathur, 2000; Lorentzen, 1994; and Lorentzen and Pettersen, 1993), solar energy-power-conversion systems

[3] Thermal and transport properties of CO_2 and water were retrieved from NIST REFPROP ver. 9.0 software (Lemmon et al., 2013). The properties of CO_2 implemented in NIST are based on the publication by Span and Wagner (1996), Fenghour et al. (1998), and Vesovic et al. (1990). The properties of water implemented in NIST are based on the 1995 formulation by the International Association for the Properties of Water and Steam (Wagner and Pruss, 2002), Huber et al. (2009), and IAPWS (2008).

(Chapman and Arias, 2009), and enhanced geothermal systems (Wan et al., 2011; and Brown, 2000).

Most recently, SC CO_2 was proposed as a prospective working fluid for large-scale district heating purposes. The proposed technology was based on the use of high-capacity heat pumps with CO_2 to transform the waste heat of NPPs to parameters corresponding to those of district heat supply systems (Kalnin et al., 2003; Kalnin et al. 2013).

Additionally, SC CO_2 may be considered as an intermediate coolant between the hydrogen production facility and SCWR. This idea is stemming from the proposed linkage of an SCWR and a hydrogen producing facility based on Copper-Chlorine (Cu-Cl) cycle that requires high temperatures (up to 550 °C). Mokry et al. (2011a) discussed integration of heat exchangers into a reactor building. However, this is a high-risk option due to the very high difference in SCWR operational pressures and those required for the Cu-Cl cycle. Thus, an intermediate loop between SCWR and hydrogen producing facility that would use low pressure superheated CO_2 may be an alternative option.

Thus, SC CO_2 recently became a very important fluid for power and engineering applications.

Recognizing the benefits of using SC CO_2 in fossil, renewable, and nuclear power plants, the SC CO_2 Power Cycle Symposium was established in the US in 2007.

All the applications of SC CO_2 mentioned above will use heat exchangers. The design of the appropriate heat exchangers (intermediate heat exchangers, recuperators, intercoolers, etc.) for these power/engineering applications will require reliable heat transfer correlations.

CHAPTER 3. LITERATURE REVIEW – FORCED CONVECTIVE HEAT TRANSFER TO FLUIDS IN SUPERCRITICAL STATE

The supercritical state is a thermodynamic state at which both the temperature and pressure of a fluid exceed those values at a critical point. If neither of these conditions are met, the fluid is said to be at the subcritical state. While liquid and gaseous phases are clearly distinct for fluid at the subcritical state, no such difference can be made for fluid at the supercritical state. Usually, a fluid at temperatures exceeding the saturation temperature at a given pressure is called a superheated vapor (Black and Hartley, 1996; Kikoin and Kikoin, 1976); and fluid at pressures exceeding the saturation pressure at a given temperature is called a compressed fluid (Black and Hartley, 1996; Kikoin and Kikoin, 1976). Quite often fluids at pressures exceeding the critical value are referred to as SC pressure fluids. However, recently more detailed definitions were proposed (Pioro and Mokry, 2011): only vapor at temperatures above that of the critical state is called a superheated vapor; only fluid at pressures above that of the critical state is called a compressed fluid; and fluid at temperatures and pressures both exceeding those of the critical point is called a supercritical fluid. Moreover, Pioro and Mokry (2011) proposed to extend the saturation line with a pseudocritical line, which represents the loci of pseudocritical temperatures (pseudocritical temperature (sometimes referred to as the pseudocritical point) is the temperature at which, for the given pressure, the specific heat, c_p, reaches its maximal value). These definitions are shown on a P-T diagram for water, which is repeated here for convenience (Figure 3.1).

Thermal and transport properties of subcritical fluids vary with temperature much more significantly than with pressure. As long as a fluid does not undergo a phase change, variations of its properties are gradual. Therefore, for modelling purposes, flow of subcritical fluids can be considered as a flow of fluid with constant properties.

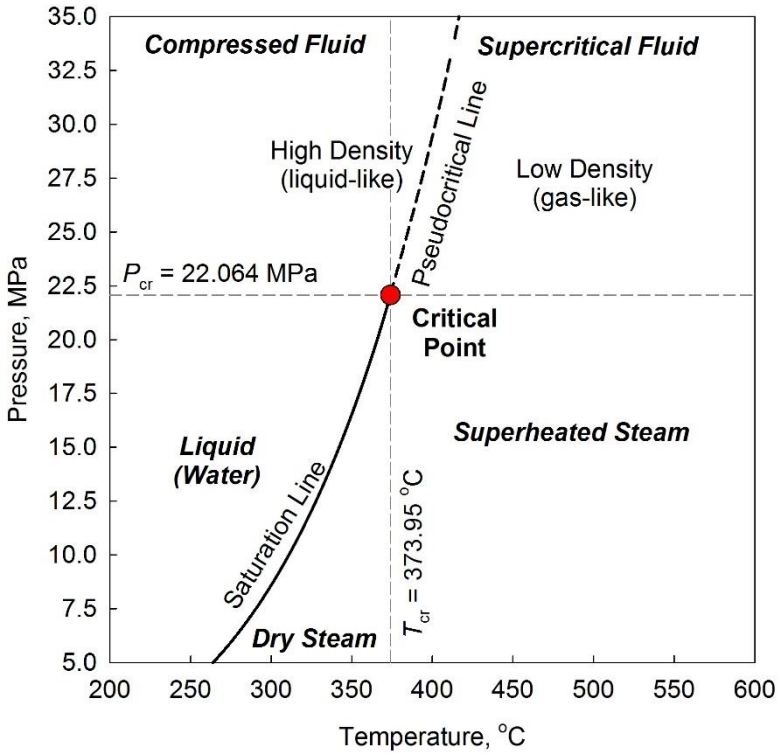

Figure 3.1. P-T diagram for water (courtesy of S. Mokry (UOIT), Mokry et al., 2011).

Based on numerous experiments, numerical solutions, and semi-empirical studies (Munson et al., 2009), the theory of the turbulent boundary layer has been established. Theory suggests that the fully developed turbulent flow consists of the following three regions: the viscous sublayer (where viscous effects are important and density effects are negligible); the buffer layer (sometimes referred to as the transitional or overlap layer), and the outer layer, or turbulent core, where the density effects are important and viscous effects are negligible.

The most common geometry used in heat transfer experiments is a circular bare tube. To relate the cross-sectional average temperature of fluid (commonly referred to as bulk fluid temperature, T_b), temperature of the cooled or heated surface (commonly referred to as wall temperature, T_w), and applied heat flux, the concept of an HTC is used. These quantities are connected through Newton's cooling law:

$$q = HTC\left(T_w - T_b\right) \tag{3.1}$$

HTCs of subcritical fluids do not experience significant changes along the heated length of tubes. On the contrary, the situation is different for fluids at the SC state (or, SCFs). The properties of fluids undergo drastic variations within a narrow region of temperatures around the pseudocritical temperature, T_{pc}. Figure 3.2 displays the variations of some of the properties of water around the pseudocritical point. These properties have the strongest influence on heat transfer.

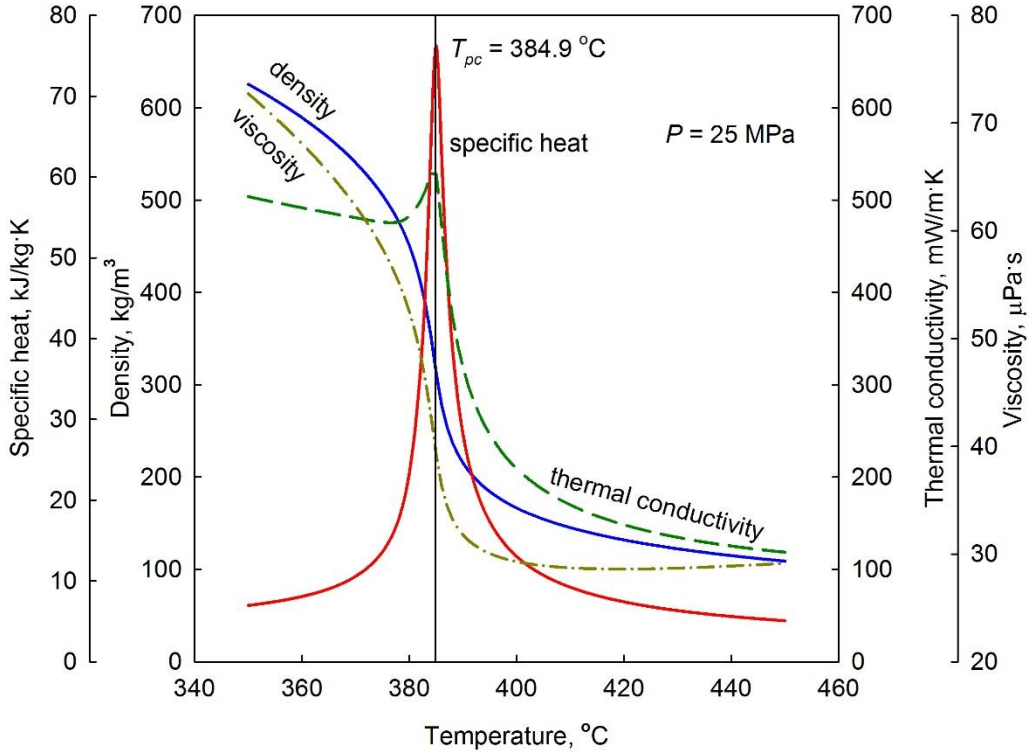

Figure 3.2. Selected thermal and transport properties of water at 25 MPa.

From Figure 3.2, the changes are non-uniform for different properties. Density, ρ, and viscosity, μ, reduce continuously; thermal conductivity, k, has a small peak at a temperature different than T_{pc}; specific heat, however, has a similar to Gaussian-type peak. If one can think of a situation when T_b = 350 °C (T_w is automatically higher than T_b) it becomes obvious that there will be generally high axial and radial variations of properties for heated flows of SCFs. Indeed, HTCs of SCFs vary significantly in the vicinity of the pseudocritical point. Some authors (Jackson and Hall, 1979a; and Pioro and Duffey, 2007) have referred to the SCFs at temperatures below T_{pc} as high-density (liquid-like) fluids,

and to those at temperatures above T_{pc} as low-density (gas-like) fluids, based on experiments with X-ray diffraction.

Based on significant deviations of HTC from the values predicted by correlations for fully developed subcritical flows (such as the one by Dittus and Boelter, 1930) for Normal Heat Transfer (NHT), the corresponding heat transfer regimes are referred to as DHT and Improved Heat Transfer (IHT). Examples of these regimes are shown on Figures 3.3 and 3.4.

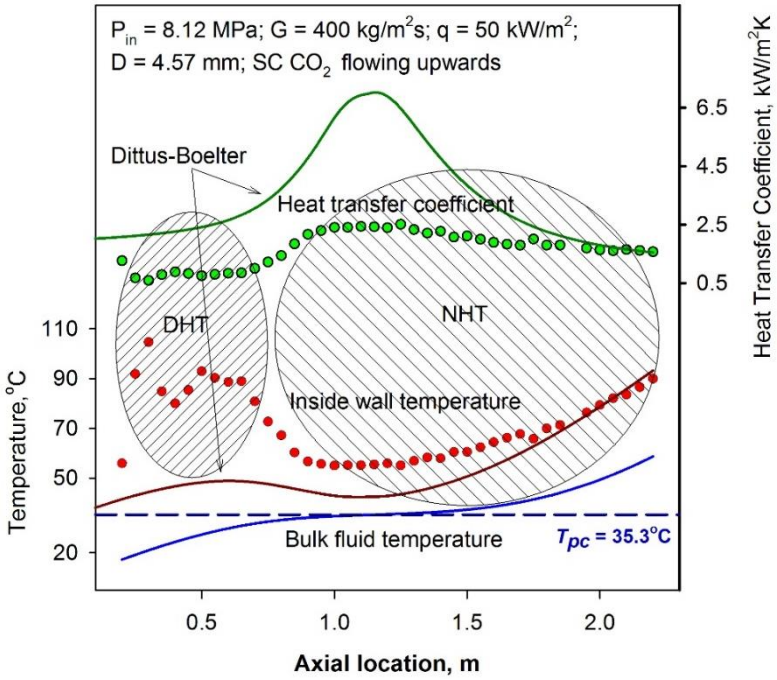

Figure 3.3. Heat transfer coefficients at deteriorated and normal heat transfer regimes (upward flow of SC CO_2 in a bare tube; IAEA, 2011).

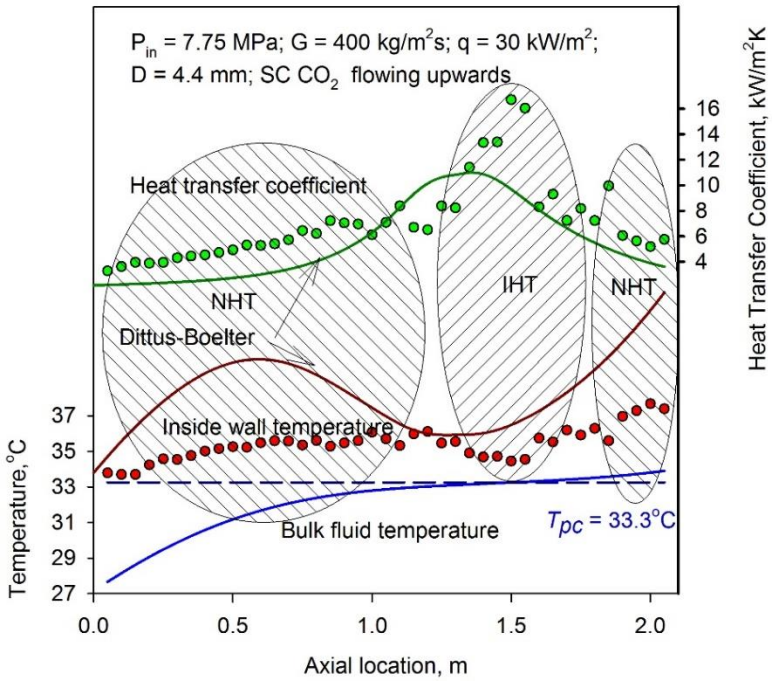

Figure 3.4. Heat transfer coefficients at improved and normal heat transfer regimes (upward flow of SC CO_2 in a bare tube IAEA, 2011).

IHT and DHT are usually observed when the bulk-fluid temperature is within T_{pc}. While the increase in specific heat and decrease in viscosity (in the pseudocritical region) should lead to an improved rate of heat transfer from the heated wall to the core of the flow, the decrease in thermal conductivity has an opposite effect.

Research often treats the flow of SCF at the inlet of the test-section as fully developed by using a long enough preceding unheated section. Nevertheless, it is important to realize that the velocity profile transforms significantly as the bulk fluid passes through the pseudocritical point, independent of the distance from the inlet to the tube. This transformation affects the shear stress and, thus, affects the rate of heat transfer, as well.

Therefore, there are several basic effects influencing the regime of heat transfer. DHT is the least desirable heat transfer regime from the point of view of power/engineering applications[4]. As a result, there is an ongoing discussion about the physics behind DHT, criteria for distinguishing it from NHT, and the approaches to correlate DHT data.

[4] Relevance of DHT to the current Canadian SCWR concept is briefly discussed in Appendix E.

3.1. Current understanding of DHT mechanisms

Current understanding and explanation of DHT mechanisms relies on numerical studies, semi-empirical calculations, and experiments. Review of these studies and their major findings is presented below.

Pioro and Duffey (2007) presented an extensive study on DHT and made a major conclusion that DHT generally occurs at higher heat fluxes and lower mass fluxes. They found that DHT is typical for upward flow of SCW, and is not specific to downward flow. DHT at upward flow is subject to possible combinations of fluid properties and specifics of experiments (surface roughness, pressure pulsations, presence of impurities in the coolant), and may occur anywhere along a test-section.

Koshizuka et al. (1995) distinguished two mechanisms of DHT: 1) thickening of the viscous sublayer and decrease of Prandtl number at high mass fluxes; and 2) laminarization of the velocity profile due to the strong influence of buoyancy forces at low mass fluxes.

Tejaswini et al. (2013) discussed that heat transfer characteristics are highly influenced by strong buoyancy effects at low flow rates and flow acceleration at high flow rates, both of which are caused by rapid density changes. The combination of a drop in velocity gradient at the boundary-layer – flow-core interface and a decrease in thermal conductivity lead to DHT.

Ambrosini et al. (2013) emphasized that the sharp variation of thermal conductivity and viscosity over the cross section is not typical for subcritical flow, which makes heat transfer behavior in SCFs different from classical single-phase flows. They additionally pointed out that the location of the peak of specific heat is different in different cross-sections of the heated tube, which potentially causes a strong effect on heat transfer.

Jackson and Hall (1979a) discussed that change in the convective term (in the equation of motion) along the tube axis, $\rho u \frac{\partial u}{\partial x}$, leads to a reduction of shear stress in the radial direction. They proposed a 5% reduction of shear stress at location $y^+ = 20$ as a criterion

for the onset of DHT due to changes in the acceleration term. The criterion is expressed as follows:

$$-\frac{q\mu_b^{0.7}}{\rho_b^{2.7}u^{1.7}D^{0.7}}\left[\left(\frac{\partial\rho}{\partial h}\right)_P\right]_b\left(\frac{\mu_w}{\mu_b}\right)\left(\frac{\rho_w}{\rho_b}\right)^{-0.5} > 2.2\cdot10^{-6} \tag{3.2}$$

This mechanism of deterioration was called the acceleration effect.

Jackson et al. (2011) presented an extended treatment of their semi-empirical model for an SCF influenced by the acceleration effects. He discussed that the decrease in the **Nu** in the flow with thermally-induced acceleration will be negligible compared to the **Nu** for the flow without such effects, if the acceleration parameters, $\mathbf{Ac_b^*}$, meets the critera below :

$$\mathbf{Ac_b^*} = \frac{\mathbf{Q_b^*}}{\mathbf{Re_b^{1.625}Pr_b}} \le 2\cdot10^{-6} \tag{3.3}$$

Jackson (2009) proposed an extended physical explanation of the effect of the bulk flow acceleration on heat transfer. The density of SCF falls with the increase in temperature (e.g., see Figure 3.2). The continuity equation requires the mass flux to be the same at any location along the flow. Therefore, the bulk of the flow accelerates, as if due to the presence of an additional pressure gradient. Jackson (2009) suggests that this additional pressure is caused by the adjusted profile of radial shear stress. He infers that at such conditions shear stress reduces more rapidly with the distance from the wall (than in the case of fully developed flow with the same **Re**), the viscous sublayer thickens and, thus, the heat transfer deteriorates.

By analyzing experimental data, Jackson and Hall (1979b) discussed that while DHT occurs for upward flows at low mass fluxes, heat transfer does not become impaired at the same experimental conditions for the downward flows. Therefore, they concluded that buoyancy effects could be significant at causing DHT at low mass fluxes. They proposed the following criterion for buoyancy effects to become significant for vertical flows:

$$\frac{\overline{\mathbf{Gr}_\mathbf{b}}}{\mathbf{Re}_\mathbf{b}^{2.7}} < 10^{-5} \tag{3.4}$$

Recently, Jackson et al. (2011) updated the analytical criterion (based on the buoyancy parameter) for the buoyancy effects to be negligible, as follows:

$$\mathbf{Bo}_\mathbf{b}^* = \frac{\mathbf{Gr}_\mathbf{b}^*}{\mathbf{Re}_\mathbf{b}^{3.425}\mathbf{Pr}_\mathbf{b}^{0.8}} \le 2 \cdot 10^{-7} \left(\frac{\overline{\mathbf{Pr}}}{\mathbf{Pr}_\mathbf{b}} \right)^{0.4} \tag{3.5}$$

Jackson et al. (2011) suggested the following framework to explain buoyancy-induced DHT. Due to the density gradient along the heated length of the tube, buoyancy forces act to aid the flow. Buoyancy leads to a higher gradient of the shear stress near the wall. Thus, the turbulence production near the wall reduces.

Zahlan et al. (2013) presented their experimental results on forced convection heat transfer to SC CO_2 flowing upward. They observed DHT when the acceleration parameter (Eq. (3.3)) exceeded $3.5 \cdot 10^{-7}$, which is in contradiction with the criterion by Jackson (2008). However, Zahlan et al. (2013) confirmed the criterion Eq. (3.5) as they observed DHT when the buoyancy parameter exceeded $3.3 \cdot 10^{-7}$.

Kiss and Aszodi (2013) performed numerical simulations of buoyancy-induced DHT (they referred to it as mixed-convection DHT) in the experiment C008 by Shitsman (1963) and acceleration-induced DHT (they referred to it as forced convection DHT) in the experiment C359 by Ornatskiy et al. (1971). Their major conclusion was that the huge radial temperature gradient in the vicinity of peak of the wall temperature peak along the heated length serves as a negative feedback mechanism to recover heat transfer.

As one can see, the mechanisms of DHT are currently attributed to the reduction in shearing stress and thickening of the viscous sublayer having low thermal conductivity. However, the proposed descriptions of the mechanisms underlying the buoyancy- and acceleration-induced DHT are overlapping, and, in fact, the same. A certain confusion arises due to the terminology, since buoyancy force acting on a differential volume fluid causes its

acceleration. However, Jackson and Hall (1979a) used the word "acceleration" to describe a convective term in the equation of motion.

Thus, based on this review it may be concluded that the most influential description of DHT was proposed by Jackson and Hall in 1979 (a, b). They proposed the two following mechanisms: 1) induced by buoyancy; and 2) induced by acceleration effect. It appears from the discussion by other authors, that buoyancy-induced mechanism is typical of low mass fluxes flows, while the acceleration-induced mechanism is typical of both high heat and mass fluxes at pure forced convection conditions. Both DHT mechanisms proposed by Jackson and Hall (1979a and 1979b) suggest that DHT would be associated with a laminarized, or flattened, velocity profile. However, in neither of the above cited works Jackson proposed an idea how to experimentally distinguish one effect from another.

Bourke and Pulling (1971) obtained profiles of mean axial velocity, RMS fluctuations of radial velocity, mean values and RMS fluctuations of temperature and radial heat flux for upward flow of SC CO_2 at 7.45 MPa in a 22.5 mm (0.886 in) bare tube with variable heated length. Only one test was reported. Heat flux, q, in their test run was approximately equal to 266 kW/m^2 and mass flux, G, approximately equal to 1517 kg/m^{2}s (thus, q/G = 0.175 kg/m^{2}s). The results of measurements of mean velocity profiles reported by Bourke and Pulling (1971) suggest that the heat transfer recovers as the velocity profile attains an M-shape. In fact, DHT develops as the velocity profile resembling a parabola at the inlet to the test section flattens to a shape resembling a rounded rectangular, with a corresponding peak in T_w. Further deformation of the velocity profile into an M-shape leads to a recovery in heat transfer. Bourke and Pulling (1971) conclude that deterioration was caused by a reduction in turbulence over a much wider region of fluid than the normal laminar boundary layer. Bourke and Pulling (1971) had a long enough heated length to observe that as the bulk temperature increased beyond the T_{pc} region and heat transfer stabilized, the velocity profile flattened to a shape similar to that at the inlet (although with a small depreciation in the center). Although, the results obtained by Bourke and Pulling (1971) represent a great interest from the qualitative perspective, Kurganov et al. (2013) discuss that numerical results might not be reliable due to several reasons. One of the reasons is

the experimental pressure being extremely close to the critical value thus affecting the accuracy of determining density.

Kurganov and Kaptil'ny (1992) conducted a series of experiments on forced convective heat transfer to SC CO_2 flowing upward and downward in bare tubes (5.22 mm long) of 8 and 22.7 mm inner diameter at the Institute for High Temperatures (Russia). It appears that a 2.951 m long central part of the tube was heated and preceded by a 1.135 m long unheated part. The following conditions were covered at their experiments: P = 9 MPa, G = 800 – 2100 kg/m^{2}s, q/G = 0.05 – 0.22 kJ/kg. Kurganov and Kaptil'ny (1992) reported direct measurements of both temperature and velocity fields. By using the continuity, conservation of mass, and energy equations, they were able to calculate profiles for radial heat and mass fluxes and shear stress over tube cross section, and, consequently, the gradient coefficients of turbulent momentum and heat diffusivities. They reported that depending on the experimental conditions, T_w peaked either prior or after T_b exceeded T_{pc}. The deterioration appeared at $q/G > 0.191$ kJ/kg. By analyzing the obtained data, Kurganov and Kaptil'ny (1992) concluded the following:

1) DHT occurred beyond the thermal entrance length ($x/D > 20$).
2) DHT was accompanied by the flattening of the velocity profile and corresponding near-zero (or slightly negative) values of the shear stress for the bulk part of the cross-section.
3) Recovery from DHT was accompanied with the formation of an M-shape velocity profile and corresponding negative shear stress for the bulk part of the cross-section.
4) In general, such changes in flow structure make analysis of hydraulic resistance and heat transfer crude based on local approximation, i.e., by ignoring flow history.

It is important to notice that Kurganov and Kaptil'ny (1992) and Bourke and Pulling (1971) presented results of measurements for the upward flow of SC CO_2 in tubes of similar diameters, but at different pressures (9.0 MPa in the paper by Kurganov and Kaptil'ny, 1992; and 7.45 MPa in the report by Bourke and Pulling, 1971). However, in both works experimental conditions leading to DHT correspond to the high heat flux type of DHT.

Additionally, both works reported that heat transfer recovery was associated with the transformation of the velocity profile into M-shape.

No other reported experimental measurement of velocity profiles were found in the literature. Therefore, it appears highly important to perform systematic experimental measurements of velocity profiles for the case of the low mass flux type of DHT. This will allow the discovery of any similarities in the velocity profile transformations at low mass flux and high heat flux types of DHT. Additionally, measurements of the velocity profiles at NHT would be valuable. A full set of velocity profiles will allow researchers to compare the effect different flow structures have on DHT. Based on the scarce experimental results found in the literature, it may be preliminary concluded, that DHT can be viewed as merely a transition between similar heat-transfer regimes as the result of the redistribution of the velocity profile. Depending on the heat loading factor q/G the redistribution of the velocity profile may occur along a very short part of the test section, thus, avoiding onset of DHT.

3.2. Onset of DHT

From the discussion in the previos section it follows that for any given mass flux, heat flux may be increased to a value that will lead to DHT. Therefore, the onset of DHT is usually reported in the form of a dimensional relationship between heat and mass flux. The existing criteria and correlations for the onset of DHT are discussed below. Unless specified, the default unit for heat flux is kW/m^2 in these correlations.

One of the most recent correlation relating mass flux and minimal heat flux at which DHT is expected to occur was proposed by Zahlan et al. (2013). They used their experimental data for SC CO_2 to predict the onset of DHT as follows:

$$q = 3 \cdot 10^{-4} G^{1.8} \tag{3.6}$$

Although, they did not specify for what kind of DHT this criterion is valid, it appears from their paper that criterion Eq. (3.6) is for the buoyancy-induced DHT.

Mokry et al. (2011b) proposed the following criterion for the onset of DHT in SCW:

$$q = -58.97 + 0.745G \tag{3.7}$$

It appears from the paper by Mokry et al. (2011b) that their correlation is valid for the following range of experimental parameters: P = 24 MPa, T_{in} = 320 – 350 °C, G = 200–1500 kg/m^2 s, $q \leq 1250$ kW/m^2, and D = 10 mm.

By using the numerical definition of Koshizuka et al. (1995) for DHT, Cheng et al. (2009) proposed the following equation to predict the onset of DHT:

$$\frac{q}{G} = 1.354 \cdot 10^{-3} \frac{c_{p,pc}}{\beta_{pc}} \tag{3.8}$$

They showed that this criterion was in a good agreement with the one by Yamagata et al. (1972). Criterion presented in Eq. (3.8) includes effect of pressure.

Kim et al. (2005) presented the following power relation for the flow of SC CO_2 in circular tubes:

$$q = 0.2G^2 \tag{3.9}$$

It appears from the paper by Kim et al. (2005) that their correlation is valid for the following range of experimental parameters: P = 8 MPa, T_{in} = 15 – 32 °C, G = 209–1230 kg/m^2 s, q = 3 – 180 kW/m^2, and D = 7.8 mm.

Kang et al. (2007) presented the data obtained at Korea Atomic Energy Research Institute (KAERI) Supercritical Pressure Heat transfer Investigation for NeXt generation (SPHINX) loop for upward flow of SC CO_2 inside a 6.32 mm diameter bare tubes at various heat and mass fluxes, inlet temperatures, and pressure fixed at 8.12 MPa. They came up with the following criteria for the onset of DHT:

$$\begin{cases} q = 18 \cdot G^{1.25} \text{ for } G < 1000 \text{ kg/m}^2\text{s} \\ q = 0.1 \cdot G^2 \text{ for } G \geq 1000 \text{ kg/m}^2\text{s} \end{cases} \tag{3.10}$$

Their criteria are valid for the following range of operating parameters: P = 8.12 MPa, T_{in} = 5 – 37 °C, G = 400 – 1200 kg/m^{2}s, q = 20 – 170 kW/m^2, and D = 6.32 mm.

Kang et al. (2007) have clearly specified what data they considered as deteriorated: if the wall temperature of at least four successive points was higher than the temperature of the following point, accounting for the uncertainties of the ThermoCouples (TC), the region was considered as deteriorated. This is an important remark, because points belonging to DHT regime are typically removed from consideration for conventional heat transfer correlations based on visual inspection. However, the definition of a point belonging to DHT is absent in the paper by Kang et al. (2007). Additionally, it appears that their definition of DHT points is rather a definition of a peak in T_w.

Grabezhnaya and Kirillov (2006) used an approximate theory of thermodynamic similarity to define the onset of DHT in any SCF as follows:

$$q \geq 0.6G\frac{M_{H_2O}}{M}, \tag{3.11}$$

where M – molecular weight.

Petukhov et al. (1972) derived the following semi-empirical relation for the (the numerical constant was fitted to the experimental data) onset of DHT in SC CO_2 and SCW:

$$\frac{q}{G} = 3.4\cdot 10^{-2}\left(\frac{c_p}{\beta}\right)_{pc}\sqrt{\frac{\xi}{8}} \approx 0.012\left(\frac{c_p}{\beta}\right)_{pc}\sqrt{\xi}, \tag{3.12}$$

where ξ – friction factor, which is calculated according to the Filonenko (1954) equation:

$$\xi = \frac{1}{\left(1.82\log_{10}\mathbf{Re} - 1.64\right)} \tag{3.13}$$

where viscosity in **Re** should be calculated at the temperature corresponding to the onset of DHT.

The criterion presented in Eq. (3.12) has ±20% uncertainty and is valid for upward flow of water (P/P_{cr} = 1.02 – 1.55; **Re** = (27 – 180)·10^3; G = 400 – 1450 kg/m^{2}s; q = (0.29 – 1.75)·10^6 W/m^2; and D = 6 – 20 mm) and CO_2 (P/P_{cr} = 1.06 – 1.33; **Re** = (34 – 850)·10^3; G = 700 – 25,000 kg/m^{2}s; q = (0.12 – 4.83)·10^6 W/m^2; and D = 2 – 4 mm). Petukhov et al. (1972) clarified that this criterion gives a value of heat loading parameter below which local DHT will not develop in any section of the heated tube.

Yamagata et al. (1972) proposed the following correlation for the onset of DHT in SCW:

$$q = 0.2G^{1.2} \tag{3.14}$$

It appears from the paper by Yamagata et al. (1972) that their correlation is valid for the following range of experimental parameters: P = 22.6 – 29.4 MPa, T_b = 230 – 540 °C, G = 310 – 1830 kg/m^{2}s, q = 116 – 930 kW/m^2, and D = 7.5 mm and 10 mm (however, the majority of the data were collected for D = 10 mm).

Cheng et al. (2007) suggested defining the onset of DHT as the onset of the low peak of HTC, since in their Computational Fluid Dynamics (CFD) calculations the appearance of low peak of HTC coincided with Yamagata et al. (1972) criterion for the onset of DHT. Unfortunately, when presented in such form, the suggested definition by Cheng et al. (2007) cannot be used directly and merely serves as a confirmation that CFD prediction of DHT coincides with the empirical correlation.

Bae et al. (2010) tested several criteria for the onset of deterioration (Yamagata et al., 1972, Eq. (3.14); Kim et al., 2005, Eq. (3.9); and Grabezhnaya and Kirillov, 2006, Eq. (3.11))[5] against their experimental data. They showed that their earlier criterion, which was presented by Kim et al. (2005) performed well at G > 1000 kg/m^{2}s. The generalized deterioration criterion suggested by Grabezhnaya and Kirillov (2006) performed poorly.

[5] Bae et al. (2010) have also referred to a criterion by Styrikovich et al. (1967), however it was not possible to find the original paper. Moreover, different authors citing the critera for the onset of deterioration by Styrikovich et al. (1967) presnt, for some reason, contradicting values. Since the original paper was not available, it was not possible to verify the correct version of the criterion allegedly proposed by Styrikovich et al. (1967).

The criteria by Styrikovich et al. (1967) and Yamagata et al. (1972) significantly over predicted the onset of DHT.

Thus, while there is a big number of criteria for the onset of DHT present in literature, the majority of them: 1) were developed for different fluids; 2) do not contain explanation for what type of DHT they were developed; and 3) involve the effects of heat and mass fluxes only. Therefore, it is important to consider the effects of these parameters as well as those of pressure and diameter on heat transfer.

3.3. Experimental parameters influencing heat transfer

Discussion below assumes that only the mentioned experimental parameter is being changed, while the rest of the parameters are kept constant, unless stated otherwise.

3.3.1. Effect of heat flux

Bae et al. (2010) observed that as heat flux increased, generally, the HTC decreased at NHT. At DHT this observation did not hold true based on one out of six reported cases breaking this tendency. They also observed that at higher heat fluxes the DHT region broadened, transformed from a double-peaked to plateau-like, and moved towards the inlet of the test-section. In addition to this, from the figures presented in the paper by Bae et al. (2010) it appears that the maximal T_w did not move and occurred at the same bulk-fluid specific enthalpy. Bae et al. (2010) showed that beyond the pseudocritical region, experimental HTCs approached the values predicted by Dittus and Boelter (1930) correlation. They explained it by the radial density distribution approaching uniform one.

Cheng et al. (2007) discussed that generally DHT is observed to develop over a longer part of the flow at high fluxes. However, the DHT region contracts with the increase of the mass flux.

Swenson et al. (1965) observed a strong dependence of HTC on heat flux. Specifically, HTC had a sharp maximum near the pseudocritical temperature at low heat fluxes, and HTC was much lower and did not have a sharp peak at high heat fluxes.

Bishop et al. (1964) noticed that HTCs decreased with an increase in heat flux.

To summarize, as a rule, researchers point out that increasing heat flux leads to occurrence of DHT with gradual broadening of the part of the test section under the deteriorated regime. The counter effect is played by an increase in mass flux.

3.3.2. Effect of mass flux

Zahlan et al. (2013) reported that decreasing the mass flux from 2006 kg/m^{2}s to 496 kg/m^{2}s lead to an increase in T_w and appearance of a mild peak in T_w at G = 496 kg/m^{2}s. Increasing the heat flux from 50 kW/m^2 to 225 kW/m^2 eventually caused DHT with two peaks in T_w (at $q \geq 175$ kW/m^2 and G = 1000 kg/m^{2}s), the second one being much milder and broader.

Bae et al. (2010) observed that increasing mass flux consistently led to reduced wall temperatures.

Bishop et al. (1964) observed that increasing mass flow rate lead to an increase of HTC over the entire range of investigated bulk fluid temperatures.

3.3.3. Effect of pressure

Zahlan et al. (2013) reported that increasing the pressure caused the maximal T_w to decrease and move downstream. Presumably, they referred to the case with buoyancy-induced DHT. They explained the observed effect by the fact that the variations of the thermal properties become less steep at higher pressures.

Bae (2011) concluded that the effect of pressure was negligible in his experiments. However, Bae et al. (2010) observed a non-negligible decrease in HTC as the pressure increased. The effect was more prominent in the DHT region rather than in the NHT region.

Bishop et al. (1964) elaborated that in their experiments the effect of pressure on the HTC was the same as that on the Prandtl number. At temperatures below the pseudocritical

temperature the HTC decreased with increasing pressure and above the pseudocritical temperature the reverse was true.

Thus, the pressure effect is less investigated, and there is some inconsistency in the reported observed effects of pressure on heat transfer.

3.3.4. Effect of the inlet temperature

Bishop et al. (1964) reported that the effect of the inlet coolant temperature was inverse to that of pressure. They observed that under similar experimental conditions the lower the inlet temperature was the higher the HTCs appeared to be in the region of the pseudocritical temperature. The effect was observed in several runs but was not explained completely.

The effect of the inlet temperature is the least discussed effect in the literature.

3.3.5. Effect of the channel shape and flow direction

Bae (2011) compared the heat transfer results between a bare tube and an annular channel, which simulated a subchannel of a fuel assembly. The heat transfer rates in the annular channel were almost the same or slightly lower than those in a tube. The DHT occurred both in the upward and downward flow, however it was less severe in the case of the downward flow.

Kurganov et al. (2009) analyzed a large set of experimental data for downward and upward flow at the same heat loading conditions. They reported that no deterioration was observed in the case of downward flow, when compared to DHT cases of upward flow with the same heat loading values.

3.3.6. Effect of the tube diameter

Recently Yildiz and Groeneveld (2014) made a comprehensive literature review on heat transfer to different SCFs (water, CO_2, Freon R-22, and Freon R-12). Yildiz and Groeneveld (2014) concluded that, for all fluids HTCs, were higher in the tubes of smaller

diameter at NHT regime. However, there was no agreement on the diameter effect on HTC at DHT regime.

Bae et al. (2010) discussed that there was a less likelihood for the DHT to develop in smaller diameter tubes. However, if occurred, HTC was higher in the bigger diameter tube up to a certain bulk-fluid specific enthalpy. Their discussion of the diameter effect is questionable, however. First of all, when discussing the upward flow experiments they kept mentioning the 6.0 mm diameter tube, not the 6.32 mm. However, the 6.0 mm tube was used only in the downward flow experiments (IAEA, 2011), the section on the diameter effect was devoted to the upward flow. Secondly, they substantiated the discussion of the diameter effect by presenting several runs, including the following conditions: G = 400 kg/m^{2}s and q = 60 kW/m^2 for D = 9.0 mm, in Figure 8 (page 1302) of their paper. There was no such experimental run provided with the data from IAEA (2011). However, data from IAEA (2011) allowed comparing a case with a lower heat flux to assure that the general trend discussed by Bae et al. (2010) indeed existed.

Thus, mass and heat fluxes are the most important experimental parameters influencing heat transfer. Conventionally, data obtained in heat transfer experiments are generalized in the form of heat transfer correlations.

The next section is devoted to the discussion of existing heat transfer correlations for SC CO_2 and SCW.

3.4. Existing heat transfer correlations for SC CO_2 and SCW for forced convection

In 1910 it was Prandtl who was the first to propose to correlate experimental heat transfer data using the following dimensional groups (Petukhov, 1970):

$$\frac{HTC \cdot D}{k} = f_1\left(\frac{\rho u D}{\mu}\right) \cdot f_2\left(\frac{\mu c_p}{k}\right) \tag{3.15}$$

This became a conventional approach to correlate heat transfer data. The groups entering Eq. (3.15) are now called (from left to right) as Nusselt number (**Nu**), Reynolds number

(**Re**), and Prandtl number (**Pr**). **Nu** is usually interpreted as the dimensionless temperature gradient. **Re** is usually interpreted as the ratio of inertia forces to viscous forces. **Pr** is usually interpreted as the ratio of momentum and heat transport by diffusion in the velocity and thermal boundary layer (Incropera and DeWitt, 2002; Bergman et al., 2011).

The following correlation is the most frequently quoted (Incropera and DeWitt, 2002) for correlating single phase subcritical data within a wide range of experimental parameters:

$$\mathbf{Nu_b} = 0.023\mathbf{Re_b^{0.8}Pr_b^n}, \tag{3.16}$$

where $n = 0.4$ for heating $n = 0.3$ for cooling of the fluid. Although it is referred to as the Dittus and Boelter (1930) correlation, Winterton (1998) proved that they developed a different correlation from Eq. (3.16). He suggested that correlation Eq. (3.16) should be referred to as the Dittus and Boelter (1930) correlation as introduced by McAdams (1942). However, later in this thesis, correlation Eq. (3.16) will be referred to as the Dittus and Boelter (1930) correlation ($n = 0.4$ is assumed by default).

Correlation Eq. (3.16) is often used as a basis to analyze unexpected effects of heat transfer to SCF compared to heat transfer to subcritical fluids.

It should be emphasized that the correlation Eq. (3.16) was developed for constant property flow, and thus, cannot be applied for heat transfer predictions for SCFs. There were different attempts to improve such form of correlation. One of the best ideas was, probably originally proposed by Petukhov et al. (1961), to use the integral average specific heat $\left(\frac{h_w - h_b}{T_w - T_b}\right)$ instead of specific heat at either wall- or bulk-fluid temperature.

In general, the majority of the correlations for SCFs, which appeared after the 1950's can be categorized as one of the following:

1) Correlations using a fixed correction factor.
2) Correlations using a variable correction factor.
3) Correlations based on Prandtl's solution.

On the other hand, correlations can be categorized based on the temperature at which properties entering the correlation are calculated. Temperature chosen for this purpose is usually referred to as a characteristic temperature and can be either:

1) bulk-fluid temperature,
2) wall temperature, or
3) film temperature (average of the two previous).

3.4.1. Legacy correlations

Properties of fluids were updated several times after the 1930's. Temperature dependences of viscosity and thermal conductivity at SC pressures have undergone major revisions since the 1980's. It was only in the 1990's that the occurrence of a peak in the thermal conductivity of water near the pseudocritical temperature was recognized. Therefore, even if the experimental data were obtained with reasonable accuracy, the fitted powers in the terms entering legacy correlations would have been altered if used with newer properties. Thus, it should be expected that the legacy correlations would perform poorly when tested using modern thermal and transport properties of the fluids.

The most frequently quoted correlations are presented below.

As cited by Pioro and Duffey (2007), Bringer and Smith (1957) developed the following correlation for SCW and SC CO_2:

$$\mathbf{Nu_x} = const \cdot \mathbf{Re_x^{0.77} Pr_w^{0.55}} \tag{3.17}$$

where *const* = 0.0266 for water and 0.0375 for CO_2; *x* denotes the characteristic temperature for calculating non-dimensional groups, as follows: $T_x = T_b$ if $\frac{T_{pc} - T_b}{T_w - T_b} < 0$,

$T_x = T_{pc}$ if $0 \le \frac{T_{pc} - T_b}{T_w - T_b} \le 1.0$, and $T_x = T_w$ if $\frac{T_{pc} - T_b}{T_w - T_b} > 1.0$

Petukhov and Kirillov (1958) used the approach of Prandt to derive an analytical solution to a problem of heat transfer to a fluid flowing inside a pipe at turbulent conditions. After

fitting unknown constants to available experimental data they obtained the following equation:

$$\mathbf{Nu} = \frac{\frac{\xi}{8}\mathbf{Re_b}\,\mathbf{Pr_b}}{12.7\sqrt{\frac{\xi}{8}}\,(\mathbf{Pr_b}^{2/3}-1)+1.07}\,, \tag{3.18}$$

where the friction factor ξ can be calculated using the Filonenko (1954) equation (3.13).

Bishop et al. (1964) conducted experiments with SCW flowing upward inside tubes and annuli. Their data for HTC in tubes were generalized with a ±15% spread based on 2σ-level using the following correlation:

$$\mathbf{Nu_b} = 0.0069\mathbf{Re_b}^{0.9}\overline{\mathbf{Pr_b}}^{0.66}\left(\frac{\rho_w}{\rho_b}\right)^{0.43}\left(1+2.4\frac{D}{x}\right) \tag{3.19}$$

Correlation Eq. (3.19) is valid within the following range of experimental parameters: P = 22.8 – 27.6 MPa, T_b = 282 – 527 ºC, G = 651 – 3662 kg/m^{2}s, q = 310 – 3460 kW/m^2, and D = 2.54 and 5.08 mm.

Prior to coming up with expression Eq. (3.19), Bishop et al. (1964) tried several different forms of correlations based both on film and bulk-fluid temperatures with various combinations of thermal and transport properties. The computational resources did not allow them to correlate more than five groups and terms at once. Their final correlation was based on at least 400 points. While comparing their experimental data with the existing correlations, Bishop et al. (1964) mentioned several times that the differences in the prediction results could have been partially accounted for by the differences in thermal and transport properties used for correlations and those available to Bishop et al. (1964).

Swenson et al. (1965) generalized their experimental data on forced convective heat transfer to SCW using the following correlation:

$$\mathbf{Nu_w} = 0.00459\mathbf{Re_w}^{0.923}\overline{\mathbf{Pr_w}}^{0.613}\left(\frac{\rho_w}{\rho_b}\right)^{0.231} \tag{3.20}$$

Correlation Eq. (3.20) is valid within the following range of experimental parameters: P = 22.8 – 41.4 MPa, G = 542 – 2150 kg/m^{2}s, T_b = 75 – 576 ºC, T_w = 93 – 649 ºC, and D = 9.4 mm. Swenson et al. (1965) reported that their correlation was based on 2951 points and covered 72.5% of the data within one standard deviation. Additionally, their correlation predicted the CO_2 data with good accuracy.

Kransoshchekov and Protopopov (1966) have generalized available to them experimental data for SC CO_2 at P = 7.85 and 9.81 MPa in the following form:

$$\mathbf{Nu_b} = \mathbf{Nu_0}\left(\frac{\rho_w}{\rho_b}\right)^{0.3}\left(\frac{\overline{c_p}}{c_{p,b}}\right)^{n}, \tag{3.21}$$

where $\mathbf{Nu_0}$ is the Nusselt number calculated using Eq. (3.18); and n is a function of both T_b and T_w. Later, as cited by Pioro and Duffey (2007), Kransoshchekov et al. (1967) have explicitly formulated the expression for n as follows:

$$n = \begin{cases} 0.4 \text{ if } \dfrac{T_w}{T_{pc}} < 1 \text{ or } \dfrac{T_b}{T_{pc}} \geq 1.2 \\ n_1 = 0.22 + 0.18\dfrac{T_w}{T_{pc}} \text{ if } 1 \leq \dfrac{T_w}{T_{pc}} < 2.5 \\ n_1 + 5\left(n_1 - 2\right)\left(1 - \dfrac{T_b}{T_{pc}}\right) \text{ if } 1 \leq \dfrac{T_b}{T_{pc}} < 1.2 \end{cases} \tag{3.22}$$

Correlation Eq. (3.21) is valid within the following range of experimental parameters: $8\cdot10^4 < \mathbf{Re_b} < 5\cdot10^5$; $0.85 < \mathbf{Pr_b} < 65$; $0.09 < \dfrac{\rho_w}{\rho_b} < 1.0$; $0.02 < \dfrac{\overline{c_p}}{c_{p,b}} < 4$; $0.9 < \dfrac{T_w}{T_{pc}} < 2.5$; $46 < q < 2600$ kW/m^2; and $x / D \geq 15$. Krasnoshchekov and Protopopov (1966) reported that their correlation performed well when tested against data for SCW.

Yamagata et al. (1972) developed a correlation based predominantly on the data for upward flow in a bare tube of D = 10 mm, excluding the data within the DHT region. Yamagata

et al. (1972) used the Eckert number (defined below in Eq. (3.23)) to classify data into three different domains.

$$\mathbf{E} = \frac{T_{pc} - T_b}{T_w - T_b} \tag{3.23}$$

They obtained the following correlation:

$$\mathbf{Nu_b} = 0.0135\mathbf{Re_b^{0.85}Pr_b^{0.8}}F\,, \tag{3.24}$$

where

$$\begin{aligned} &F = 1.0 \text{ for } \mathbf{E} > 1 \\ &F = 0.67\mathbf{Pr}_{pc}^{-0.05}\left(\frac{\overline{c_p}}{c_{p,b}}\right)^{n_1} \text{ for } 0 \le \mathbf{E} \le 1; \quad n_1 = -0.77\left(1 + \frac{1}{\mathbf{Pr}_{pc}}\right) + 1.49 \\ &F = \left(\frac{\overline{c_p}}{c_{p,b}}\right)^{n_2} \text{ for } \mathbf{E} < 0; \quad n_2 = 1.44\left(1 + \frac{1}{\mathbf{Pr}_{pc}}\right) - 0.53 \end{aligned} \tag{3.25}$$

The correlation Eq. (3.24) fitted their data within a ±20% band. Although not clearly stated in the results, it appears that this correlation is valid within the following experimental conditions (horizontal, upward and downward flows): P = 22.6 – 29.4 MPa, T_b = 230 – 540 °C, G = 310 – 1830 kg/m^{2}s, q = 116 – 930 kW/m^2, and D = 7.5 mm and 10 mm, excluding the DHT region.

Gnielinski (1976) modified and improved the correlation developed by Petukhov and Kirillov (1958) Eq. (3.18) for SC CO_2 as follows:

$$\mathbf{Nu_b} = \frac{\frac{\xi}{8}\left(\mathbf{Re_b} - 1000\right)\mathbf{Pr_b}}{1 + 12.7\sqrt{\frac{\xi}{8}}\left(\mathbf{Pr_b}^{2/3} - 1\right)}\,, \tag{3.26}$$

where the friction factor ξ can be determined from an appropriate relation, such as the Filonenko (1954) equation (3.13).

The Gnielinski correlation, Eq. (3.26), is valid within the following range of experimental conditions: $0.5 \le \mathbf{Pr_b} \le 2000$ and $3 \cdot 10^3 < \mathbf{Re_b} < 5 \cdot 10^6$.

Jackson and Hall (1979a) performed an extensive review of the existing correlations. They tested them against predicted **Nu** using experimental data for q, G, $T_{b,}$ and T_w, and explicitly mentioned that a different result would be expected if instead of T_w only heat flux q was used. They discovered that the correlation by Kransoshchekov and Protopopov (1966) was the most effective. Therefore, Jackson and Hall (1979a) have used it as a basis for their own correlation, where instead of the $\mathbf{Nu_0}$ defined in Eq. (3.18) they used a simpler Dittus and Boelter (1930) form, as follows:

$$\mathbf{Nu_b} = 0.0183 \mathbf{Re_b^{0.82}} \mathbf{Pr_b^{0.5}} \left(\frac{\rho_w}{\rho_b} \right)^{0.3} \left(\frac{\overline{c_p}}{c_{p,b}} \right)^n , \tag{3.27}$$

where n is equal to:

$$n = \begin{cases} 0.4 \text{ if } \dfrac{T_w}{T_{pc}} < 1 \text{ or } \dfrac{T_b}{T_{pc}} \ge 1.2 \\ 0.4 + 0.2 \left(\dfrac{T_w}{T_{pc}} - 1 \right) \text{ if } \dfrac{T_b}{T_{pc}} < 1 \text{ and } \dfrac{T_w}{T_{pc}} > 1 \\ 0.4 + 0.2 \left(\dfrac{T_w}{T_{pc}} - 1 \right) \left[1 - 5 \left(\dfrac{T_b}{T_{pc}} - 1 \right) \right] \text{ if } \dfrac{T_b}{T_{pc}} > 1.2 \end{cases} \tag{3.28}$$

This expression only looks different from expression Eq. (3.22), although it appears to be based on exactly the same data presented by Krasnoshchekov and Protopopov (1966). The reason for apparent dissimilarity of expressions (3.22) and (3.28) is because they were derived from a graph, which Krasnoshchekov and Protopopov (1966) provided to relate T_b / T_{pc}, T_w / T_{pc}, and n.

Jackson and Hall (1979a) proposed the following modified and simplified version of the correlation Eq. (3.27):

$$\mathbf{Nu_b} = 0.0183\mathbf{Re_b^{0.82}}\overline{\mathbf{Pr}}_\mathbf{b}^{\mathbf{0.5}}\left(\frac{\rho_w}{\rho_b}\right)^{0.3} \tag{3.29}$$

They claimed that this correlation performed well against SCW and SC CO_2. This correlation is often referred to as the Jackson and Fewster (1975) correlation (e.g., see the book by Pioro and Duffey, 2007) and , however, the original reference was not found. The ranges of applicability were not shown neither for the correlation Eq. (3.27) nor for the correlation Eq. (3.29), in the paper by Jackson and Hall (1979a).

Watts and Chou (1982) developed the following correlation for the mixed-convective flow of SCW:

$$\mathbf{Nu_b} = 0.021\mathbf{Re_b^{0.8}}\overline{\mathbf{Pr}}_\mathbf{b}^{\mathbf{0.55}}\left(\frac{\rho_w}{\rho_b}\right)^{0.35} f\left(\mathbf{Bu}^*\right) \tag{3.30}$$

where $f\left(\mathbf{Bu}^*\right) = \begin{cases} \left(1.27 - 19{,}500\mathbf{Bu}^*\right)^{0.7} \text{ if } \mathbf{Bu}^* \le 4.5\cdot 10^{-5} \\ \left(2600\mathbf{Bu}^*\right)^{0.305} \text{ if } \mathbf{Bu}^* > 4.5\cdot 10^{-5} \end{cases}$ for minimum in **Nu**

$\begin{cases} \left(1 - 3000\mathbf{Bu}^*\right)^{0.295} \text{ if } \mathbf{Bu}^* \le 1.0\cdot 10^{-4} \\ \left(7000\mathbf{Bu}^*\right)^{0.295} \text{ if } \mathbf{Bu}^* > 1.0\cdot 10^{-4} \end{cases}$ normal heat transfer , (3.31)

where

$$\mathbf{Bu}^* = \frac{\overline{\mathbf{Gr}}_\mathbf{b}}{\mathbf{Re_b^{2.7}}\overline{\mathbf{Pr}}_\mathbf{b}^{\mathbf{0.5}}} \tag{3.32}$$

is the modified parameter from relation Eq. (3.4).

The correlations Eq. (3.30) by Watts and Chou (1982) is valid within the following range of experimental parameters: P = 25.0 MPa, T_b = 150 – 310 °C, G = 106 – 1060 kg/m^{2}s, q = 175 – 440 kW/m^2, and D = 25 and 32.2 mm. There is ambiguity in choosing the expression for $f\left(\mathbf{Bu}^*\right)$ because of the overlapping regions for $\mathbf{Bu}^*$. Indeed, Watts and Chou (1982) did not propose a way to predict an onset in DHT to make it clear how to use

the part of their correlation for calculating a minimum in **Nu**. Nevertheless, this correlation attracted attention because it was one of the earliest attempts to predict heat transfer at mixed-convection.

Griem (1996) proposed a new calculation procedure and the following correlation for the flow of near critical and supercritical water:

$$\mathbf{Nu_b} = 0.0169\mathbf{Re_b^{0.8356}Pr_b^{0.432}}F\,, \tag{3.33}$$

where 1) c_p in **Pr** should be evaluated at 5 different temperatures (in equal increments from the bulk-fluid- to the wall temperatures), its two highest values should be dropped (since they do not appear on the average in the turbulent flow), and the average of the remaining three should be used for the correlation; 2) the average value of thermal conductivity between the values at bulk-fluid- and wall-temperatures should be used; and 3) the correction factor F for **Nu** depends on the different values of bulk fluid enthalpy as follows:

$$F = \begin{cases} 0.82 \text{ if } h_b < 1540 \text{ kJ/kg} \\ 9\cdot 10^{-4} h_b - 0.566 \text{ if } 1540 \text{ kJ/kg} \le h_b \le 1740 \text{ kJ/kg} \\ 1.0 \text{ if } h_b > 1740 \text{ kJ/kg} \end{cases} \tag{3.34}$$

The correlation Eq. (3.33) by Griem (1996) is valid within the following range of experimental parameters: P = 22.0 – 27.0 MPa, G = 300 – 2500 kg/m^{2}s, q = 200 – 700 kW/m^2, D = 10, 14, and 20 mm. Griem (1996) observed no pseudo boiling crisis at near critical pressures.

The plot of the 1967 data for SCW presented in the paper by Griem (1996) shows that the old values of thermal properties are significantly inconsistent with those currently accepted. Moreover, Griem (1996) noticed that his correlation was prone to instability. Numerical instability of correlations is discussed in Appendix E.

The reason to include his correlation into the list of the legacy correlation is that Griem (1996) used the properties of water formulated in 1967 (Schmidt, 1969).

3.4.2. Most recent correlations

Gupta et al. (2011) proposed the following correlation for the upward flow of SCW:

$$\mathbf{Nu_w} = 0.0033\mathbf{Re_w^{0.941}}\overline{\mathbf{Pr_w}}^{\mathbf{0.764}}\left(\frac{\mu_w}{\mu_b}\right)^{0.398}\left(\frac{\rho_w}{\rho_b}\right)^{0.156} \tag{3.35}$$

Correlation Eq. (3.35) is valid within the following range of experimental parameters: P = 24 – 25 MPa, inlet T_b = 320 – 350 °C, G = 200 – 1500 kg/m^{2}s, q = 70 – 1250 kW/m^2, and D = 10 mm. They reported that their correlation is for the NHT regime only. DHT points, outliers, and the readings of the first and the last TC's along the test-section were removed. Their correlation was based on approximately 6336 points. The correlation predicted the majority of the HTC data within a ±25% error band.

Earlier, Mokry et al. (2009) proposed a correlation based on the same experimental data as the correlation by Gupta et al. (2011), however using a bulk-fluid temperature approach. Mokry et al. (2009) came up with the following correlation:

$$\mathbf{Nu_b} = 0.0061\,\mathbf{Re_b^{0.904}}\,\overline{\mathbf{Pr_b}}^{0.684}\left(\frac{\rho_w}{\rho_b}\right)^{0.564} \tag{3.36}$$

Correlation Eq. (3.36) predicted the majority of the original HTC data within a ±25% error band. Morky et al. (2009) reported that, when tested against an extended set of data for SCW, their correlation performed well (apparently, the authors meant that the fit was within the same error band). Thus, in a later publication, Mokry et al. (2011b) have specified the following range of experimental parameters within which their correlation was considered to be valid: P = 22.8 – 29.4 MPa, G = 200 – 1500 kg/m^{2}s, q = 70 – 1250 kW/m^2, and D = 3 – 38 mm.

Cheng et al. (2009) proposed the following correlation based on the Herkenrath et al. (1967) data for the upward of SCW:

$$\mathbf{Nu_b} = 0.023\mathbf{Re_b^{0.8}}\mathbf{Pr_b^{1/3}}F\,, \tag{3.37}$$

where

$$
\begin{aligned}
&F = \min\left(F_1, F_2\right): \\
&F_1 = 0.85 + 0.776\left(\boldsymbol{\pi}_{\mathbf{A}} \cdot 10^3\right)^{2.4}; \\
&F_2 = \frac{0.48}{\left(\boldsymbol{\pi}_{\mathbf{A,pc}} \cdot 10^3\right)^{1.55}} + 1.21 \cdot \left(1 - \frac{\boldsymbol{\pi}_{\mathbf{A}}}{\boldsymbol{\pi}_{\mathbf{A,pc}}}\right),
\end{aligned}
\tag{3.38}
$$

where the acceleration number is defined as:

$$
\boldsymbol{\pi}_{\mathbf{A}} = \frac{\beta}{c_{p,b}} \frac{q}{G} \tag{3.39}
$$

Cheng et al. (2009) came up with the correlation (3.37) by investigating a possibility of having a simple correlation containing as few parameters as possible and having no explicit dependence on wall temperature. They also intended the correlation to describe both NHT and DHT. Their approach was to correlate the correction factor F against the ratio of experimental Nusselt number and Nusselt number calculated using Dittus and Boelter (1930) correlation. However, they used 1/3 as the power of the Prandtl, not 0.4 as in the Dittus and Boelter (1930) correlation. Cheng et al. (2009) discussed that the most promising parameter to correlate the ratio of Nusselt numbers against would be the acceleration number defined above in Eq. (3.39).

Additionally to the uncertainties in experimental parameters published by Herkenrath et al. (1967), Cheng et al. (2009) calculated the uncertainties in HTCs and dimensionless parameters. They found that only 9% of the digitized test data had uncertainty in HTC less than 10%, and about 43% of the data had uncertainty greater than 20%. The summary of their findings are in Table 3.1.

Table 3.1. Uncertainties of heat transfer coefficients obtained by digitizing data by Herkenrath et al. (1967) (Adapted from Cheng et al., 2009).

Uncertainty range	**≤10%**	**10 – 20%**	**≥20%**
No. of data points (in total: 4599)	419	2186	1995
Percentage	9.1	47.5	43.4

Cheng et al. (2009) used only those HTC data which had uncertainty less than 20%. Additionally, they included only the data which had less than 20% uncertainty in Reynolds number, less than 50% uncertainty in Prandtl number, less than 20% uncertainty in acceleration parameter, and less than 30% uncertainty in Nusselt number. They also excluded test data with length to diameter ratios less than 50 to avoid entrance effect. This filtering process left 2152 data points (out of 4599 original) for the correlation. Cheng et al. (2009) emphasized that an extensive uncertainty analysis is required for the selection of the test data and dimensionless numbers to be used in the development of a heat transfer correlation.

Researchers at KAERI proposed several correlations for the flow of SC CO_2 in vertical bare tubes. Only those developed for the upward flow are presented here.

Bae and Kim (2009) reported experimental results for the following three geometries of the KAERI SPHINX facility: tubes of 4.4 mm ID, 9.0 mm ID, and an annular channel between an 8 mm OD heater rod and a 10 mm ID tube. The experimental results covered both forced and mixed convection, with buoyancy-induced DHT occurring in some of their runs. They estimated a 40% uncertainty (presumably in HTC) for heat fluxes below 20 kW/m^2 and $T_w - T_b$ of about 5 °C.

Bae and Kim (2009) generalized their data by multiplying **Nu** obtained from the correlation by Krasnoshchekov and Protopopov (1966) Eq. (3.21) by correction factors depending on the simplified buoyancy parameter defined in Eq. (3.4). The correction factors were defined as follows:

$$F = \begin{cases} \left(1 + 1.0 \cdot 10^{8} \mathbf{Bu}\right)^{-0.032} \text{ for } 5.0 \cdot 10^{-8} < \mathbf{Bu} < 7.0 \cdot 10^{-7} \\ 0.0185 \cdot \mathbf{Bu}^{-0.4365} \text{ for } 7.0 \cdot 10^{-7} < \mathbf{Bu} < 1.0 \cdot 10^{-6} \\ 0.75 \text{ for } 1.0 \cdot 10^{-6} < \mathbf{Bu} < 1.0 \cdot 10^{-5} \\ 0.0119 \cdot \mathbf{Bu}^{-0.36} \text{ for } 1.0 \cdot 10^{-5} < \mathbf{Bu} < 3.0 \cdot 10^{-5} \\ 32.4 \cdot \mathbf{Bu}^{0.40} \text{ for } 3.0 \cdot 10^{-5} < \mathbf{Bu} < 1.0 \cdot 10^{-4} \end{cases} \tag{3.40}$$

Their correlation predicted 86.0% data for $400 < G < 1200$ kg/m^{2}s within ±30% range. The maximal deviations were not provided. Based on the 20.8% standard deviation of $\mathbf{Nu_{calc}}/\mathbf{Nu_{exp}}$ provided in their paper, the RMS of their correlation is 45.6%. Additionally they reported that 93.3% (97.2%) of the data were within 40% (50%) error bound. Bae and Kim (2009) inferred that the ability to predict the onset of DHT was one of the strongest features of their proposed correlation. They suggested regarding their correlation as the first step in formulating a universal correlation applicable for both NHT and DHT.

Bae et al. (2010) generalized their data for upward flow of SC CO_2 in tube of 6.32 mm ID by multiplying **Nu** obtained from the correlation by Krasnoshchekov and Protopopov (1966) Eq. (3.21) by a correction factor. The correction factor, F, has the following dependency on the parameter defined in the paper by Jackson and Hall (1979a) (see Eq. (3.4)):

$$F = \begin{cases} \left.\begin{array}{l} 1.0 \text{ for } \dfrac{\overline{\mathbf{Gr_b}}}{\mathbf{Re_b^{2.7}}} < 2\cdot 10^{-7} \\ 0.043\left(\dfrac{\overline{\mathbf{Gr_b}}}{\mathbf{Re_b^{2.7}}}\right)^{-0.2} \text{ for } 2\cdot 10^{-7} < \dfrac{\overline{\mathbf{Gr_b}}}{\mathbf{Re_b^{2.7}}} < 6\cdot 10^{-6} \\ 1120\left(\dfrac{\overline{\mathbf{Gr_b}}}{\mathbf{Re_b^{2.7}}}\right)^{0.64} \text{ for } 6\cdot 10^{-6} < \dfrac{\overline{\mathbf{Gr_b}}}{\mathbf{Re_b^{2.7}}} < 1.5\cdot 10^{-5} \\ 3.6\cdot 10^{-8}\left(\dfrac{\overline{\mathbf{Gr_b}}}{\mathbf{Re_b^{2.7}}}\right)^{-1.53} \text{ for } 1.5\cdot 10^{-5} < \dfrac{\overline{\mathbf{Gr_b}}}{\mathbf{Re_b^{2.7}}} < 4\cdot 10^{-5} \\ 200\mathbf{Bu}^{0.68} \text{ for } 4\cdot 10^{-5} < \mathbf{Bu} < 2\cdot 10^{-4} \end{array}\right\} \text{deteriorated heat transfer} \\ \left.\begin{array}{l} \left(1+3\cdot 10^{5}\dfrac{\overline{\mathbf{Gr_b}}}{\mathbf{Re_b^{2.7}}}\right)^{0.35} \text{ for } \dfrac{\overline{\mathbf{Gr_b}}}{\mathbf{Re_b^{2.7}}} < 2\cdot 10^{-6} \\ 0.48\left(\dfrac{\overline{\mathbf{Gr_b}}}{\mathbf{Re_b^{2.7}}}\right)^{-0.07} \text{ for } \dfrac{\overline{\mathbf{Gr_b}}}{\mathbf{Re_b^{2.7}}} > 2\cdot 10^{-6} \end{array}\right\} \text{normal heat transfer} \end{cases} \tag{3.41}$$

The RMS of their correlation is 52.3%[6] (46.6% for NHT and 57.3% for DHT). Its overall performance was prediction of 78.7% data within the ±30% error range.

Bae (2011) reported the experimental results for the tests with the upward flow of SC CO_2 through a 4.57 mm ID bare tube. He estimated that the uncertainties in HTC were between 7.7 – 12.6 %. However, these estimations were made assuming average difference of 21.8 °C for $T_w - T_b$ and maximal difference of 34.7 °C (for the highest achieved wall temperature, T_w, of 190 °C). Such choice of values appears to significantly underestimate the HTC error, because the difference in temperatures can actually be as low as few degrees. This can be clearly seen from Fig. 3 of the paper by Bae (2011) or from their numerical experimental data (IAEA, 2011).

Bae (2011) proposed to correlate data for upward flow using the correlation by Watts and Chou (1982) Eq. (3.30) multiplied by a correction factor. His final correlation has the following form:

$$\mathbf{Nu_b} = 0.021\,\mathbf{Re_b}^{0.8}\overline{\mathbf{Pr}}_{\mathbf{b}}^{0.55}\left(\frac{\rho_w}{\rho_b}\right)^{0.35} F\,, \tag{3.42}$$

where the correction factor F is based on the parameter defined in Eq.(3.4).

$$F = \begin{cases} \left(1 - 8000\,\dfrac{\overline{\mathbf{Gr_b}}}{\mathbf{Re_b}^{2.7}}\right)^{0.5} & \text{for} \quad \dfrac{\overline{\mathbf{Gr_b}}}{\mathbf{Re_b}^{2.7}} < 1.0\cdot 10^{-4} \\ f = 15\left(\dfrac{\overline{\mathbf{Gr_b}}}{\mathbf{Re_b}^{2.7}}\right)^{0.38} & \text{for} \quad \dfrac{\overline{\mathbf{Gr_b}}}{\mathbf{Re_b}^{2.7}} > 1.0\cdot 10^{-4} \end{cases} \tag{3.43}$$

This correlation predicted 74.5% (86.5%) data for $G < 200$ kg/m^{2}s ($G > 400$ kg/m^{2}s) within ±30% range. The maximal deviations were not provided. Bae (2011) reported very odd cases with the experimental data increasing and decreasing several times at fixed estimated **Nu**. Bae (2011) made a major conclusion that it is very difficult to formulate a single correlation in the region of high buoyancy influence. This conclusion was based on the

[6] This value of RMS was calculate based on the value for standard deviation (27.4%) that was provided in the paper by Bae et al. (2010) for combined normal and deteriorated data

failure of his correlation against experimental buoyancy-induced DHT data by Shitsman (1963), although he expected his correlation, which included buoyancy regime, to perform well.

3.5. Assessment of correlations

Gu et al. (2013) compared the correlations by Dittus and Boelter (1930), Krasnoshchekov and Protopopov (1966), Watts and Chou (1982), Cheng et al. (2009), and Jackson and Hall (1979a) (Eq. (3.27)) against the experimental data on forced-convective heat transfer to SCW flowing upward through a 7.6 mm ID bare tube obtained at Supercritical Water Multipurpose test facility in Shanghai Jiao Taong University. Gu et al. (2013) concluded that the deviations between the predictions of the existing correlations were large, especially at the high heat fluxes. They interpreted it as the validity of the correlations being limited to experimental data they were obtained from.

Bae (2011) showed that the previous correlations (by Bishop et al., 1964; Jackson and Hall, 1979a Eq. (3.27); Watts and Chou, 1982; and Dittus and Boelter, 1930) significantly over predicted the experimental data within the DHT regime. When the mass flux was increased further to 1000 kg/m^2s, all the correlations, except those by Bishop et al. (1964) and Dittus and Boelter (1930), performed well.

Bae et al. (2010) used their data to test their correlation (Eq. (3.21) with correction factors defined by Eq. (3.41)), as well as those by Bishop et al. (1964), Jackson and Hall (1979a) (Eq. (3.27)), Watts and Chou (1982), and Jackson and Hall (1979a) (Eq. (3.29)). They concluded that all the four latter correlation were able to predict less than 70% of all data within ±30% error range. Among those correlations, Bishop et al. (1964) correlation was the most accurate by predicting 66.9% of the experimental data within the ±30% error range. However, Bae et al. (2010) clarified that only their proposed correlation and the Watts and Chou (1982) correlation were tested again the DHT data. The remaining correlations were tested only against NHT data.

Cheng et al. (2009) compared their correlation Eq. (3.37) , as well as correlations by Bishop et al. (1964), Swenson et al. (1965), Krasnoshchekov and Protopopov (1966), Yamagata et

al. (1972), Jackson and Hall (1979a) Eq. (3.27), and Griem (1996) against a wide range of data. The new correlation by Cheng et al. (2009) had the lowest bias in the predicted HTC; however, the lowest RMS was achieved by Bishop et al. (1964) and Swenson et al. (1965).

A comparison done by Mokry et al. (2009) showed that the Dittus and Boelter correlation (1930) significantly overestimated experimental HTC values within the pseudocritical range. The Bishop et al. (1964) and Jackson and Hall (1979a) (1.25) correlations also tended to deviate significantly from the experimental data within the pseudocritical range. The Swenson et al. (1965) correlation provided a better fit, within some flow conditions, for the experimental data than the latter three correlations; however it did not follow up closely the experimental data within other flow conditions (Mokry et al., 2009).

The most extensive assessment of the correlations was performed by Zahlan et al. (2011). After removing unreliable and duplicate data they compiled an SCW databank at the University of Ottawa containing 24,000 data points. Zahlan et al. (2011) tested 12 correlations for SCFs and four single-phase correlations. With the exception of the correlations proposed by Bringer and Smith (1957), Petukhov and Kirillov (1958), and those by KAERI researchers, the rest of the correlations reviewed above were covered in the tests by Zahlan et al. (2011). They split the experimental regions into three: liquid-like, close to pseudocritical point, and gas-like. Based on the minimal for all three regions RMS for the relative deviation of calculated HTC from the experimental HTC, they ranked the correlation by Mokry et al. (2009) the first, the one by Gupta et al. (2011) the second, and the one by Swenson et al. (1965) the third.

3.6. Recent CFD results in modelling DHT

Numerous recent worldwide CFD studies showed that current models are able to capture temperature trends at normal conditions and predict the onset of deterioration; however these models fail to capture DHT numerically (Sharabi et al. 2007 and 2009; Gu et al., 2009; Shams et al., 2011; Jaromin and Anglart, 2011). It should be noted that in the majority of the reviewed papers, CFD results were validated based on the old data by Yamagata et al. (1972), Ornatiskiy et al. (1971), and Shitsman (1963).

Further discussion is mainly devoted to the most recent or the most often cited results of CFD modelling of DHT, in chronological order.

Koshizuka et al. (1995) conducted quite a successful CFD modelling (based on a k-ε model by Jones-Launder) of Yamagata et al. (1972) experimental data that correspond to the NHT and IHT. They used an arbitrary definition of the deterioration as:

$$\frac{HTC_{CFD}}{HTC_{Dittus-Boelter}} < 0.3 \tag{3.44}$$

Gu et al. (2009) used different CFD models to predict deterioration in the case of Ornatskiy et al. (1971) and showed that drop in thermal conductivity was the main dominant contributor to DHT.

Kao et al. (2010) were able to predict qualitatively DHT in the experiments by Shitsman (1963). They had such discrepancy between their predicted values and the experimental values that appeared as if the specific enthalpy axis for the experimental data was shifted.

A recent sensitivity analysis of various thermal parameters on the onset of DHT was conducted by Jaromin and Anglart (2011) using CFD. Using data from an experiment by Shitsman (1963) (the experimental run cited from the paper by Shitsman, 1963 was at G = 430 kg/m^{2}s and q = 319.87 kW/m^2, thus q/G = 0.74 kJ/kg) they showed that their CFD model had low sensitivity to variation of system pressure, medium sensitivity to variation in inlet temperature, and high sensitivity to variation to changes in heat and mass fluxes. They determined that in the case of low mass fluxes, buoyancy was the dominant cause of DHT. However, in the case of high mass fluxes (an experimental run by Ornatskiy et al., 1971; G = 1500 kg/m^{2}s and q = 1810 kW/m^2, thus q/G = 1.21 kJ/kg), their model showed insignificant sensitivity to variation in the system pressure and temperature, and only medium sensitivity to changes of mass and heat fluxes.

Kiss and Aszodi (2013) used the Shear Stress Transport (SST) eddy viscosity turbulence model with enhanced wall treatment and adopted the Best Practice Guidelines (refer to Menter et al., 2002 for details) to model mixed-convection DHT case in the experiment C008 by Shitsman (1963) and forced convection DHT case in the experiment C359 by

Ornatskiy et al. (1971). They calculated the temperature distributions at the conditions of the C008 experiment (Shitsman, 1963) and suggested that the huge radial temperature gradient in the vicinity of the temperature peak of the wall-temperature serves as a negative feedback mechanism to recover heat transfer. However, there was another peak in the C008 experiment by Shitsman (1963), which Kiss and Aszodi (2013) did not comment on at all. Kiss and Aszodi (2013) claimed that they managed to obtain qualitatively right distributions of the wall-temperature and HTC. However, they achieved this by doing sensitivity analysis of the inlet experimental conditions.

The general numerical discrepancy of their results appears as a shift of the modelled values compared to the experimental with respect to the specific bulk-fluid enthalpy axis. This is similar to the discrepancy Kao et al. (2010) obtained for the same modelled experiment. Such reproduction of discrepancies may indicate that either: 1) the CFD modelling has an inherent deficiency; or 2) this is an effect of plotting the results obtained at the currently accepted thermal and transport properties against the old version of those, or 3) there is something wrong with the Shitsman (1963) data. If the latter is the case, then it may be either due to incorrectly reported experimental conditions in the original paper or an error introduced in the process of digitizing data.

Kiss and Aszodi (2013) concluded that calculated values of wall-temperature and HTC are very sensitive to small changes of the global flow parameters (inlet temperature, heat flux, mass flux, nominal pressure, and specific enthalpy). It is apparent from their figures that even minor discrepancies between the calculated and published values of bulk-fluid specific enthalpy cause noticeable shifts in the positions of calculated wall-temperature peaks.

Jaromin and Anglart (2013) studied the sensitivity of CFD results on the formulation of the turbulent Prandtl number. They validated the results against five different experimental runs with DHT (Shitsman, 1963; Ornatskiy et al., 1971; Pis'menny et al., 2006; Glushchenko, in *Supercritical water experiments database*, 2008; and Vikhrev, in *Supercritical water experiments database*, 2008) and one experimental run with NHT (Ackerman, in *Supercritical water experiments database*, 2008). They found good

numerical agreement between the calculations and experiments for each of the experiments, however, at different values of the turbulent Prandtl number. They did not discuss the possible reasons for such discrepancy from the point of view of physics. Therefore, it may be concluded that there is no consistency on how to choose a fixed set from all the possible numerical options in CFD calculations to obtain the results matching different experiments. However, Jaromin and Anglart (2013) concluded that the best-fit values for the turbulent Prandtl number (for the experimental cases were DHT occurs) were proportional to **Re** and inversely proportional to **Pr** at the inlet. There is still an inconsistency in the discussion of the results of their modelling: Jaromin and Anglart (2013) obtained an increase in the turbulent kinetic energy in the DHT region when modelling an experiment by Ornatskiy et al. (1971), and a significant reduction in the turbulent kinetic energy in the DHT region when modelling an experiment by Glushchenko (in *Supercritical water database*, 2008). However, they found an explanation (which was missing in the paper by Kiss and Aszodi, 2013) for the occurrence of the second DHT peak in the C008 experiment by Shitsman (1963), as follows: it is the reduction in the turbulence kinetic energy after the recovery from the first DHT region, which leads to impairment of heat transfer and caused the second DHT region.

Wang et al. (2013) performed CFD modelling of the data by Yamagata et al. (1972). They chose re-normalization groups k-ε turbulence model with enhanced wall treatment for turbulence simulation. After choosing an appropriate value for non-dimensional wall coordinate y^+, they were able to make an "outstanding prediction of heat transfer enhancement and heat transfer deterioration" (Wang et al., 2013). While the first part of their statement is justified by the presented data on the graphs, the last part related to DHT may be misleading. It appears that they related their conclusions to the decrease in the values of HTC after the huge enhancement around the T_{pc}. However, this is not what was regarded by DHT in the work by Yamagata et al. (1972). The apparent deterioration that Wang et al. (2013) referred to was merely due to the rapid decrease of specific heat past the pseudocritical point.

Ose et al. (2013) presented the results of their modelling of upward and downward flow of SCW. For modelling the flow, they used their in-house CFD code (Advanced Code for

Evaluation of 3-Dimensional Two-Phase Flow) with standard k-ε and Launder-Sharma turbulence models. They simulated a heat transfer experiment proposed as an IAEA benchmark exercise (Churkin et al., 2011). Ose et al. (2013) claimed that the Launder-Sharma model predicted the DHT for the upward flow well. While the graph that they presented shows that the qualitative prediction is right, the results appears to be shifted quantitatively along the heat tube, which is similar to the problem that Kao et al. (2010) and Kiss and Aszodi (2013) encountered. This means that either their CFD model was not able to properly capture physics of the process, or the experimental data they used contained systematic errors.

Ambrosini et al. (2013) studied the capabilities of several low-Reynolds number CFD models to predict heat transfer to SCW and SC CO_2. They verified the models based on the experimental data of Kim and Kim (2011), Jackson (2009), Ornatskiy et al. (1971), and Pis'menny et al. (2005). They concluded that k-ε low Reynolds number model available in STAR-CCM+ code predicted the deterioration well when T_b was below T_{pc}; however it consistently over predicted T_w when T_b approached or exceeded T_{pc}. The SST k-ω model was unable to predict buoyancy-induced DHT, with the exception of modelling data of Ornatskiy et al. (1971). All the models predicted SC CO_2 data much worse than SCW data. Ambrosini et al. (2013) suggested that this could be due to the lower subcooling of the SC CO_2 data with respect to T_{pc} at the inlet to the test-section.

Xiong et al. (2013) tested the combination of k-ε-ζ-f turbulence model and general gradient diffusion hypothesis, simple gradient diffusion hypothesis, algebraic flux model, and elliptic blending algebraic flux model against the direct simulation data by Bae et al. (2005). The general conclusion was that all the models were deficient in calculation of heat transfer to SCF. Even the simple gradient diffusion hypothesis model, which was the best in prediction of radial turbulent heat flux, appeared to be completely incapable of modelling streamwise heat flux which determines the onset of DHT and recovery from it (Xiong et al., 2013).

Li et al. (2013) tested capabilities of ANSYS CFX CFD code against one experimental run of Yamagata et al. (1972) and one experimental run of Pis'menny et al. (2006). Li eat al.

(2013) chose these runs so that one of them would correspond to NHT (the run of Yamagata et al., 1972), and another would correspond to the buoyancy-induced DHT (the run of Pis'menny et al., 2006). Li et al. (2013) tested 12 different turbulence models. For the case of the run with DHT, the lowest among all models RMS of predicted wall temperature was 11%, which is quite high.

Farah et al. (2013) tested capabilities of FLUENT-12 CFD code against experimental data of Kirillov obtained at IPPE (in 2005) on heat transfer to SCW flowing vertically upward. It seems that Farah et al. (2013) had access to the original data and did not have to digitize any from the graphs. This means that their error analysis was free from any bias associated with transformation of data. Farah et al. (2013) mentioned that they had to go through many options available for the Realisable k-ε and SST k-ω turbulence models to find those that would provide the best fit. Both models predicted NHT data adequately. However, SST model showed a better fit for DHT with maximal deviations of ±10% for temperature and ±40% for HTC. Both models tended to overestimate wall temperature.

3.7. Scaling heat transfer data

In general, heat transfer data can be scaled using either of the two following approaches:

1) Directly, by applying a correlation developed for one fluid to the experimental conditions of the other fluid.
2) Indirectly, by scaling experimental conditions to another fluid, for which a correlation is established; running a correlation and comparing it with the scaled data.

Scaling factors are usually obtained from the basic governing equations (continuity, momentum, and energy) written in the non-dimensional form. The most frequently encountered scaling laws are those for geometry, pressure, and temperature as follows (from fluid A to fluid B):

$$D_A = D_B \text{ (geometric similarity)} \tag{3.45}$$

$$\left(\frac{P}{P_{cr}}\right)_A = \left(\frac{P}{P_{cr}}\right)_B \text{ (pressure)} \tag{3.46}$$

$$\left(\frac{T}{T_{cr}}\right)_A = \left(\frac{T}{T_{cr}}\right)_B \text{ (temperature)} \tag{3.47}$$

Sometimes, scaling of temperature is done by reducing it to the pseudocritical temperature. Such approach indirectly involves similarity in pressure.

Jackson and Hall (1979a) proposed 12 non-dimensional similarity groups and stated that they were unlikely to be satisfied simultaneously. Of those groups proposed by Jackson and Hall (1979a), the most important ones for forced-convective heat transfer are the following:

$$\left(\frac{qD}{k_{b,in}T_{b,in}}\right)_A = \left(\frac{qD}{k_{b,in}T_{b,in}}\right)_B \text{ (heat flux)} \tag{3.48}$$

$$\left(\frac{GD}{\mu_{b,in}}\right)_A = \left(\frac{GD}{\mu_{b,in}}\right)_B \text{ (Reynolds number or mass flux)} \tag{3.49}$$

Using Eqs. (3.45) – (3.49) it is possible to scale the basic thermal hydraulic parameters of the current Canadian SCWR concept (Dominguez et al., 2013; and Yetisir et al., 2013) to SC CO_2 conditions (see Table 3.2).

Table 3.2. Critical parameters of water and CO_2 and operating parameters of the current Canadian SCWR concept scaled to CO_2.

Parameter	Critical parameters	
	Water	**CO_2**
P_{cr}, MPa	22.064	7.3773
T_{cr}, K	647.1	304.13
ρ_{cr}, kg/m^3	322.0	467.6
	Operating parameters	
P_{in}, MPa	25	8.36
T_{in} / T_{out}, °C	350 / 625	20 / 149
G_{in}, kg/m^{2}s	794	844
q, kW/m^2	776	68
D_{hy}, mm	7.30	7.30

In addition to the scaling laws above (Eqs. (3.45) – (3.49)), Pioro and Duffey (2007) proposed a modified law for geometric similarity, a law for wall superheat, and a law for HTC:

$$\left(\frac{x}{D}\right)_A = \left(\frac{x}{D}\right)_B \text{ (modified geometric similarity)} \tag{3.50}$$

$$\left(\frac{T_w - T_b}{T_{cr}}\right)_A = \left(\frac{T_w - T_b}{T_{cr}}\right)_B \text{ (wall superheat)} \tag{3.51}$$

$$\mathbf{Nu}_A = \mathbf{Nu}_B \text{ (HTC)} \tag{3.52}$$

Gupta (2012) compared profiles of certain thermal and transport properties reduced to their values at critical and pseudocritical temperatures and plotted them against reduced pressures and temperatures. He found that, in general, profiles of properties for water and carbon dioxide were quite similar. However, none of the approaches allowed combining data into a single profile per each property. Gupta (2012) concluded that the approach based on the properties reduced to their values at pseudocritical temperature gave better similarity for profiles of volumetric expansivity (within the whole range of reduced pressures), density, and Prandtl number (within the pseudocritical point and beyond).

Cheng et al. (2011) proposed to base the scaling law for temperature neither on T_{cr} nor T_{pc}, but on the difference between those. Having compared dimensionless specific heat, density, thermal conductivity, and viscosity they concluded that this approach showed the best similarity of properties variations for water, CO_2, and R134a. Cheng et al. (2011) also proposed mass flux scaling law based on the distortion approach, which was originally introduced by Ahmad (1973). In comparison to the scaling laws proposed by Jackson and Hall (1979a) for heat flux and HTC, the difference in the approach by Cheng et al. (2011) is only in the choice of the reference temperature. In summary, the modified scaling laws proposed by Cheng et al. (2011) are as follows:

$$\left(\frac{T - T_{pc}}{T_{pc} - T_{cr}}\right)_A = \left(\frac{T - T_{pc}}{T_{pc} - T_{cr}}\right)_B \text{ (temperature)} \tag{3.53}$$

$$\left(\frac{G}{\mu_b}\mathbf{Pr}_b^{5/12}\right)_A = \left(\frac{G}{\mu_b}\mathbf{Pr}_b^{5/12}\right)_B \text{ (mass flux)} \tag{3.54}$$

$$\left(\frac{q}{k_b\left(T_{pc}-T_{cr}\right)}\right)_A = \left(\frac{q}{k_b\left(T_{pc}-T_{cr}\right)}\right)_B \text{ (heat flux)} \tag{3.55}$$

$$\left(\frac{HTC\cdot D}{k_b}\right)_A = \left(\frac{HTC\cdot D}{k_b}\right)_B \text{ (heat transfer coefficient)} \tag{3.56}$$

The scaling rule for mass flux should be used with care, because Cheng et al. (2011) defined this law for the NHT regime. The law is based on the assumption of similarity:

$$\left(\mathbf{Re}^m\mathbf{Pr}^n\right)_A = \left(\mathbf{Re}^m\mathbf{Pr}^n\right)_B \tag{3.57}$$

Preliminary, Cheng et al. (2011) chose the following correlation for heat transfer region to pick exponents *m* an *n* and incorrectly referred to is as to Dittus and Boelter (1930) correlation:

$$\left(\mathbf{Re}^{0.8}\mathbf{Pr}^{1/3}\right)_A = \left(\mathbf{Re}^{0.8}\mathbf{Pr}^{1/3}\right)_B \tag{3.58}$$

Finally, Cheng et al. (2011) validated their scaling laws based on the available to them test data bank of heat transfer to SCFs. They first scaled the data to another fluid according to the scaling laws above and then tested the data against an appropriate correlation for that fluid. The correlation by Bishop et al. (1964) was tested against data scaled to SCW conditions and the correlation by Kransoshchekov and Protopopov (1966) was tested against data scaled to SC CO_2 conditions. Cheng et al. (2011) claimed that the validation results showed reasonable accuracy of the proposed scaling method, although they obtained standard deviation of the parameters for the runs in the range of 19% – 38%. Cheng et al. (2011) made an interesting conclusion that R134a appeared to be a better modelling fluid for water than CO_2. The conclusion was based on the comparison of expected experimental uncertainties in HTCs and temperatures in SC CO_2 and SC R134a at scaled to SCW conditions.

Ambrosini (2011) brought to attention that a qualitative similarity of dimensionless density (based on T_{pc}) and Prandtl number as functions of dimensionless enthalpy (see the definition in Eq. (3.59) below) at SC conditions was observed between water, CO_2, ammonia, and R23.

$$h^* = \left(h - h_{pc}\right)\frac{\beta_{pc}}{c_{p,pc}} \tag{3.59}$$

A greater quantitative similarity was observed between water and ammonia rather than between water and CO_2 or R23. According to Ambrosini (2011), however, this does not qualify ammonia as better modelling fluid, because of its high critical parameters (P_{cr} = 11.33 MPa, T_{cr} = 132.25 °C) and chemical characteristics.

Ambrosini (2011) also discussed that it was never possible to obtain real fully developed working conditions with SCFs in the presence of wall heating and the fluid passing the pseudocritical threshold. Therefore, any heat transfer model which disregards the upstream history, i.e., based on the local conditions, is by default limited in its predictive capabilities.

When comparing similarities in the flow instabilities of channels cooled with SCW and SC CO_2, Chatoorgoon et al. (2013) concluded that scaling parameters based on the temperature at which $\left(\frac{\partial \rho}{\partial h}\right)_P$ peaks showed a better similarity between fluids than scaling parameters based on temperature at which c_p peaks (T_{pc}).

3.8. Remarks

The majority of the experimental data were obtained for the flow of SCW in the 1960's-1980's. Unfortunately, at least half of these data was lost; other data are proprietary; and the bulk of the remaining data comes in the form of graphs (Kurganov et al., 2009; Groeneveld et al., 2007).

The majority of empirical correlations for SCFs where proposed and developed for SCW in the 60's – 70's, when experimental techniques were not at the same advanced level as

they are today. For example, Yamagata et al., 1972 mentioned that accuracy of 2 °C could be assumed for their calculations of the inside wall temperature.

Additionally, thermal and transport properties of fluids were updated and standardized several times since then. Thus, a peak in thermal conductivity of water in critical and pseudocritical points within a range of pressures from 22.1 to 25 MPa was not officially recognized until the 1990's (Pioro and Mokry, 2011; Sharabi et al. 2009). For example, Swenson et al. (1965) used smoothed properties around the pseudocritical point. Moreover, they discussed that they had to rely on five different references to obtain values of specific enthalpies, specific volumes, thermal conductivities and viscosities for the whole range of their experimental parameters. Finally, they emphasized that with the availability of more accurate values of viscosities and thermal conductivities the exponents of their correlation Eq. (3.20) should be re-evaluated.

Thus, independent of the experimental accuracy, all the correlation developed prior to 1996 (see IAPWS, 2008; IAPWS, 2005; and IAPWS, 1998 for more details) where fitted to the experimental data based on obsolete thermal and transport properties. Therefore, the legacy correlations cannot be used with the current properties and should be abandoned.

Literature review also revealed that, generally, correlations for SCW cannot be applied to SC CO_2; and vice versa. Moreover, the reviewed recent SC CO_2 correlations are based on the mixed-convection heat transfer data (at low mass and heat flux conditions) and, additionally, are not very reliable. Specifically, researchers at KAERI: a) could not generalize their data for tubes of different diameters; and b) despite using very complicated forms of correlations to fit their data failed to reduce the spread of the data to ±20% band. Thus, none of the existing methodologies for developing correlations allows improving prediction accuracy of the correlations.

Generally, the performance of correlations can be assessed based on either the "T-approach" or "Q-approach" (Kurganov et al., 2011; Kurganov et al., 2013a,b). HTC is calculated based on the experimental T_w and heat flux (q) in the T-approach, while it is calculated based on the knowledge of only q in the Q-approach. This distinction is rarely clearly mentioned in the publication. Among the reviewed papers, it was only in the paper

by Jackson and Hall (1979a) that was clearly mentioned that the authors used the T– approach. However, the rest of the reviewed papers contained no mentioning neither of the approach they used nor the tolerance for convergence criteria. Incomplete and insufficient procedures of assessing performance and presenting statistics for the correlations are present in the literature. Finally, no full analysis of uncertainties in HTCs obtained from the original experimental data was found in the literature. Such analysis is vital ground to substantiate the inclusion of the experimental data for the development of a correlation. It was only the paper by Cheng et al. (2009) where a full assessment of digitized data was made (those were the digitized data of Herkenrath et al., 1967).

An alternative to using one-dimensional correlations is using CFD. Generally, CFD models can predict NHT and IHT very well (Kao et al., 2010). However, there are certain problems in predicting DHT (see Figure 2.13) when CFD models are used. The problems arise mainly due to the following reasons (Kao et al., 2010):

1) The choice of a turbulence model; and
2) Incorporation of buoyancy and acceleration effects due to large variations of thermal properties.

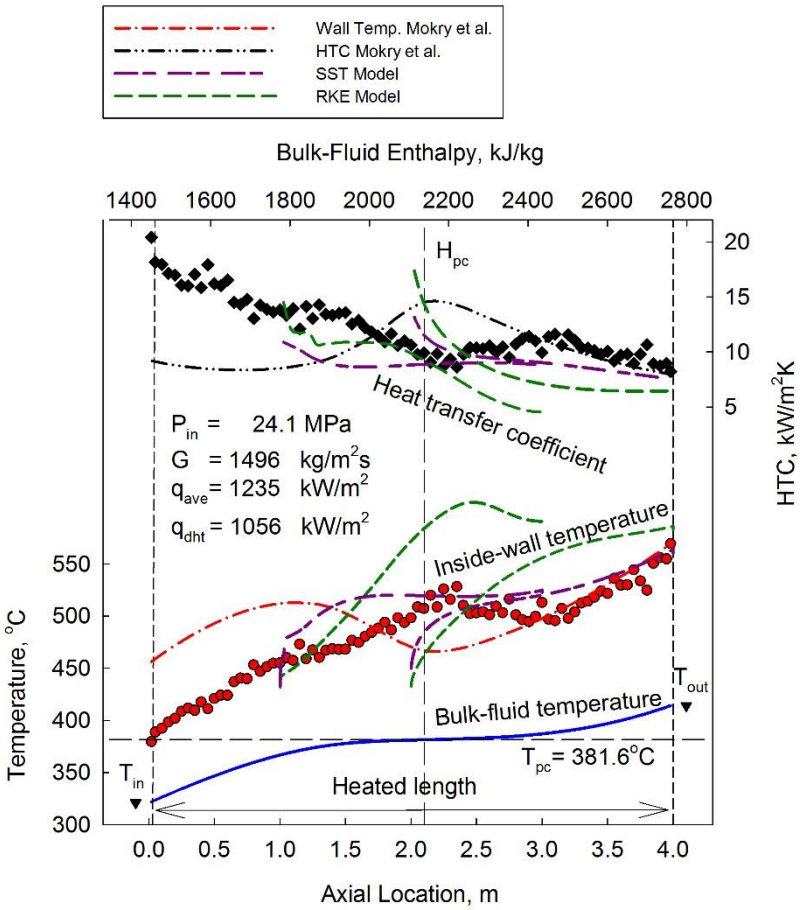

Figure 3.5. Depiction of DHT region within which CFD predictions are inconsistent between different models (upward flow of SCW in a bare tube; courtesy of A. Farah (UOIT), Farah et al., 2013)).

CFD modelling has not been validated for supercritical conditions yet. No CFD software has obtained a licensing from the domestic regulatory body recently (Lee et al., 2013). Licht et al. (2009) pointed out that experimental data were missing for the validation of the numerical results, obtained from the codes which are dedicated to modelling microscopic mechanisms of heat transfer. These experimental data were missing mainly due to the technical difficulties in measuring microscopic turbulence parameters near the heat transfer surface.

The literature review showed that the capabilities of current turbulence models to predict DHT are unsatisfactory.

Therefore, there is still a great reliance on 1D-heat-transfer correlations. Heat transfer correlations are widely used in the system and subchannel thermalhydraluic codes (Samuel

et al., 2014, Yang. et al., 2013; Shan et al., 2009). These codes are often coupled with neutronics codes to analyze fuel channels of nuclear reactors (Liu et al., 2013; Feng et al., 2013; Shan et al., 2010; Liu et al., 2010)

Although numerous supercritical heat transfer correlations were proposed in the past several decades, a search for a reliable and accurate correlation is still going on due to a wide discrepancy in the predictions of those correlations. Specifically, in the deteriorated or mixed convection heat transfer regime, no correlation successfully produces accurate predictions.

3.9. Objectives of the thesis

Based on the performed literature review, the following objectives are set for this thesis:

1) To develop forced-convective heat transfer correlations for SC CO_2 flowing upward in vertical bare tubes. These will be correlations for normal and improved heat transfer regimes. The correlations will be developed based on the conventional methodology. However, the correlations will be based on the biggest available data sets, covering a wide range of experimental parameters (pressures, inlet temperatures, mass fluxes, and heat fluxes).

2) Since SC CO_2 is mainly considered to be used in forced convective regime in power and engineering applications, it is important to develop a correlation for the onset of deteriorated heat transfer. In forced convection regime, the deteriorated heat transfer occurs at high heat and mass fluxes.

3) To propose, verify, and validate an innovative methodology for the development of forced-convective heat transfer correlations for SC CO_2 flowing upward in vertical bare tubes. This methodology should allow a significant reduction (more than 25%) in RMS for HTCs and T_w.

CHAPTER 4. AVAILABLE DATASETS

As discussed above, the objective of this thesis is to develop forced-convective heat transfer correlations for power/engineering applications. Development of any correlation starts from choosing an appropriate set of data. There were two sets available:

1) from the experiments at KAERI SPHINX loop (officially obtained under collaboration and agreement with IAEA); and

2) from the experiments at the AECL MR-1 loop (officially obtained by Dr. Pioro). The next sections discuss the experimental set-ups, reason to prefer one over the other, and the methodology for developing heat transfer correlations.

4.1. Dataset obtained at the SPHINX loop

A heat transfer test loop, named SPHINX (Supercritical Pressure Heat transfer Investigation for NeXt generation), was constructed at Korea Atomic Energy Research Institute (KAERI). The test loop uses CO_2 as a modelling fluid for water. Tests in bare tubes and annular tubes were performed.

The test facility was designed so that the heat transfer characteristics of SC CO_2 could be investigated at various combinations of heat and mass fluxes, at a given pressure. Figure 4.1 shows the test facility layout.

Experiments were performed using bare tubes of 4.4 mm, 4.57 mm, 6.0 mm (for downward flow only), 6.32 mm, and 9.0 mm ID as well as using annulus of 10.0 mm ID with a central heater rod (with an Inconel 600 sheath, heated by alternating current) of 8.0 mm OD (Kang et al., 2007; Song et al., 2008; Kim et al., 2008; Bae and Kim, 2009; Bae et al., 2010; and Bae, 2011).

In order to ensure a hydrodynamically fully developed flow at the entrance to the heated section, a 500 mm long unheated developing section was provided for tests with 4.57 mm ID tubes (650 mm, 550 mm, and 200 mm developing sections were provided for tests with

4.4 mm, 6.32 mm, and 9.0 mm tubes, respectively). The heated length was 2250 mm for tests with 4.57 mm ID tubes (2100 mm for tests with 4.4 mm and 2650 mm for tests with 6.32 mm, and 9.0 mm tubes, respectively).

The test section with a bare tube of 4.57 mm ID and the locations of the measuring points are shown in Figure 4.2. The test section was comprised of an Inconel 625 tube with circular cross-section with inside diameter of 4.57 mm. Heat to the test section was supplied by a direct current power source to impose a uniform heat flux on the tube surface. The heat flux on the inner wall was varied by adjusting the voltage between the clamped terminals. A proper insulation was provided to limit heat loss to a negligible level. The flanges were electrically insulated by the high heat-resisting plastic material (polyether ether ketone) capable of continuous exposure to 250 °C. (Bae, 2011).

A number of tests were conducted under different combinations of mass flux and heat flux at a given pressure. In order to investigate the effect of pressure on heat transfer, the experiments were performed at either three different pressures, for 4.4 mm tube (1.05, 1.10 and 1.20 times the critical pressure), or two different pressures, for tubes of other diameters (1.05 and 1.10 times the critical pressure). For the given mass flux for each test, heat flux and pressure were selected so that the fluid crossed the pseudocritical point inside the test section. This allowed for an investigation of heat transfer deterioration.

Table 4.1 contains test-matrix for the experiments with upward flow of SC CO_2. The test matrix was summarized based on the KAERI SPHINX loop data, which were provided in 2011 under the agreement with IAEA

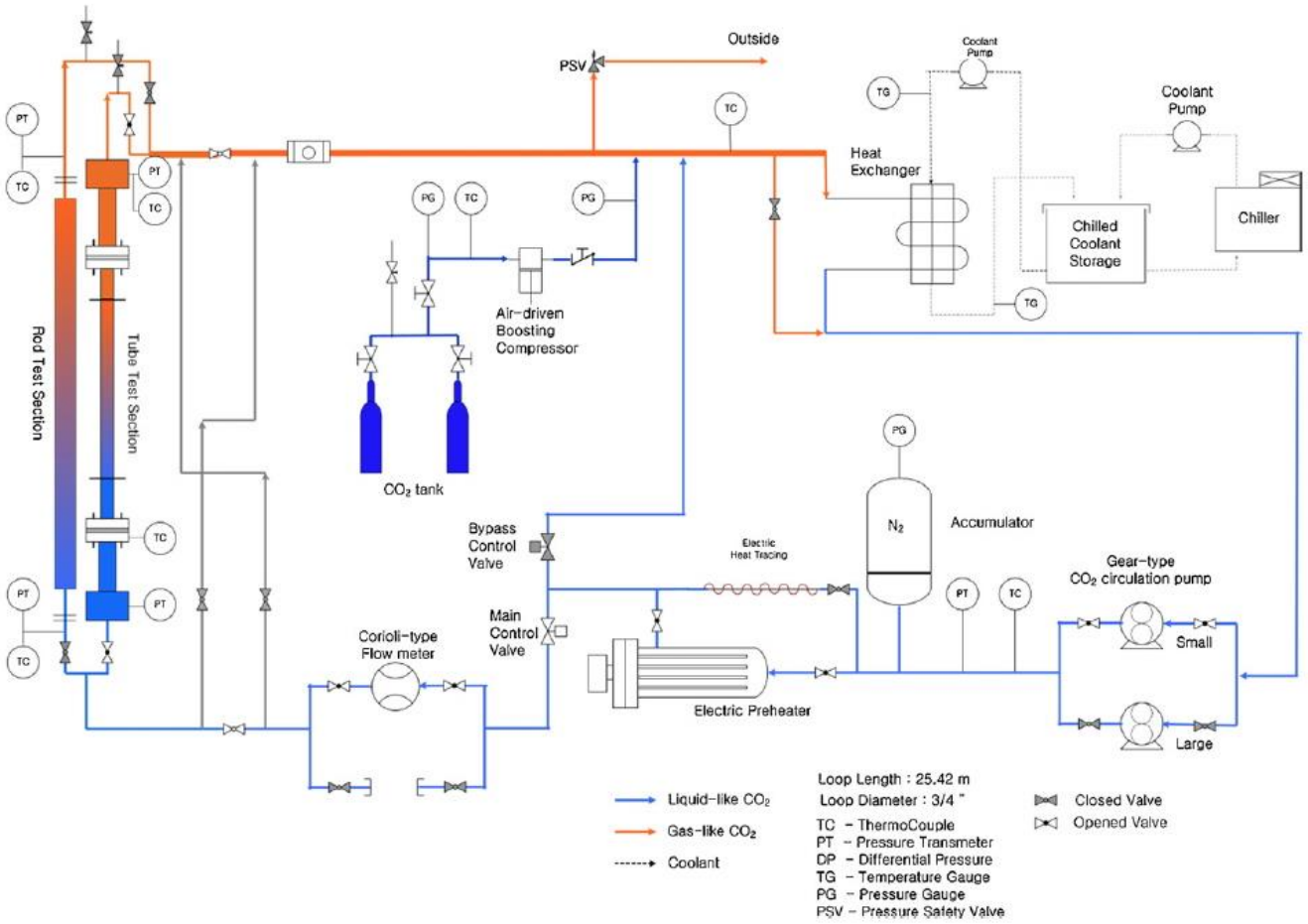

Figure 4.1. SPHINX test facility layout[7].

[7] Reprinted from Nuclear Engineering and Design, Vol 241, Bae Y.Y., "Mixed convection heat transfer to carbon dioxide flowing upward and downward in a vertical tube and an annular channel", pp. 3164–3177, Copyright 2011, with permission from Elsevier.

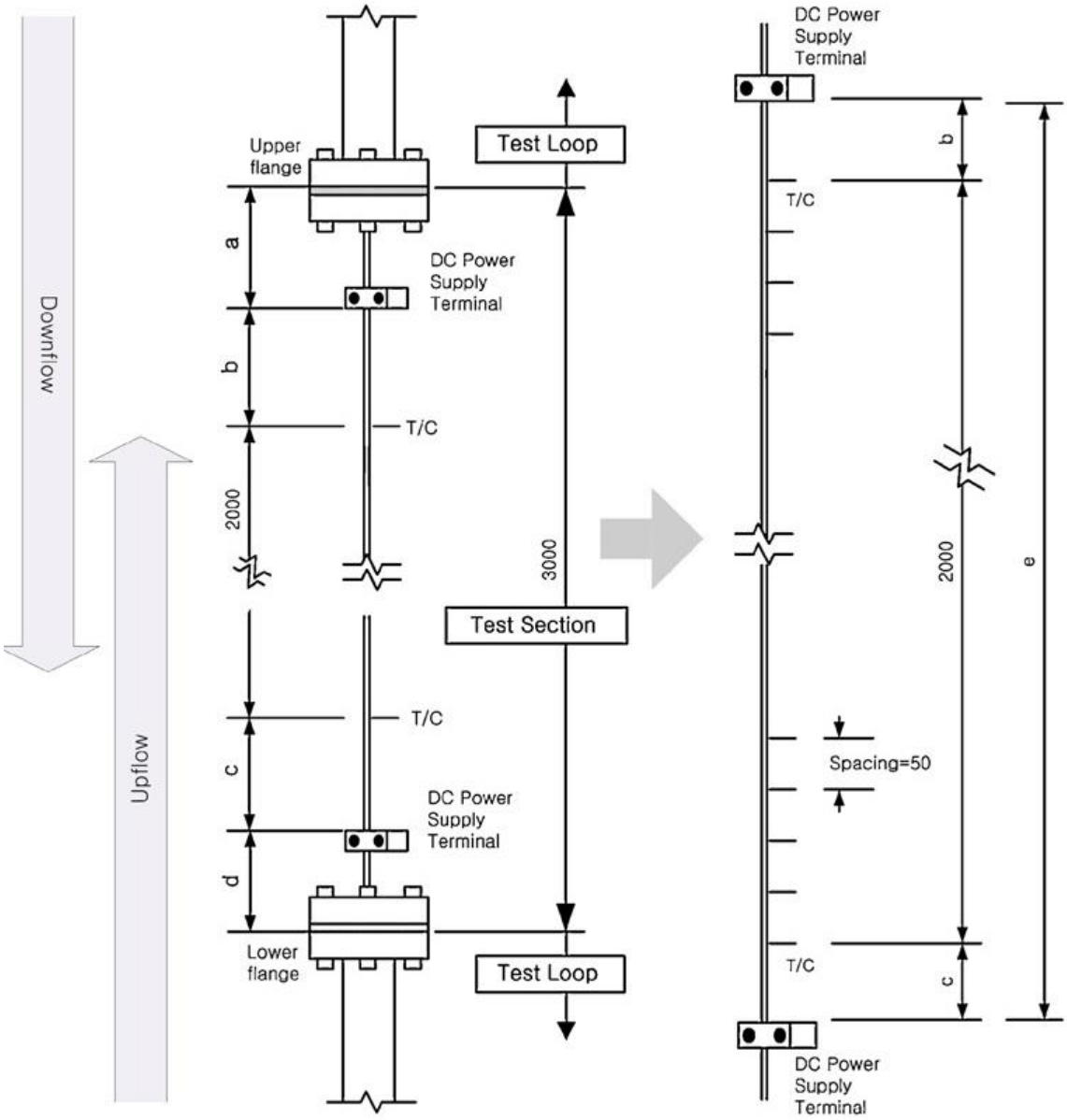

Figure 4.2. Test-section and locations of measurements[8]. Although the original paper does not clarify what the letters on the schematic stand for, it appears that meaning is the following: d – unheated region to allow hydrodynamic fully developed flow at the entrance to the test-section; c – thermal entrance region (no TCs[9] were installed at this part of the test-section); b –region of the heated part of the test-section, located at its end with no TCs installed, a – unheated end of the test section; e – heated part of the test-section.

[8] Reprinted from Nuclear Engineering and Design, Vol 241, Bae Y.Y., "Mixed convection heat transfer to carbon dioxide flowing upward and downward in a vertical tube and an annular channel", pp. 3164–3177, Copyright 2011, with permission from Elsevier.

[9] TC – ThermoCouple.

Table 4.1 Test-matrix parameters for experiments with upward flow of SC CO_2 at SPHINX loop (IAEA, 2011).

***D*, mm**	***P*, MPa**	**T_{in}, °C**	***q*, kW/m^2**	***G*, kg/m^{2}s**
4.4	7.75, 8.12, 8.85	5 – 41	10-150	400; 500; 750; 1000; 1200
4.57	7.75; 8.12	7 – 38	30-130	400; 500; 600; 700; 800
6.32	7.75, 8.12	4 – 37	20-170	285; 400; 500; 750; 854 1000; 1200
9.0	7.75, 8.12	6 – 34	30-50	200; 400; 600; 1200

Data in Table 4.1 show that the maximal heat flux was 170 kW/m^{2}K, while the maximal T_w temperature was about 181 °C (IAEA, 2011). Thus, the majority of the KAERI SPHINX loop data are more suited for the mixed- or natural-convective heat transfer applications. Additionally, Bae (2011) mentions that the circulation pump was stopped at extremely low mass fluxes and the flow was maintained only by natural circulation. This fact and analysis of KAERI SPHINX loop experimental data infers that the DHT observed during their experiments was caused by strong buoyancy forces (which are relevant to accident conditions), but not high heat fluxes (which are relevant to normal operation of power/engineering).

4.1.1. Instrumentation

The following test-section parameters were measured or calculated during the experiments (Bae, 2011):

- Pressure at the test section inlet and outlet.

- Fluid temperatures at the inlet and outlet of the test section. Mixing chambers upstream of the test section inlet and downstream of the test section outlet were used to minimize non-uniformity in the cross-sectional temperature distribution.

- Wall temperatures at equal intervals (50 mm) along the test section. 41 K–type TCs, each located 5 cm apart, were soldered on to the external surface of the tube to measure the wall temperatures.

- CO_2 mass-flow rate. Coriolis-type flowmeter was used.

A gear-type circulation pump was used to minimize flow fluctuations. An accumulator filled with N_2 in gaseous state installed downstream of the pumps to absorb any pressure fluctuations in the main loop. An auxiliary chiller system was used to cool CO_2 below the environment temperature and well below the pseudocritical temperature. (Bae, 2011).

4.1.2. Uncertainties of measured and calculated parameters

Table 4.2 shows the uncertainties of measured and calculated parameters (Bae and Kim, 2009). The expressions for calculation of uncertainties of the measuring devices supplied by the vendors were not provided.

Table 4.2. Vendor-supplied uncertainty parameters for experiments held at SPHINX loop with 4.4 mm and 9.0 mm ID bare tubes and annular tube of 10 mm ID and central heated rod of 8.0 mm OD (Bae and Kim, 2009).

Parameter	Accuracy
Test section power	neglected
Absolute pressure	±0.25% of full scale for P = 0–16.0 MPa
Differential pressure	±0.055% of span for P = 0–58.8 kPa
Temperature	±0.75% or ±2.2°C for T = 0–1260 °C
Mass-flow meter	±0.15% for 0-680 kg/h
Total calculated uncertainty for calculation of HTC	2.14%

A different estimate for HTC uncertainty was provided for tests with 4.57 mm bare tubes. Bae (2011) estimated that the uncertainties in HTC were between 7.7 – 12.6 %. However, he estimated these uncertainties assuming the average $T_w - T_b$ difference was 21.8 °C for and the maximal difference was 34.7 °C for the highest achieved wall temperature of 190 °C. Such choice of values appears to significantly underestimate the HTC error, because the difference in temperatures can be as low as few degrees. This is clearly seen on the Figure 3 of the original paper by Bae (2011), or from their numerical experimental data (IAEA, 2011).

Additionally, no details of the calibration of the flow-meter or comparison of its readings with a direct-weighting method were reported for KAERI tests (Kang et al., 2007; Song et al., 2008; Kim et al., 2008; Bae and Kim, 2009; Bae et al., 2010; Bae, 2011, and IAEA, 2011). Since improperly calibrated flow-meter automatically affects the calculation of the distribution of bulk-fluid temperature along the heated test-section, and thus, calculated HTC, some of the KAERI SPHINX loop data may be unreliable due to highly underestimated uncertainty in HTC calculations. Thus, consistent reduction and uncertainty analysis are impossible for KAERI data.

Further analysis of the KAERI SPHINX loop data (provided by IAEA, 2011) showed:

1) readings of every 35^{th} TC in the tests with 4.57 mm ID tubes were previously removed without any explanation; and
2) there were multiple runs, were the HTC was above 100 kW/m^2K, which is unrealistic.

Thus, there is strong evidence that the results of the KAERI test were submitted to the IAEA with partial and undocumented filtering of the data. Additional analysis of KAERI SPHINX loop data lead to removal of many points, for which experimental HTC became negative after accounting for the uncertainty in TCs. Finally, the a significant part of KAERI data were obtained at low mass and heat fluxes that do not correspond to pure forced-convective conditions.

Therefore, the dataset provided by IAEA (2011) and based on the KAERI SPHINX loop experiments cannot be directly used for the objective of the thesis. However, after proper reduction, data points belonging to the mixed-convective can be screened out, and the rest of the data can be used for the development of correlations. Additionally, these data can be used to verify correlations obtained using other datasets and to validate unconventional methodologies for the development of correlations.

4.2. Dataset obtained at the MR-1 loop

A large set of experimental data was obtained from the Fuel Channel Thermalhydraulics (FCT) laboratory at AECL. The experimental dataset was obtained at the MR-1 loop (see Figure 4.3), a high pressure and high-temperature pump loop adapted for use with SC CO_2 (Pioro and Duffey, 2007). The operating range of the MR-1 test facility was within high pressures up to 10.3 MPa and temperatures as high as 310°C. CO_2 was charged into the loop with 99.9% purity and 0.8 ppm content of hydrocarbons. The details of purity are especially important, since, as discussed by Kurganov(1998) and Kurganov et al. (2012), appreciable amounts of dissolved gases having low critical temperature (such, as components of air) can significantly decrease the maximum of specific heat and distort dependences of density and specific enthalpy on temperature.

The CO_2 passed through a 25 kW preheater before entering the test section. The test section was powered by a 350 kW (175 V, 2000 A) direct current power supply. Heat was removed in two places within the loop. A small amount of heat was removed from the test section downstream of the test section with the use of helicoid coolers. River water provided coolant to the coolers. However, most of the heat from the test section was removed in the discharge circuit of the pump using the main loop heat exchanger. Pressurization was achieved by applying electrical power to the heating elements in two vessels (Pioro and Duffey, 2007).

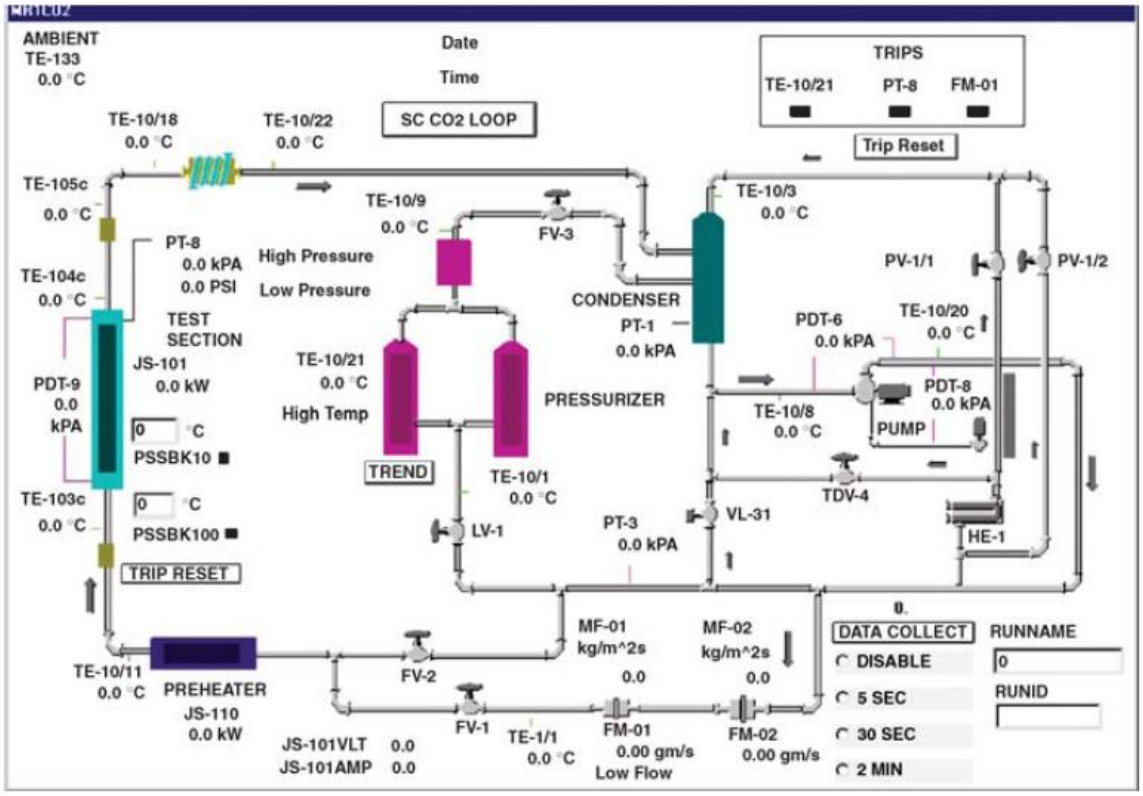

Figure 4.3. MR-1 loop (courtesy of Dr. Pioro (Pioro and Khartabil, 2005)).

The test section is shown in Figure 4.4. It was made up of 2.4 m long Inconel 600 tube with 8 mm ID and 10 mm OD. Only 2.208 m of the tube was heated. A 308 mm long (38 diameters) calming unheated part of the test section was located downstream of the mixing chamber. Direct electrical current passed through the tube wall and heated the fluid from the inlet to the outlet power terminals with the use of copper clamps. The test section and mixing chambers are wrapped with thermal insulation to minimize heat loss. The test section was attached with structural supports to a post to maintain its vertical orientation.

The experimental data were recorded using a Data Acquisition System (DAS) when the desired flow conditions and power level were reached and stabilized. Stable conditions meant no visible variations in parameters with time. After that a new power level or/and new flow conditions were set up. The data were recorded in 5 seconds intervals for a duration of one minute. Additionally, the test were re-run after one week time to verify the reproducibility of the data.

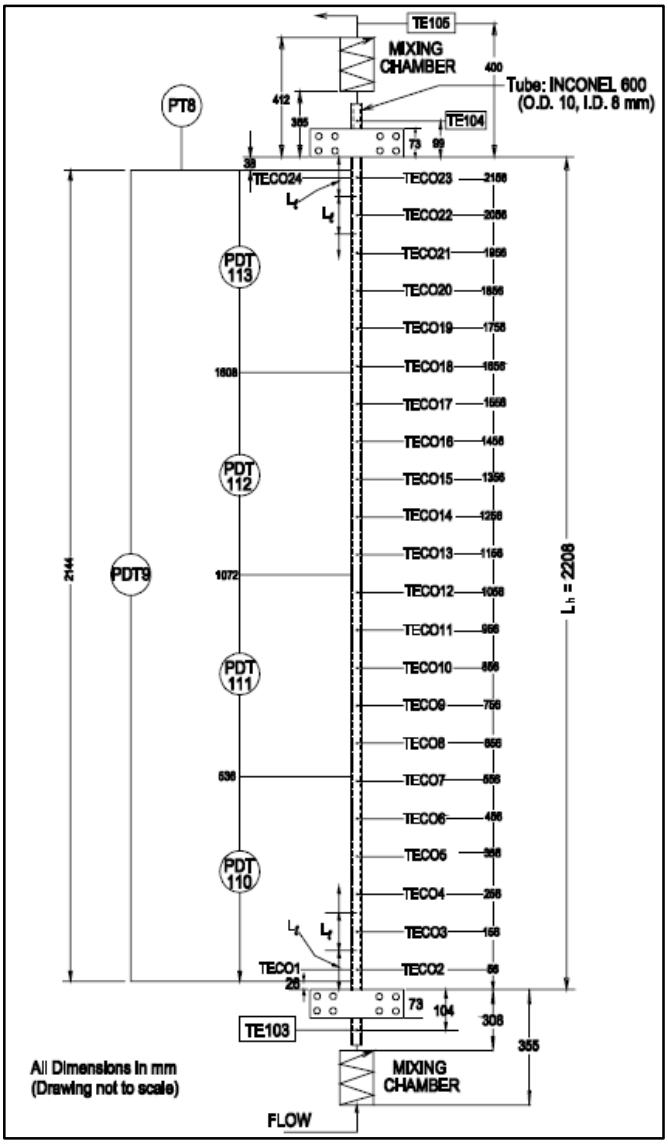

Figure 4.4. Test Section of MR-1 Loop Schematic (courtesy of Dr. Pioro (Pioro and Khartabil, 2005).

The test-matrix parameters are listed in Table 4.3.

Table 4.3. Test matrix parameters (Pioro and Duffey, 2007).

***P*, MPa**	***T_{in}*, °C**	***T_w*, °C**	***q*, kW/m^2**	***G*, kg/m^{2}s**
7.6; 8.4; 8.8	20–40	29–234	9.3–616	446–3048

Data in Table 4.3 shows that the maximal heat flux was 616 kW/m^2, the maximal mass flux was 3048 kg/m^{2}s, and the maximal T_w temperature was about 234 °C. Thus, the majority of the AECL MR-1 loop data are suited for the forced-convective heat transfer applications. Moreover, the selected range of the experimental parameters covers the experimental conditions of a generic SCWR (see Table 3.2). Preliminary analysis of experimental data infers that the DHT observed during MR-1 experiments was caused by high heat fluxes (which are relevant to normal operation of power/engineering). Furthermore, the majority of the MR-1experiments were held at 8.4 MPa pressures, which is equivalent to the operating pressure of the current Canadian SCWR concept (see Appendix E). The hydraulic diameter of the heated part of the test-section of MR-1 loop (8.058 mm) is very close to that of the concept (7.30 mm). The rest of the MR-1 loop test parameters are also within the range of equivalent parameters of the concept. Thus, these data can be considered as model data.

4.2.1. Instrumentation

The following test-section parameters were measured or calculated during the experiments (Pioro and Duffey, 2007):

- Test-section current (based on the measured voltage drop across a calibrated shunt) and voltage. These parameters were used to calculate the power.
- Pressure at the test-section outlet.
- Four pressure drops over equal lengths (536 mm) along the test section.
- Temperatures at the test-section inlet and outlet. These temperatures were measured using 1/16″ K-type ungrounded sheathed TCs inserted into the fluid stream. The TCs were installed immediately downstream of the mixing chambers. All TCs were calibrated *in situ* within the temperature range of 0 – 100 °C. Mixing chambers were used to minimize non-uniformity in the cross-sectional temperature distribution. Measurements of the bulk-fluid temperatures at the outlet revealed the absolute need to have a mixing chamber, for the following reason. In some cases,

the bulk-fluid temperature on the axis of the flow at the outlet was lower than that downstream of the mixing chamber, showing high temperature variation across the flow.

- Wall temperatures at equal intervals (100 mm) along the test section. 24 fast response K-type TCs with self-adhesive fiberglass backing were attached to the tube outer wall and were wrapped with Teflon tape and fiberglass string to achieve proper contact with the wall. The temperature trip for the external wall temperature was set at 250°C. Thermocouples TEC02 to TEC023 were located at one side of the test section. Thermocouples TEC01 and TEC024 were located at the same axial locations as thermocouples TEC02 and TEC023, but 180° apart. All fast-response thermocouples were calibrated *in situ* within the range of 0 – 100 °C prior to use.

- CO_2 mass-flow rate. Loop mass-flow rate was calculated based on the measured pressure drop over a small orifice plate, which was monitored with a differential-pressure cell. Comparison of the readings of the calibrated mass-flow meter with the direct weighting method showed that readings became considerably inaccurate at mass-flow rate below 45 g/s.

- Ambient temperature.

4.2.2. Uncertainties of measured and calculated parameters

Basic uncertainties of measured and calculated parameters at MR-1 loop are listed in Table 2.4.

The raw experimental data were provided. Detailed expressions for the uncertainty of the devices supplied by vendors were provided.

Thus, this dataset is appropriate for the forced-convective heat transfer applications; proper data reduction, and data uncertainty analysis are possible.

Table 4.4. Uncertainties of measured and calculated parameters at MR-1 Loop (Pioro and Duffey, 2007).

Parameter	Uncertainty
Test Section Power	±0.5%
Outlet Pressure	±0.2%
Local Pressure Drops	±0.8% at ΔP=30 kPa ±5.0% at ΔP=30 kPa
Temperatures	±0.3 °C within 0 – 100 °C ±2.2 °C beyond 100 °C
Mass Flow rates	±0.9% at 155 g/s (G = 3084 kg/m^{2}s) ±8.2% at 46 g/s (G = 915 kg/m^{2}s)

Therefore, the experimental dataset obtained at AECL MR-1 loop was chosen as the primary basis for the development of heat transfer correlations.

4.3. Data reduction

Conventionally, data reduction consists of the following steps:

1) calculation of time-averaged values of experimental parameters;

2) analysis of uncertainties of measured and calculated parameters;

3) removal of outliers; and

4) removal of the points within the mixed-convection regimes (if the purpose is to obtain a forced-convective heat transfer correlation).

4.3.1. Full analysis of uncertainties of measured and calculated parameters

Pioro and Duffey (2007) provided a very detailed description for the calibration of their instrumentation; they also provided data from the manufacturer on the uncertainties of the individual measuring devices. Pioro and Duffey (2007) suggested how to account for the

numerical errors due to using NIST REFPROP, as well. However, their book contained only the range of errors for the measured parameters, and no estimation for the error in HTCs (see Section 4.2, Table 4.4). Therefore, equations for the directly measured experimental parameters, as well as the rules for the calculation of the absolute and relative errors for commonly used function, given in the book by Pioro and Duffey (2007), were used to calculate the errors in estimation of the indirect experimental parameters. The used and developed equations are listed in Tables 4.5 – 4.7.

Table 4.5. Expression for the absolute and/or relative errors for the directly measured experimental parameters (Pioro and Duffey, 2007).

Parameter	Absolute error	Relative error
Temperatures T	±0.3 °C within 0-100 °C; ±2.2 °C beyond 100 °C	$\frac{\Delta T}{T}$
Absolute pressure P	-	$\frac{\Delta P}{P} = \pm\sqrt{\left(\frac{10\text{ kPa}}{P}\right)^2 + \left(10^{-3}\right)^2 + \left(\frac{3.2\text{ kPa}}{P}\right)^2 + \left(\frac{1.56\text{ kPa}}{P}\right)^2}$
Test-section pressure drop ΔP	-	$\frac{\Delta(\Delta P)}{P} = \pm\sqrt{\left(\frac{\%\text{ of span in kPa}}{P}\right)^2 + \left(10^{-3}\right)^2 + \left(\frac{0.0092\text{ kPa}}{P}\right)^2 + \left(\frac{0.0058\text{ kPa}}{P}\right)^2}$ the percentage of span in kPa is given in Table 3.2
ID and OD	±0.02 mm	$\frac{\Delta D}{D}$
Heated length of the test section L	±0.5 mm	$\frac{\Delta L}{L}$

Table 4.6. Basic characteristics of differential-pressure cells (Pioro and Duffey, 2007).

Instrument name	Description	Output, V	Output, kPa	Span, kPa	Accuracy of span, %
PDT-1*	Test-section pressure drop	10–50	0–300	300	0.5
PDT-2	Test-section pressure drop	1–5	0–50	50	0.5
PDT-3	Test-section pressure drop	1–5	0–50	50	0.5
PDT-4	Test-section pressure drop	1–5	0–50	50	0.5
PDT-5	Test-section pressure drop	1–5	0–50	50	0.5
PDT-FM-1**	Orifice-plate pressure drop	10–50	0–37	37	0.5

* PDT – Pressure Differential Transducer

** FM – Flow Meter

Table 4.7. Expression for the absolute and/or relative errors for the calculated (indirect) experimental parameters (based on the book by Pioro and Duffey, 2007).

Parameter	Absolute error	Relative error
Test-section power POW_{TS}	-	$\frac{\Delta POW_{TS}}{POW_{TS}} = \sqrt{\left(\frac{0.25}{100}\right)^2 + \left(\frac{0.02}{100}\right)^2 + \left(\frac{0.1}{100}\right)^2 + \left(\frac{0.09}{100}\right)^2 + \left(\frac{0.5\ \text{A}}{I}\right)^2 + \left(\frac{0.04\ \text{V}}{U}\right)^2}$
Heated area A_h	-	$\frac{\Delta A_h}{A_h} = \sqrt{\left(\frac{\Delta D}{D}\right)^2 + \left(\frac{\Delta L}{L}\right)^2}$
Flow area A_{fl}	$A_{fl} = \frac{\pi D \cdot \Delta D}{2}$	$\frac{\Delta A_{fl}}{A_{fl}}$
Mass-flow rate m	-	$\frac{\Delta m}{m} = \sqrt{(8\text{E-}4)^2 + \left(\frac{0.5\Delta\rho}{\rho}\right)^2 + \left(\frac{0.5\Delta(\Delta P)}{\Delta P}\right)^2}$, where $\frac{\Delta\rho}{\rho} = \sqrt{2.5\text{E-}7 + \frac{\max\left(\Delta\rho(T_b + \Delta T_b; P - \Delta P); \Delta\rho(T_b - \Delta T_b; P + \Delta P)\right)}{\rho}}$ The first term in the expression for the relative error in density corresponds to the maximum calculation uncertainty from the equation of state

Parameter	Absolute error	Relative error
Mass flux	-	$\frac{\Delta G}{G}=\sqrt{\left(\frac{\Delta m}{m}\right)^2+\left(\frac{\Delta A_{fl}}{A_{fl}}\right)^2}$
Average heat flux q_{ave}	-	$\frac{\Delta q_{ave}}{q_{ave}}=\sqrt{\left(\frac{\Delta POW_{TS}}{POW_{TS}}\right)^2+\left(\frac{\Delta A_h}{A_h}\right)^2}=\sqrt{\left(\frac{\Delta POW_{TS}}{POW_{TS}}\right)^2+\left(1.4\text{E-}3\right)^2}$
Bulk-fluid specific enthalpy at the inlet $h_{b,in}$	-	$\frac{\Delta h_{b,in}}{h_{b,in}}=\sqrt{\frac{\max\left(\Delta h_{b,in}\left(T_b-\Delta T_b;P+\Delta P\right);\Delta h_{b,in}\left(T_b+\Delta T_b;P-\Delta P\right)\right)}{h_{b,in}}}$
Bulk-fluid temperature at any calculation step $T_{b,i}$	-	$\frac{\Delta T_{b,i}}{T_{b,i}}=\sqrt{\frac{\max\left(\Delta T_{b,i}\left(h_b-\Delta h_b;P-\Delta P\right);\Delta T_{b,i}\left(h_b+\Delta h_b;P+\Delta P\right)\right)}{T_{b,i}}}$
Bulk-fluid specific enthalpy at any calculation step $h_{b,i}$	-	$\frac{\Delta h_{b,\mathrm{i}}}{h_{b,i}}=\sqrt{\left(\frac{\Delta h_b}{h_b}\right)_{i-1}^2+\left(\frac{\Delta POW_{TS}}{POW_{TS}}\right)^2+\left(\frac{\Delta m_{fr}}{m_{fr}}\right)^2+\left(\frac{\Delta A_h}{A_h}\right)^2}$
Volumetric heat generation rate q_{vol}	-	$\frac{\Delta q_{vol}}{q_{vol}}=(\,6.250\text{E-}6+4.0\text{E-}9+1\text{E-}6+8.1\text{E-}7+\left(\frac{0.5\ \mathrm{A}}{I}\right)^2+3.6\text{E-}5+$ $+(5.245\text{E-}2)^2+\frac{\Delta T_{w,ext}^2+\Delta T_{amb}^2}{\left(T_{w,ext}-T_{amb}\right)^2}+\left(2.623\text{E-}2\right)^2\,)^{0.5}$
Internal wall temperature $T_{w,int}$	-	$\frac{\Delta T_{w,\mathrm{int}}}{T_{w,\mathrm{int}}}=\sqrt{a^2+b^2+c^2}$, where *a*- uncertainty of the directly measured external temperature of the wall; $b=\sqrt{\left(\frac{\Delta q_{vol}}{q_{vol}}\right)^2+6.25\text{E-}4+\left(1.036\text{E-}2\right)^2}$ $c=\sqrt{\left(\frac{\Delta q_{vol}}{q_{vol}}\right)^2+6.25\text{E-}4+8.0\text{E-}6+\left(1.036\text{E-}2\right)^2}$

Parameter	Absolute error	Relative error
Heat transfer coefficient	-	$\frac{\Delta HTC}{HTC} = \sqrt{\left(\frac{\Delta q_{ave}}{q_{ave}}\right)^2 + \left(\frac{\Delta T_{w,\text{int}}^2 + \Delta T_b^2}{T_{w,\text{int}} - T_b}\right)^2}$

Although part of the data on heat transfer to the upward flow of SC CO_2 obtained at the MR–1 experiments were published earlier (Pioro and Duffey, 2007; Mokry and Pioro, 2011; Gupta et al. 2012; and Yang, 2013) no uncertainties of calculated T_b, T_w, or HTC were ever presented.

Additionally, from personal communication, Mr. Sahil Gupta confirmed that although he processed the data before, he never calculated the actual experimental uncertainties. Moreover, he used a combination of time-averaged and instantaneous raw data to compile the reduced dataset.

Yang (2013) clearly mentioned that he used 1416 points for a correlation for NHT and 1172 points for a correlation for DHT. These total 2588 points. No explanation was provided on how the rest of the points (approximately 2212 out of 4800) were eliminated.

Therefore, all the raw data and the above listed uncertainties were re-calculated (please see Appendix A for the listing of the corresponding MATLAB code). The process of re-calculation is briefly explained below.

Each of the original files contains directly measured data from all the reading instruments corresponding to the run within a day. In total, there were 23 files containing both the original and the processed data (labeled as ver.7). The original data correspond to approximately 4800 averaged data points.

First, the data had to be processed to calculate the average values of the following parameters as well as their absolute and relative errors:

- Bulk fluid temperature and specific enthalpy along the test section.

- Internal wall temperature based on the applied heat flux and present heat losses to the ambient air.

- Pressure loss due to the gravity and acceleration.

Careful inspection of the original data revealed a number of the erroneous runs, when the DAS interrupted the measurements because of either a power trip, huge mass-flow rate fluctuation, or a sudden jump or drop of current. However, there were just a few of such cases. Although the data were supposed to be collected 13 times per minute (every 5 seconds), at least a half of the data contained 14 measurements. Dr. Pioro suggested that it could have been simply due to an additional measurement done by electronics.

After calculating the temperature distribution (the heat losses were accounted for), the code extracts each of the parameters relevant for the future creation of a correlation (i.e., distribution of the bulk-fluid, wall temperatures, and HTC along the test section, inlet pressure, mass flux, and heat flux); and writes them into an Excel file with a corresponding name.

Additional filtering of the averaged data was done to determine the cases when the inside wall temperature was within the uncertainty of the calculated bulk-fluid temperature (in the majority of such cases the calculated values of HTC were negative and, therefore, meaningless). These cases where eliminated as erroneous. Also three cases, which where nearly exact duplicates of the other cases, where ignored and set aside for future verification of the correlation.

The calculated uncertainties for HTCs were found to range from 4.7% (for high heat and mass fluxes) to 69.2% (such huge errors were associated with the data collected at both low heat and mass fluxes) (see Table 4.8). Also, independent of the absolute values of the heat and mass fluxes, high uncertainties (of the order of 20%) were often encountered within the pseudocritical region and beyond it due to higher uncertainties in the measured temperatures.

Table 4.8. Uncertainties of heat transfer coefficients obtained by processing the data from MR–1 loop.

Uncertainty range	≤10%	10 – 20%	≥20%
No. of data points (in total: 4599)	3249	1002	457
Percentage	69.0	21.3	9.7

In the end, 229 files representing all the AECL MR-1 Loop data were created (one experimental run per file).

4.3.2. Data filtering

The filtering process of MR-1 data consisted of the following steps:

1) Removal of the data corresponding to low mass-flow rates. According to the description of the flow meter operation (Pioro and Duffey, 2007), accuracy of its measurements decreased significantly for mass-flow rates below 45 g/s. This value of mass-flow rate corresponds to the mass flux G = 882 kg/m^2·s. 748 points were removed at this step.

2) Removal of the buoyancy-affected data according to the criterion by Jackson and Hall (1979a) (see Eq. (3.4)). This step was needed to remove any cases were mixed convection effects could be possible. Only 16 points were removed, mainly because the majority of the buoyancy-affected data were collected at low mass fluxes, which were eliminated at the previous step.

3) Removal of the data points collected in the vicinity of the PDTs. From the visual analysis of the data it was evident that TC– measurements were affected by the presences of PDTs. It appears that PDTs acted as turbulizers. During private discussions Dr. Pioro mentioned that this could have been caused by the structure of the PDT. Five measurements in each run were determined to be affected by the PDTs. Table 4.9 provides information on the location of the affected TCs and PDTs. As one can see from the Table 4.9, PDT-2 is located immediately downstream of the TC7 (6th measurement point), and PDT-4 is located immediately

upstream of the TC18. PDT-3, however, is located almost at exactly same distance from the TC12 and TC13. Therefore, PDT-2 and PDT-4 acted as turbulizers and disturbed the flow enough for the wall temperature to conspicuously decrease at some distance downstream (PDT-2), as well as upstream (PDT-4) of its location. This means, that the MR-1 loop data are not the pure data for the bare tube, but the data for a tube with local turbulizers of flow. Although the effect of presence of PDT-3 is barely distinguishable, knowing how the other two PDTs affected the flow, the decision was made to remove the readings of the 11^{th} and 12^{th} points as well. It was, however, unclear how to correct the remaining data to the bare tube case because of the caused turbulence. An assumption was made that due to the large amount of data obtained at gradual variation of parameters, the removed readings were reproduced in the consequent run. Therefore, it is expected that the final correlation would reproduce the removed data well. Thus, five measurement points were removed per run. 900 points were removed at this step. The effect of PDTs is shown in Figure 4.5.

4) Removal of data points with high HTC uncertainty (≥20%). 258 points were removed at this step.

Table 4.9. Locations of the PDTs and TCs in their proximity

Name of a PDT	Location of a PDT, cm	Name of a TC	Location of a TC, cm
PDT-2	56.2	TC7	55.6
		TC8	65.6
PDT-3	109.8	TC12	105.6
		TC13	115.6
PDT-4	163.4	TC18	165.5

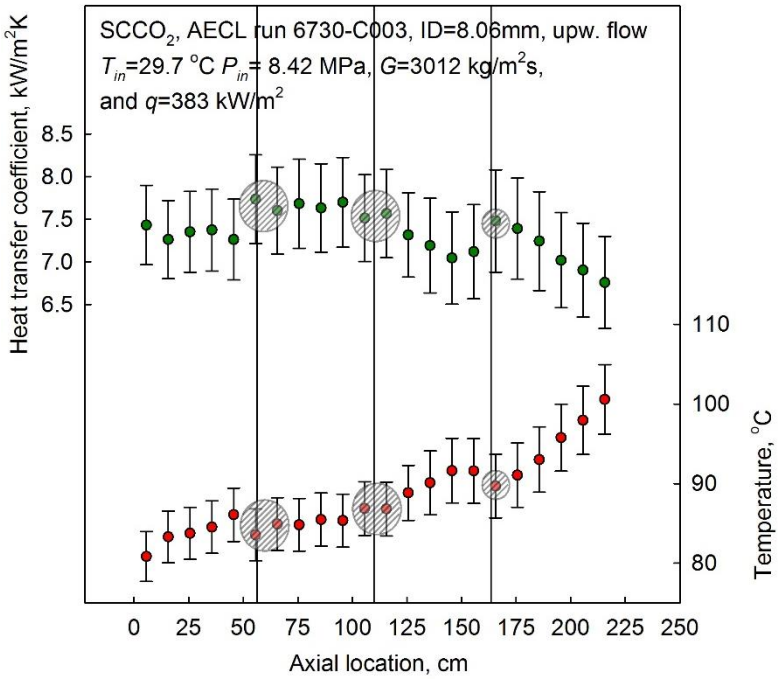

Figure 4.5. Effect of PDTs.

Therefore, 2786 points were left for the development of the correlations. This is one of the biggest known datasets used to develop heat transfer correlations for SC CO_2.

4.4. Observed effects of experimental parameters on heat transfer

This section summarizes the observed effects of experimental parameters on heat transfer. All the data obtained at MR-1 loop were analyzed. The full set of graphs is presented in Appendix F. The main conclusions along with the supporting graphs are presented below.

4.4.1. Effect of heat flux.

Increasing heat flux leads to higher wall temperatures (see Figures 4.6 (a) and (b)) and a significant HTC deterioration. An inlet effect is also clearly visible on Figure 4.6 (a). Also it appears that if the heated length were longer, HTCs for q = 466 kW/m^2 and 289 kW/m^2

would become equal; however, wall temperature would still be lower at lower heat flux (in accordance with Newton's cooling law).

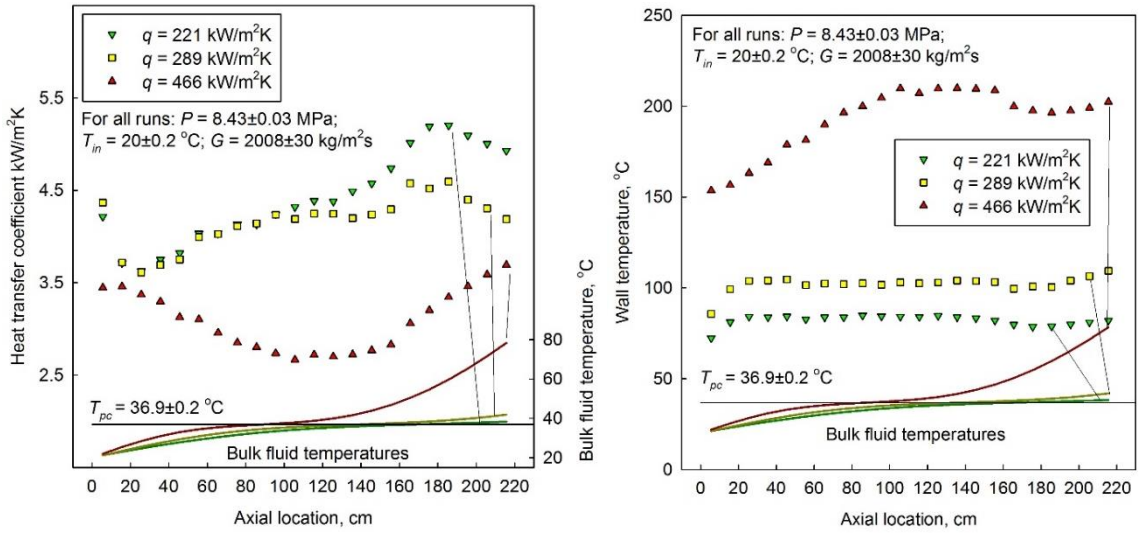

Figure 4.6. Effect of heat flux on heat transfer: (a) – HTCs; (b) – wall temperatures (upward flow of SC CO_2 in a bare tube).

The observed heat flux effect on MR-1 loop data is in agreement with the previous observations, as discussed in Chapter 1. Additionally, it is seen that in the case of the maximal heat flux, the deterioration in wall temperatures starts at bulk fluid temperatures below T_{pc}, and the deterioration stops developing when bulk fluid temperature reaches T_{pc}.

4.4.2. Effect of mass flux.

Increasing mass flux leads to nearly proportional increase in HTC and much lower wall temperatures (see Figures 4.7 (a) and (b)).

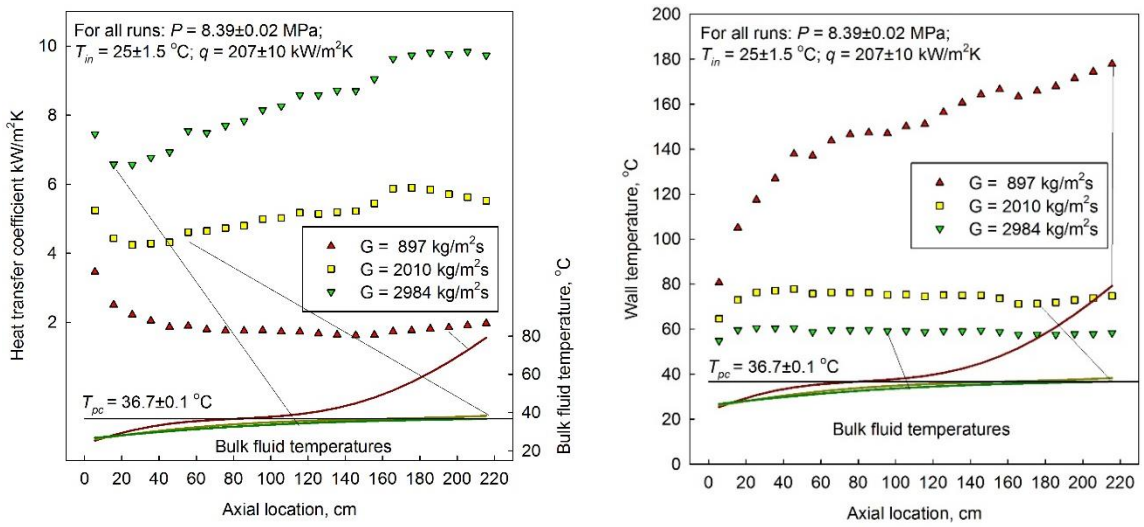

(a) **(b)**

Figure 4.7. Effect of mass flux on heat transfer: (a) – HTCs; (b) – wall temperatures (upward flow of SC CO_2 in a bare tube).

The observed mass flux effect on MR-1 loop data is in agreement with the previous observations, as discussed in Chapter 2. Additionally, it is seen that at low mass fluxes heat transfer deteriorates to steady HTC values prior to bulk fluid reaching T_{pc}. Further increase of bulk fluid temperature does not lead to HTC deterioration at low fluxes.

4.4.3. Effect of pressure.

The effect of pressure is generally discussed less in the literature than the effects of mass and heat fluxes. Additionally, a literature review did not reveal any regularity in the observed pressure effect. Moreover, the effect could be opposite on HTC depending whether the bulk fluid is below or above the pseudocritical temperature. Unfortunately, the majority of the data was collected for P = 8.4 MPa. It was very hard to find runs with the rest of the experimental parameters being the same at different pressures. For example, in Figures 4.8 (a) and (b) the presented run at P = 8.8 MPa was obtained at a heat flux, which was 20 kW/m^{2}k less than the heat flux for the other two runs obtained at different pressures. Therefore it is hard to make a convincing conclusion. However, it appears that increasing pressure leads to a decrease in HTC independent of the bulk fluid temperature.

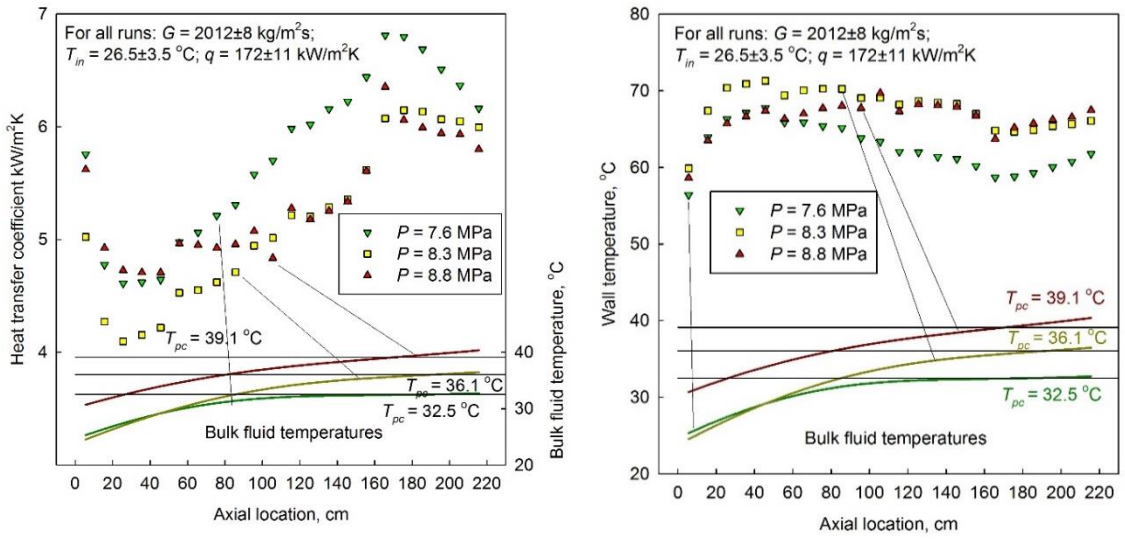

(a) **(b)**

Figure 4.8. Effect of pressure on heat transfer: (a) – HTCs; (b) – wall temperatures (upward flow of SC CO_2 in a bare tube).

It should also be noted that the presented runs all correspond to NHT. The effect of pressure on HTC at DHT conditions may be different.

4.4.4. Effect of inlet temperature

Only one reference (of those considered in the literature review) mentioned the inlet effect. The observed inlet temperature effect on MR-1 loop data is presented below in Figures 4.9 (a) and (b).

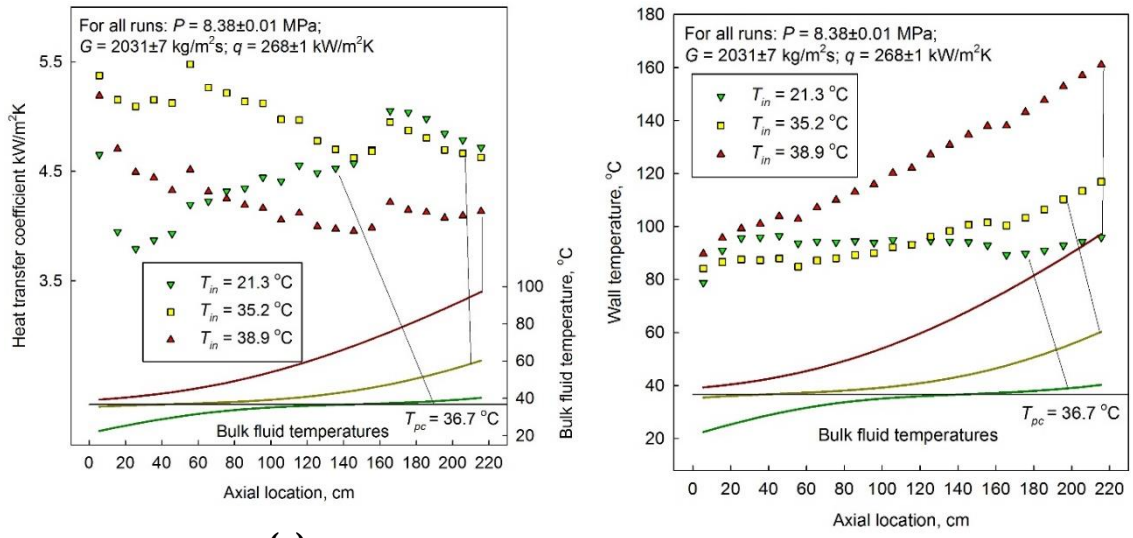

Figure 4.9. Effect of inlet temperature on normal heat transfer: (a) – HTCs; (b) – wall temperatures (upward flow of SC CO_2 in a bare tube).

The observed effect is only consistent at bulk fluid temperatures above T_{pc}; i.e. HTC increases (T_w decreases) with the decrease in inlet temperatures. However it seems that both T_w and HTC assume the same values at the same T_b for the runs that only differ in the inlet temperature. Thus, it may mean that the effect of velocity profile transformation around the pseudocritical point is similar to the entrance effect.

The next chapter is devoted to the discussion of general properties of CO_2.

CHAPTER 5. PROPERTIES OF CO_2[10]

This section is devoted to the discussion of thermal and transport properties of CO_2. Although, general behavior of SCFs was discussed in Chapter 2, consideration of the properties of CO_2 is still important to be aware of their specifics. The author feels that such consideration is especially relevant before discussing methodology for development of heat transfer correlations. P-T and T-s diagrams for CO_2 are presented in Figure 5.1 (a) and (b).

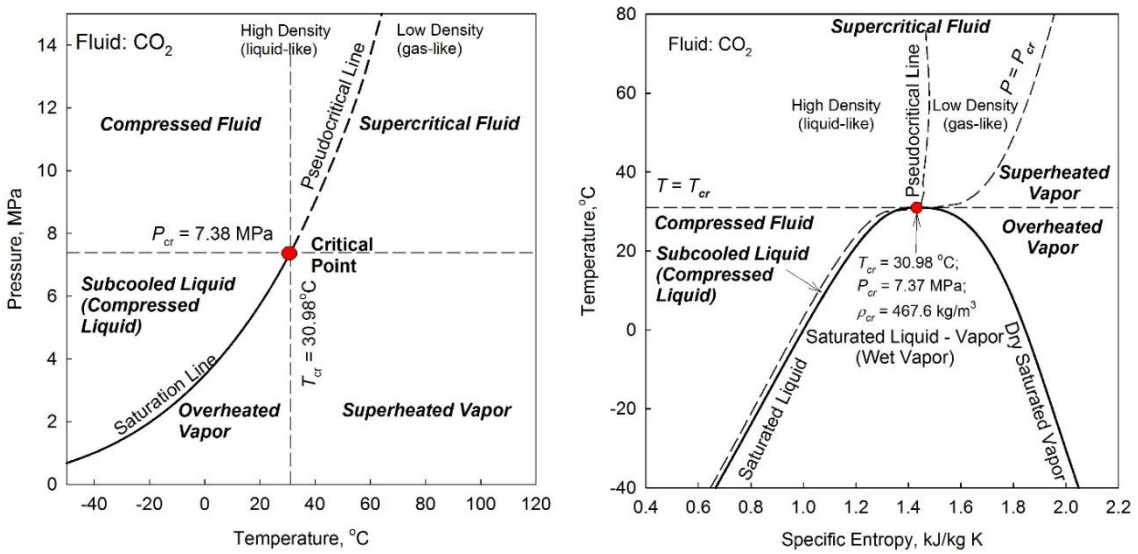

Figure 5.1. P-T (a) and T-s (b) diagrams for CO_2.

It was established using X-ray diffraction methods that the molecular structure of SCFs at temperatures below the pseudocritical resembles that of liquid, and at temperatures above the pseudocritical resembles that of gas (Jackson and Hall, 1979a; Pioro and Duffey, 2007). The mere presence of a peak in c_p in a very narrow region of temperatures suggests that fluid is undergoing a certain change in its molecular structure. This interpretation is based on the definition of c_p as unit energy required to increase temperature of unit mass by unit degree. Therefore, extremely high values of c_p near T_{pc} show that the energy transferred

[10] Thermal and transport properties of CO_2, water, and refrigerant R-134a were retrieved from NIST REFPROP ver. 9.0 software (Lemmon et al., 2013). The properties of CO_2 implemented in NIST are based on the publication by Span and Wagner (1996), Fenghour et al. (1998), and Vesovic et al. (1990). The properties of water implemented in NIST are based on the 1995 formulation by the International Association for the Properties of Water and Steam (Wagner and Pruss, 2002), Huber et al. (2009), and IAPWS (2008).

into SCF is not readily transferred to increase bulk temperature, but rather consumed for something else (Bishop et al., 1964).

In general, the differences in thermal and transport properties of CO_2 at subcritical and SC state are as radical as they are for water (as discussed in Chapter 2). Specific heat, density, viscosity, and thermal conductivities are plotted at three subcritical and three SC pressures in Figures 5.2 – 5.5. The three SC pressures are chosen as those representing the three nominal pressures at the AECL MR-1 loop experiments (7.6 MPa, 8.4 MPa, and 8.8 MPa, which correspond to $1.03P_{cr}$, $1.14P_{cr}$, and $1.19P_{cr}$, respectively). The three subcritical pressures are chosen equal to be multiple of the inverse of the ratios of the chosen SC pressures to the critical pressures (7.16 MPa, 6.47 MPa, and 6.20 MPa, which correspond to $P_{cr}/1.03$, $P_{cr}/1.14$, and $P_{cr}/1.19$).

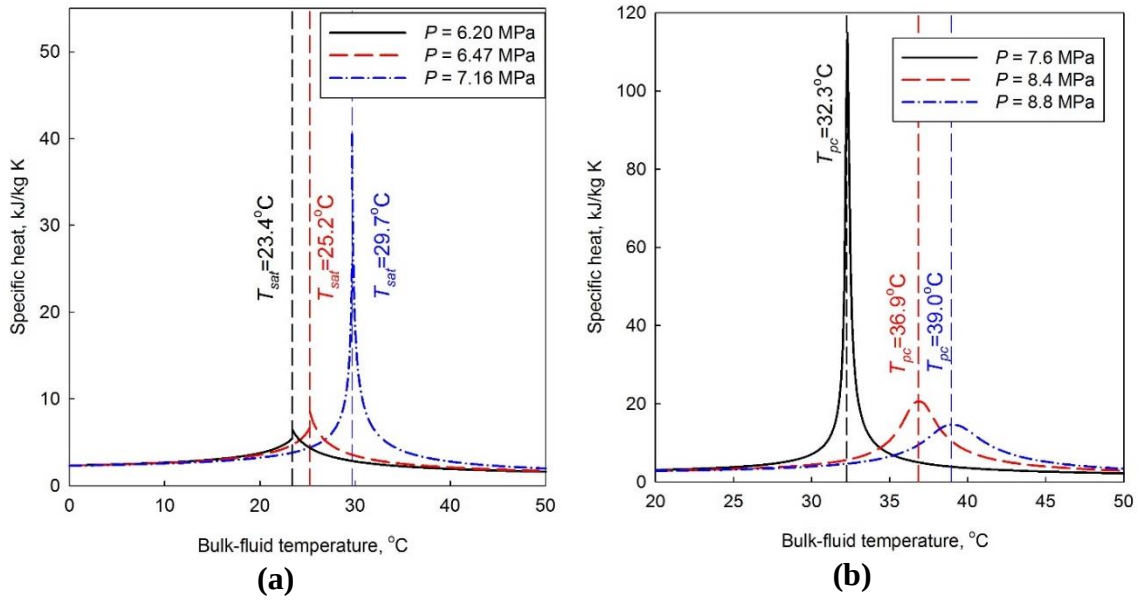

Figure 5.2. Specific heat of CO_2 at three subcritical (a) and three supercritical (b) pressures.

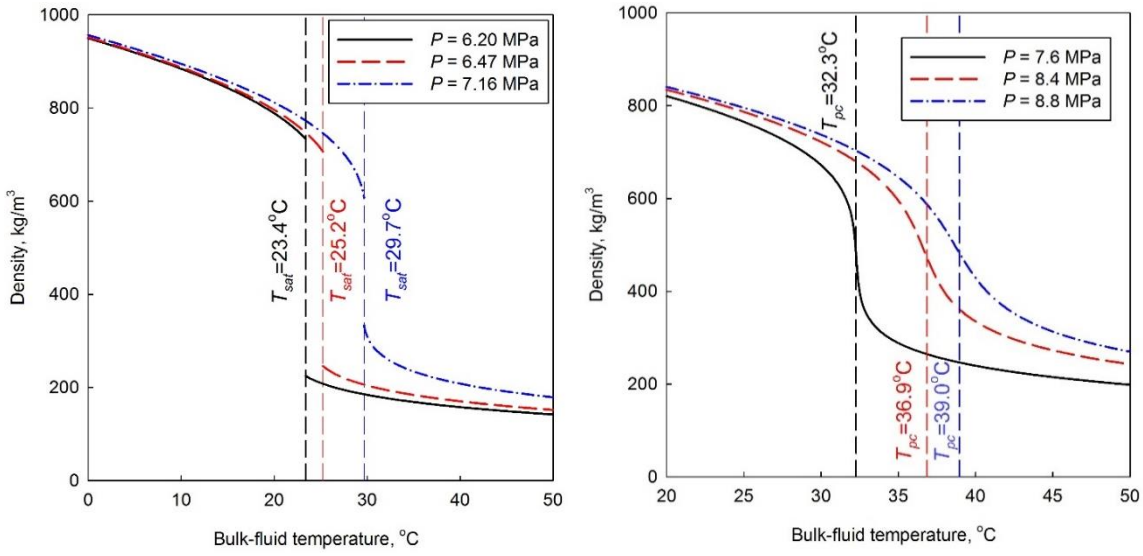

Figure 5.3. Density of CO_2 at three subcritical (a) and three supercritical (b) pressures.

From Figure 5.2 (a) it is seen specific heat of CO_2 increases with temperature at liquid state and decreases with temperature at vapor state. The shape of specific heat at subcritical pressures is similar to that at SC pressures. However, the maximal specific heat is always higher at vapor state. Additionally, the peak in specific heat increases with the increase in pressure and shifts towards higher bulk fluid temperatures. However, at SC pressures the peak in specific heat reduces dramatically with the increase in pressure and shifts towards higher bulk fluid temperatures (see Figure 5.2 (b)).

Figure 5.3 reveals that the general trends of density with temperatures are remarkably similar both at subcritical and SC pressures. It is seen that the depreciation in density becomes less pronounced with the increase in pressure (Figure 5.3 (b)) at SC state, and the difference between the values of density at saturation temperature becomes less with the pressure (Figure 5.3 (a)). Additionally, the depreciation shifts towards higher bulk fluid temperatures with pressure at SC state. According to NIST, maximal uncertainty in calculated values of ρ of SC CO_2 is less between between 0.03% – 0.05%.

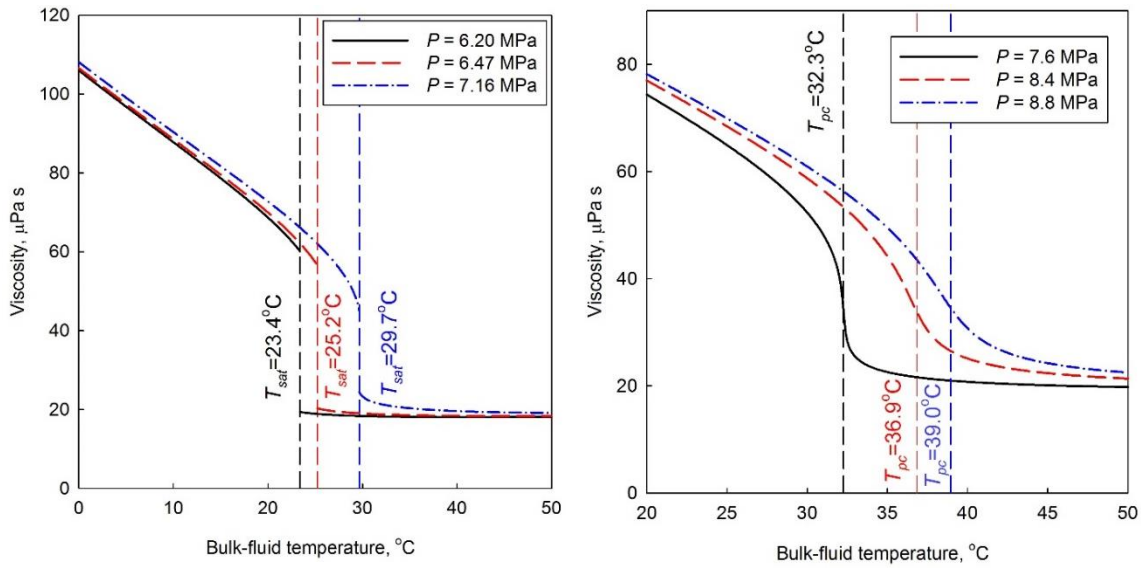

Figure 5.4. Viscosity of CO_2 at three subcritical (a) and three supercritical (b) pressures.

From Figure 5.4 it is seen that the patterns of viscosity dependence on temperature is very similar to that of the density both at sub- and SC state; namely, the difference in the values of viscosity at saturation temperature becomes less with the pressure at subcritical state, and the depreciation becomes less pronounce and shifts towards higher bulk fluid temperatures with pressure at SC state. According to NIST, maximal uncertainty in calculated values of μ of SC CO_2 is between 0.3% – 5%.

Figure 5.5 (b) shows that the peak in thermal conductivity reduces and shifts towards higher bulk fluid temperatures with the increase in pressure at SC state. The peak in thermal conductivity is not coinciding with the pseudocritical temperature. Also, values of thermal conductivity at temperatures beyond pseudocritical are higher at higher pressures. The temperature dependence of thermal conductivity at subcritical state (Figure 5.5 (b)) is different than that of the other properties. While at low pressures there is an expected break in the values of thermal conductivity at saturation temperature, there is an unexpected peak in thermal conductivity of liquid CO_2 at pressure approaching that of critical states (namely, P_{cr}/1.03). In other words, its behavior is extremely similar at near-critical sate for CO_2. This conclusion, however, is based on the belief that the values of thermal conductivity obtained from NIST REFPROP are true. According to NIST, maximal uncertainty in calculated values of k of SC CO_2 is less than 5%.

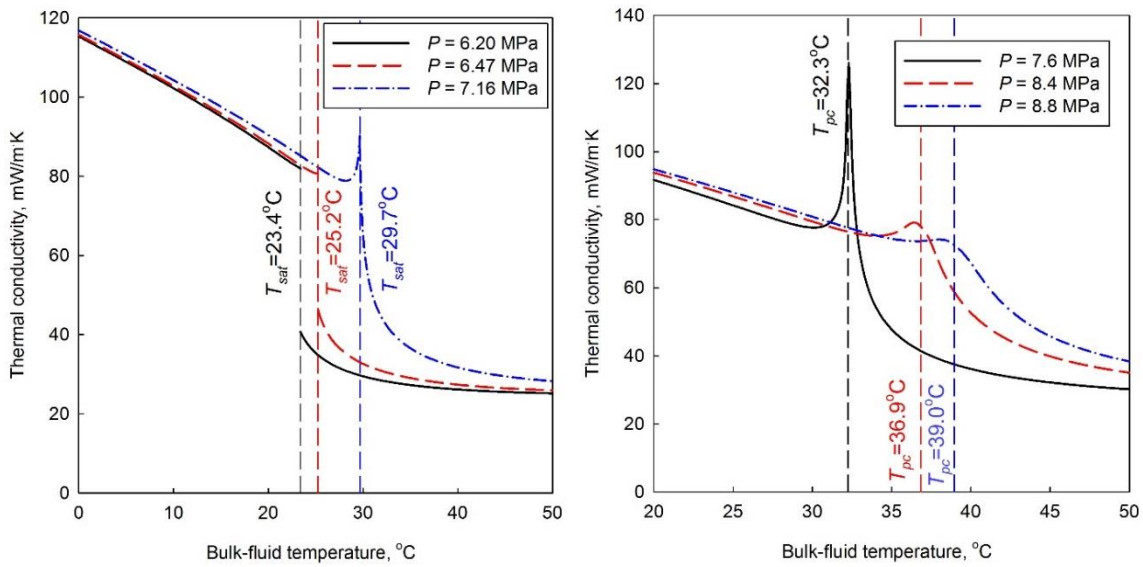

Figure 5.5. Thermal conductivity of CO_2 at three subcritical (a) and three supercritical (b) pressures.

There is a general similarity in the trends of specific heat, c_p, density, ρ, viscosity, μ, and thermal conductivity, k, between water and CO_2, at their respective SC states. Specifically, c_p has a symmetrical peak at certain temperature (T_{pc}); ρ and μ undergo a significant reduction around T_{pc}; and k has a small peak near T_{pc}, although it does not possess symmetry.

It is also important to realize that specific heat, thermal conductivity, and isobaric thermal expansion coefficient, β, all peak at specific, however, different temperatures at the SC state. These properties are plotted at 8.4 MPa in Figure 5.6. It is seen that the profiles of c_p and β are very similar. However, peaks in both decrease rapidly with pressure (e.g., see Figure 5.2 (b) for c_p). According to NIST REFPROP, maximal uncertainty in calculated values of c_p and β of SC CO_2 can be taken to be 1.5%. Thus, considering values of these properties at reference temperature T = 20 °C, pressures at which peaks become within the calculated uncertainty can be found. The corresponding pressure for c_p is 42.9 MPa, and that for β is 132.3 MPa. Both pressures are extremely high. However, consideration of the disappearance of peak in β elicits pressure at which SC CO_2 could be considered as compressed liquid.

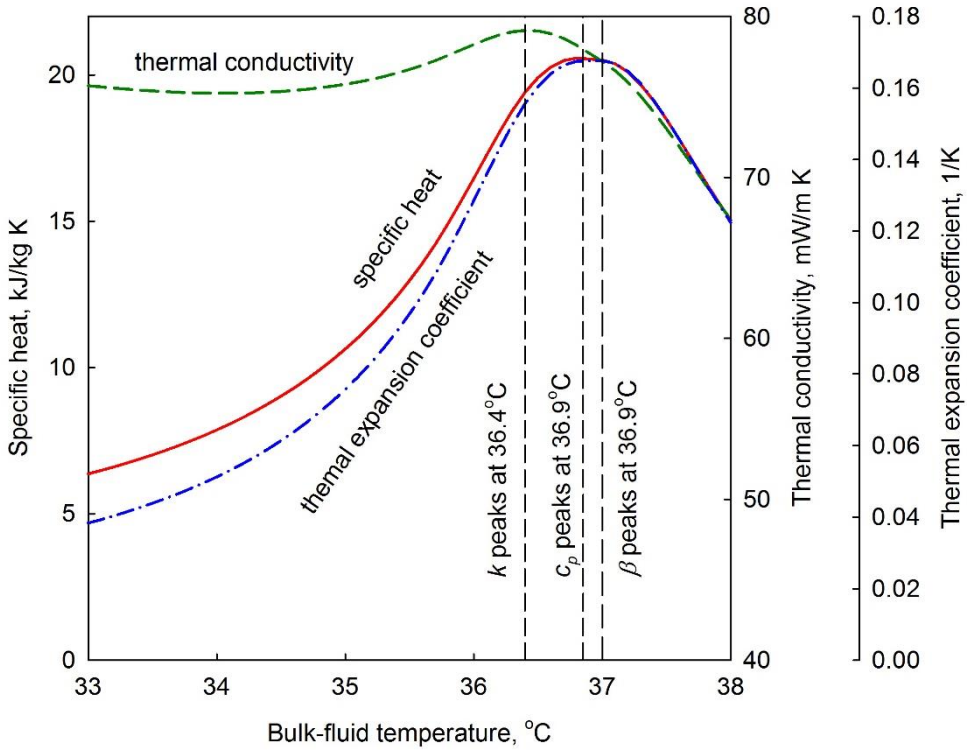

Figure 5.6. Peaks in specific heat, thermal conductivity, and isobaric thermal expansion coefficient of SC CO_2 at P = 8.4 MPa.

5.1. Proposed numerical definition of the width of the pseudocritical region.

The region of temperatures within which thermal and transport properties undergo such drastic changes is usually arbitrarily considered to be 2 – 5 °C wide. It may be observed in Figures 5.2 – 5.6. However, no exact numerical definition or the basis for the definition of the pseudocritical region was proposed before. Therefore, it was decided to compare the rate of change of the properties. Their derivatives were plotted in Figures 5.7 – 5.10. With the most recently updated properties of SCFs there is an increased confidence in numerical prediction of properties at different pressures.

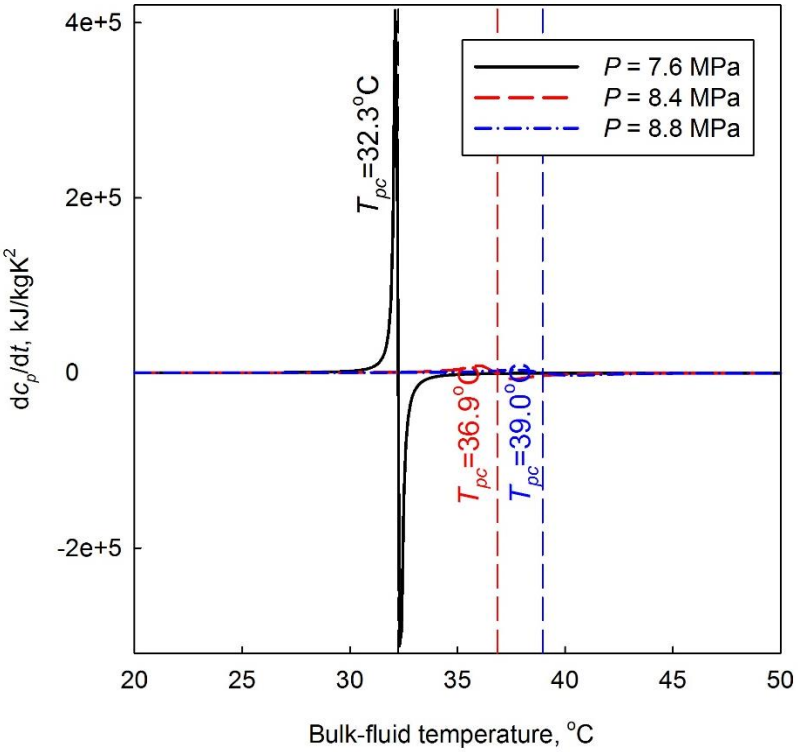

Figure 5.7. Specific heat derivative temperature dependence for three pressures.

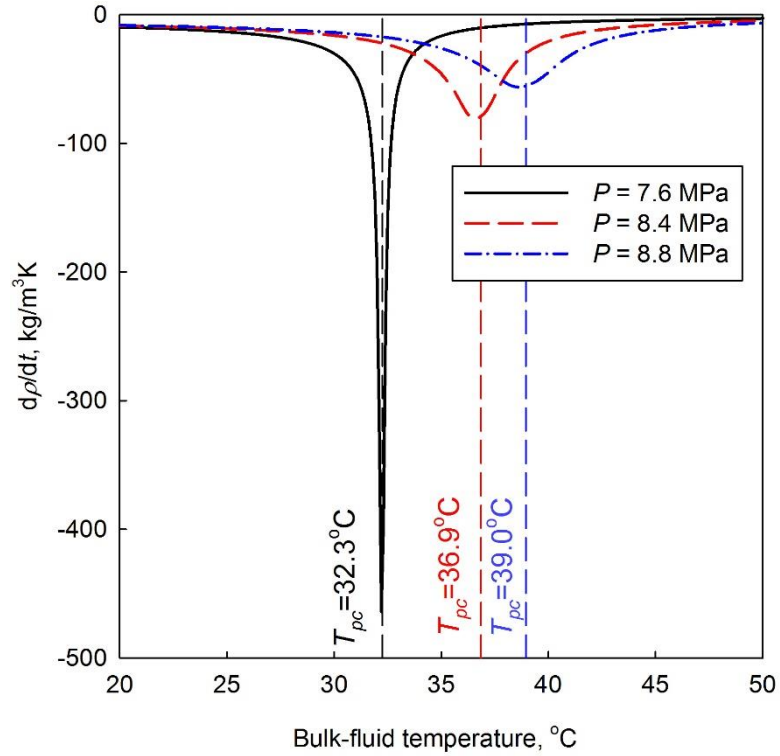

Figure 5.8. Density derivative temperature dependence for three pressures.

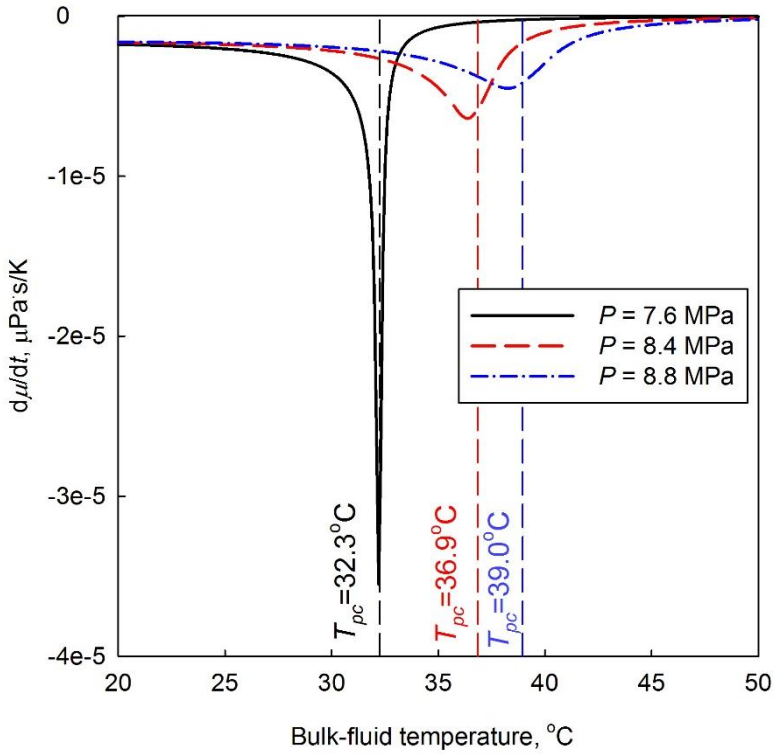

Figure 5.9. Viscosity derivative temperature dependence for three pressures.

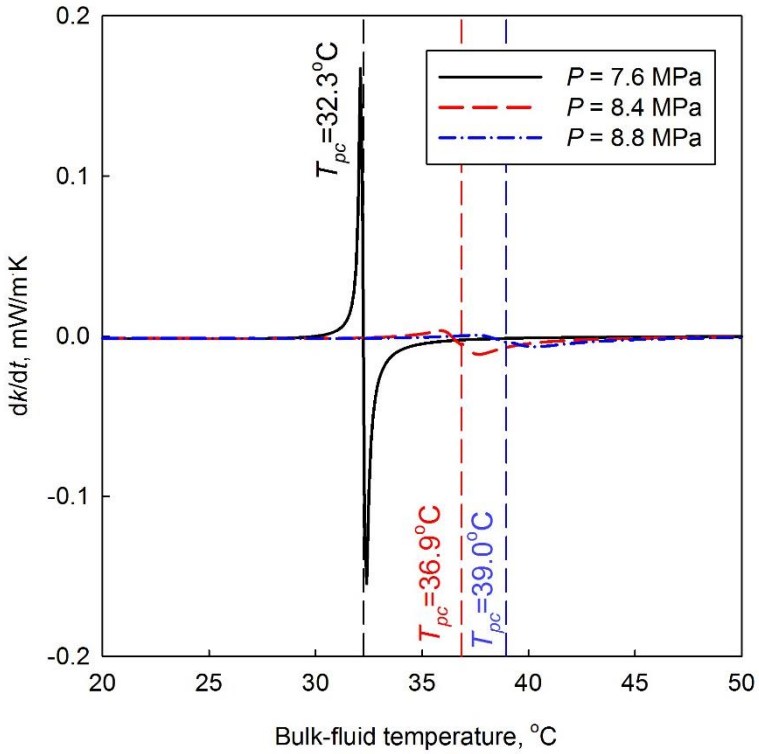

Figure 5.10. Thermal conductivity derivative temperature dependence for three pressures.

Figures 5.7 – 5.10 confirm the above mentioned conclusions about the temperature dependencies of the properties. However, it is additionally seen that the rate of change of properties decreases approximately 8 times with the increase of pressure from 1.03 to 1.14 times P_{cr}. The patterns of derivatives of c_p and k are remarkably similar. The patterns of derivatives of ρ and μ are even more similar. It is also interesting to see that the latter are very similar to the profile of negative c_p.

It is seen from Figures 5.2 – 5.5, 5.7 – 5.10 that the range of temperatures within which the rapid changes of properties widens with the change in pressure. It is proposed here to call these rapid changes as pseudocritical phase change. Since the change in c_p is nearly symmetrical around the pseudocritical temperature it appears reasonable to define the region of temperature within which the pseudocritical phase change occurs based on the changes in c_p.

The proposition is to define pseudocritical phase change region as the temperature range within which the absolute value of the increment in c_p with unit change in temperature relative to the value of c_p at T = 20 °C (approximately $0.96T_{pc}$) is more than 5%:

$$\left| \frac{dc_p(T)}{c_p(T = 0.96T_{cr})} \right| \geq 0.05 \tag{5.1}$$

Of course, this criterion is to determine the start and end of the rapid increase in c_p and should not be used in the proximity of the peak in c_p, where the derivative changes sign and may satisfy Eq. (5.1). The choice of temperature for the reference value of c_p is based on the fact that at this temperature the variation in c_p is negligible. The graphs of all properties at different pressures with the pseudocritical phase change region outlined are shown in Figures 5.11 – 5.13.

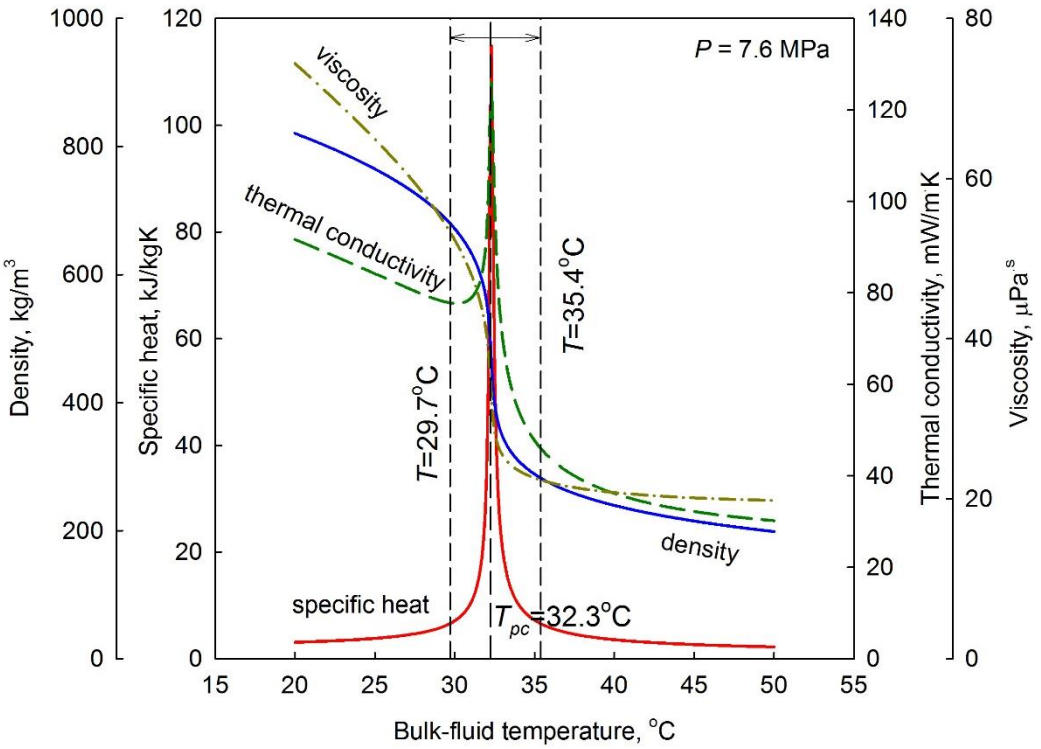

Figure 5.11. Major thermal and transport properties of CO_2 at 7.6 MPa.

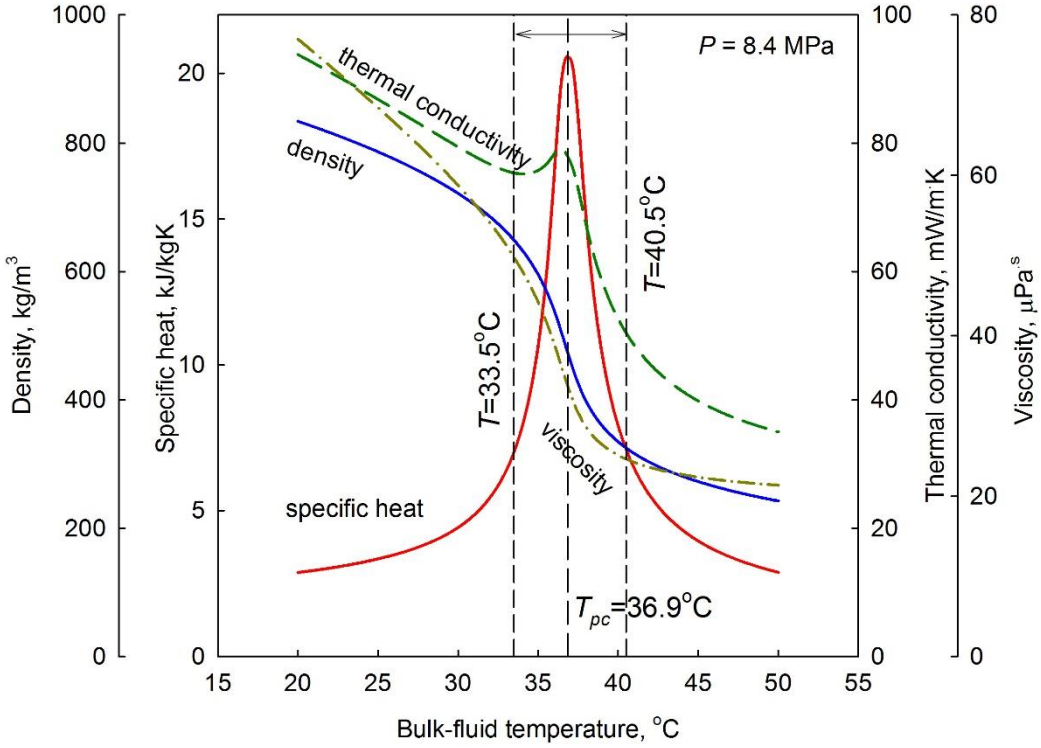

Figure 5.12. Major thermal and transport properties of CO_2 at 8.4 MPa.

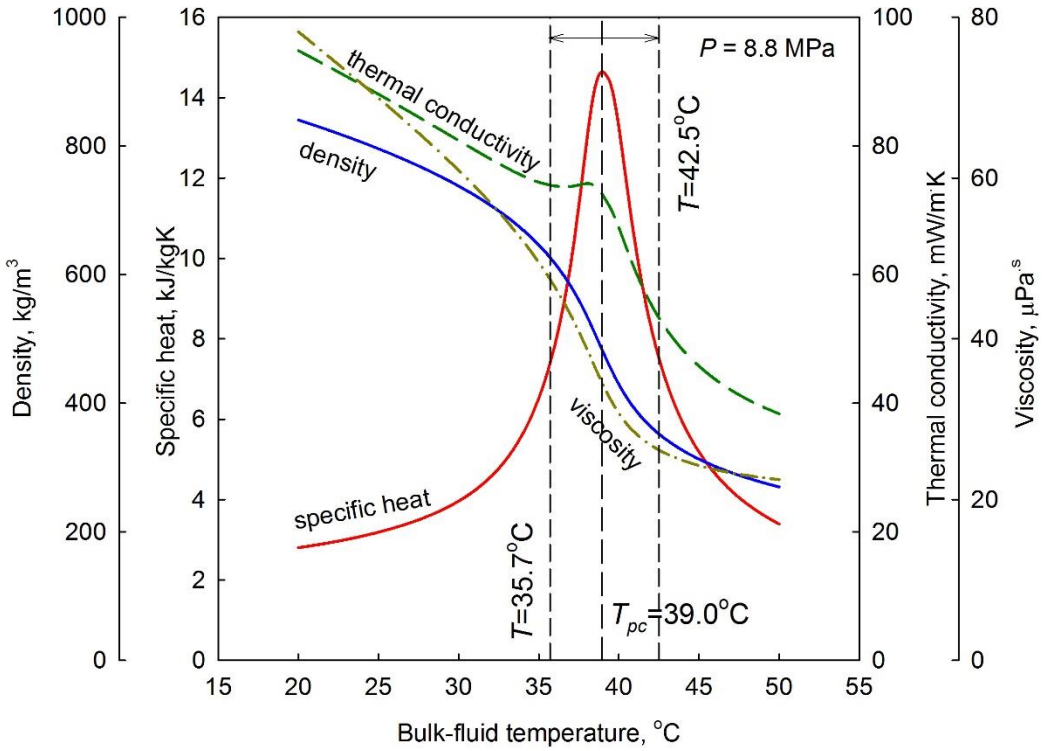

Figure 5.13. Major thermal and transport properties of CO_2 at 8.8 MPa.

As it is seen from Figures 5.11 – 5.13, the proposed definition is able to track the shift of the pseudocritical region. However, the widening of the region is not tracked. This is caused by the choice of the fixed temperature to define the reference c_p value. This can be mitigated by multiplying proposed 5% criterion by P_{cr} / P. Thus, the proposed numerical definition Eq. (5.1) of the borders of the pseudocritical phase change region is the following:

$$\left|\frac{dc_p(T)}{c_p(T=0.96T_{cr})}\right| \geq 0.05\left(\frac{P}{P_{cr}}\right) \tag{5.2}$$

5.2. Comparison of transport properties of CO_2 with those of water, and R134a at SC state.

It was discussed in Chapter 2 that approach based on comparison of the properties reduced to their values at pseudocritical temperature may lead to similar properties within pseudocritical region. To verify this, values of reduced specific heat, density, viscosity, and thermal conductivity were plotted in terms of the reduced temperature (to that of

critical state) for pressures equivalent to 25 MPa in water. The critical parameters of water, CO_2, and R134a are presented in Table 5.1.

Table 5.1 Critical parameters of water, CO_2, and R134a.

Fluid	P_{cr}, MPa	T_{cr}, K (°C)	ρ_{cr}, kg/m^3
Water	22.064	647.1 (373.95)	322.0
CO_2	7.3773	304.13 (30.98)	467.6
R134a	4.0593	374.21 (101.06)	511.9

The equivalent pressures (to 25 MPa in water) and the range of the compared temperatures are presented in Table 5.2.

Table 5.2. Range of compared temperatures of CO_2, and R134a at pressures equivalent to 25 MPa in water.

Fluid	P, MPa	T/T_{cr} range	T range, K (°C)
Water	25	0.8 – 1.2	517.7 – 776.5 (244.55 – 503.35)
CO_2	8.4	0.8 – 1.2	243.3 – 365.0 (-29.85 – 91.85)
R134a	4.6	0.8 – 1.2	299.4 – 449.1 (26.25 – 175.95)

Maximal temperature was set to $1.2T_{cr}$, because of R134a, for which this was the maximal temperature for which properties did not have to be extrapolated.

Figures 5.14 – 5.17 show the values of reduced specific heat, density, viscosity, and thermal conductivity, respectively.

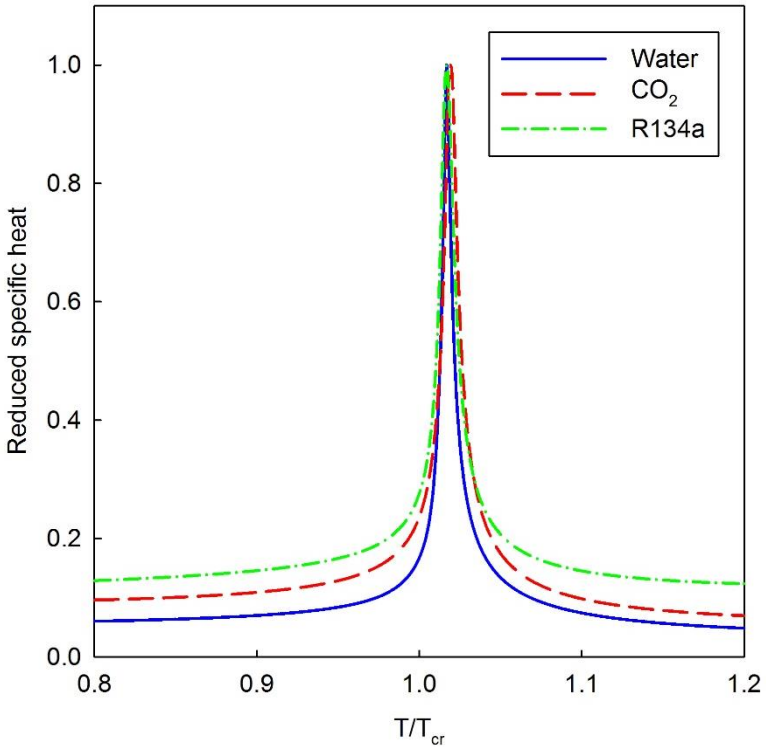

Figure 5.14. Comparison of the reduced values of specific heat of water, CO_2, and R134a.

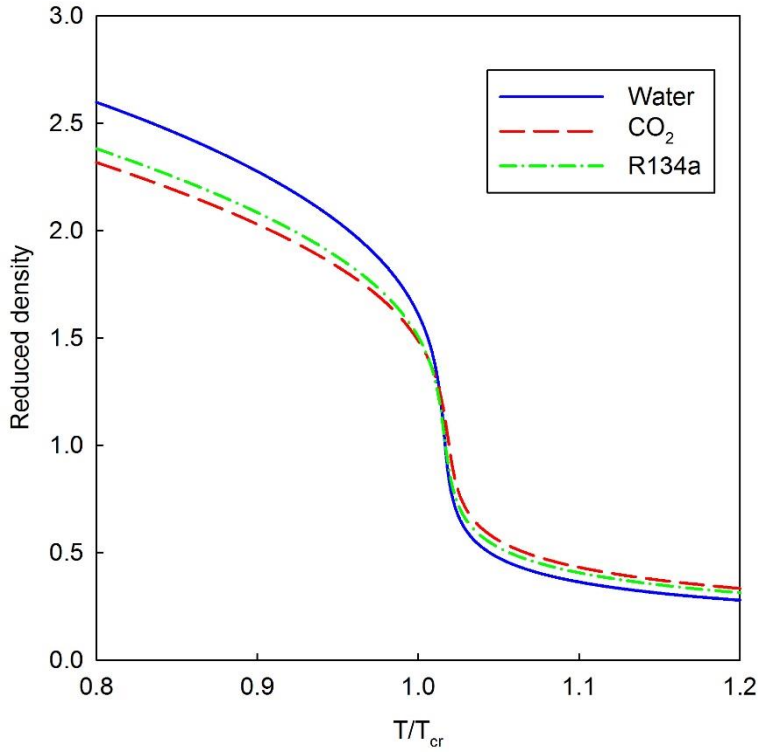

Figure 5.15. Comparison of the reduced values of density of water, CO_2, and R134a.

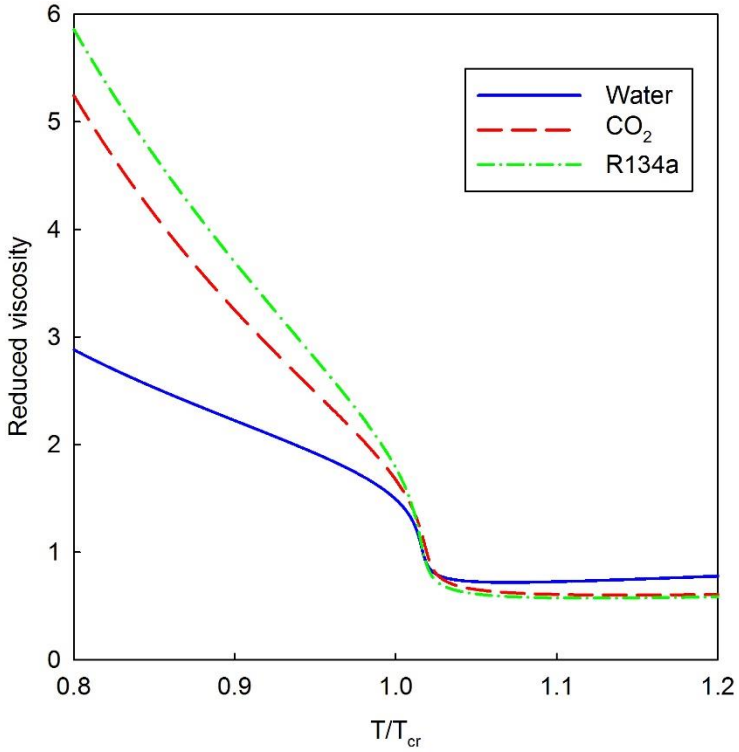

Figure 5.16. Comparison of the reduced values of viscosity of water, CO_2, and R134a.

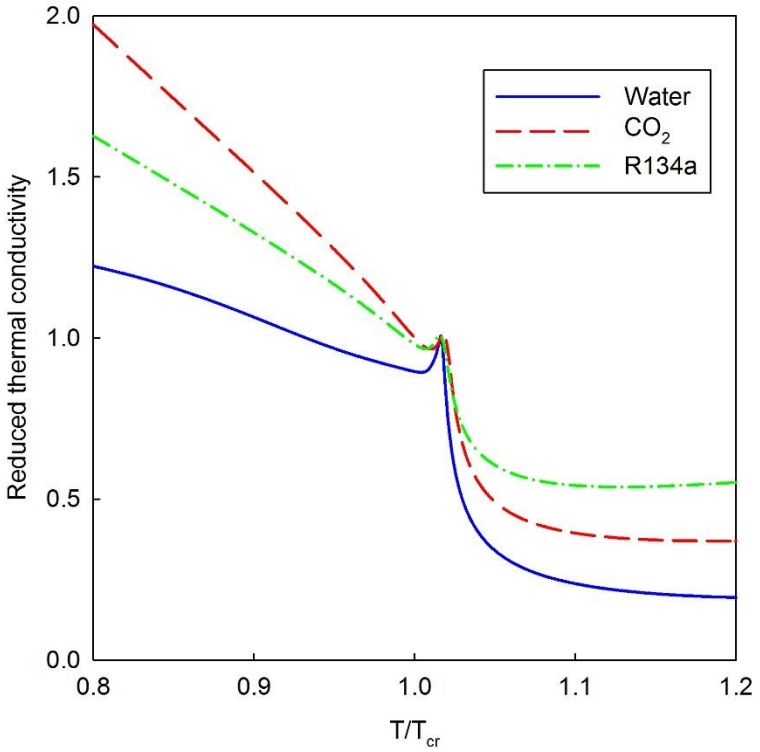

Figure 5.17. Comparison of the reduced values of thermal conductivity of water, CO_2, and R134a.

Consideration of Figures 5.14 – 5.17 reveals the following:

1) All reduced properties are extremely close to each other within a very narrow region around T_{pc}.
2) Outside of this region properties differ significantly. The difference is more pronounced in the cases of specific heat (see Figure 5.14) and thermal conductivity (see Figure 5.17). Thus, inclusion of the ratios of these properties into correlation may lead to its worse performance when used to model heat transfer in fluids different from CO_2.
3) Reduced densities and viscosities (see Figures 5.15 and 5.16) and are much closer beyond T_{pc} (gas-like state) than prior to T_{pc} (liquid-like state).
4) Values of reduced densities and viscosities of CO_2 and R134a are much closer to each other than to those of water.

Therefore, using correlations developed for SCW directly to model heat transfer in SC CO_2 (and vice versa) is prone to inaccuracies. Thus, modelling should be done by scaling operational conditions.

CHAPTER 6. METHODOLOGY

In this chapter:

1) Conventional methodology for the development of heat transfer correlations is thoroughly discussed.
2) Methodology for correlating the mass flux and the heat flux, at which DHT onsets, is discussed.
3) A new methodology for the development of heat transfer correlations, which is partially based on 1) and 2), is introduced and discussed.

6.1. Methodologies for development of heat transfer correlations

6.1.1. Development of heat transfer correlations for NHT

After data reduction and preliminary filtering of the data were done (as described in section 4.3), the next step was to distinguish data corresponding to NHT and IHT from those corresponding to DHT. This is a subjective process, since it relies purely on a visual check. Only the data within a run judged as belonging to DHT were removed. The readings affected by the entrance effect were removed as well, based on the visual check. Thus, 2209 points remained as the basis for the development of a heat transfer correlation for NHT and IHT.

It should be remembered that the literature review (Chapter 2) did not reveal any common approach to deciding which ratios of thermal and transport properties should be included in a heat transfer correlation. The most common where those based on density, viscosity, thermal conductivity, and average specific heat. The latter, however, is redundant since the average specific heat is included in the average Prandtl number. Thus, the ratio of specific heats would be used instead. Therefore, a heat transfer correlation describing forced convection to SCFs may be expressed as follows in most general way:

$$\mathbf{Nu} = const\mathbf{Re}^{n_1}\overline{\mathbf{Pr}}^{n_2}\left(\frac{\rho_{w\,or\,f}}{\rho_b}\right)^{n_3}\left(\frac{\mu_{w\,or\,f}}{\mu_b}\right)^{n_4}\left(\frac{k_{w\,or\,f}}{k_b}\right)^{n_5}\left(\frac{c_{p,w\,or\,f}}{c_{p,b}}\right)^{n_6} \qquad (6.1)$$

where dimensionless groups can be calculated at either bulk-fluid, wall, or film temperatures; thermal and transport properties are calculate at either wall or film temperature and divided by their values at bulk-fluid temperature; and *const* and powers n_1 … n_6 are fitted either using conventional step-by-step fitting approach (Incropera and DeWitt, 2002), linear least mean squares approach, used in the papers by Saltanov et al. 2013b; Saltanov et al. 2014b, or the weighted non-linear least mean squares approach, used in the papers by Gupta et al. 2013; Gupta et al. 2014. The first two approaches are applied to the expression (6.1) in logarithmic form. The third approach is more complicated and is usually implemented in the software for scientific calculations (such as Mathematica, Matlab, and SigmaPlot). The approach is based on the Levenberg – Marquardt algorithm usually referenced to the paper by Marquardt (1963).

While it could be shown by means of non-dimensional analysis that **Nu**, **Re**, and **Pr** form a basic set of non-dimensional groups to describe forced-convective heat transfer (see Appendix B), a rationale for including ratios of thermal and transport properties should be discussed separately. The discussion is based on the inspection of the continuity, conservation of momentum and conservation of energy equations (see Appendix B).

Density variation affects the radial transfer of momentum and heat. Additionally, as it was discussed in Chapter 1, variations in density along the vertical is the fundamental cause of buoyancy forces, which may become significant to affect the heat transfer at low mass fluxes.

Viscosity variation affects the radial transfer of momentum. Additionally, viscosity is the primary cause of the energy dissipation.

Variations in both thermal conductivity and specific heat affect the radial and axial energy transfer.

To illustrate the effect of the discussed properties, their ratios and comparison of c_p, **Pr**, $\overline{c_p}$, and $\overline{\mathbf{Pr}}$ are shown in Figures 6.1 – 6.8 for one of the AECL MR-1 loop runs.

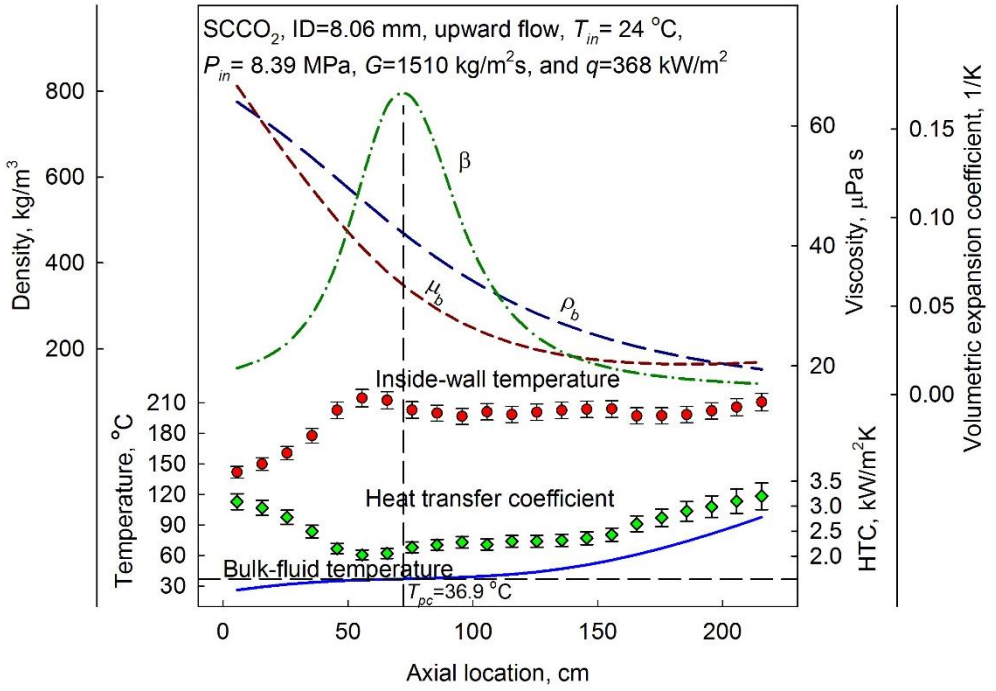

Figure 6.1. Density, viscosity, and volumetric expansion coefficient calculated at bulk-fluid temperature along the heated length.

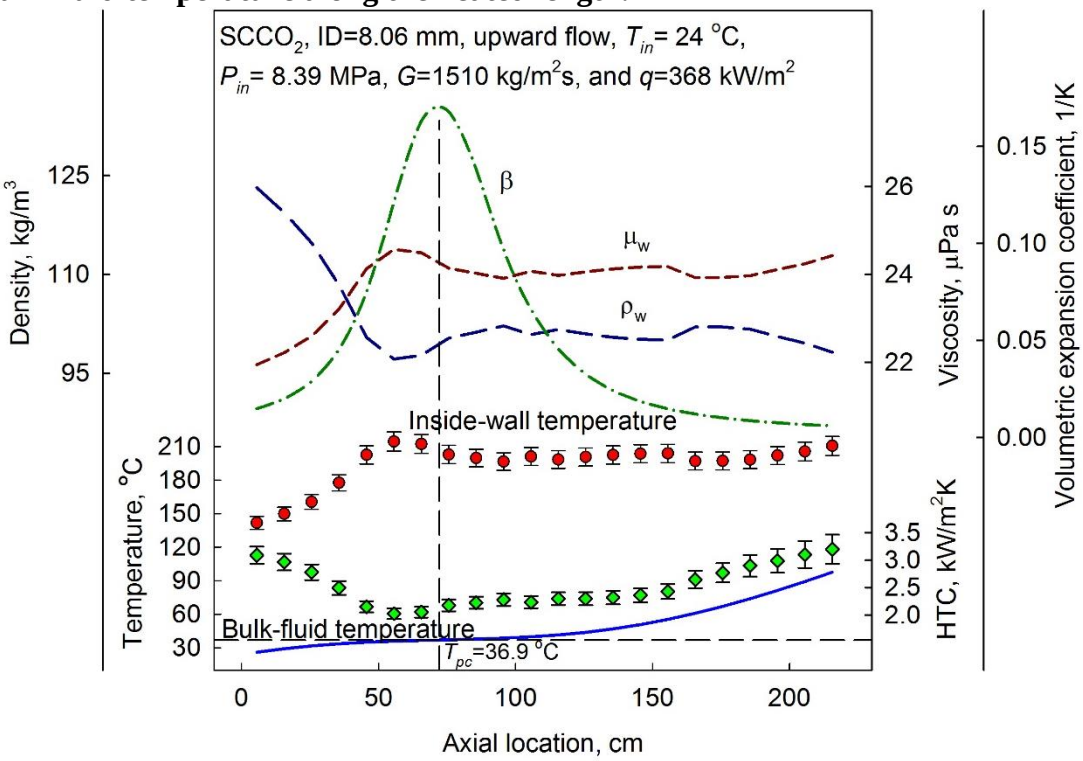

Figure 6.2. Density, viscosity, and volumetric expansion coefficient calculated at wall temperature along the heated length.

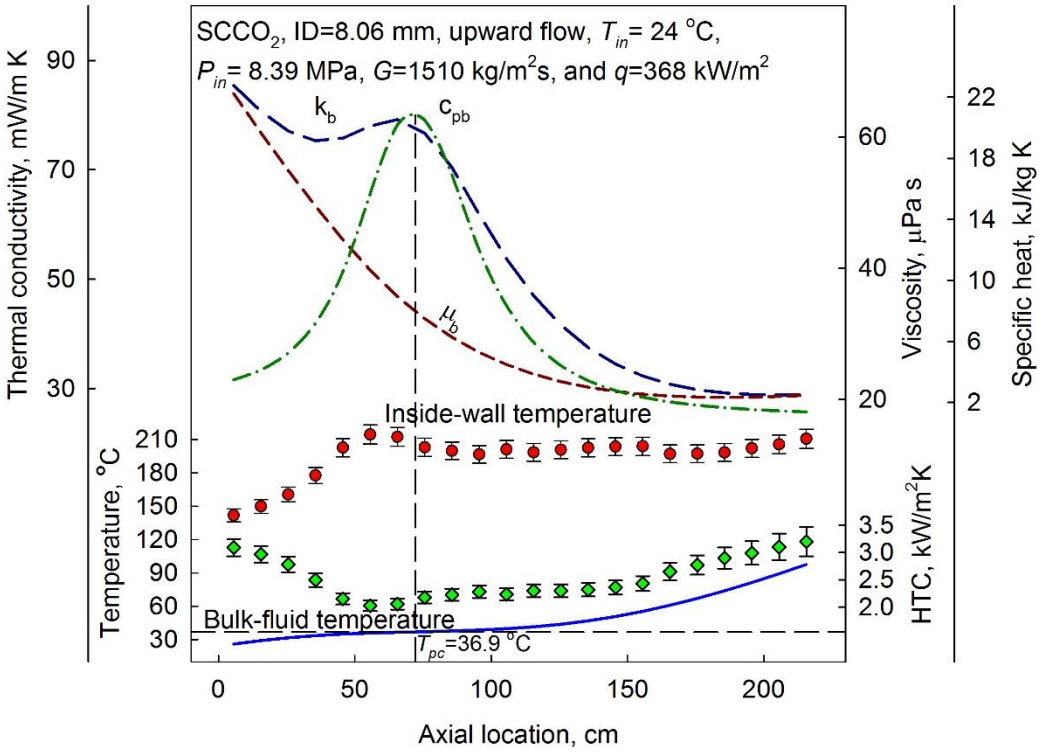

Figure 6.3. Thermal conductivity, viscosity, and specific heat calculated at bulk-fluid temperature along the heated length.

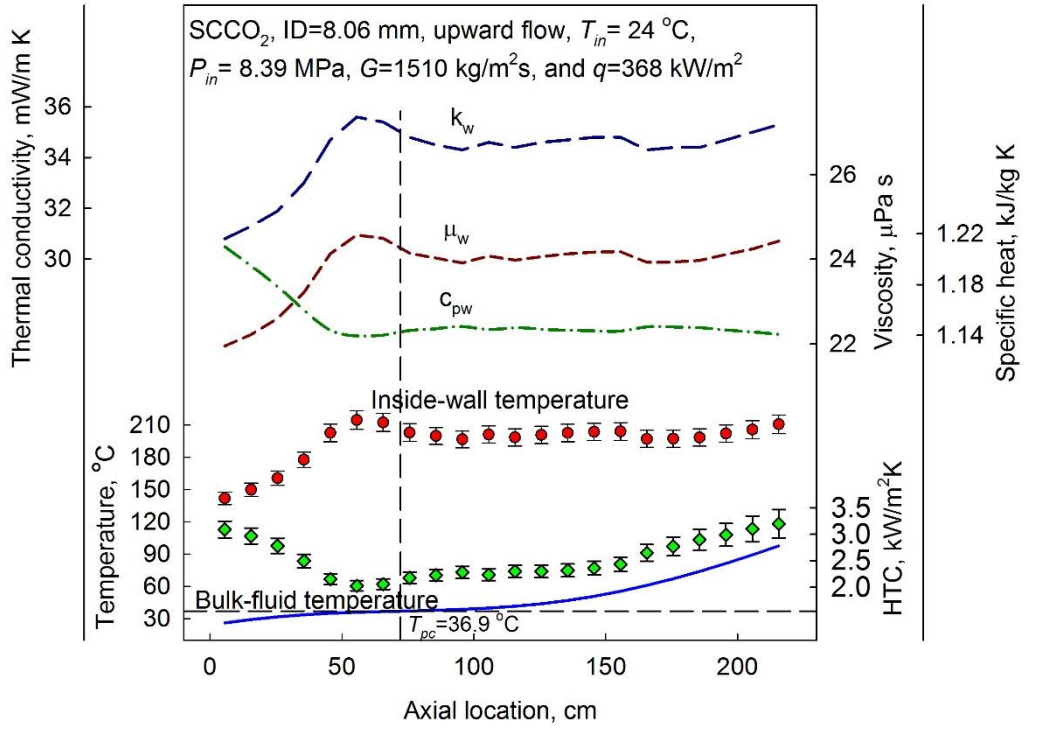

Figure 6.4. Thermal conductivity, viscosity, and specific heat calculated at wall temperature along the heated length.

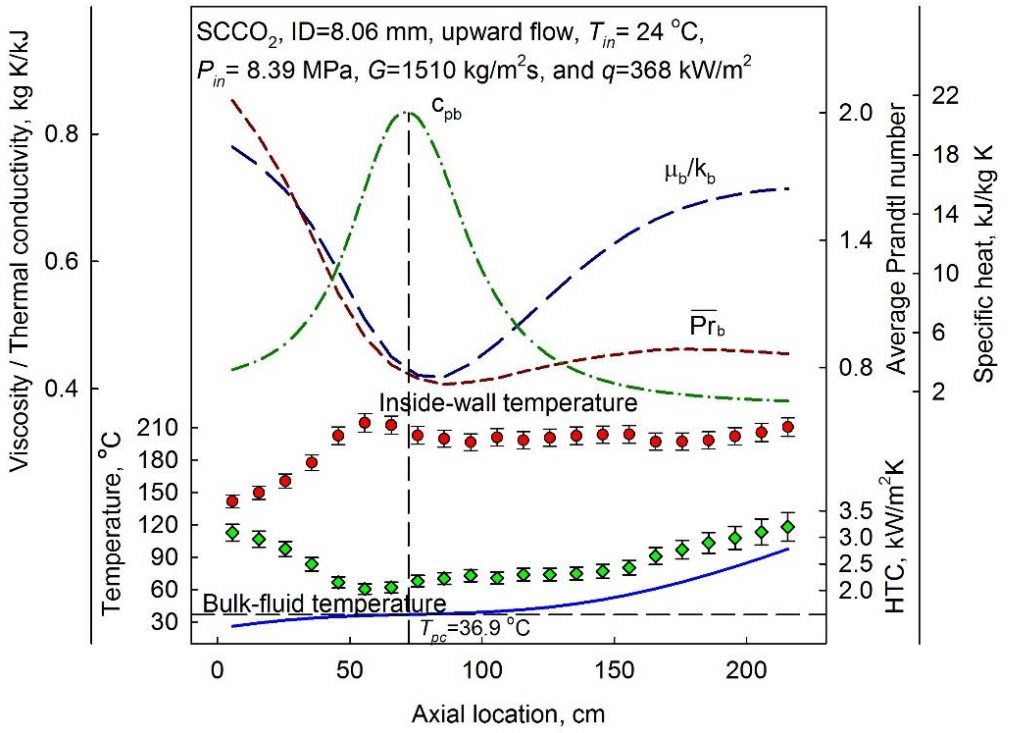

Figure 6.5. Viscosity over thermal conductivity ratio, average Prandtl number, and specific heat calculated at bulk-fluid temperature along the heated length.

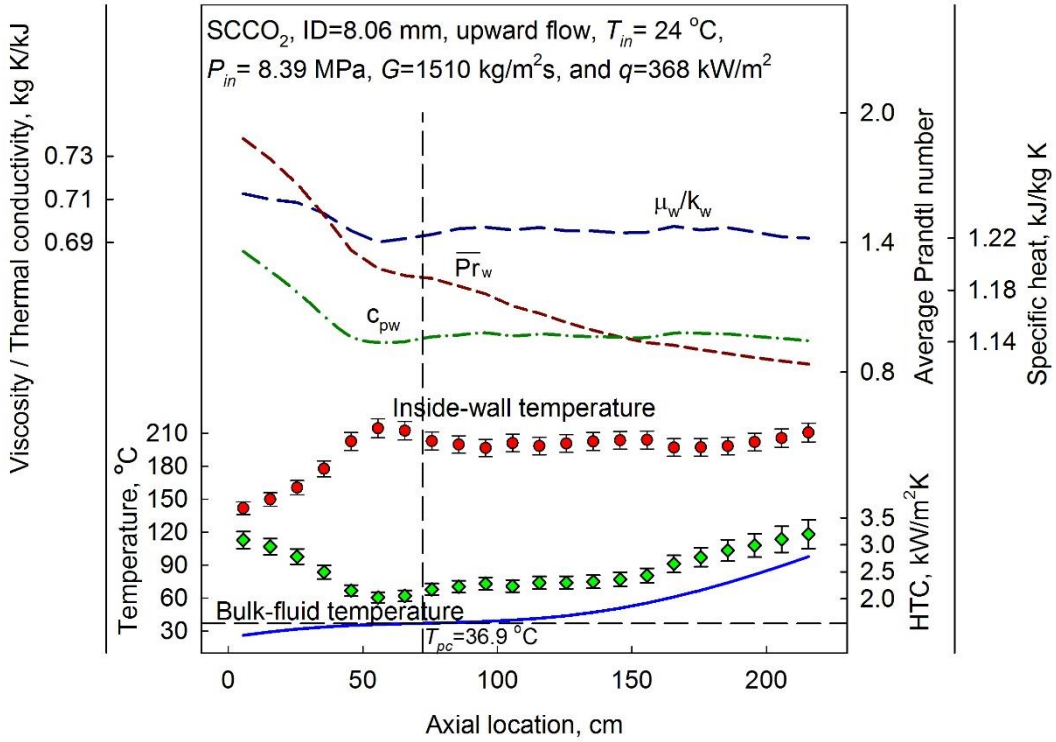

Figure 6.6. Viscosity over thermal conductivity ratio, average Prandtl number, and specific heat calculated at wall temperature along the heated length.

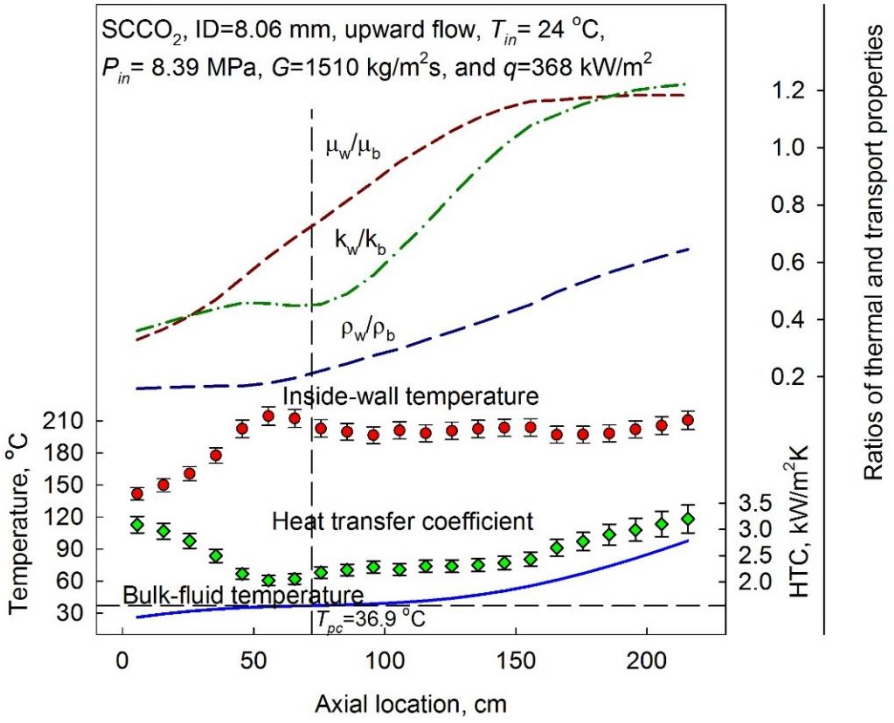

Figure 6.7. Ratios of viscosities, thermal conductivities, and density at wall- and bulk-fluid temperatures along the heated length.

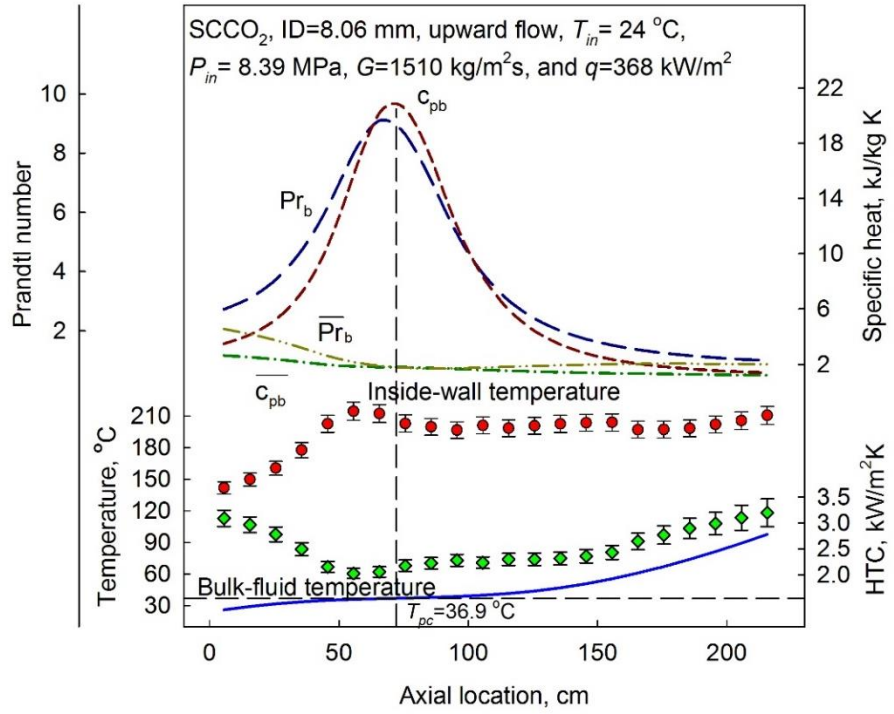

Figure 6.8. Effect of heat flux: comparison of specific heat and average specific heat, Prandtl number and average Prandtl number calculated at bulk-fluid temperature along the heated length.

However, with all of the described above properties having effect on forced-convective heat transfer, they should not be used all at once to obtain the final form Eq. (6.1). Rather each of the terms containing ratios of properties should be added one by one while checking *t*-statistics and improvement in R^2_{adj} statistics at each step.

Strictly speaking, if the *t*-statistic is below its critical value, the corresponding coefficient should be dropped at the next stage of improvement of the correlation. However, it was noticed that after the addition of another term, the *t*-statistic for a coefficient, which was non-meaningful at the previous step, improved and exceeded the critical value. Thus, this term was retained.

If *F*-statistics for the comparison of R^2_{adj} after the new term was added and R^2_{adj} of the previous form of the correlation is higher than the critical value, the reduction in the spread of data for the new correlation (i.e., containing an additional term) is considered to be meaningful.

After the correlation is obtained, the corresponding RMS for HTC and T_w are calculated. When assessing performance of a heat transfer correlation, RMS is typically calculated in the sense of percent deviations of HTC or T_w from the experimental values. The definition of RMS for HTC is as follows:

$$RMS = \sqrt{\frac{\sum_{i=1}^{n}\left(1-\frac{HTC_{calc,i}}{HTC_{\exp,i}}\right)^2}{n-1}} \tag{6.2}$$

RMS for T_w is calculated in the exact same way.

The maximal deviations of HTC and T_w should be reported as well, since after the rigorous reduction and filtering of the data they cannot be considered as just random outliers. The literature review showed that these are not usually reported, although they represent the maximal possible over- and under-estimations of the calculated parameters. Instead, average deviations are presented, which do not have much value.

The expression for calculating relative deviation for HTC is as follows:

$$\text{HTC deviation} = 1 - \frac{HTC_{calc,i}}{HTC_{\exp,i}} \tag{6.3}$$

A negative deviation means that predicted HTC is overestimated and the corresponding T_w is lower than the actual. Thus, the bigger the magnitude of the maximal negative deviation, the worse the performance of the correlation is. In the same way, the bigger the magnitude of the maximal positive deviation in T_w (underestimation of temperature), the worse the performance of the correlation is.

Additionally, the convergence of the correlation should be assessed. Potentially, inclusion of the term containing the ratios of specific heats may lead to numerical instability (see Appendix D). Therefore, if the correlation is found to be failing to converge even at one point, the term in the correlation responsible for this should be dropped; and the process of the assessment of the performance of the correlation should be repeated from the beginning.

Finally, the graphs in the form of calculated versus experimental values of HTCs and T_w should be plotted with the confidence band based on the chosen level of significance. Such representation shows the overall performance of a correlation. As a substitute, graphs of probability density function for the deviations or density function for the prediction of a correlation can be shown.

It should be noted that the conventional approach for the development of the correlation is based on the following steps: correlating **Nu** against **Re**; then correlating the ratio **Nu**/**Re** against **Pr**; then correlating the ratio **Nu/(RePr)** against ρ_w/ρ_b , and so on. However, the iterative fitting of the exponents of the terms of Eq. (6.1) was already done based on non-linear least mean squares approach in the works by Bishop et al. (1964), Swenson et al. (1965), and Yamagata et al. (1972). The main deficiency of the conventional approach is that the fitted exponents of the terms are not updated with the addition of the new terms to minimize the RMS.

6.1.2. Development of heat transfer correlations for the onset DHT

Literature review showed that there is no impartial numerical definition of the DHT. Therefore, the conventional procedure to establish the onset of DHT was used, similar to the one presented in the paper by Saltanov et al. (2014b). In this procedure, the data should be sorted by the ascending mass fluxes and ascending heat fluxes. For the given mass flux, heat flux, at which the increase in the wall temperature becomes non-linear and a "hump" in the distribution of wall temperatures along the test-section becomes visible, is judged as the minimal heat flux that leads to DHT.

6.1.3. Development of heat transfer correlations without distinguishing heat transfer mode

Literature review has shown that the vast majority of the existing correlations were developed for NHT and IHT. A few attempts to correlate buoyancy-induced DHT data were done by KAERI researchers. However, their results were unsatisfactory. Therefore, an innovative approach to correlate data without distinguishing heat transfer modes was developed (Saltanov et al. 2014a). The approach is based on the following proposed non-dimensional number[11]:

$$\mathbf{X} = \frac{h_b - h_{pc}}{q / G}, \tag{6.4}$$

where h_b - bulk-fluid specific enthalpy; h_{pc} – specific enthalpy at the pseudocritical temperature; and q / G – heat flux to mass flux ratio.

The idea in coming up with this non-dimensional number was the following. HTC is known to become non-linear in pseudocritical region, however, it stabilizes prior to and beyond this region. Many of the graphs in the previous papers had bulk-fluid specific enthalpy as an independent coordinate. Such choice seems to by unphysical for the following reason: in classical thermodynamics, enthalpy is introduced as a thermodynamic *potential*. Therefore, not only its absolute value depends on the chosen reference state, but

[11] This non-dimensional number can be viewed as an extension of the boiling number or as a modification of Stanton number. Although the non-dimensional number **X** was introduced in author's common papers with co-authors, it is the author of this thesis who invented this number.

it also carries *no physical meaning*. Just like for the electric potential, it is the *difference in the values between enthalpy values at two states*, which is meaningful. Therefore, the numerator of Eq. (6.4) has sense of the specific energy that should be added to the fluid at current state to reach the pseudocritical state. The denominator of Eq. (6.4) has a meaning of a specific rate of heat addition to the fluid. Thus, a large negative number may mean both a fluid at a temperature significantly below T_{pc} under average heat loading conditions and a fluid at temperature very close to T_{pc} under extremely low heat loading conditions.

It is proposed that the new approach to group data based on non-dimensional number **X** (see Eq. (6.4)) should be considered. This approach may be helpful in picking some general heat transfer trends. At the preliminary stage, the bins will be identified based on the commond trends in HTC from different experimental runs within the same range of **X**. Indeed, a comprehensive analysis of MR-1 loop data, which is presented in Appendix F, revealed that grouping the data into bins based on the values of the non-dimensional number **X** (see Eq. (6.4)) allows reducing RMS for HTC. Moreover, it was found by correlating the data using both bulk-fluid- and wall temperature approach (film-temperature approach was found to be worse than the other two) that within the pseudocritical region, these approaches tend to produce deviations of opposite signs. Thus, setting calculated HTC as the average of the two approaches allowed not only to reduce the spread of the data, but to also reduce RMS.

It was also found that the correlation having fewer number of the ratios of thermal properties and thus having slightly higher RMS than the correlation having all the possible properties, may have a more narrow maximal spread of the data. This is especially important in terms of overestimation of HTC, which leads to too optimistic values of T_w, which, in its turn, is potentially dangerous in engineering and power applications.

However, it was decided to include two other factors, which are not present in the general form of correlation (Eq. (6.1)).

One of these two factors is the reduced pressure. This term was chosen to be added based on the analysis of the effect of pressure (see Chapter 1). Additionally, since the peak in

the specific heat is a strong function of pressure, inclusion of the reduced pressure term should account for such dependency.

The other factor is the inlet effect. Based on the commonly recognized inlet effect, the following fade-away term was added to account for it:

$$1+38\frac{D}{z}, \tag{6.5}$$

where 38 is the ratio of the length of the calming unheated part of the test section (between the mixing chamber and the heated part) to the diameter of the test section, D; and z is the distance from the mixing chamber (not from the beginning of the heated part). The idea to use the fade-away term in such form came up during the discussion with Dr. Harvel, who mentioned that improvement in CFD modelling of the heat transfer to SCW flowing in a bare tube was made after the inclusion of the unheated calming part of the test section into the model. It is expected that the fade-away term in the form of Eq. (6.5) can account for the flow history.

It was also found that addition of the ratios of thermal conductivities and specific heats did not lead to the decrease of the standard error of **Nu**. From the other side, the values of thermal conductivity are known to be generally less accurate than the rest of the properties (for example, the peak in it was not recognized until the 90's). Therefore, inclusion of thermal conductivity would potentially require a re-evaluation of the exponents of the developed correlations if more accurate values become available later. Specific heat, in turn, is a strong function of temperature at SC pressure. Temperature variations even within a 0.1 K of the pseudocritical point would lead to significant variations in the values of specific heat. Therefore, inclusion of specific heat would lead to potentially strong dependence of the correlation performance on the convergence criteria.

It was discovered that the acceleration number Eq. (3.39) introduced by Cheng et al. (2009) allowed for a drastic reduction of the standard error of **Nu**. However, the correlations involving it and other ratios dependent on T_w failed to converge. Probably, Cheng et al.

(2009) noticed it as well, since they mentioned possible numerical instabilities of correlations relying on properties dependent on T_w.

Therefore, the general form of the correlations proposed for the binned data according to criterion Eq. (6.4) that do not require distinguishing heat transfer regimes is the following:

$$\mathbf{Nu} = const\mathbf{Re}^{n_1}\overline{\mathbf{Pr}}^{n_2}\left(\frac{\rho_w}{\rho_b}\right)^{n_3}\left(1+\frac{l_{unheated}}{l_{unheated}+z_{heated}}\right)^{n_4}\left(\frac{P}{P_{cr}}\right)^{n_5}\left(\frac{\mu_w}{\mu_b}\right)^{n_6}, \quad (6.6)$$

where the characteristic temperature is either of the bulk-fluid or that at the wall; $l_{unheated}$ is the calming region (distance between the mixing chamber and the beginning of the heated part of the test-section); z_{heated} is the distance from the beginning of the heated part of the test section. The **Nu** calculated from the correlation Eq. (6.6) is the local, not average, **Nu**.

According to the structure of the fully developed turbulent flow, it is expected that the inclusion of the ratios of densities and viscosities should account for the variation of the velocity profile across the flow.

Thus, there is hope that the correlation in the form of Eq. (6.6) will overcome the general deficiency of conventional correlations that are based on the local parameters and, thus, ignore the history of the flow.

During the fitting of the data grouped into bins it was found that at very high values of heat loading factors, the right border of the bin including the data around the pseudocritical point (i.e., data corresponding to both negative and positive values of **X**) should be extended towards higher values of **X** to reduce the RMS.

It is important to emphasize that there is no need to remove *any* points because of the possible entrance effects or because of the presence in the DHT region.

Finally, it should be reminded that the proposed approach to group data according to the criterion Eq. (6.4) is innovative and has never been discussed in the open literature.

CHAPTER 7. DEVELOPED CORRELATIONS

The three correlations (Mokry et al., 2009; Gupta et al., 2011; and Swenson et al., 1965) that were shown in the literature review (see Chapter 2) to be the most accurate in predicting HTCs for SCFs were tested against the final AECL dataset containing NHT and IHT points only. All of these correlation were originally developed based on data for SCW. The summary of the performance of these correlations is given in Table 7.1. Here and onwards only the Q-approach is used (with the convergence criteria set as the difference between the two successive iterations of T_w becoming less than 0.1 K) to assess the performance of the correlations, unless mentioned otherwise. Comparisons of Q- and T-approach, and convergence criteria are given in the Appendix C.

Table 7.1. Summary of the performance of the three most accurate correlations for NHT and IHT dataset.

Statistics	**Characteristic temperature**		
	Mokry et al. (2009)	**Gupta et al. (2011)**	**Swenson et al. (1965)**
RMS of HTC, %	108.2	113.4	122.9
RMS of T_w, %	4.6	3.5	4.2
HTC spread, %	–374.7 - +52.8	–414.7 - +35.2	–483.1 - +33.0
T_w spread, %	–37.5 - +10.5	–10.0 - +13.1	–9.1 - +14.9

It is obvious from Table 7.1 that even the most recent and the most accurate correlations developed for SCW are not directly applicable to SC CO_2. Also, it should be emphasized that all of these correlations contained ratios of different thermal properties and were based on different characteristic temperatures. Moreover, the correlation by Swenson et al. (1965) was based on extremely old properties, prior to those established by now obsolete 1967 formulation (Schmidt, 1969; IAPWS, 2005). Another observation from Table 7.1 suggests that a low RMS of T_w does not guarantee low RMS of HTC. Finally, all the correlations have asymmetrical spread in HTC tending to over-predict HTC to a larger degree rather than to under-predict it. To assure that this is the case, the plots comparing calculated and experimental values of HTCs and T_w, as well as plots of relative deviations of HTCs and T_w were made (see Figures 7.1 – 7.6).

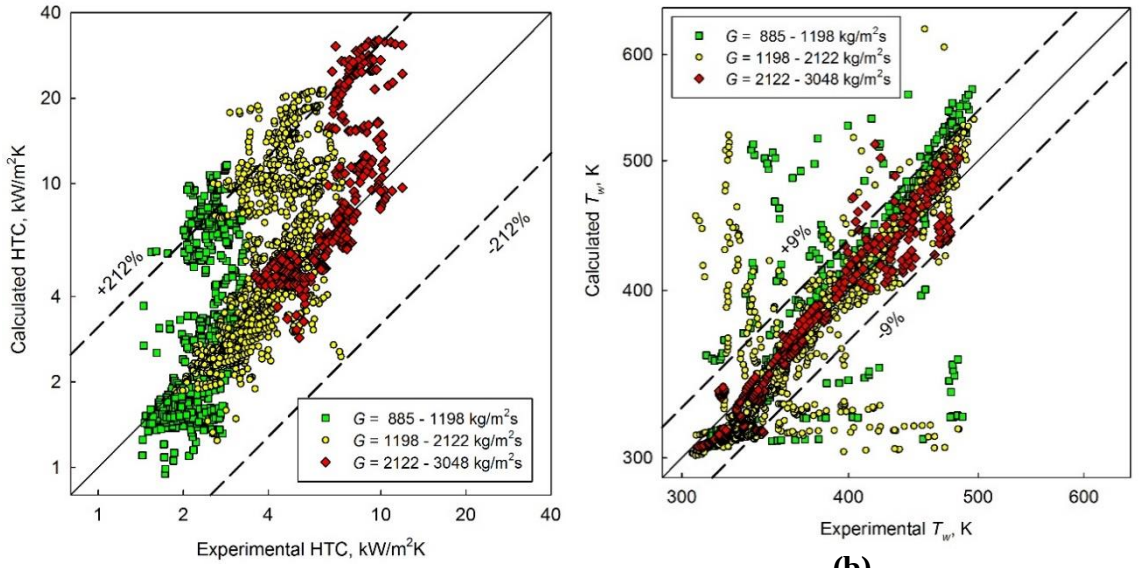

(a) **(b)**

Figure 7.1. Calculated vs experimental values of HTC (a) and T_w (b) using Mokry et al. (2009) correlation (data on upward flow of SC CO_2 in a bare tube).

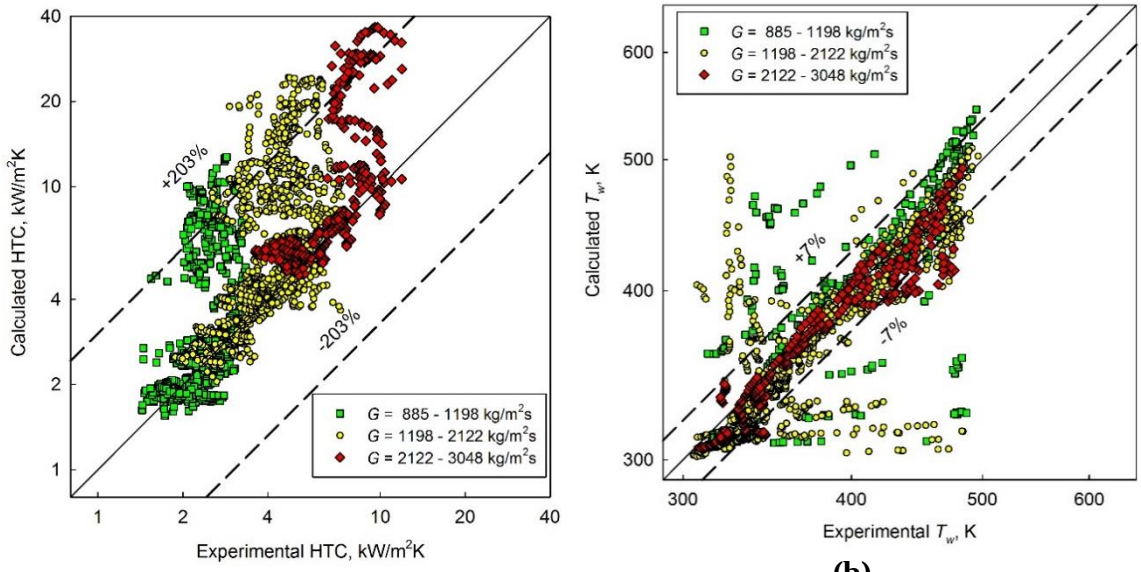

(a) **(b)**

Figure 7.2. Calculated vs experimental values of HTC (a) and T_w (b) using Gupta et al. (2011) correlation (data on upward flow of SC CO_2 in a bare tube).

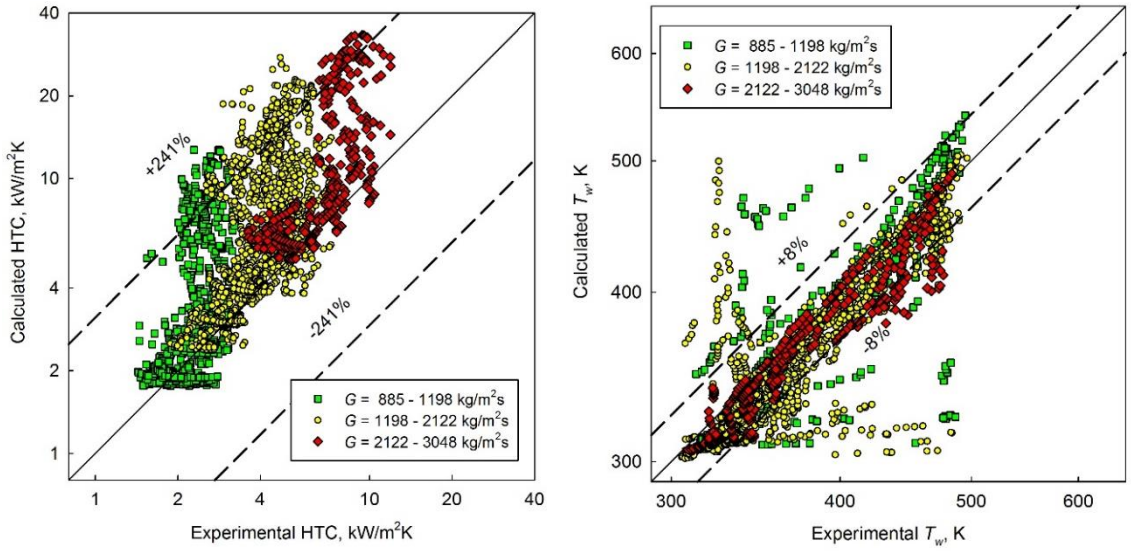

(a) **(b)**

Figure 7.3. Calculated vs experimental values of HTC (a) and T_w (b) using Swenson et al. (1965) correlation (data on upward flow of SC CO_2 in a bare tube).

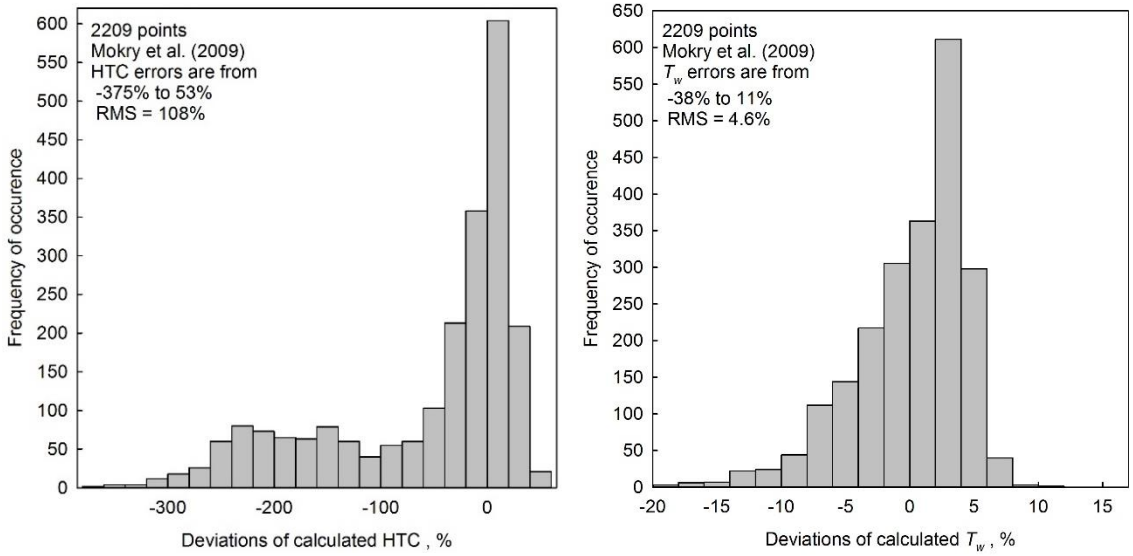

(a) **(b)**

Figure 7.4. Distribution of relative deviations of HTC (a) and T_w (b) using Mokry et al. (2009) correlation (data on upward flow of SC CO_2 in a bare tube).

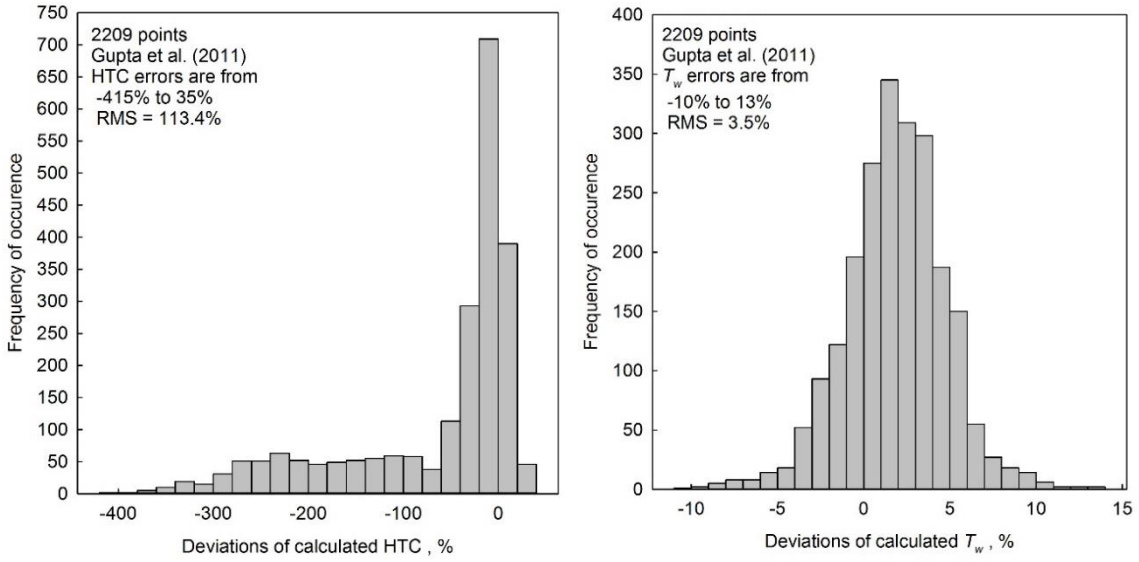

(a) **(b)**

Figure 7.5. Distribution of relative deviations of HTC (a) and T_w (b) using Gupta et al. (2011) correlation (data on upward flow of SC CO_2 in a bare tube).

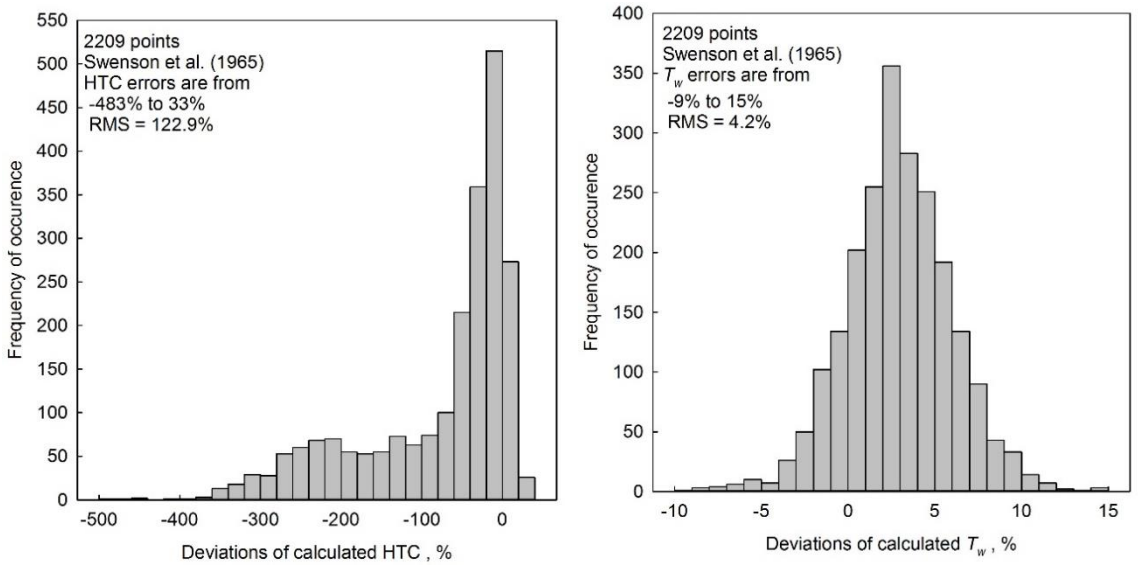

(a) **(b)**

Figure 7.6. Distribution of relative deviations of HTC (a) and T_w (b) using Swenson et al. (1965) correlation (data on upward flow of SC CO_2 in a bare tube).

Figures 7.1 – 7.6 confirm the conclusions of the numerical assessment of the performance of the best correlations developed for NHT and IHT regimes for water. These correlations are not applicable to wide range of SC CO_2 experimental parameters, because they tend to

overestimate HTCs. However, it is seen from Figure 7.1 – 7.3 that these correlations perform well at high mass fluxes ($G \geq 2122$ kg/m^{2}s).

The above analysis confirms the need to develop a separate set of correlations for the finalized AECL dataset for SC CO_2.

7.1. Correlations for NHT and IHT

As discussed in Chapter 6, the conventional approach to correlate heat transfer data consists of step-by-step fitting of the data by adding consequently the most important non-dimensional groups. This approach was tested for the finalized AECL data set containing data points corresponding to the NHT and IHT regimes. The results for the bulk-fluid temperature approach are shown in the Figures 7.7 – 7.9.

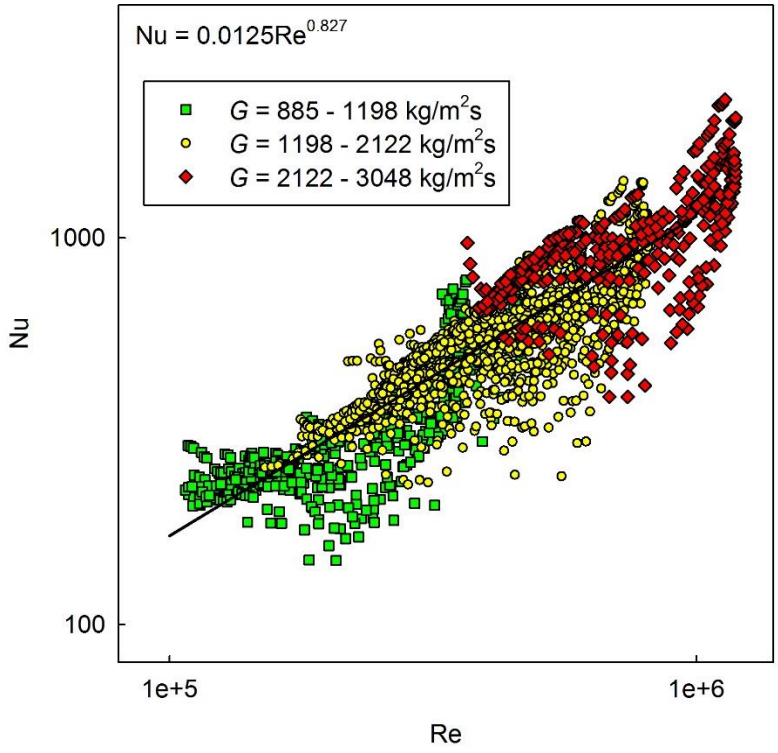

Figure 7.7. Linear least mean squares approach to correlate Nu vs Re (data on upward flow of SC CO_2 in a bare tube).

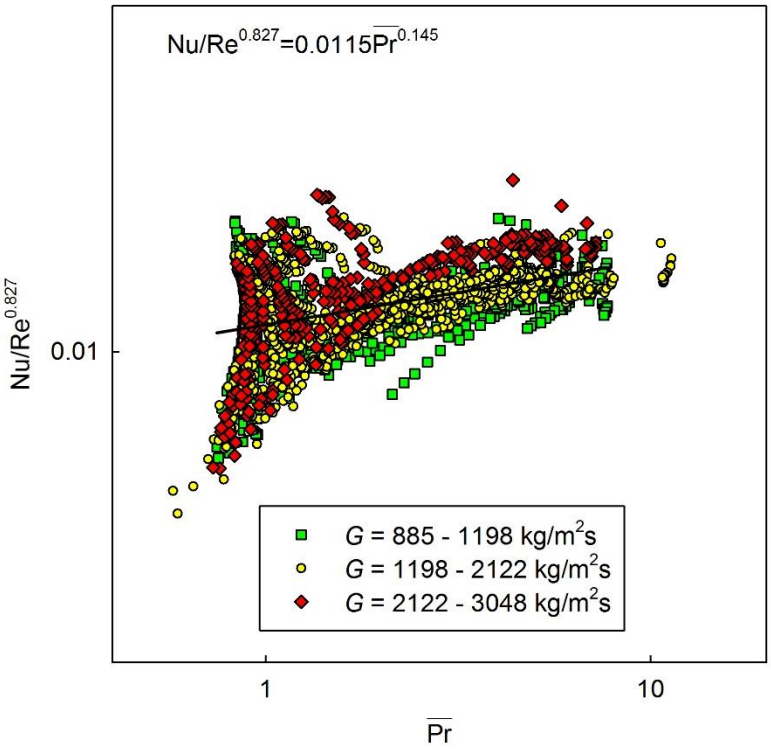

Figure 7.8. Linear least mean squares approach to correlate Nu/Re vs $\overline{Pr}$ (data on upward flow of SC CO_2 in a bare tube).

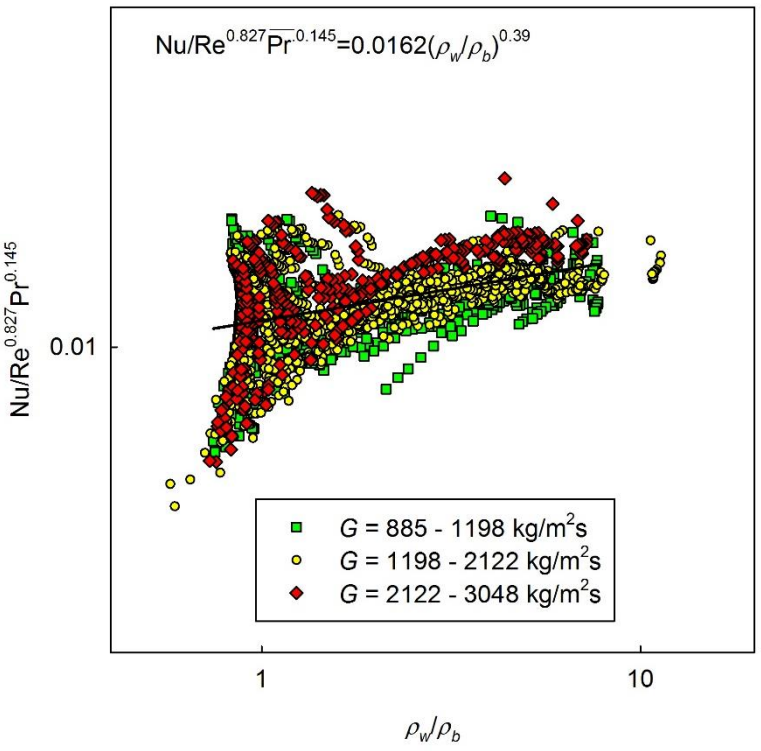

Figure 7.9. Linear least mean squares approach to correlate $Nu / Re\overline{Pr}$ vs ρ_w / ρ_b.

It is seen that **Re** (ratio of inertial forces over the viscous) has the strongest influence on the forced-convective heat transfer. Since the experimental data cover a much wider range of **Re** than of any other property, the effect of $\overline{\mathbf{Pr}}_\mathbf{b}$ and $\frac{\rho_w}{\rho_b}$ is less pronounced. Thus the preliminary correlation according to the conventional approach has the following form:

$$\mathbf{Nu_b} = 0.0162\mathbf{Re_b^{0.827}}\overline{\mathbf{Pr}}_\mathbf{b}^{\mathbf{0.145}}\left(\frac{\rho_w}{\rho_b}\right)^{0.39} \tag{7.1}$$

If the linear least squares approach is used to the same data, the following correlation is obtained:

$$\mathbf{Nu_b} = 0.0069\mathbf{Re_b^{0.891}}\overline{\mathbf{Pr}}_\mathbf{b}^{\mathbf{0.249}}\left(\frac{\rho_w}{\rho_b}\right)^{0.418} \tag{7.2}$$

If the weighted non-linear least squares approach is used to the same data, the following correlation is obtained:

$$\mathbf{Nu_b} = 0.0060\mathbf{Re_b^{0.901}}\overline{\mathbf{Pr}}_\mathbf{b}^{\mathbf{0.256}}\left(\frac{\rho_w}{\rho_b}\right)^{0.455} \tag{7.3}$$

As one can see, the difference between Eq. (7.1) – (7.3) is minor. The comparison of the performance of correlations Eq. (7.1) – (7.3) is summarized in Table 7.2.

Table 7.2. Summary of the performance of the preliminary correlations.

Statistics	**Approach**		
	conventional Eq. (7.1)	**linear Eq. (7.2)**	**weighted non-linear Eq. (7.3)**
RMS of HTC, %	21.9	21.4	20.9
RMS of T_w, %	3.6	3.8	4.4
HTC spread, %	–162.3 - +45.2	–149.6 - +46.3	–135.3 - +53.1
T_w spread, %	–14.1 - +17.9	–19.4 - +16.6	–26.2 - +15.4

While the smallest T_w RMS is obtained using the conventional approach, the smallest HTC RMS is obtained using the weighted non-linear least mean squares approach. The lowest maximal underestimation is attained when using the latter approach, as well. It seen that spread of data is biased towards overestimation of HTCs. Therefore, Eqs. (7.1) – (7.3) are not final and not recommended for use.

Therefore, based on the methodology discussed in Section 2.4.1, the following correlations for NHT and IHT were fitted to the lowest standard error of estimate based on 2209 points.

$$\mathbf{Nu_b} = 0.0057\mathbf{Re_b^{0.936}}\overline{\mathbf{Pr}}_{\mathbf{b}}^{\mathbf{-0.338}}\left(\frac{\rho_w}{\rho_b}\right)^{1.157}\left(\frac{\mu_w}{\mu_b}\right)^{-2.561}\left(\frac{k_w}{k_b}\right)^{1.586}\left(\frac{c_{p,w}}{c_{p,b}}\right)^{-0.324} \quad (7.4)$$

$$\mathbf{Nu}_w = 0.0057\mathbf{Re_w^{0.936}}\overline{\mathbf{Pr}}_{\mathbf{w}}^{\mathbf{-0.338}}\left(\frac{\rho_w}{\rho_b}\right)^{1.157}\left(\frac{\mu_w}{\mu_b}\right)^{-1.288}\left(\frac{k_w}{k_b}\right)^{0.248}\left(\frac{c_{p,w}}{c_{p,b}}\right)^{-0.324} \quad (7.5)$$

$$\mathbf{Nu_f} = 0.0051\mathbf{Re_f^{0.935}}\overline{\mathbf{Pr}}_{\mathbf{f}}^{\mathbf{-0.245}}\left(\frac{\rho_f}{\rho_b}\right)^{1.468}\left(\frac{\mu_f}{\mu_b}\right)^{-1.569}\left(\frac{k_f}{k_b}\right)^{0.372}\left(\frac{c_{p,f}}{c_{p,b}}\right)^{-0.375} \quad (7.6)$$

It was a surprise to get identical constants, and powers for **Re**, $\overline{\mathbf{Pr}}$, and ratios of densities and specific heats for bulk-fluid- and wall temperature approaches. However, the effect of viscosity and thermal conductivity turned out to be different for these two approaches. It is important to emphasize that literature review (Chapter 2) revealed that there is no consistent methodology for choosing ratios of thermal and transport properties and verifying the difference in the performance of the correlations based on different characteristic temperature, but having the same ratios of thermal and transport properties.

The summary of the performance of the correlations Eqs. (7.4) – (7.6) is given in Table 7.3. The statistics were obtained using four significant digits for the fitted parameters.

Table 7.3. Summary of the performance of the correlations for NHT.

Statistics	**Characteristic temperature**		
	bulk-fluid	**wall**	**film**
RMS of HTC, %	15.3	15.3	15.0
RMS of T_w, %	3.1	3.1	3.1
HTC spread, %	–102.8 - +41.6	–102.8 - +41.6	–98.2 - +46.9
T_w spread, %	–22.1 - +14.0	–22.0 - +14.0	–28.9 - +13.1

Thus, the film-temperature approach produced the lowest RMS in HTC and the lowest overestimation in HTC. The bulk-fluid- and the wall-temperature approach produced

identical statistics and thus can be used interchangeably. However, all of the correlations Eqs. (7.4) – (7.6) failed to converge for a different number of points: one point (bulk-fluid temperature approach), two points (wall temperature approach), and four points (film temperature approach). The convergence was not reached because of the instability, but because of the proximity of iterated wall temperatures to T_{pc}. The maximal deviation was 1.2 K from the actual temperature. The failure to converge was mainly caused by the inclusion of the ratio of specific heats, which are very sensitive to variations even within 0.1 K around the pseudocritical points. Thus a flexible convergence criteria, allowing convergence within 1.2 K, may be used.

The next best fit to the data was performed by dropping the term containing the ratios of specific heats. The rationale was to develop correlations, which would not be prone to entering infinite convergence loop. The following three correlations were developed at the next stage:

$$\mathbf{Nu_b} = 0.0052\mathbf{Re_b^{0.937}}\overline{\mathbf{Pr}}_\mathbf{b}^{\mathbf{-0.242}}\left(\frac{\rho_w}{\rho_b}\right)^{0.854}\left(\frac{\mu_w}{\mu_b}\right)^{-1.37}\left(\frac{k_w}{k_b}\right)^{0.426} \tag{7.7}$$

$$\mathbf{Nu}_w = 0.0052\mathbf{Re_w^{0.937}}\overline{\mathbf{Pr}}_\mathbf{w}^{\mathbf{-0.242}}\left(\frac{\rho_w}{\rho_b}\right)^{0.854}\left(\frac{\mu_w}{\mu_b}\right)^{-0.195}\left(\frac{k_w}{k_b}\right)^{-0.816} \tag{7.8}$$

$$\mathbf{Nu_f} = 0.0034\mathbf{Re_f^{0.957}}\overline{\mathbf{Pr}}_\mathbf{f}^{\mathbf{-0.143}}\left(\frac{\rho_f}{\rho_b}\right)^{1.08}\left(\frac{\mu_f}{\mu_b}\right)^{-0.313}\left(\frac{k_f}{k_b}\right)^{-0.839} \tag{7.9}$$

It is seen that similar to the correlations obtained at the previous step, the exponents of **Re**, $\overline{\mathbf{Pr}}$, and ratios of densities are the same, meaning that these parameters have the highest descriptive ability.

The summary of the performance of the correlations Eqs. (7.7) – (7.9) is given in Table 7.4. The statistics were obtained using four significant digits for the fitted parameters.

Table 7.4. Summary of the performance of the final correlations for NHT.

Statistics	Characteristic temperature		
	bulk-fluid	wall	film
RMS of HTC, %	16.6	16.6	16.7
RMS of T_w, %	3.2	3.2	3.5
HTC spread, %	–123.8 - +38.6	–123.8 - +38.6	–115.3 - +42.3
T_w spread, %	–17.8 - +14.2	–17.8 - +14.2	–19.5 - +13.7

All of the developed correlations Eqs. (7.1) – (7.9) are valid within the following range of experimental parameters: P = 7.58 – 8.91 MPa, T_b = 22 – 142 °C, T_w = 32 – 223 °C, G = 885 – 3048 kg/m^{2}s, q = 27 – 616 kW/m^{2}K, D = 8.1 mm.

The performance of the new correlations Eqs. (7.7) – (7.9) is also shown in the Figures 7.10 – 7.12. All confidence bands are based on the 2σ-level.

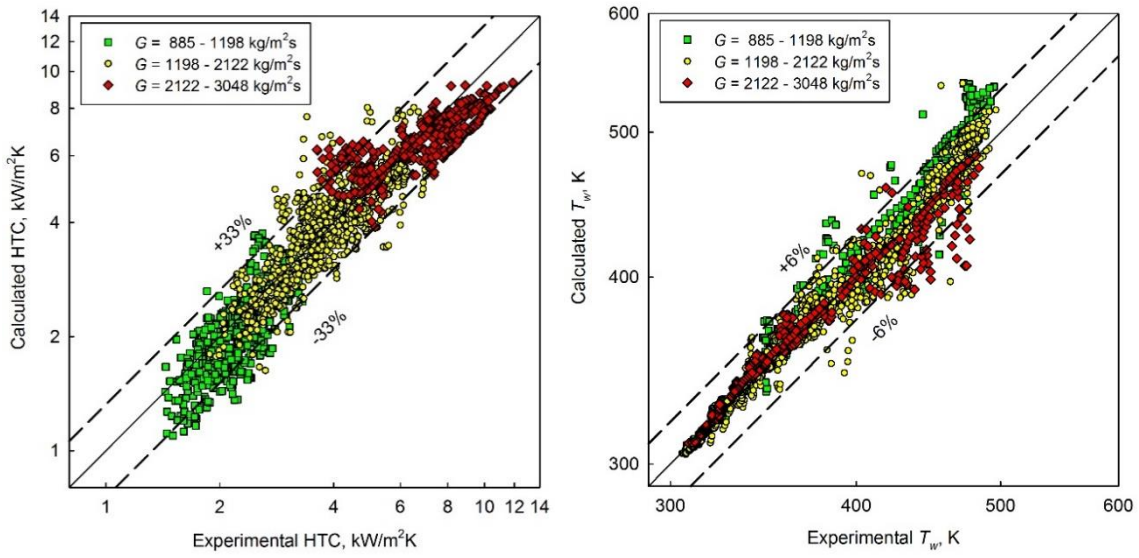

(a) **(b)**

Figure 7.10. Calculated vs experimental values of HTC (a) and T_w (b) for bulk-fluid temperature approach (data on upward flow of SC CO_2 in a bare tube).

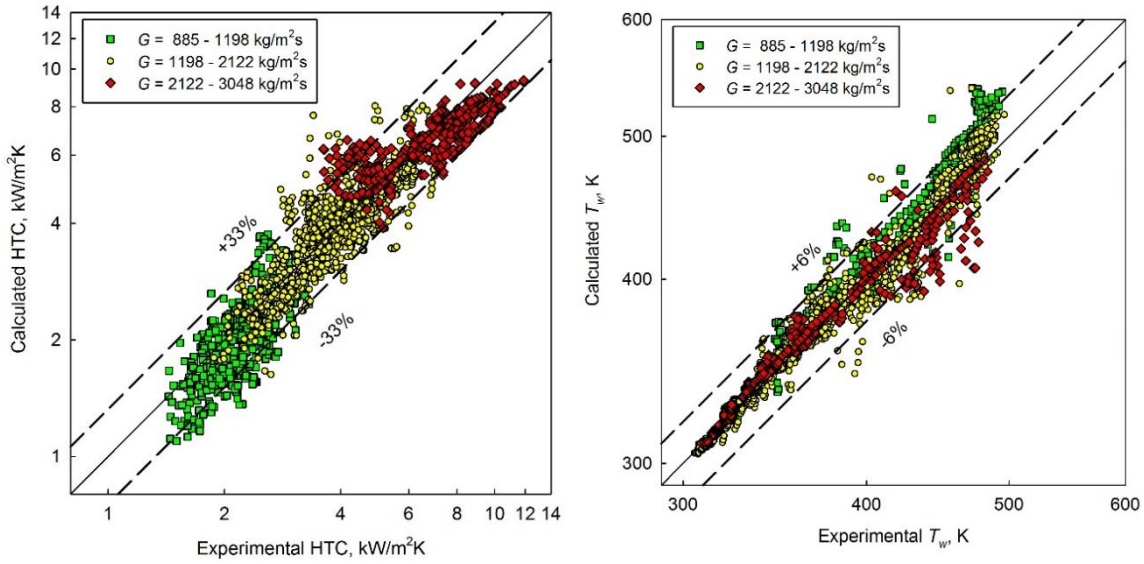

(a) **(b)**

Figure 7.11. Calculated vs experimental values of HTC (a) and T_w (b) for wall temperature approach (data on upward flow of SC CO_2 in a bare tube).

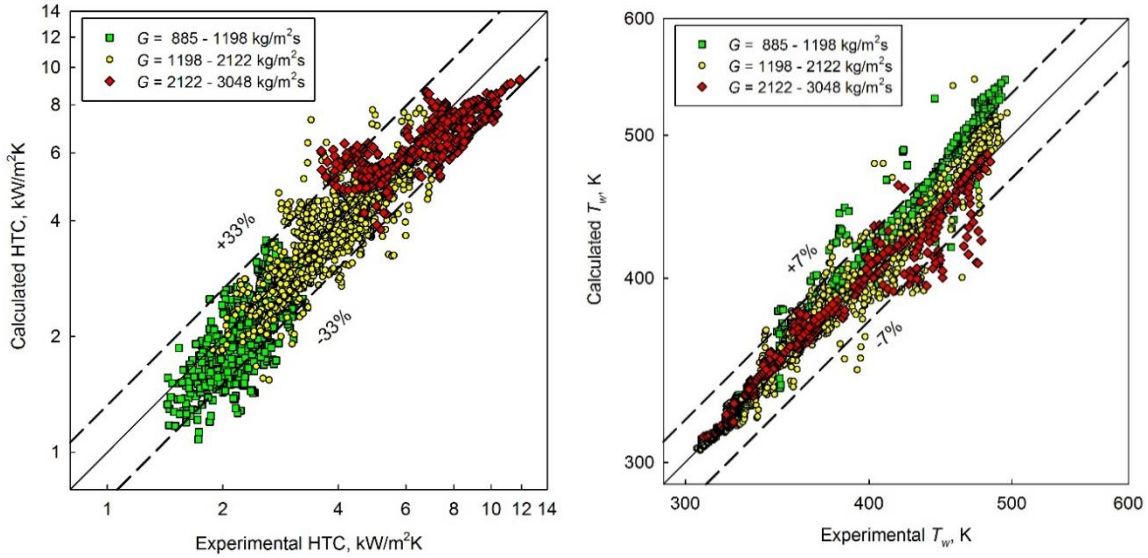

(a) **(b)**

Figure 7.12. Calculated vs experimental values of HTC (a) and T_w (b) for film temperature approach (data on upward flow of SC CO_2 in a bare tube).

Inspection of Figures 7.10 – 7.12 reveals that all the developed correlations are slightly biased towards under-prediction of HTC at the lowest mass fluxes. It is also seen that the prediction of HTC and T_w is identical for bulk-fluid- and wall temperature approaches. Indeed, numerical check showed that the temperatures predicted by the bulk-fluid- and wall

temperature approaches are identical up to the 8th figure. To clarify whether there is a difference in the spread of the deviations between the approaches, additional statistical graphs were plotted (in accordance with methodology discussed in Chapter 6) and are show in Figures 7.13 – 7.15.

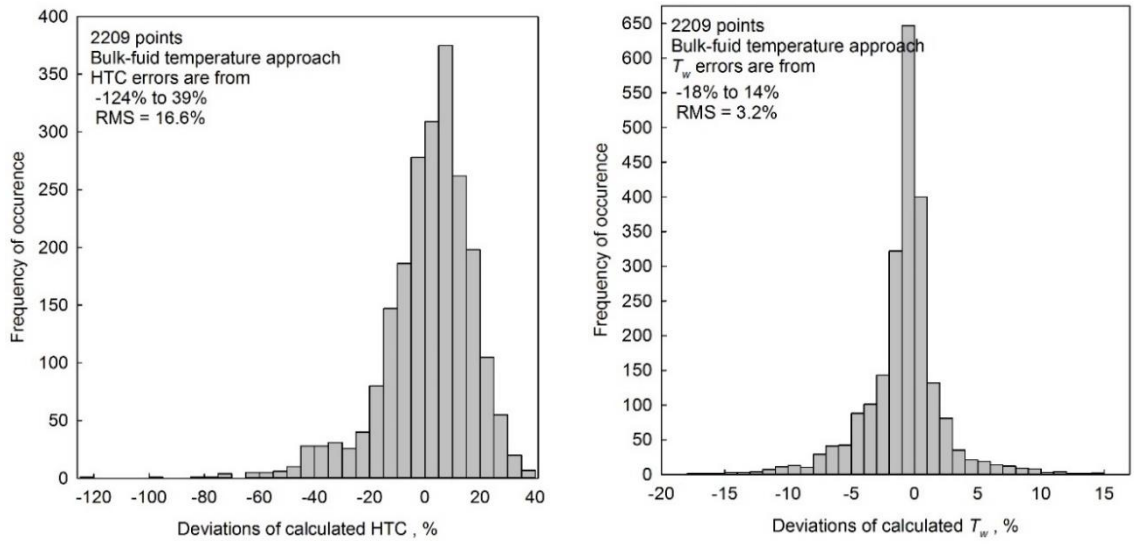

(a) **(b)**

Figure 7.13. Distribution of relative deviations of HTC (a) and T_w (b) for bulk-fluid temperature approach (data on upward flow of SC CO_2 in a bare tube).

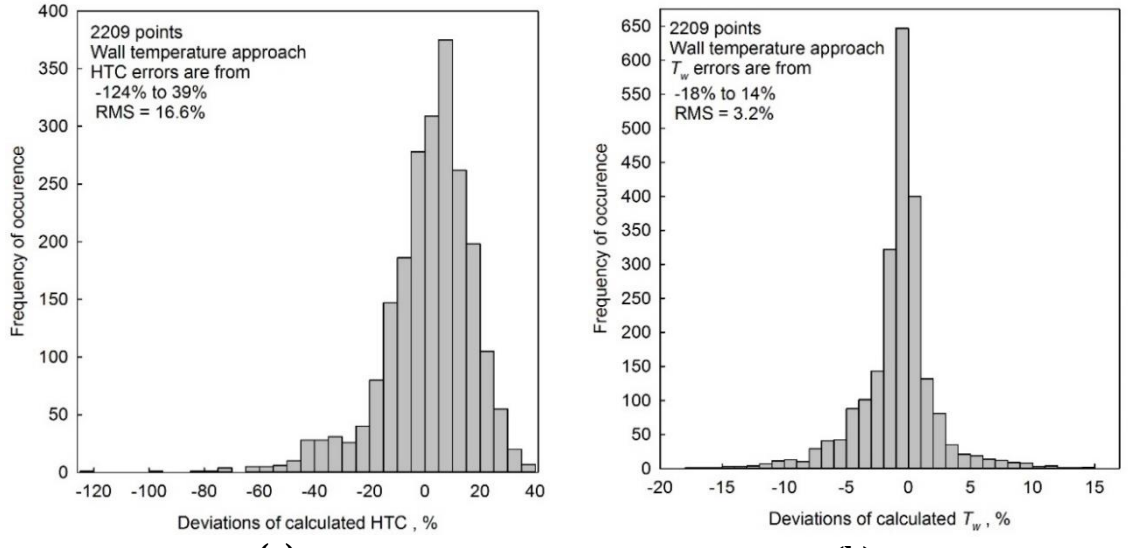

(a) **(b)**

Figure 7.14. Distribution of relative deviations of HTC (a) and T_w (b) for wall temperature approach (data on upward flow of SC CO_2 in a bare tube).

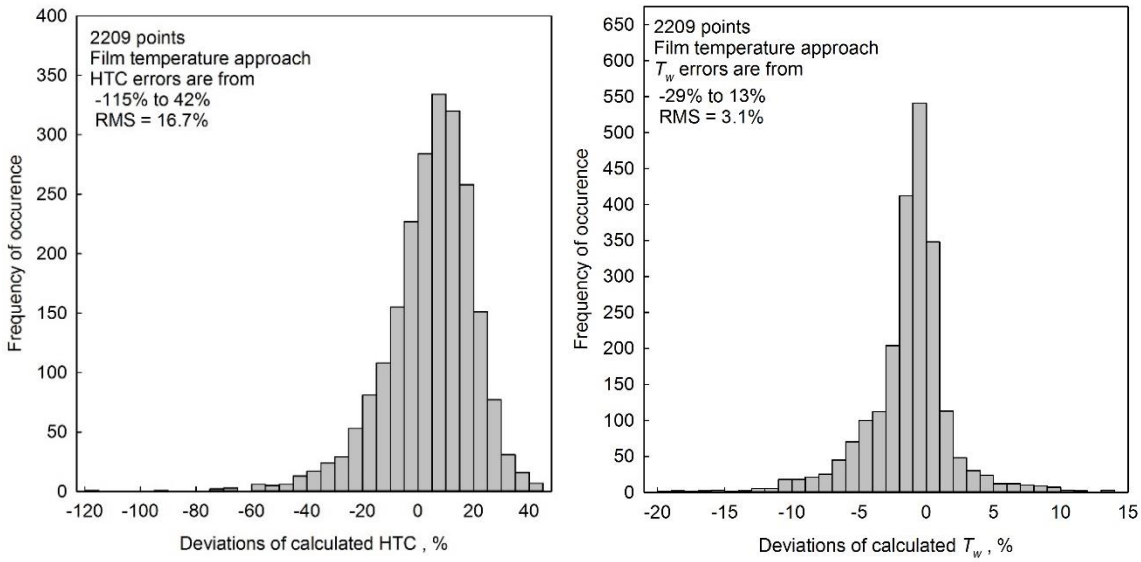

Figure 7.15. Distribution of relative deviations of HTC (a) and T_w (b) for film temperature approach (data on upward flow of SC CO_2 in a bare tube).

Inspection of Figures 7.12 – 7.15 reveals that correlations having RMS different only by fraction of percent can have a different spread of data. Indeed, that relative deviations of calculated HTC are spread within (–124%, +39%) interval for the bulk-fluid- and wall-temperature-based correlations, and within (–115%, +42%) for the film-temperature-based correlation. Thus, RMS alone can be a misguiding parameter when presented for a huge sample of data, because it levels the input of several significantly deviating points. Again, it is important to remind that from the perspective of calculation, the correlation having a slightly higher RMS, but smaller tendency to overestimate HTC (underestimate T_w) should be preferred over the other correlations.

Therefore, the correlations based on bulk-fluid- and wall temperature approaches (Eqs. (7.7) and (7.8)) have exact same statistics and both can be recommended for prediction of HTC and T_w for the forced convective heat transfer to SC CO_2 flowing upward at NHT and IHT. Since Eqs. (7.4) – (7.6)) require a special convergence relaxation criterion and Eq. (7.8) is based on the less frequently used wall temperature approach, Eq. (7.7) is recommended.

7.2. Correlation for the onset of DHT

Based on the methodology discussed in the Section 6.4.2, the following correlation for the onset of DHT was developed with 8.7% RMS:

$$q = 64 + 0.18G, \tag{7.10}$$

where q is the heat flux (kW/m^{2}K), and G is the mass flux (kg/m^{2}s). At heat fluxes exceeding those calculated from Eq. (7.10) deterioration of heat transfer is expected to occur. This correlation is valid within the following range of experimental parameters: P = 7.6 – 8.8 MPa, $T_{b,in}$ = 20 – 35 °C, G = 887 – 2987 kg/m^{2}s, q = 180 – 616 kW/m^{2}K, D = 8.1 mm.

The deterioration predicted by Eq. (7.10) is due to high heat flux, rather than strong buoyancy forces.

7.3. Heat transfer correlations without distinguishing heat transfer mode

Based on the methodology described in the Section 6.4.3, six correlations were developed without distinguishing heat transfer regimes. For convenience, the general form of the correlations is repeated again, as follows:

$$\mathbf{Nu} = const\mathbf{Re}^{n_1}\overline{\mathbf{Pr}}^{n_2}\left(\frac{\rho_w}{\rho_b}\right)^{n_3}\left(\frac{P}{P_{cr}}\right)^{n_4}\left(1+\frac{l_{unheated}}{l_{unheated}+z_{heated}}\right)^{n_5}\left(\frac{\mu_w}{\mu_b}\right)^{n_6} \tag{7.11}$$

The fitted constant and powers are presented in Table 7.5.

The summary of the performance of the correlations according to Eq. (7.11) with fitted exponents in Table 7.5 is given in Table 7.6. The statistics where calculated using: 1) four significant figures of the fitted parameters; 2) Q-approach is used; and 3) the convergence criteria set as the difference between the two successive iterations of T_w becoming less than 0.5 K (discussion of the sensitivity of the performance of the correlations is presented in Appendix C). Since it was discussed in Chapter 6 that using the average of the HTCs predicted by bulk-fluid- and wall temperature approaches may reduce the spread or RMS,

the performance of this approach is also presented. The recommended choice of the temperature approach is highlighted in green. The preference was made to the approach, which, with comparable with the RMS of other approaches for HTC, produced the smallest negative relative deviation for HTC (meaning the lowest tendency to over-predict HTC) or the smallest spread of the predicted values data.

Table 7.5. Fitted constants and powers for the correlations according to Eq. (7.11).

Bin*	**Approach/ parameter**	***const***	n_1	n_2	n_3	n_4	n_5	n_6
X<–1000	bulk-fluid	0.00342	0.912	0.189	0.110	0.0	0.556	0.0
	wall	0.00506	0.871	0.295	–1.44	0.0	0.810	1.82
–1020≤**X**<–500	bulk-fluid	0.00160	0.985	0.248	0.159	–0.679	0.523	0.0
	wall	0.00297	0.983	0.123	0.0	–1.39	0.552	0.571
–520≤**X**<–200	bulk-fluid	0.00202	0.922	0.498	0.0	0.331	0.515	0.0
	wall	0.00614	0.921	0.185	0.392	–0.882	0.526	0.0
–220≤**X**<300	bulk-fluid	0.00604	0.857	0.564	0.218	1.23	0.0	0.0
	wall	0.0156	0.905	–0.244	1.17	–1.39	0.244	–1.24
280≤**X**<500	bulk-fluid	0.0148	0.871	0.141	1.19	0.0	0.0	0.0
	wall	0.0172	0.860	0.0	0.915	0.0	0.0	–1.27
480≤**X**	bulk-fluid	0.0204	0.841	0.224	0.971	–0.357	–0.181	0.0
	wall	0.0211	0.839	0.285	0.774	–0.516	–0.178	–-0.737

* Boundaries for bins were chosen based on the analysis of all experimental HTC data plotted against **X**. For details see Appendix F.

It should be noted that fitting of the exponents in Table 7.5 was done for data belonging to the bins of **X** overlapping each other by 20 units. This allowed to smoothen the change in the predicted values of HTCs by the correlations for neighboring bins.

Based on the idea described in the Section 6.4.3, the right border of bin #4 should be extended to **X** = 380 at heat fluxes equal to or higher than those corresponding to Eq. (7.10). This suggests that the difference between the data around the pseudocritical state becomes less pronounced over the extended range of thermodynamic states of fluid at high heat loading factors. Since the deterioration at high heat fluxes is mainly assumed to be caused by the thickening of the viscous sublayer and delayed transformation of the velocity profile (see Chapter 3), this may mean that the correlations developed based on

Eq. (7.11) are able to capture the heat transfer trends over a wider range of experimental conditions than those they were based on.

Table 7.6. Summary of the performance of the correlations according to Eq. (7.11).

Bin	Statistics	Characteristic temperature		
		bulk-fluid	**wall**	**average**
X<–1000	**RMS of HTC, %**	9.8	10.0	9.5
	RMS of T_w, %	0.5	0.5	0.5
	HTC spread, %	–20.7- +32.9	–17.9 - +31.6	–15.1 - +31.9
	T_w spread, %	–1.7 - +1.1	–1.5 - +1.1	–1.5 - +1.1
–1020≤**X**<–500	**RMS of HTC, %**	8.4	9.1	8.7
	RMS of T_w, %	1.0	1.0	1.0
	HTC spread, %	–38.1- +33.7	–38.1 - +30.0	–38.1 - +31.7
	T_w spread, %	–5.3 - +2.3	–4.7 - +1.9	–4.9 - +2.0
–520≤**X**<–200	**RMS of HTC, %**	10.7	11.4	10.9
	RMS of T_w, %	1.9	1.9	1.9
	HTC spread, %	–29.8- +44.9	–40.8 - +46.7	–34.6 - +45.8
	T_w spread, %	–11.0 - +4.9	–11.8 - +4.3	–11.4 - +4.6
–220≤**X**<300	**RMS of HTC, %**	15.3	13.7	11.8
	RMS of T_w, %	3.4	4.9	2.7
	HTC spread, %	–55.0- +42.0	–43.5 - +54.9	–41.2 - +42.0
	T_w spread, %	–14.1 - +12.3	–41.0 - +7.4	–12.4 - +8.6
280≤**X**<500	**RMS of HTC, %**	9.3	9.5	9.2
	RMS of T_w, %	2.3	2.3	2.4
	HTC spread, %	–26.3 - +19.6	–29.2 - +21.8	–28.3 - +20.8
	T_w spread, %	–8.1 - +4.1	–10.0 - +4.7	–9.8 - +3.9
480≤**X**	**RMS of HTC, %**	7.7	7.8	7.7
	RMS of T_w, %	1.6	1.6	1.6
	HTC spread, %	–28.0- +20.7	–32.4 – 21.9	–30.2 - +21.3
	T_w spread, %	–5.0 - +3.7	–5.3 - +2.8	–5.1 - +3.1

The cells highlighted in green represent the recommended approach for that bins.

The final intervals for the bins are shown in Table 7.7.

Table 7.7. Recommended bins for predicting data.

Bin #	1	2	3	4	5	6
Interval for **X**	(–∞,–1000]	[–1000, –520)	[–520, –200)	[–200, 300)	[300, 480)	[480, +∞)
Adjustment if criterion in Eq. (7.10) is met	No	No	No	[–200, 380)	[380, 480)	No

The performance of the overall binned correlation over the whole range of data used for the development of the binned correlation with the recommended bins (according to Table 7.5)[12] is summarized in Table 7.8.

Table 7.8. Summary of the overall performance of the binned correlation.

RMS of HTC, %	RMS of T_w, %	HTC spread, %	T_w spread, %
10.0	2.0	–41.2 - +44.9	–12.4 - +8.6

The developed binned correlation Eq. (7.11) is valid within the following range of experimental parameters: P = 7.58 – 8.91 MPa, T_b = 20 – 142 °C, T_w = 32 – 231 °C, G = 885 – 3048 kg/m^{2}s, q = 26 – 616 kW/m^{2}K, D = 8.1 mm.

The convergence criterion was relaxed to 1 K if the iterations did not stop after 50 attempts. This relaxation was never invoked. The performance of the binned correlation Eq. (7.11) is shown in the Figures 7.16 – 7.19.

Although the confidence band (based on the 2σ-level) for the predicted values of HTC should be ±20%, 95% of the predicted data fall within a narrower band, which is ±18%. However, 95% of the predicted T_w values fall within the ±4% band, which coincides with the one corresponding to the 2σ-level. This indeed may be seen from Figures 7.16 – 7.19, the predicted HTCs and T_w values lie within a much narrower band than those predicted by Eq. (7.7). It is also seen from Figure 7.18 that the residuals have normal distribution, which conforms to one of the presumptions of the least-squares fit method.

[12] Onwards the correlations based on Eq. (7.11) with the fitted exponents in Table 7.5 and used on the bins defined in Table 7.7 will be referred to as binned correlation Eq. (7.11); the approach to correlate the data for each of the bins will be called binned approach.

Finally, it should be reminded that the data presented in Figures 7.16 – 7.19 include inlet points and points considered as DHT from the conventional approach.

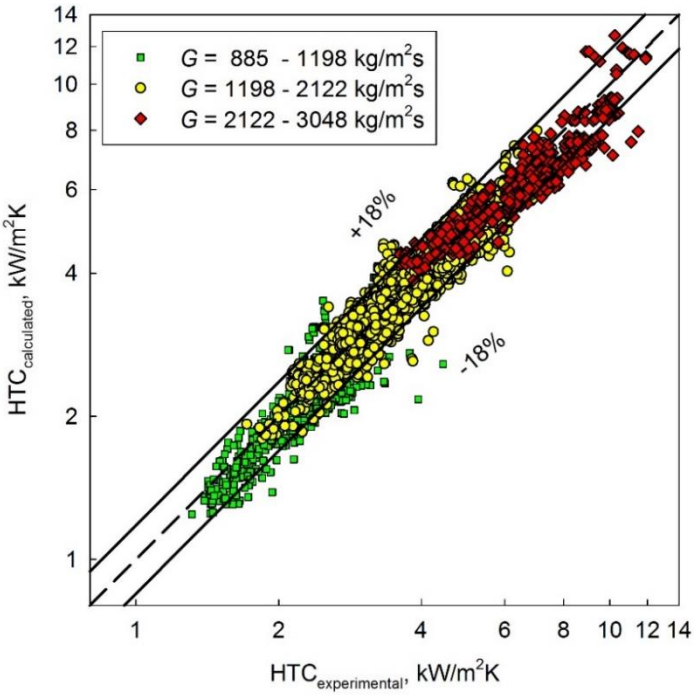

Figure 7.16. Calculated vs experimental values of HTC for the binned approach (data on upward flow of SC CO_2 in a bare tube).

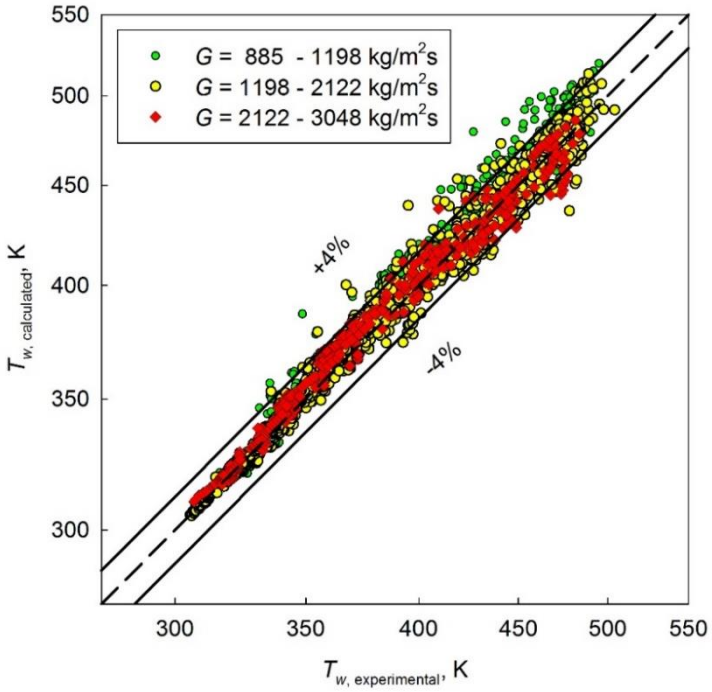

Figure 7.17. Calculated vs experimental values of T_w for the binned approach (data on upward flow of SC CO_2 in a bare tube).

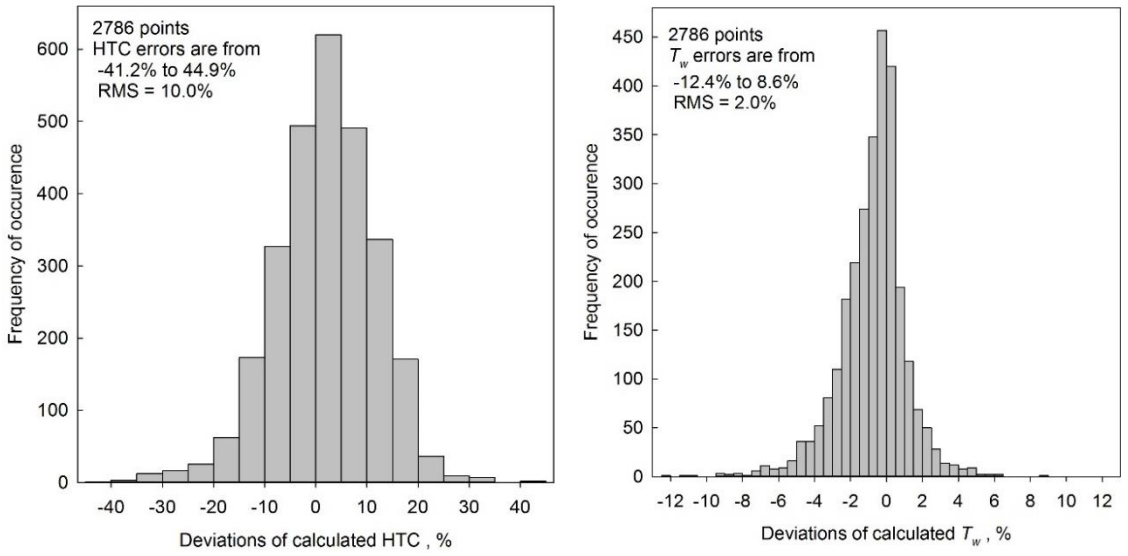

(a) **(b)**

Figure 7.18. Distribution of relative deviations of HTC (a) and T_w (b) for the binned approach (data on upward flow of SC CO_2 in a bare tube).

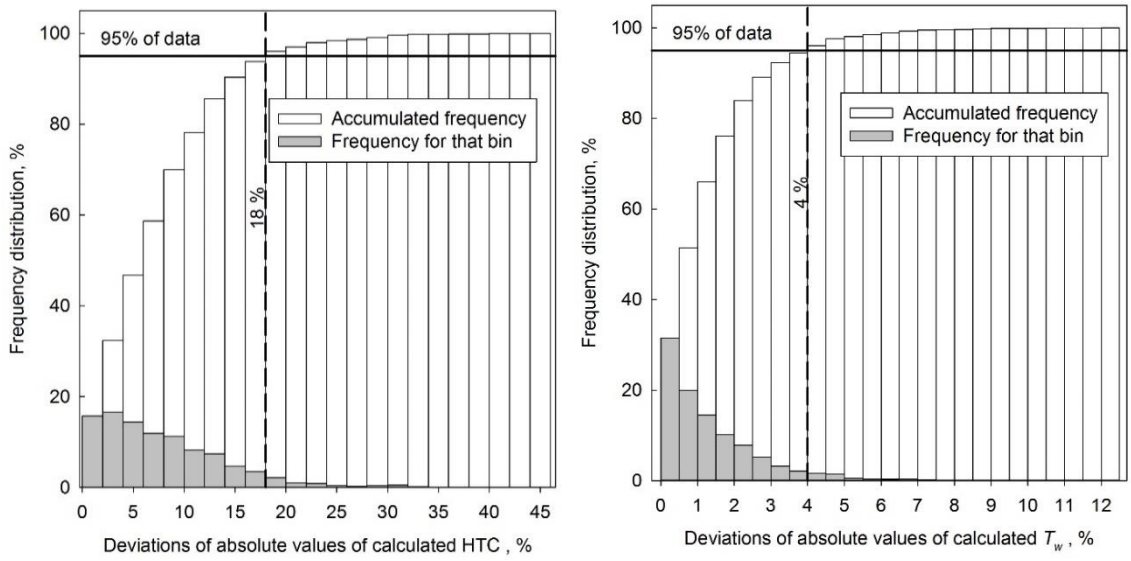

(a) **(b)**

Figure 7.19. Distribution of absolute values of relative deviations of HTC (a) and T_w (b) for the binned approach (data on upward flow of SC CO_2 in a bare tube).

The results presented in Table 7.8 and Figures 7.16 – 7.19, in fact, validate the proposed methodology. Still, further discussion of the results and verification of the developed correlations are presented in the next chapter.

CHAPTER 8. DISCUSSION OF RESULTS

Inspection of the results obtained by using different approaches to fit the data based on the conventional methodology (Eqs. (7.1) – (7.3)) shows that there is insignificant difference between the approaches. However, the weighted non-linear least mean squares approach seems to produce better fit than the others.

Addition of the terms in the forms of ratios of thermal conductivities and viscosities leads to a better performance of the correlations (compare Eqs. (7.1) – (7.3) with Eqs. (7.7) – (7.9)). This was expected, because these transport properties affect the transport of energy (see Literature review (Chapter 2) and Appendix B)

Using film temperature approach does not lead to improvement of the fitted results for forced convection to SC CO_2. Both bulk-fluid and wall temperature approaches produce smaller RMS (see Tables 7.2 – 7.4).

However, using new methodology to bin and correlate the data leads to a drastic reduction in RMS (see Figures 8.1 and 8.2 below).

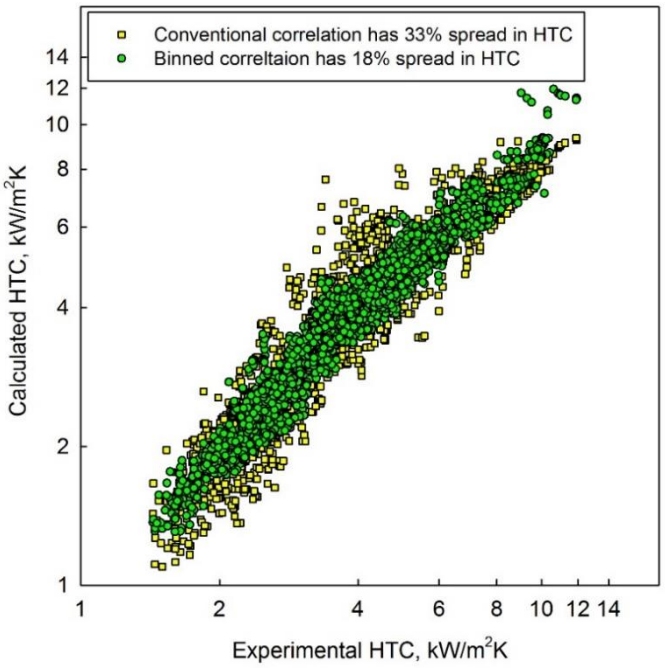

Figure 8.1. Comparison of the spread in the prediction of HTC by correlations based on conventional and new methodology. NHT MR-1 loop data are compared (data on upward flow of SC CO_2 in a bare tube).

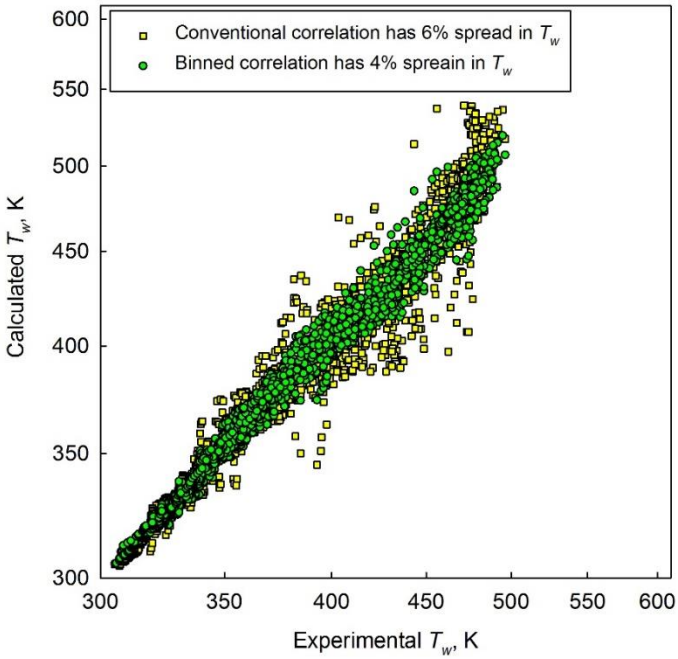

Figure 8.2. Comparison of the spread in the prediction of wall temperatures by correlations based on conventional and new methodology. NHT MR-1 loop data are compared (data on upward flow of SC CO_2 in a bare tube).

The new methodology not only allows reducing RMS, but also gives ideas for the discussion of the effects of flow history, pressure, and relative effects of density and viscosity on heat transfer.

Examination of exponents of the terms of the binned correlation (see Table 7.5) reveals the following for the investigated data.

Correlations based on the bulk-fluid temperatures did not require the inclusion of the viscosity term within any of the bins to improve description of heat transfer. However, correlations based on wall temperature approach did not require the viscosity term only on the second bin (moderate subcooling, the near wall layer may be within the pseudocritical region, but the bulk of the flow is definitely subcooled), and on the fifth bin (exit from the pseudocritical region).

Flow history had zero effect on heat transfer description on the fifth bin (exit from the pseudocritical region). Probably, the transformation of the velocity profile corresponding to the values of **X** within this bin are significant and similar to those that can occur at the entrance to the heated part of the test-section. Correlation based on the bulk-fluid approach

did not require inclusion of the flow history term on the fourth bin (pseudocritical region). Most likely, the reason is similar. Here, the axial gradient of velocity profile is significant within the bulk of the flow, however not to the same extent as within the near wall layer.

Effect of pressure on heat transfer was found to be negligible from the prediction point of view for both temperature approaches within the first bin (high subcooling level) and within the fifth bin (exit from the pseudocritical region) and beyond the pseudocritical point (fifth bin). However, it has the strongest effect within the pseudocritical region. It has the inverse effect within the 3rd (bulk fluid is subcooled, but near wall is beyond pseudocritical) and 4th bin (pseudocritical region) on heat transfer depending on the chosen description: heat transfer is predicted to increase with an increase in pressure according to the bulk-fluid approach, and the opposite is true according to the wall temperature approaches. Within two other bins where the pressure term is important it has a stronger influence when the bulk fluid approach is chosen for the description of heat transfer.

Density turned out to have negligible effect on numerical description of heat transfer based on the wall temperature approach only within the 2nd bin, which corresponds to the region when bulk of the fluid is subcooled, and the near wall part of the flow is approaching pseudocritical state. In the next bin, it was the bulk-fluid temperature approach, which showed negligible effect of density on heat transfer.

Average Prandtl number showed no influence on improvement of prediction of heat transfer only within the fifth bin (exit from the pseudocritical region) and for the wall temperature approach only.

Additionally, the bulk-fluid approach was the best on three out of six bins (third, fifth, and sixth), what is in agreement with the idea that conventional bulk-fluid temperature based correlations should predict heat transfer to SCFs well in the regions well away from the pseudocritical regions.

The wall temperature approach was the best only on the 2nd bin, which corresponds to bulk fluid being subcooled and the near wall part of the flow within pseudocritical region.

Averaging HTCs obtained from the bulk-fluid and wall-temperature approach proved to be very significant in the pseudocritical region (4^{th} bin). This is the bin, where bulk-fluid and wall temperature based correlations produced deviations of the opposite signs. More specifically, averaging the results allows better reproducibility of the experimental data due to a more symmetrical spread of errors. The averaged approach also allowed reducing RMS within the first and fifth bins.

It should be clearly stated that the binned correlation obtained using new methodology is tuned to the data it was based on. However the tuning is not as subjective as in the case of conventional approach (removal of entrance effect, DHT points, and outliers that significantly deviate from the prediction trend). The new methodology requires scrupulous uncertainty analysis to screen out the data that have high experimental error. Finally, change of the boundaries of the bins may be required if:

1) set of data in study was obtained for a wider range of experimental conditions (especially if the chiller was used to cool down the fluid below the ambient temperature);
2) data were obtained at a test-section with a different length of unheated part; and
3) full uncertainty analysis of HTCs is impossible due to missing expressions for the uncertainties of the measuring devices from the vendors.

8.1. Verification of the obtained correlations

Correlation Eq. (7.7) (recommended based on the conventional methodology) and binned correlation Eq (7.11) are verified in this section by plotting their predictions against:

1) Data they were developed based on. Figures 8.3 – 8.5 represent NHT runs.
2) Data correlation Eq. (7.11) was developed on. Figures 8.6 – 8.8 represent DHT runs.
3) Data for three runs that were not used for the development of either of the correlations Figures 8.9 – 8.11 represent these three runs.

The runs presented in Figures 8.3 – 8.11 were selected to represent all the heat transfer regimes encountered in the MR-1 loop test data. Whenever bulk-fluid temperature crossed T_{pc} within the heated length, location of intersection was denoted with a vertical dashed lines.

It is expected that correlation Eq. (7.7) will produce significant deviations in the presence of entrance effects and DHT, since it was developed to NHT and IHT regimes only. Both correlations Eq. (7.7) and Eq. (7.11) are expected to reproduce the removed readings in the vicinity of the PDTs well (6th. 7th, 11th, 12th, and 17th data points within each run). Verification of the predictions of these removed readings be the developed correlations is summarized in Table 8.1.

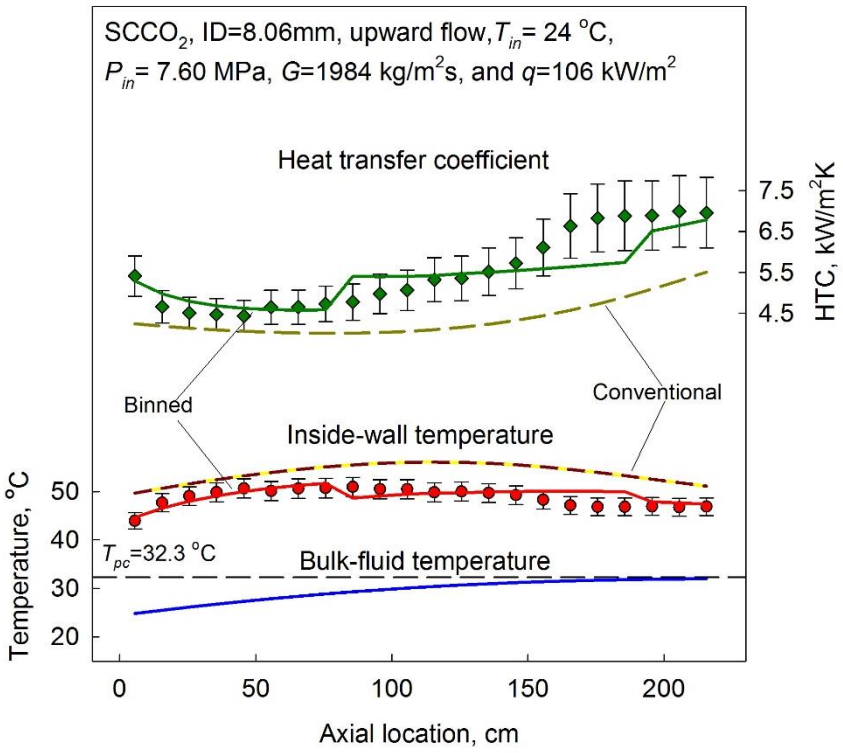

Figure 8.3. Verification of developed correlations for NHT run #1.

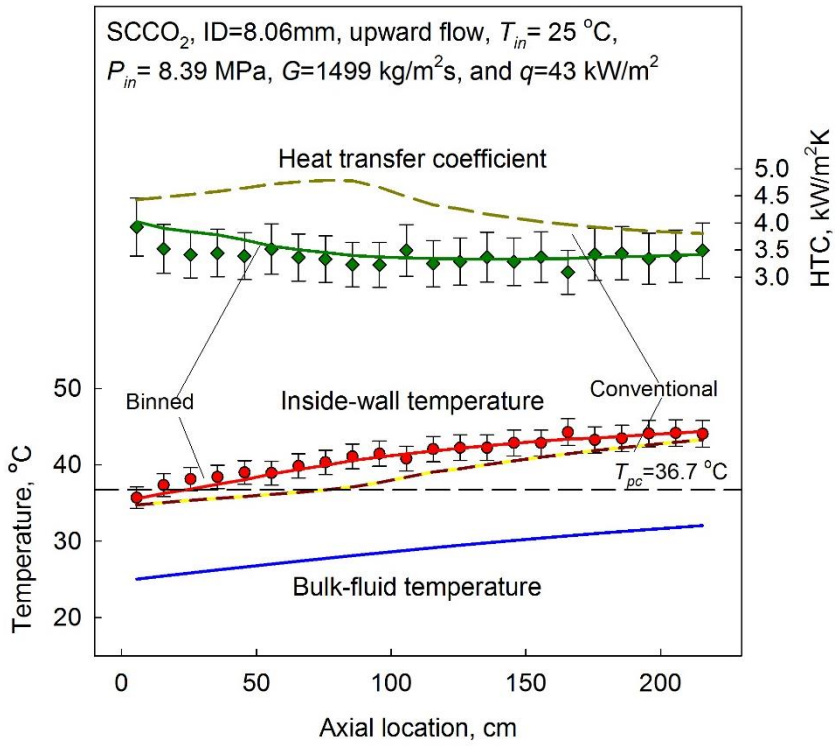

Figure 8.4. Verification of developed correlations for NHT run #2.

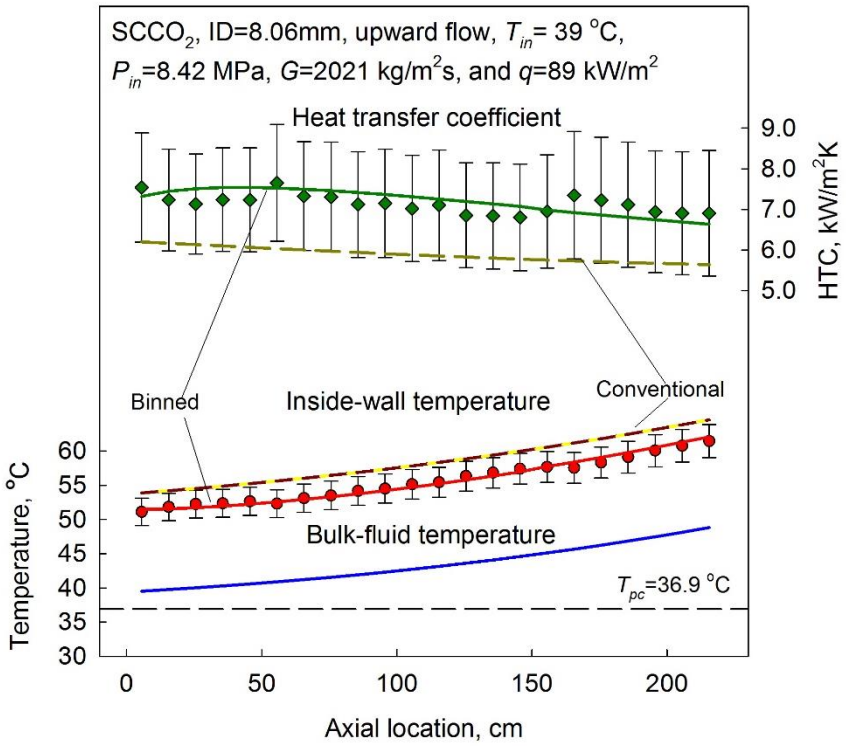

Figure 8.5. Verification of developed correlations for NHT run #3.

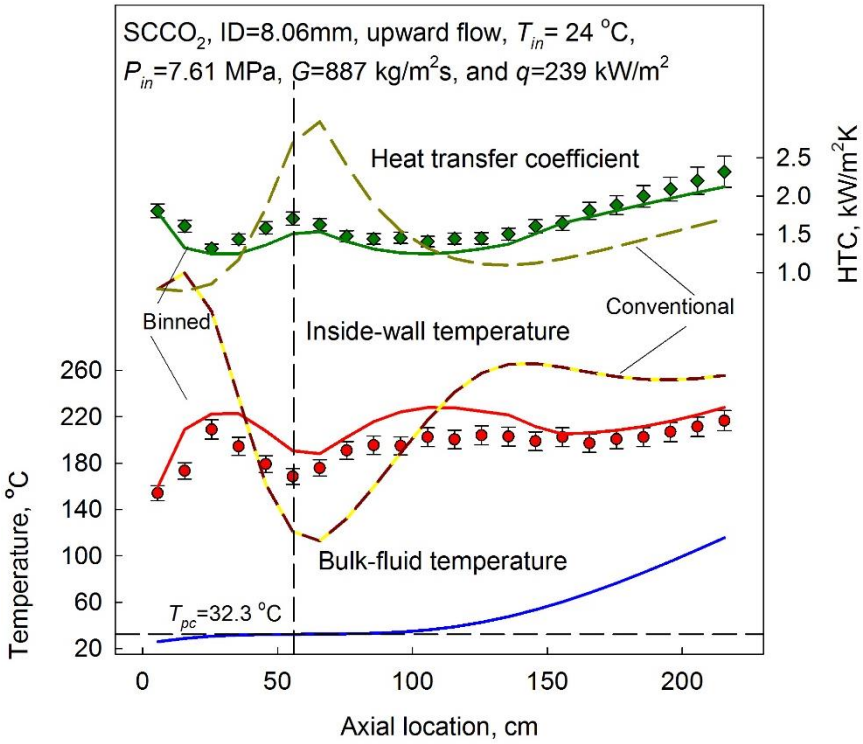

Figure 8.6. Verification of developed correlations for DHT run #1.

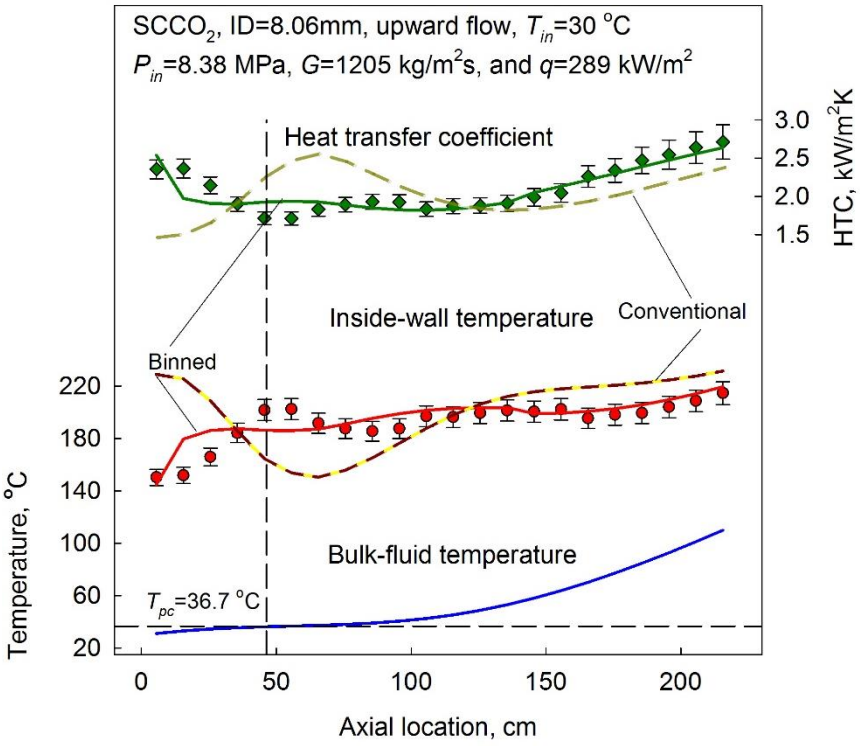

Figure 8.7. Verification of developed correlations for DHT run #2.

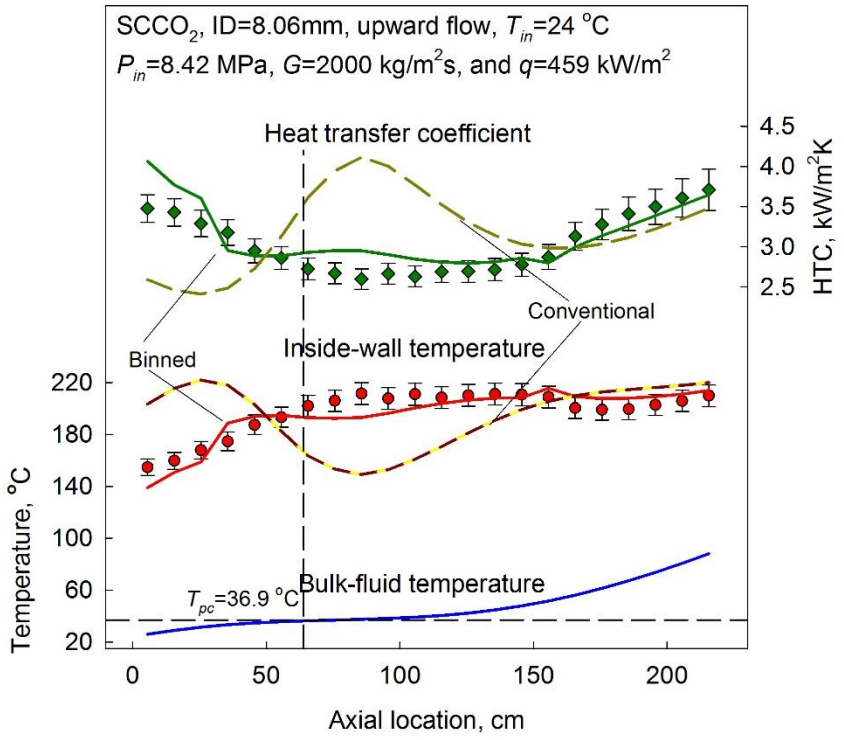

Figure 8.8. Verification of developed correlations for DHT run #3.

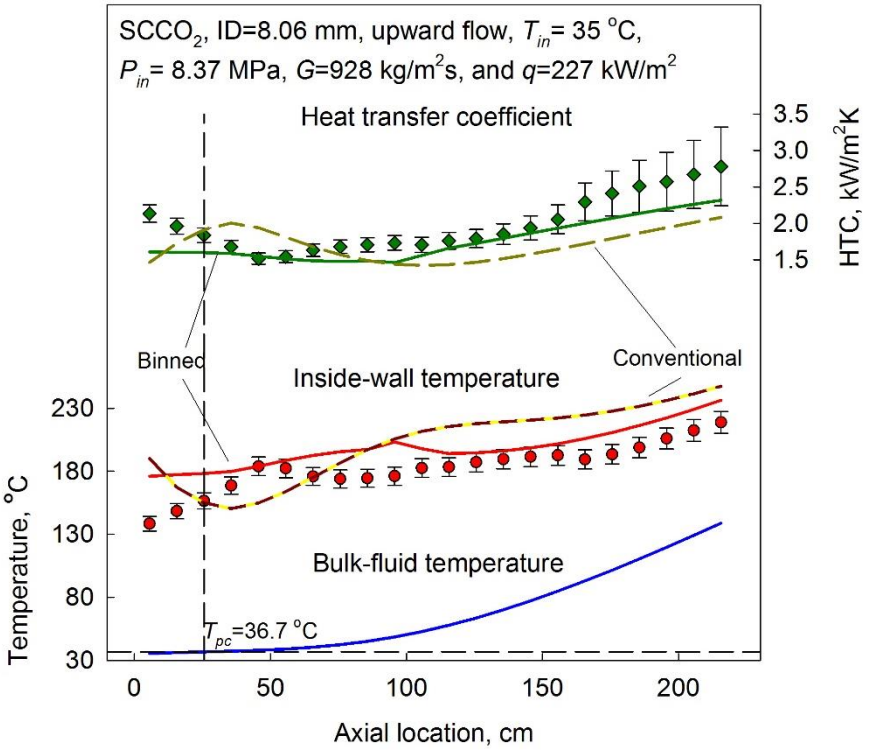

Figure 8.9. Verification of developed correlations for a set aside run #1.

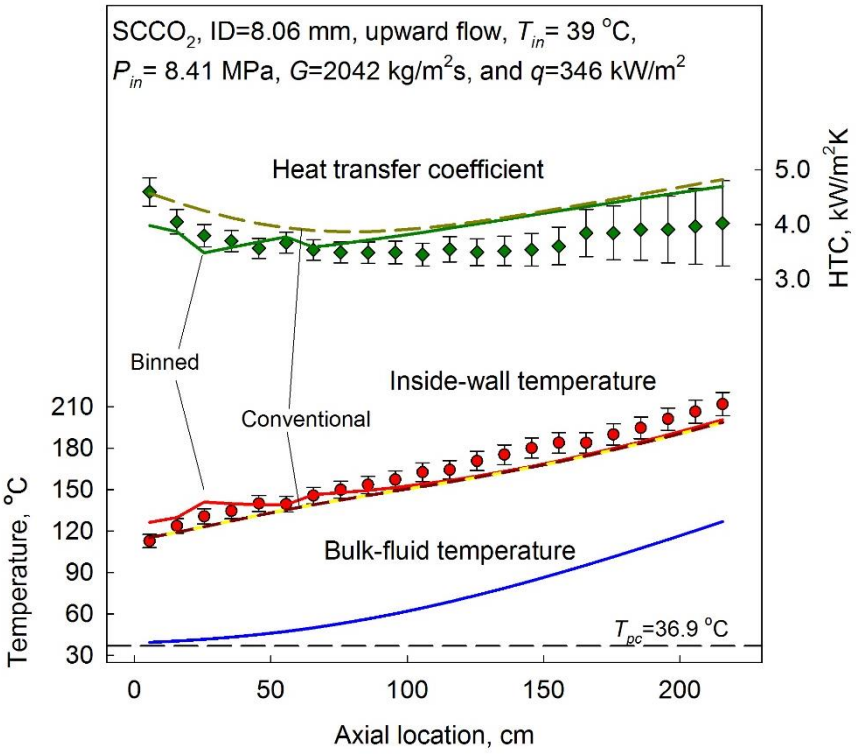

Figure 8.10. Verification of developed correlations for a set aside run #2.

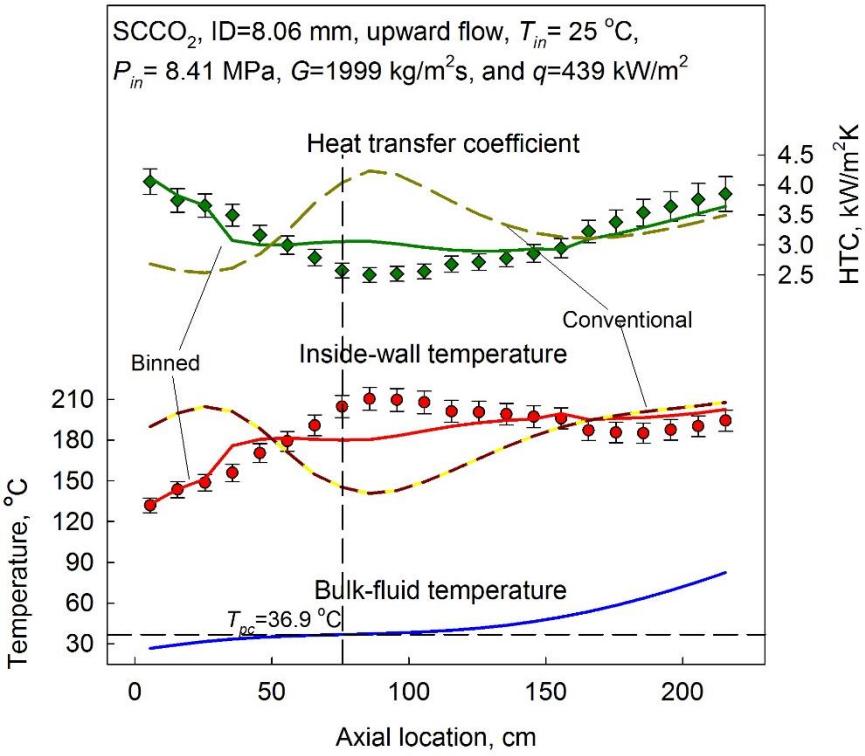

Figure 8.11. Verification of developed correlations for a set aside run #3.

Figures 8.3 – 8.11 show that the correlation Eq. (7.7) developed using on the conventional methodology describes NHT well, whether this regime is developed within the whole test-section (e.g., Figure 8.5) or within end where the fluid is well beyond the pseudocritical state (e.g., Figure 8.7).

The binned correlation Eq. (7.11) predicts DHT well. The deviation in HTCs is no more than 22% for the set aside runs, two of which had DHT data. Although the binned correlation is formulated in a piecewise-like form, transitions in predictions at the borders of the bins appear to be gradual.

Table 8.1. Summary of the predictions of the removed readings affected by PDTs.

Statistics	**Test of 829 points; data with more than 20% experimental uncertainty in HTC were excluded.**	
	Eq. (7.7) (conventional)	**Eq. (7.11) (binned)**
RMS of HTC, %	21	10
RMS of T_w, %	4	2
HTC spread, %	–154 - +42	–35 - +27
T_w spread, %	–13 - +22	–10 - +9

The conventional correlation Eq. (7.7) produced slightly higher RMS (1.2 times) for the removed data compared to the data it was developed on. However, the removed data contained DHT points. Therefore, this small increase in RMS can be attributed by this. The binned correlation Eq. (7.11) predicted the removed data within the smaller spread in HTCs and T_w, and with the same RMS as the data it was developed on.

8.2. Verification of the binned correlation on the external data

As discussed in Chapter 2, KAERI SPHINX loop data represent a "black box", because of the absence of the description of calibration of flow-meter and absence of the vendors' supplied expression for the uncertainties for other measuring devices. However, it was still possible to remove conspicuous outliers and erroneous runs (see Chapter 4 for details).

The remaining data represented forced, mixed and natural circulation convection data. Mixed and natural circulation data (according to the criterion Eq. (3.4)) as well as DHT data were removed. The remaining data were correlated using both conventional and new methodology. The patterns of the data (in terms of HTC vs **X**) were not examined;

therefore, the boundaries of the bins for the development of the correlation (Table 7.5) and for the use of the correlation (Table 7.7) were not changed.

A comparison of the performance of the conventional correlation and binned correlation was made for NHT KAERI SPHINX loop data. The summary is presented in Table 8.2.

Table 8.2. Summary of the predictions of the conventional and binned correlations against NHT KAERI SPHINX loop data.

Statistics	**Test of 7142 KAERI SPHINX loop data points within NHT**	
	Conventional	**Binned**
RMS of HTC, %	21	19
RMS of T_w, %	1.5	1.6
HTC spread, %	–152 - +71	–145 - +75
T_w spread, %	–11 - +6	–26 - +5

It is seen that the binned correlation performs as well as the conventional one on the "black box" data. A more detailed study of the patterns could have led to change in the boundaries of the bins and improvement of the predictions by the binned correlation. Since in the case of KAERI data there is no significant improvement when using new methodology, and a significant improvement was shown on the scrutinized AECL data, the results in the Table 8.2 may serve as a justification of the need to perform full uncertainty analysis of the experimental data.

CHAPTER 9. SUMMARY AND CONCLUSIONS

Several heat transfer correlations were developed for forced convection to SC CO_2 at NHT using different characteristic temperatures. All of the developed correlations are for the heating of SC CO_2. Comparison of the performance of these correlations leads to conclusion that the following correlation based on the bulk-fluid temperature approach should be preferred:

$$\mathbf{Nu_b} = 0.0052\mathbf{Re_b^{0.937}}\overline{\mathbf{Pr_b}}^{\mathbf{-0.242}}\left(\frac{\rho_w}{\rho_b}\right)^{0.854}\left(\frac{\mu_w}{\mu_b}\right)^{-1.37}\left(\frac{k_w}{k_b}\right)^{0.426} \tag{9.1}$$

This correlation was developed based on 2209 points with a spread of ±33% (based on 2σ-level). It is valid within the following range of experimental parameters: P = 7.58 – 8.91 MPa, T_b = 22 – 142 °C, T_w = 32 – 223 °C, G = 885 – 3048 kg/m^{2}s, q = 27 – 616 kW/m^{2}K, D = 8.1 mm.

Additionally, the following correlation for the onset of DHT occurring at high heat and mass flux was developed with a 9% RMS:

$$q = 64 + 0.18G, \tag{9.2}$$

where q is the heat flux (kW/m^{2}K), and G is the mass flux (kg/m^{2}s). This correlation is valid within the following range of experimental parameters: P = 7.6 – 8.8 MPa, $T_{b,in}$ = 20 – 35 °C, G = 887 – 2987 kg/m^{2}s, q = 180 – 616 kW/m^{2}K, D = 8.1 mm.

A new methodology was proposed to correlate data. According to this methodology, data can be binned according to the following non-dimensional number:

$$\mathbf{X} = \frac{h_b - h_{pc}}{q / G} \tag{9.3}$$

When this non-dimensional number is used, there is no need to preliminary visually and, therefore, subjectively distinguish and discriminate entrance effects, normal and deteriorated heat transfer regimes.

Using this methodology normal heat transfer data were predicted with a spread of ±19%. (1.74 times narrower compared to the conventional methodology), while all the data (2786 points, including entrance effects and deteriorated heat transfer) were predicted with a spread of ±20% (based on 2σ-level). This is a significant improvement compared to the conventional methodology. The correlation developed based on the new methodology is valid within the following range of experimental parameters: P = 7.58 – 8.91 MPa, T_b = 20 – 142 °C, T_w = 32 – 231 °C, G = 885 – 3048 kg/m^{2}s, q = 26 – 616 kW/m^{2}K, D = 8.1 mm.

The binned correlation is formulated as follows.

$$\mathbf{Nu} = const\mathbf{Re}^{n_1}\overline{\mathbf{Pr}}^{n_2}\left(\frac{\rho_w}{\rho_b}\right)^{n_3}\left(\frac{P}{P_{cr}}\right)^{n_4}\left(1+\frac{l_{unheated}}{l_{unheated}+z_{heated}}\right)^{n_5}\left(\frac{\mu_w}{\mu_b}\right)^{n_6}, \tag{9.4}$$

where the exponents depend on the parameter as indicated in Table 9.1.

The new methodology includes inlet effect and effects of pressure. Addition of density and viscosity terms and using the average of HTCs calculated from bulk-fluid- and wall temperature approaches allowed improvement of predictions in the pseudocritical region when deterioration occurred.

It was found that varying the convergence criteria form 0.01 K to 0.5 K had almost no effect on RMS and maximal spread of HTC and T_w. Therefore, 0.5 K can be safely used as a convergence criterion both for the conventional correlation Eq. (7.7) and the binned correlation Eq. (7.11). No instabilities occur with such choice of the convergence criterion.

Two types of instabilities in convergence were observed. The first type happens when the rather correlation runs in an infinite iterative loop. It was noticed that in a pair of iterations, one of the T_w may be very close to the solution, while averaging with the next iteration, shifts the former away from the solution by at least double the convergence tolerance. Changing the convergence tolerance or using "biased" value for the T_w in the next iteration (as proposed by Griem, 1996) may solve the issue. The second type of instability occurs in very rare instances when T_w increases to thousands of K. Changing the convergence criterion and the starting value of T_w for iterations could help avoiding this instability.

Table 9.1 Exponents of the terms entering binned correlations, boundaries of the bins, recommended characteristic temperature approaches.

Bin / recommended approach	**Characterisitc temperature approach**	***const***	n_1	n_2	n_3	n_4	n_5	n_6
X<–1000 (average)	bulk-fluid	0.00342	0.912	0.189	0.110	0.0	0.556	0.0
	wall	0.00506	0.871	0.295	–1.44	0.0	0.810	1.82
–1020≤**X**<–500 (wall)	bulk-fluid	0.00160	0.985	0.248	0.159	–0.679	0.523	0.0
	wall	0.00297	0.983	0.123	0.0	–1.39	0.552	0.571
–520≤**X**<–200 (bulk-fluid)	bulk-fluid	0.00202	0.922	0.498	0.0	0.331	0.515	0.0
	wall	0.00614	0.921	0.185	0.392	–0.882	0.526	0.0
–200≤**X**<300 (average)								
–200≤**X**<380 (if q is higher than q calculated from Eq. (9.2))	bulk-fluid	0.00604	0.857	0.564	0.218	1.23	0.0	0.0
	wall	0.0156	0.905	–0.244	1.17	–1.39	0.244	–1.24
300≤**X**<480 (bulk-fluid)								
380≤**X**<480 (if q is higher than q calculated from Eq. (9.2))	bulk-fluid	0.0148	0.871	0.141	1.19	0.0	0.0	0.0
	wall	0.0172	0.860	0.0	0.915	0.0	0.0	–1.27
480≤**X (**bulk-fluid)	bulk-fluid	0.0204	0.841	0.224	0.971	–0.357	–0.181	0.0
	wall	0.0211	0.839	0.285	0.774	–0.516	–0.178	–0.737

Analysis of heat transfer data using parameter defined in Eq. (6.4) allowed to reveal the following effects of experimental parameters on heat transfer that are not clearly described in the literature:

1) Decrease in pressure enhances heat transfer at NHT, and decreases the minimal HTC when DHT occurs.
2) If the inlet effect is present, then deterioration develops to the same level as it would in case of DHT in the middle of the test-section. This conclusion support the idea discussed in the analysis of the works by Bourke and Pulling (1971) and Kurganov and Kaptil'ny (1992). Specifically, consistent measurements of velocity profiles should be performed to find whether there are common trends in the transformation of velocity profiles at the entrance to the test section, at what is considered as NHT, DHT at high heat fluxes, and DHT at low mass fluxes.
3) At the same mass fluxes, HTCs appear to be higher in the liquid-like region than in the gas-like region.

Comparison of AECL and KAERI data showed absolute need to perform full analysis of uncertainties in experimental HTCs to avoid inclusion of skewed data in the development of correlations.

Additionally, subcritical Rankine, SC Rankine, and SC CO_2 Brayton cycles were considered. It was shown that SC CO_2 Brayton cycles are a promising option for power-conversion side of SFR. SC CO_2 Brayton cycle with regeneration was considered for the temperature conditions corresponding to the BN-600 SFR; and SC CO_2 Brayton cycle with reheat and intercooling was considered for the temperature conditions corresponding to the Monju SFR. It was discovered that addition of a stage of reheat lead to a 3% increase in thermal efficiency. An efficiency of 43% of the ideal two-stage compression with intercooling and single reheat was found for the SC CO_2 power conversion cycle with as low as 480 °C turbine inlet temperature.

REFERENCES

Ahmad, S.Y., 1973 (as cited by Cheng et al., 2011). Fluid to Fluid Modelling of CHF: a Compensated Distortion Model, *International Journal of Heat and Mass Transfer*, 16, pp. 641–662.

Ambrosini, W., 2011. Discussion of Similarity Principles for Fluid-to-Fluid Scaling of Heat Transfer Behaviour at Supercritical Pressures, *Nuclear Engineering and Design*, 241. pp. 5149–5173.

Ambrosini, W., Forgione, N., Badiali, S., Jackson, J.D., and Sharabi, M., 2013. Heat Transfer of Supercritical Water Flowing Upward and Downward in a Circular Tube, proceedings of the 15th International Topical Meeting on Nuclear Reactor Thermalhydraulics (NURETH-15), May 12–17, Pisa, Italy, paper #482, 10 pages.

Anglart, H., 2009. Heat Transfer Deterioration in Application to HPLWR – Mechanisms Identification and Ranking Table, proceedings of 4th International Symposium on Supercritical Water-Cooled Reactors (ISSCWR-4), March 8-11, Heidelberg, Germany, paper #18, 10 pages.

Bae, J.H., Yoo, J.Y., and Choi, H., 2005. Direct Numerical Simulation of Turbulent Supercritical Flows with Heat Transfer, *Physics of Fluid*, 17, pp. 105104-1 – 105104-24.

Beznosov, A.V., Dragunov, Yu.G., and Rachkov, V.I., 2007. Heavy-Liquid Metal Coolants in Nuclear Engineering (in Russian), IzdAT Publishing House, Moscow, Russia, 434 pages.

Bae, Y.Y., 2011. Mixed Convection Heat Transfer to Carbon Dioxide Flowing Upward and Downward in a Vertical Tube and an Annular Channel, *Nuclear Engineering and Design*, 241, pp. 3164–3177.

Bae, Y.Y. and Kim, H.Y., 2009. Convective Heat Transfer to CO_2 at a Supercritical Pressure Flowing Vertically in Tubes and an Annular Channel, *Experimental Thermal and Fluid Science*, 33, pp. 329–339.

Bae Y.Y., Kim, H.Y., and Kang, D.J., 2010. Forced and Mixed Convection Heat Transfer to Supercritical CO_2 Vertically Flowing in a Uniformly-Heated Circular Tube, *Experimental Thermal and Fluid Science*, 34, pp. 1295–1308.

Bergman, T.L., Lavine, A.D., Incropera, F.P., and DeWitt, D.P. *Fundamentals of Heat and Mass Transfer*, 7th edition, John Wiley & Sons, ISBN 13 978-0470-50197-9, 1048 pages.

Bishop, A.A., Sandberg, R.O. and Tong, L.S., 1964. Forced Convection Heat Transfer to Water at Near-Critical Temperatures and Super-Critical Pressures, Report WCAP-2056, Westinghouse Electric Corporation, Atomic Power Division, Pittsburgh, PA, USA, December, 85 pages.

Black, W.Z. and Hartley, J.G., 1996. *Thermodynamics*, 3rd edition, English/SI Version, published by HarperCollins, NY, USA, 919 pages.

Bourke, P.J. and Pulling D.J., 1971. An Experimental Explanation of Deterioration in Heat Transfer to Supercritical Carbon Dioxide, Report AERE-R.6765, Chemical Engineering Division, U.K.A.E.A. Research Group, Atomic Energy Research Establishment, HARWELL, March, 12 pages.

Bringer, R.P. and Smith, J.M., 1957 (as cited by Pioro and Duffey, 2007). Heat Transfer in the Critical Region, AIChE Journal, 3 (1), pp.49–55.

Brown, D.W., 2000. A Hot Dry Rock Geothermal Energy Concept Utilizing Supercritical CO_2 Instead of Water, proceedings of the 25th Workshop on Geothermal Reservoir Engineering, January 24–26, Stanford University, Stanford, CA, USA, SGP-TR-165, 6 pages.

Cengel, Y.A. and Boles, M.A., 2006. *Thermodynamics: an Engineering Approach*, 5th edition, published by McGraw-Hill College, Boston, MA, USA, 988 pages.

Chapman, D.J. and Arias, D.A., 2009. An Assessment of the Supercritical Carbon Dioxide Cycle for Use in a Solar Parabolic Trough Power Plant, proceedings of the Supercritical CO_2 Power Cycle Symposium, Troy, NY, USA, 5 pages.

Chatoorgoon, V., Yeganeh-Dahrsarab, H, and Leung, L., 2013. Further Studies of Supercritical Flow Stability in Parallel Channels, proceedings of the 6th International Symposium on Supercritical Water-Cooled Reactors (ISSCWR-6), March 3–7, Shenzhen, Guangdong, China, paper #13110, 16 pages.

Cheng, X., Liu, X., and Gu, H., 2011. Fluid-to-Fluid Scaling of Heat Transfer in Circular Tubes Cooled with Supercritical Fluids, *Nuclear Engineering and Design*, 241, pp. 498–508.

Cheng, X., Kuang, B., and Yang, Y.H., 2007. Numercial Analysis of Heat Transfer in Supercritical Water Cooled Flow Channels, *Nuclear Engineering and Design*, 237, pp. 240–252

Cheng, X., Yang, Y.H., and Huang, S.F., 2009. A Simplified Method for Heat Transfer Prediction of Supercritical Fluids, *Annals of Nuclear Energy*, 36, pp. 1120–1128.

Churkin, A., Bilbao y Leon, S., and Yamada, K., 2011. Results of Calculations of the IAEA Benchmark Exercise on Steady-State Flow of Supercritical Water in a Heated Pipe, proceedings of the International Symposium on Supercritical Water-Cooled Reactors (ISSCWR-5), March 13–16, Vancouver, British Columbia, Canada, paper #78, 10 pages.

Churkin, A.N. and Deev, V.I., 2013. Ambiguity of Calculation Results of Heat Transfer to Water Using Empirical Correlations in the Region of Supercritical Pressure, proceedings

of the International Symposium on Supercritical Water-Cooled Reactors (ISSCWR-6), March 3–7, Shenzhen, Guangdong, China, paper #13057, 18 pages.

Cleveland, J., Nusret, A., and Duffey, R., 2007. Status and Plan for the IAEA Coordinated Research Programme on Heat Transfer Behaviour and Thermo-hydraulics Code Testing for Super-Critical Water-Cooled Reactors, proceedings of the 3rd International Symposium on Supercritical Water-Cooled Reactors – Design and Technology (ISSCWR-3), March 12-15, Shanghai, China, paper #I005, pp.138-149.

Dittus, F.W. and Boelter, L.M.K., 1930. Heat Transfer in Automobile Radiators of the Tubular Type, University of California, Berkeley, Publications in Engineering, Vol. 2, No. 13, pp. 443-461 (or Int. Communications in Heat and Mass Transfer, 1985, Vol. 12, pp. 3-22).

Dominguez, A.N., Onder, E.N., Pencer, J., and Watts, D., 2013. Canadian SCWR Bundle Optimization for the New Fuel Channel Design, proceedings of the 6th International Symposium on Supercritical Water-Cooled Reactors (ISSCWR-6), March 3–7, Shenzhen, Guangdong, China, paper #13022, 16 pages.

Dragunov, A., 2013. Development of Thermodynamic Cycles for Sodium-Cooled-Fast Reactors, MASc thesis, UOIT, 150 pages.

Dragunov, A., Saltanov**,** Eu., Bedenko, S. and Pioro, I., 2012. A Feasibility Study on Various Power-Conversion Cycles for a Sodium-Cooled Fast Reactor, Proceedings of the 20th International Conference On Nuclear Engineering (ICONE-20) – ASME 2012 POWER Conference, July 30 - August 3, Anaheim, California, USA, Paper #55130, 9 pages.

Dragunov, A., Saltanov, Eu., Pioro, I., Harvel, G. and Ikeda, B., 2013a. Study on Primary and Secondary Heat-Transport Systems for Sodium-Cooled Fast Reactor, Proceedings of

the 21st International Conference on Nuclear Engineering (ICONE-21), July 29-August 2, Chengdu, China, Paper #16014, 9 pages.

Dragunov, A., Saltanov, Eu., Pioro, I., Ikeda, B., Miletic, M., and Zvorykina, A., 2013b. Investigation of Thermophysical and Nuclear Properties of Prospective Coolants for Generation-IV Nuclear Reactors, Proceedings of the 21st International Conference on Nuclear Engineering (ICONE-21), July 29-August 2, Chengdu, China, Paper #16020, 11 pages.

Environment Canada, 2014. Appendix 3 – Refrigerant Ozone-depletion Potential (Odp), Global
Warming Potential (Gwp) And Container Colours, available at: http://www.ec.gc.ca/Air/default.asp?lang=En&n=4CA440F8-1 , retrieved on October 15, 2014.

Farah, A., Harvel, G., and Pioro, I., 2013. Assessment of FLUENT CFD Code as an Analysis Tool for Supercritical-Water Heat-Transfer Applications, proceedings of the 15th International Topical Meeting on Nuclear Reactor Thermalhydraulics (NURETH-15), May 12–17, Pisa, Italy, paper #118, 13 pages.

Feng, J., Shan, J., and Zhang, B., 2013. Coupled Neutronics/Thermal-hydraulics Analysis of 54-element Bundle Sesign with SiC Material as Cladding, proceedings of the 6th International Symposium on Supercritical Water-Cooled Reactors (ISSCWR-6), March 3–7, Shenzhen, Guangdong, China, paper #13123, 16 pages.

Fenghour, A., Wakeham, W.A., and Vesovic, V., 1998. The Viscosity of Carbon Dioxide, *Journal of Physical and Chemical Reference Data*, 27 (1), pp. 31–44.

Fewster, J. and Jackson, D., 2004. Experiments on Supercritical Pressure Convective Heat Transfer Having Relevance to SPWR, proceedings of the International Congress on

Advances in Nuclear Power Plants 2004 (ICAPP'04), June 13–17, Pittsburgh, PA, USA, paper #4342, 15 pages.

Filonenko, G.K., 1954. Hydraulic Resistance of the Pipelines, (in Russian) *Thermal Engineering*, 4, pp. 40–44.

Generation IV Annual Report, 2013. Available at: https://www.gen-4.org/gif/upload/docs/application/pdf/2014-06/gif_2013_annual_report-final.pdf , retrieved on September 17, 2014, 121 pages.

Generators Output and Capability Report, 2014. http://reports.ieso.ca/public/GenOutputCapability/PUB_GenOutputCapability_20141010.xml , retrieved on October 15, 2014.

Gnielinski, V., 1976. New Equation for Heat and Mass Transfer in Turbulent Pipe and Channel Flow, *International Journal of Chemical Engineering*, 16 (2), pp. 359–368.

Grabezhnaya, V.A. and Kirillov, P.L., 2006. Heat Transfer under Supercritical Pressures and Heat Transfer Deterioration Boundaries, *Thermal Engineering*, 53 (4), pp. 296–301.

Griem, H., 1996. A New Procedure for the Prediction of Forced Convection Heat Transfer at Near- and Supercritical Pressure. *Heat and Mass Transfer*, 31, Springer-Verlag, pp. 301–305.

Grigoryev, V.A. and Zorin, V.M., 1989. Thermal and Nuclear Power Plants, (in Russian), Energoatomizdat Publ. House, Moscow, Russia, 608 pages.

Groeneveld, D.C., Tavoularis, S., Gudla, P.R.S.S., Yang, S.K., and Leung, L.K.H., 2007, Analytical and Experimental Program of Supercritical Heat Transfer Research at the University of Ottawa, proceedings of the 3rd International Symposium on Supercritical

Water-Cooled Reactors – Design and Technology (ISSCWR-3), March 12-15, Shanghai, China, paper #17, pp. 380-391.

Gu, H.Y., Cheng, X., and Yang, Y.H., 2009. CFD Study on Heat Transfer Deterioration Phenomenon in Supercritical Water Through Vertical Tube, proceedings of 4th International Symposium on Supercritical Water-Cooled Reactors (ISSCWR-4), March 8–11, Heidelberg, Germany, paper# 22, 17 pages.

Gu, H.Y., Zhao, M., and Cheng, X., 2013. Heat Transfer of Supercritical Water Flowig Upward and Downward in a Circular Tube, proceedings of the 15th International Topical Meeting on Nuclear Reactor Thermalhydraulics (NURETH-15), May 12–17, Pisa, Italy, paper #269, 9 pages.

Gupta, S., 2012. Developing Heat Transfer Correlations for Supercritical Fluids Flowing in Bare Vertical Tubes, Thesis design II Final Report, UOIT, 143 pages.

Gupta, S., McGillivray, D., Surendran, P., Trevani, L. and Pioro, I., 2012. Developing Heat-Transfer Correlations for Supercritical CO2 Flowing in Vertical Bare Tubes, proceedings of the 20th International Conference On Nuclear Engineering (ICONE-20) – ASME 2012 POWER Conference, July 30 - August 3, Anaheim, California, USA, paper #54626, 13 pages.

Gupta, S., Mokry, S. and Pioro, I., 2011. Developing A heat-transfer correlation for supercritical-water flow in vertical bare tubes and its application in SCWRS, proceedings of the 19th International Conference On Nuclear Engineering (ICONE-19), Osaka, Japan, October 24-25, Paper# 43503, 11 pages.

Gupta, S., Saltanov, Eu**.** and Pioro, I., 2013. Heat-Transfer Correlation for Supercritical Carbon Dioxide Flowing in Vertical Bare Tubes, Proceedings of the 21st International Conference on Nuclear Engineering (ICONE-21), July 29-August 2, Chengdu, China, Paper #16453, 12 pages.

Gupta, S., Saltanov, Eu., and Pioro, I., 2014. Uses of Supercritical Fluids and their Characteristics within Deteriorated Heat Transfer Region, Proceedings of the 22nd International Conference on Nuclear Engineering (ICONE-22), July 7-11, Prague, Czech Republic, Paper #30274, 12 pages.

Handbook on Lead-bismuth Eutectic Alloy and Lead Properties, Materials Compatibility, Thermal-hydraulics and Technologies, 2007 Edition, Nuclear science.

Hejzlar, P., Dostal, V. and Driscoll, M., 2005. Assessment of Gas Cooled Fast Reactor with Indirect Supercritical CO_2 Cycle, proceeding of the International Congress in Advances of Nuclear Power Plants 2005 (ICAPP'05), Seoul, Korea, May 15–19, paper #5090, 11 pages.

Herkenrath, H., Mörk-Mörkenstein, P., Jung, U., Weckermann, F.J., 1967 (as cited by Cheng et al., 2009). Wärmeübertragung an Wasser bei erzwungener Strömung im Druckbereich von 140 bis 250 bar, EUR 3658d, Euratom.

Huber, M.L., Perkins, R.A., Laesecke, A., Friend, D.G., Sengers, J.V., Assael, M.J., Metaxa, I.M., Vogel, E., Mares, R., and Miyagawa, K., 2009. New International Formulation for the Viscosity of H_2O, *Journal of Physical and Chemical Reference Data*, 38 (2), pp. 101–125.

IAEA, 2011: Heat Transfer Behaviour and Thermohydraulics Code Testing for Supercritical Water Cooled Reactors, www.oecd-nea.org/cpr_scwr_ht , retrieved on October 10, 2011.

IAEA-TECDOC-1746, 2014. *Heat Transfer Behaviour and Thermohydraulics Code Testing for Supercritical Water Cooled Reactors (SCWRs)*. Available at: http://www-pub.iaea.org/MTCD/publications/PDF/TE-1746_web.pdf , 510 pages.

IAPWS, 1998. Revised Release on the IAPS Formulation 1985 for the Thermal Conductivity of Ordinary Water Substance, publication by the International Association for the Properties of Water and Steam. Available at: http://www.15icpws.de/IAPWS_documents/Releases/thcond.pdf , 23 pages.
IAPWS, 2005. Obsolete IAPWS Recommendations. Available at: www.**iapws**.org/relguide/**Obsolete**.pdf , 4 pages.

IAPWS, 2008. Release on the IAPWS Formulation 2008 for the Viscosity of Ordinary Water Substance. Available at: http://www.iapws.org/relguide/visc.pdf , 9 pages.

Incropera, F.P. and DeWitt, D.P., 2002. *Fundamentals of Heat and Mass Transfer*, 5th edition, John Wiley & Sons, New York, NY, USA, 999 pages.

Jackson, J.D., 2008. A Semi-Empirical Model of Turbulent Convective Heat Transfer to Fluids at Supercritical Pressures, proceedings of the 16th International Conference on Nuclear Engineering (ICONE16), May 11–15, 2008, Orlando, Florida, USA, paper #48914, 11 pages.

Jackson, J.D., 2009 (as cited by Ambrosini et al., 2013). Contribution to the IAEA Coordinated Research Programme (CRP) on Heat Transfer Behaviour and Thermo-Hydraulics Code Testing for SCWRs. University of Manchester.

Jackson, J.D., 2009. Validation of an Extended Heat Transfer Equation for Fluids at Supercritical Pressure, proceedings the 3rd International Symposium on Supercritical Water-Cooled Reactors – Design and Technology (ISSCWR-3), March 12–15, Shanghai, China, paper #24, 16 pages.

Jackson, J.D. and Hall W.B., 1979a. Forced Convection Heat Transfer to Fluids at Supercritical Pressure, in book: Turbulent Forced Convection in Channels and Bundles, Editors S. Kakaç and D.B. Spalding, Hemisphere Publishing Corp., New York, New York, USA, Vol. 2, pp. 563–612.

Jackson, J.D. and Hall W.B., 1979b. Influences of Buoyancy on Heat Transfer to Fluids Flowing in Vertical Tubes under Turbulent Conditions, in book: Turbulent Forced Convection in Channels and Bundles, Editors S. Kakaç and D.B. Spalding, Hemisphere Publishing Corp., New York, New York, USA, Vol. 2, pp. 613–640.

Jackson, J.D., Jiang, P.X., Liu, B., and Zhao, C.R., 2011. Interpreting and Categorizing Experimental Data on Forced and Mixed Convection Heat Transfer to Supercritical Pressure Fluids Using Physically-Based Models, proceedings of the International Symposium on Supercritical Water-Cooled Reactors (ISSCWR-5), March 13–16, Vancouver, British Columbia, Canada, paper #103, 13 pages.

Jaromin, M and Anglart, H., 2011. Sensitivity Analysis of Heated Wall Temperature and Velocity Distribution in CFD Simulations of the Upward Flow of Supercritical Water, proceedings of the 14th International Topical Meeting on Nuclear Reactor Thermal Hydraulics (NURETH-14), September 25-29, Toronto, Canada, paper #231, 17 pages.

Jaromin, M. and Anglart, H., 2013. A Numerical Study of the Turbulent Prandtl Number Impact on Heat Transfer to Supercritical Water Flowing Upward under Deteriorated Conditions, proceedings of the 15th International Topical Meeting on Nuclear Reactor Thermalhydraulics (NURETH-15), May 12–17, Pisa, Italy, paper #134, 14 pages.

Kalnin, I.M., Pustovalov, S.B., and Krivtsov, D.V., 2013. CO_2 Heat Pump Technology for Heating Supply System (presentation), European Heat Pump Summit, October 15-26, Nurnberg, Germany.

Kalnin, I.M., Vasutin, V.A., and Pustovalov, S.B., 2003. Conditions for Efficient Application of Carbon Dioxide as a Working Fluid for Heat Pumps (in Russian), *Science and Technology*, 7, pp. 8–12.

Kang, D.J., Kim, S., Bae, Y.Y., and Kim, H.W., 2007. Deterioration Criteria for Heat Transfer to a Vertically Upward Flowing Supercritical CO_2 in a Circular Tube, *Transactions of the Korean Nuclear Society Autumn Meeting*, PyeongChang, Korea, October 25–26, pp. 447–448.

Kao, M.T., Lee, M., Ferng, Y.M., and Chieng, C.C., 2010. Heat Transfer Deterioration in a Supercritical Water Channel. *Nuclear Engineering and Design*, 240, pp. 3321–3328.

Kato, Ya., Muto, Ya., Ishizuka, T., and Mito, M., 2005. Design of Recuperator for the SC CO_2 Gas Turbine Fast Reactor, proceedings of the International Congress on Advances in Nuclear Power Plants 2005 (ICAPP'05), Seoul, Korea, May 15–19, paper #5196, 10 pages.

Kikoin, A.K and Kikoin, I.K., 1976. *Molecular Physics* (in Russian), 2nd edition, Science Publishing House, Moscow, Russia, 480 pages.

Kim, D.E. and Kim, M.H., 2010, Experimental Investigation of Heat Transfer in Vertical Upward and Downward Supercritical CO_2 Flow in a Circular Tube, *International Journal of Heat and Fluid Flow*, 32, pp. 176–191.

Kim, J.K., Jeon, H.K., Yoo, J.Y., and Lee, J.S., 2005. Experimental Study on Heat Transfer Characteristics of Turbulent Supercritical Flow in Vertical Circular / Non-Circular Tubes, proceedings of the 11th International Topical Meeting on Nuclear Reactor Thermal-Hydraulics (NURETH-11), Avignon, France, October 2–6, paper #266, 10 pages.

Kirillov, P., Terent'eva, M., and Deniskina, N., 2007, Thermophsical Properties of Nuclear Engineering Materials (in Russian), 2nd ed., IzdAT Publishing House, Moscow, Russia.

Kiss, A. and Aszodi, A., 2013. Numerical Investigation on the Physical Background of Deteriorated Heat Transfer Mode in Supercritical Pressure Water, proceedings of the 6th International Symposium on Supercritical Water-Cooled Reactors (ISSCWR-6), March 3–7, Shenzhen, Guangdong, China, paper #13071, 21 pages.

Koshizuka, S., Takano, O., and Oka, Y., 1995. Numerical Analysis of Deterioration Phenomena in Heat Transfer to Supercritical Water, *International Journal of Heat and Mass Transfer*, 38 (16), pp. 3307–3084.

Kostyuk, A.G. and Frolov, V.V., 2001. Turbines of Thermal and Nuclear Power Plants, (in Russian). MEI Publ. House, Moscow, Russia, 488 pages

Krasnoshchekov, E.A. and Protopopov, V.S., 1966. Experimental Study of Heat Exchange in Carbon Dioxide in the Supercritical Range at High Temperature Drops, *High Temperatures* (Теплофизика Высоких Температур, стр. 389–398), 4 (3), pp. 375–382.

Krasnoshchekov, E.A. and Protopopov, V.S., 1967 (as cited by Pioro and Duffey, 2007). A Generalized Relationship for Calculation of Heat Transfer to Carbon Dioxide at Supercritical Pressure (π = 1.02–5.25), *High Temperatures* (Теплофизика Высоких Температур, стр. 1314), 9(6), pp. 1215.

Kurganov, V.A., 1998. Heat Transfer and Pressure Drop in Tubes under Supercritical Pressure of the Coolant. Part 1: Specifics of the Thermophysical Properties, Hydrodynamics, and Heat Transfer of the Liquid. Regimes of Normal Heat Transfer, *Thermal Engineering*, 45 (3), pp. 177–185.

Kurganov, V.V. and Kaptil'ny, A.G., 1992. Velocity and Enthalpy Fields and Eddy Diffusivities in a Heated Supercritical Fluid Flow, *Experimental Thermal and Fluid Science*, 5 (4), pp. 465–478.

Kurganov, V.A., Zeigarnik, Yu. A., and Maslakova, I.V., 2009. Problems and Results of Generic Description of Heat-Transfer Mechanism to Coolants at Supercritical Pressures (in Russian), proceedings of the International Workshop "Supercritical Water and Steam in Nuclear Power Engineering: Problems and Solutions", Moscow, Russia, October 22–23, 16 pages.

Kurganov, V.A., Zeygarnik, Yu.A., and Maslakova, I.V., 2012. Heat Transfer and Hydraulic Resistance of Supercritical-Pressure Coolants. Part I: Specifics of Thermophysical Properties of Supercritical Pressure Fluids and Turbulent Heat Transfer under Heating Conditions in Round Tubes (State of the Art), *International Journal of Heat and Mass Transfer*, 55, pp. 3061–3075.

Kurganov, V.A., Zeygarnik, Yu.A., and Maslakova, I.V., 2013a. Heat Transfer and Hydraulic Resistance of Supercritical-Pressure Coolants. Part II: Experimental Data on Hydraulic Resistance and Averaged Turbulent Flow Structure of Supercritical Pressure Fluids During Heating in Round Tubes under Normal and Deteriorated Heat Transfer Conditions, *International Journal of Heat and Mass Transfer*, 58, pp. 152–167.

Kurganov, V.A., Zeygarnik, Yu.A., and Maslakova, I.V., 2013b. Heat Transfer and Hydraulic Resistance of Supercritical-Pressure Coolants. Part III: Generalized Description of SCP Fluids Normal Heat Transfer, Emprirical Calculating Correlations, Integral Method of Theoretical Calculations, *International Journal of Heat and Mass Transfer*, 67, pp. 535–547.

Kurganov, V.A., Zeygarnik, Yu.A., Maslakova, I.V., and Ivanov, F.P., 2011. *Heat Transfer and Hydraulic Resistance in Tubes at the Flow of Coolant at Supercritical Pressures* (in Russian), preprint #2-507, Institute of High Temperatures, Russian Academy of Sciences, Moscow, 168 pages.

Lee, G.H., Bang, Y.S., and Woo, S.W., 2013. Performance Assessment of the Commercial CFD Software for Nuclear Reactor Problems, proceedings of the 15th International Topical Meeting on Nuclear Reactor Thermalhydraulics (NURETH-15), May 12–17, Pisa, Italy, paper #527, 9 pages.

Lemmon, E.W., Huber, M.L., McLinden, M.O., 2013. NIST Standard Reference Database 23: Reference Fluid Thermodynamic and Transport Properties-REFPROP, Version 9.0,

National Institute of Standards and Technology, Standard Reference Data Program, Gaithersburg.

Li, Ho., Kruizenga, A., Anderson, M., Corradini, M., Luo, Y., Wang, H., and Li, Hu., 2011. Development of a New Forced Convection Heat Transfer Correlation for CO_2 in both Heating and Cooling Modes at Supercritical Pressures, *International Journal of Thermal Sciences*, 50, pp. 2430–2442.

Li, J., Jiang, Gm., Yu, Jc., and Yu, Jy., 2013. Assessment of Performance of Turbulence Models of CFX in Predicting Supercritical Water Heat Transfer in a Vertical Tube, proceedings of the 15th International Topical Meeting on Nuclear Reactor Thermalhydraulics (NURETH-15), May 12–17, Pisa, Italy, paper #176, 9 pages.

Licht, J., Anderson, M., and Corradini, M., 2009. Heat Transfer and Fluid Flow Characteristics in Supercritical Pressure Water, *ASME Journal of Heat Transfer*, 131 (7), 072051, 14 pages.

Liu, W., Zhu, Y., Bai, N., Shan, J., and Zhang, B., 2013. Coupled Neutronics/Thermal-hydraulics Analysis of PT–SCWR Fuel Channel, proceedings of the 6th International Symposium on Supercritical Water-Cooled Reactors (ISSCWR-6), March 3–7, Shenzhen, Guangdong, China, paper #13007, 15 pages.

Liu, X., Yang, T., and Cheng, X., 2010. Core and Sub-channel Analysis of SCWR with Mixed Spectrum Core, proceedings of the 2nd Canada-China Joint Workshop on Supercritical Water-Cooled Reactors (CCSC-2010), April 25–28, Toronto, Ontario, Canada, 11 pages.

Lorentzen, G., 1994. Revival of Carbon Dioxide as a Refrigerant, *International Journal of Refrigeration*, 17 (5), pp. 292–301.

Lorentzen, G and Pettersen, J., 1993. A New, Efficient and Environmentally Benign System for Car Air-Conditioning, *International Journal of Refrigeration*, 16 (1), pp. 4–12.

Marquardt, D., 1963. Algorithm for Least Squares Estimation of Nonlinear Parameters. *Journal of the Society for Industrial and Applied Mathematics*, 11 (2), pp. 431–441.

Mathur, G.D., 2000. Carbon Dioxide as an Alternative Refrigerant for Automotive Air Conditioning Systems, American Instituite of Aeronautics and Astronautics, AIAA-2000-2858, pp. 371–379.

McAdams, W.H., 1942. Heat Transmission, 2nd edition, McGraw-Hill, New York, NY, USA, 459 pages.

Menter, F. et al., 2002. (as cited in Kiss and Aszodi, 2013) CFD Best Practice Guidelines for CFD Code Validation for Reactor-Safety Applications, ECORA project, FIKS-CT-2001-00154, Brussels, Belgium.

Miyahara, S., Ishikawa, H., and Yoshizawa, Y., 2011. Experimental Investigation of Reaction Behaviour Between Carbon Dioxide and Liquid Sodium, *Nuclear Engineering and Design*, 241, pp. 1319–1328.

Moisseytsev, A. and Sienicki, J.J., 2009. Investigation of Alternative Layouts for the Supercritical Carbon Dioxide Brayton Cycle for a Sodium-Cooled Fast Reactor, *Nuclear Engineering and Design*, 239, pp. 1362–1371.

Mokry, S., Gospodinov, Ye., Pioro, I., and Kirillov, P., 2009. Supercritical Water Heat-Transfer Correlation for Vertical Bare Tubes, Proceedings of the 17th International Conference on Nuclear Engineering (ICONE-17), July 12–16, Brussels, Belgium, paper #76010, 8 pages.

Mokry, S. and Pioro, I., 2011. Heat Transfer Correlation for Supercritical Carbon Dioxide Flowing Upward in a Vertical Bare Tube, Proceedings of the Supercritical CO_2 Power Cycle Symposium, May 24–25, Boulder, CO, USA, 10 pages.

Mokry, S., Lukomski, A., Gabriel, K., Pioro, I., and Naterer, G., 2011a. Thermalhydraulic and Heat Transfer Correlation for an Intermediate Heat Exchanger Linking a Supercitical Water-Cooled Reactor and a Copper-Chlorine Cycle for Hydrogen Production, Proceedings of the International Conference on Hydrogen Production (ICH2P-11), June 19–22, Thessaloniki, Greece, paper #101THE, 17 pages.

Mokry, S., Pioro, I., Farah, A., King, K., Gupta, S., Peiman, W, and Kirillov, P., 2011b. Development of supercritical water heat-transfer correlation for vertical bare tubes, *Nuclear Engineering and Design*, 241, pp .1126–1136.

Munson, B.R. Young, D.F., Okiishi, T.H., and Huebsch, W.W., 2009. *Fundamentals of Fluid Mechanics*, 6th edition, John Wiley & Sons, USA, ISBN 978-0470-26284-9, 784 pages.

Ornatskiy, A.P., Glushchenko, L.F. and Kalachev, S.I., 1971. Heat transfer with rising and falling flows of water in tubes of small diameter at supercritical pressures, *Thermal Engineering* (Теплоэнергетика, стр. 91–93), 18 (5), pp. 137–141.

Ose, Y., Suzuki, T., Misawa, T., Yoshida, H., and Takase, K., 2013. Numeric al Analysis on Heat Transfer Characteristics of Supercritical Pressure Water in a Heated Tube Base on Three Dimensional Two-Fluid Model, proceedings of the 2013 21st International Conference on Nuclear Engineering (ICONE-21), July 29 – August 2, Chengdu, China, paper #16435, 8 pages.

Palko, D. and Anglart, H., 2009. Investigation of the Onset of Heat Transfer Deterioration to Supercritical Water, proceedings of 4th International Symposium on Supercritical Water-Cooled Reactors (ISSCWR-4), March 8-11, Heidelberg, Germany, paper #19, 13 pages.

Pencer, J., Watts, D., Colton, A., Wang, X., Blomeley, L., Anghel, V., and Yue, S., 2013. Core Neutronics for the Canadian SCWR Conceptual Design, proceedings of the 6th International Symposium on Supercritical Water-Cooled Reactors (ISSCWR-6), March 3–7, Shenzhen, Guangdong, China, paper #13021, 15 pages.

Petukhov, B.S., 1970. Heat Transfer and Friction in Turbulent Pipe Flow with Variable Physical Properties. *Advances in Heat Transfer*, 6, pp. 503–564.

Petukhov, B.S., Ghenin, L.G., Kovalev, S.A., 1974. *Heat Transfer in Nuclear Power Systems* (in Russian: Теплообмен в ядерных энергетических установках), Atomizdat Publishing House, Moscow, Russia, 408 pages.

Petukhov, B.S. and Kirillov, V.V., 1958. About heat transfer at turbulent fluid flow in tubes, (In Russian), *Thermal Engineering* (Теплоэнергетика, стр. 63–68), (4), pp. 63–68.

Petukhov, B.S., Krasnoschekov, E.A. and Protopopov, V.S., 1961. An Investigation of Heat Transfer to Fluids Flowing in Pipes Under Supercritical Conditions, in book: International Developments in Heat Transfer: Papers presented at the 1961 International Heat Transfer Conference, ASME, University of Colorado, Boulder, CO, USA, January 8–12, Part III, paper #67, pp.569–578.

Petuhkov, B.S., Protopopov, V.S., and Silin, V.A., 1972. Experimental Investigation of Worsened Heat-Transfer Conditions with the Turbulent Flow of Carbon Dioxide at Supercritical Pressure, *Teplofizika Vysokikh Temperatur* 10 (2), pp. 347–354.

Pioro, I., 2014. Nuclear Power as a Basis for Future Electricity Generation, proceedings of the 19th Pacific Basin Nuclear Conference (PBNC 2014), August 24-28, Vancouver, BC, Canada, paper #386, 19 pages.

Pioro, I.L. and Duffey, R.B., 2007. *Heat Transfer and Hydraulic Resistance at Supercritical Pressures in Power Engineering Applications*, ASME Press, New York, NY, USA, 334 pages.

Pioro, I.L. and Khartabul, H.F., 2005. Experimental Study on Heat Transfer to Supercritical Carbon Dioxide Flowing Upward in a Vertical Tube, proccedings of the 13th International Conference on Nuclear Engineering (ICONE-13), May 16–20, Beijing, China, paper #50118, 9 pages.

Pioro, I. and Mokry, S., 2011. Thermophysical Properties at Critical and Supercritical Conditions, Chapter in book *Heat Transfer - Theoretical Analysis, Experimental Investigations and Industrial Systems*, Editor: Belmiloudi, A., available at: http://cdn.intechopen.com/pdfs-wm/13204.pdf , retrieved on October 14, 2014, INTECH, Rijeka, Croatia, pp. 573-592

Pis'menny, E.N., Razumovskiy, V.G., and Maevskiy, E.M., 2005. Experimental Study on Temperature Regimes to Supercritical Water Flowing in Vertical Tubes at Low Mass Fluxes, proceedings of the International Conference GLOBAL-2005 "Nuclear Energy Systems for Future Generation and Global Sustainability, Tsukuba, Japan, October 9–13, paper #519, 9 pages.

Pis'menny, E., Razumovskiy, V., Maevskiy, E., Koloskov, A., and Pioro, I., 2006 (as cited by Jaromin and Anglart, 2013). Heat Transfer to Supercritical Water in Gaseous State or Affected by Mixed Convection Vertical Tubes, Proceedings of the 14th International Conference on Nuclear Engineering (ICONE 14), 2006, Miami, FL, USA.

Razumovskiy, V.G., Mayevskiy, E.M., Koloskov, A.E., and Pis'menny, E.N., 2013. Heat Transfer to Water at Supercritical Parameters in Vertical Tubes, Annular Channels, 3- and 7-Rod Bundles, proceedings of the 2013 21st International Conference on Nuclear Engineering (ICONE-21), July 29 – August 2, Chengdu, China, paper #16442, 8 pages.

Richards, G., Harvel, G.D., Pioro, I.L., Shelegov, A.S., and Kirillov, P.L., 2012. Heat Transfer Profiles of a Vertical, Bare, 7-Element Bundle Cooled with Supercritical Freon R-12, *Nuclear Engineering and Design*, 264, pp. 246–256.

Saltanov, Eu., Preda, T., Pioro, I., and Harvel, G., 2013a. Power-Conversion Cycles for Sodium-Cooled Fast Reactors, Proceedings of the 34th Annual Canadian Nuclear Society Conference and 37th CNS/CNA Student Conference, Toronto, ON, Canada, June 9-12, Paper #23, 5 pages.

Saltanov, Eu., Pioro, I. and Harvel, G., 2013b. Preliminary Investigation of Heat-Transfer Correlation for Upward Flow of CO_2 at Supercritical Pressure, Proceedings of the 21st International Conference on Nuclear Engineering (ICONE-21), July 29-August 2, Chengdu, China, Paper #16399, 10 pages.

Saltanov, Eu., Mann, D., Pioro, I., and Harvel, G., 2014a. Specifics of Forced-Convective Heat Transfer in Supercritical Carbon Dioxide, Proceedings of the 38th Annual CNS/CNA Student Conference at the 19th Annual Pacific Basin Nuclear Conference (PBNC), August 24-28, Vancouver, BC, Canada, Paper #30, 8 pages.

Saltanov, Eu., Pioro, I., Mann, D., Gupta, S., Mokry, S. and Harvel, G., 2014b. Study on Specifics of Forced-Convective Heat Transfer in Supercritical Carbon Dioxide, Proceedings of the 22nd International Conference on Nuclear Engineering (ICONE-22), July 7-11, Prague, Czech Republic, Paper #30122, 12 pages.

Samuel, J., Lerchl, G., Harvel, G.D., and Pioro, I., 2014, Investigation of ATHLET System Code for Supercritical Water Applications, proceedings of the 2014 22nd International Conference on Nuclear Engineering (ICONE-22), July 7–11, Prague, Czech Republic, paper #30136, 12 pages.

Schmidt, E., 1969. Properties of Water and Steam in SI-Units, Springer-Verlag New York Inc., 205 pages.

Shams, A., Visser, D.C., and Roelofs, F., 2011. Influence of Numerical Tools on the Flow and Heat Transfer of Supercritical Water, proceedings of the 14th International Topical Meeting on Nuclear Reactor Thermal Hydraulics (NURETH-14), September 25-29, Toronto, Canada, paper #445, 12 pages.

Shan, J., Chen, W., Rhee, B., and Leung, L., 2010. Coupled Neutronics/Thermal-hydraulics Analysis of CANDU-SCWR Fuel Channel, *Annals of Nuclear Energy*, 37, pp. 58–65.

Shan, J., Zhang, B., Li, C., and Leung, L., 2009. SCWR Subchannel Code ATHAS Development and CANDU-SCWR Analysis, *Nuclear Engineering and Design*, 239, pp. 1979–1987.

Sharabi, M., Ambrosini, W., Forgione, N, and He, S., 2007. Prediction of Experimental Data on Heat Transfer to Supercritical Water with Two-equation Turbulence Models, proceedings of the 3rd International Symposium on SCWR – Design and Technology (ISSCWR-3), March 12–15, Shanghai, China, paper #28, pp. 413-428.

Sharabi, M., Manera, A., and Andreani, M., 2009. Implementation of Improved Heat Transfer Correlations in RELAP5 and Application to HPLWR, proceedings of 4th International Symposium on Supercritical Water-Cooled Reactors (ISSCWR-4), March 8–11, Heidelberg, Germany, paper #79, 12 pages.

Shitsman, M.E., 1963. Impairment of the Heat Transmission at Supercritical Pressurre, *High Temperatures*, 1 (2), pp. 237–244.

Simon, N., Latge, C., and Gicquel, L., 2007. Investigation of Sodium – Carbon Dioxide Interactions With Calorimetric Studies, proceedings of the International Congress on Advances in Nuclear Power Plants 2007 (ICAPP'07), May 13-18, Nice, France, Paper #7547, 8 pages.

Sohn, M., Yoo, Yo., and Suh, K., 2005. Recuperator for Supercritical Carbon Dioxide Brayton cycle, proceedings of the International Congress on Advances in Nuclear Power Plants 2005 (ICAPP'05), Seoul, Korea, May 15–19, paper #5584, 5 pages.

Span, R. and Wagner, W., 1996. A New Equation of State for Carbon Dioxide Covering the Fluid Region from the Triple-Point Temperature to 1100 K at Pressures up to 800 MPa, *Journal of Physical and Chemical Reference Data*, 25 (6), pp. 1509–1596.

Styrikovich, M.A., Margulova, T.Kh., and Miropol'skii, Z.L., 1967 (as cited by Bae et al., 2010). Problems in the Development of Designs of Supercritical Boilers, *Thermal Engineering*, 13 (7), pp. 61–68.

Supercritical Water Experiments Database, 2008 (as cited by Jaromin and Anglart, 2013). HPLWR project.

Swenson, H.S., Carver, J.R. and Kakarala, C.R., 1965. Heat Transfer to Supercritical Water in Smooth-Bore Tubes, *Journal of Heat Transfer*, Transactions of the ASME, Series C, 87 (4), pp. 477–484.

Technology Roadmap for Generation IV Nuclear Energy Systems, 2002. Issued by the U.S. DOE Nuclear Energy Research Advisory Committee and the Generation IV International Forum, GIF-002-00, available at: https://www.gen-4.org/gif/upload/docs/application/pdf/2013-09/genivroadmap2002.pdf , retrieved on September 17, 2014, 97 pages.

Technology Roadmap Update for Generation IV Nuclear Energy Systems, 2014. Issued by the OECD Nuclear Energy Agency for the Generation IV International Forum, available at: https://www.gen-4.org/gif/upload/docs/application/pdf/2014-03/gif-tru2014.pdf , retrieved on September 17, 2014, 66 pages

Tejaswini, U.S., Basu, D.N., and Pandey, M., 2013. CFD Investigation of Heat Transfer Deterioration in Supercritical Water Flowing Through Vertical Annular Channels, proceedings of the 2013 21st International Conference on Nuclear Engineering (ICONE-21), July 29 – August 2, Chengdu, China, paper #16720, 7 pages.

US Energy Information Administration, 2014. International Energy Statistics, available at: http://www.eia.gov/cfapps/ipdbproject/iedindex3.cfm?tid=2&pid=82&aid=12&cid=ww,&syid=2008&eyid=2012&unit=BKWH , retrieved on September 21, 2014.

Vesovic, V., Wakeham, W.A., Olchowy, G.A., Sengers, J.V., Watson, J.T.R., and Millat, J., 1990. The Transport Properties of Carbon Dioxide, *Journal of Physical and Chemical Reference Data*, 19 (3), pp. 763–808.

Vikhrev, Yu.V., Barulin, Yu.D. and Kon'kov, A.S., 1967. A Study of Heat Transfer in Vertical Tubes at Supercritical Pressures, *Thermal Engineering*, 14 (9), pp. 116–119.

Wagner, W. and Pruss, A., 2002. The IAPWS Formulation 1995 for the Thermodynamic Properties of Ordinary Water Substance for General and Scientific Use, *Journal of Physical and Chemical Reference Data*, 31(2), pp. 387–535.

Wan, Yu., Xu, Ti., and Pruess, K., 2011. Impact of Fluid-Rock Interactions on Enhanced Geothermal Systems with CO_2 as Heat Transmission Fluid, proceedings of the 36th Workshop on Geothermal Reservoir Engineering, January 31 – February 2, Stanford University, Stanford, CA, USA, SGP-TR-191, 9 pages.

Wang, F., Cui, B., Zhang, Sh., and Qin, X., 2013. Numerical Simulation of Supercritical Water Heat Transfer in the Vertically Heated Tube, proceedings of the 2013 21st International Conference on Nuclear Engineering (ICONE-21), July 29 – August 2, Chengdu, China, paper #16158, 5 pages.

Watts, M.J. and Chou C.T., 1982. Mixed convection heat transfer to supercritical pressure water, proceedings of the 7th International Heat Transfer Conference, Munchen, Germany, Vol. 3, Paper No. 6–10, pp. 495–500.

Winterton, R.H.S., 1998. Where Did the Dittus and Boelter Equation Come From*? International Journal of Heat and Mass Transfer*, 41 (4–5), pp. 809–810.

Xiong, J., Cheng, X., and Yang, Y., 2013 Turbulence Modelling for Supercritical Fluid Heat Transfer in a Round Tube, proceedings of the 15th International Topical Meeting on Nuclear Reactor Thermalhydraulics (NURETH-15), May 12–17, Pisa, Italy, paper #347, 14 pages.

Yamagata, K., Nishikawa, K., Hasegawa, S., Fujii, T., and Yoshida, S., 1972. Forced Convective Heat Transfer to Supercritical Water Flowing in Tubes, *International Journal of Heat and Mass Transfer*, 15, pp. 2575–2593.

Yang, S.K., 2013. Heat Transfer Modes in Supercritical Fluids, proceedings of the 15th International Topical Meeting on Nuclear Reactor Thermalhydraulics (NURETH-15), May 12–17, Pisa, Italy, paper #547, 12 pages.

Yang, T., Yang., J., Cheng, X., Liu, X., and Gu, H., 2013. Development and Validation of a Subchannel Code Applicable for SCWR, proceedings of the 6th International Symposium on Supercritical Water-Cooled Reactors (ISSCWR-6), March 3–7, Shenzhen, Guangdong, China, paper #13020, 17 pages.

Yetisir, M., Gaudet, M., and Rhodes, D., 2013. Development and Integration of Canadian SCWR Concept with Counter-Flow Fuel Assembly, proceedings of the 6th International Symposium on Supercritical Water-Cooled Reactors (ISSCWR-6), March 3–7, Shenzhen, Guangdong, China, paper #13059, 9 pages.

Yildiz, S. and Groeneveld, D.C., 2014. Diameter Effect on Supercritical Heat Transfer, *International Communications in Heat and Mass Transfer*, 54, pp. 27–32.

Zahlan, H., Groeneveld, D.C., Tavoularis, S., Mokry, S., and Pioro, I., 2011. Assessment of Supercritical Heat Transfer Prediction Methods, proceedings of the International Symposium on Supercritical Water-Cooled Reactors (ISSCWR-5), March 13–16, Vancouver, British Columbia, Canada, paper #8, 20 pages.

Zahlan, H., Jiang, K., Tavoularis, S., and Groeneveld, D., 2013. Measurements of Heat Transfer Coefficient, CHF and Heat Transfer Deterioration in Flows of CO_2 at Near-critical and Supercritical Conditions, proceedings of the 6th International Symposium on Supercritical Water-Cooled Reactors (ISSCWR-6), March 3–7, Shenzhen, Guangdong, China, paper #13006, 18 pages.

Zvorykina, A., Gupta, S., Peiman, W., Fialko, N., and Pioro, I., 2012. Current Status and Future Applications of Supercritical Pressures in Power Engineering, proceedings of the 2012 20th International Conference on Nuclear Engineering (ICONE-20), July 30 – Aug. 3, Anaheim, CA, USA, paper #54558, 16 pages.

Appendix A. Developed Code for Structuring AECL MR-1 Loop Raw Data and Calculation of Relative Errors of Experimental Heat Transfer Coefficients and Other Related Experimental Parameters.

```
%The code was developed in Matlab
clear all;
tic
%open the excel file with the raw data; first, enter the proper name.
%fin='C:\Users\100407492\Desktop\Transfer\Pioro''s data\CO2
data\07_03_2003_corrected ver
7\07_03_2003_MR1CO2Prop2_v9_corr_nf_Normal.xls';
%fin='C:\Users\100407492\Desktop\Transfer\Pioro''s data\CO2
data\10_03_2003_corrected ver
7\10_03_2003_MR1CO2Prop2_v8_corr_nf_Normal.xls';
%fin='C:\Users\100407492\Desktop\Transfer\Pioro''s data\CO2
data\13_02_2003 corrected ver 7\&MR1CO2Prop2_v8_corr_nf_Normal.xls';
%fin='C:\Users\100407492\Desktop\Transfer\Pioro''s data\CO2
data\18_02_2003 corrected ver
7\18_02_2003_MR1CO2Prop2_v8_corr_nf_Normal.xls';
%fin='C:\Users\100407492\Desktop\Transfer\Pioro''s data\CO2
data\20_02_2003_corrected ver
7\20_02_2003_MR1CO2Prop2_v8_corr_nf_Normal.xls';
%fin='C:\Users\100407492\Desktop\Transfer\Pioro''s data\CO2
data\21_02_2003 corrected ver 7\MR1CO2Prop2_v8_corr_nf_Normal.xls';
%fin='C:\Users\100407492\Desktop\Transfer\Pioro''s data\CO2
data\26_02_2003_corrected ver 7 Part
1\&MR1CO2Prop2_v8_corr_nf_Normal.xls';
fin='C:\Users\100407492\Desktop\Transfer\Pioro''s data\CO2
data\26_02_2003_corrected ver 7 Part
2\&MR1CO2Prop2_v8_corr_nf_Normal.xls';

runid='s0';
runid_c='s0';
pos=1;
excel_n=1;
while runid~=' ' & length(runid) >=2

ki=0;

while runid_c==runid
    pos=pos+1;
    pos_s=num2str(pos);
    ki=ki+1;
[num, b, runid] = xlsread(fin,strcat('B',pos_s,':B',pos_s));
[num, b, runid_c] =
xlsread(fin,strcat('B',num2str(pos+1),':B',num2str(pos+1)));
end;

pos = pos - ki+1;
pos_s=num2str(pos);

[num, rundate] = xlsread(fin,strcat('C',pos_s,':C',pos_s));
[num, runtime] = xlsread(fin,strcat('D',pos_s,':D',pos_s));
```

```
range=strcat('E',pos_s,':','AR',num2str(pos+ki-1));
asdf = xlsread(fin,range);
%let's calculate average values of experimental parameters, bulk-fluid
and
%internal wall temperatures!
coolant = 'co2';
data = zeros(2,40);
data(1,:) = mean(asdf);
L = 2.208; % m

TC_loc =   zeros(22,1);
TC_loc_l = zeros(22,1);
Q_loc = zeros(22,1);
Q_vol = zeros(22,1);
HTC_error = zeros(22,1);

j=1;
for i = 57:100:2157
    TC_loc(j,1)=i; %in mm
    TC_loc_l(j,1)=100; %in mm
    j=j+1;
end

TC_loc_l(1,1) = 106; %mm
TC_loc_l(22,1) = 102; %mm

PDT_loc(1:5,1) = [2171; 563; 1099; 1635; 2171];
PDT_data = zeros (5,9);
PDT_data(1:5,1) = [0; 1; 2; 3; 4];
PDT_data(1:5,2) = (PDT_loc(1:5,1)-1)/10;
PDT_data(1:5,3) = data(1,6:10);
PDT_data(1,4) = PDT_error(data(1,6),300);

for i=2:5
    PDT_data(i,4) = PDT_error(data(1,i+5),50);
end

n_rows = size(asdf,1)

    for i = 1:40

    sum = 0;

    for j = 1:n_rows

        sum = sum + (asdf(j,i)/data(1,i)-1)^2;

    end

    data(2,i) = sum/n_rows;

end;

T_bf = zeros(2209,1);
```

```
p = zeros(2209,1);
h = zeros(2209,1);
T_w_ext = zeros(22,1);
T_w_int = zeros (22,1);

D = 10.0e-3;
D_in = 8.058e-3;
Acr = pi/4*(D^2 - D_in^2);

T_bf(1,1) = data(1,12);  %Used to be 16 -- don't forget to subtract 4!
because of the string data in the intermediate Excel sheet!!
p(1,1) = (data(1,6) + data(1,3));
%dp = p(1,1)*P_in_error(p(1,1));
dp = data(1,5);
[tbe hbe] = T_b_in_error(T_bf(1,1),p(1,1));

m_fr = data(1,11);
G = 4*m_fr / (pi*D_in^2);
G_e = G_error(dp,p(1,1), T_bf(1,1));

T_amb = data(1,16);

I = data(1,2);
POW_TS = data(1,1)*1d3;
V = POW_TS/I;
[POW_e POW_a] = POW_TS_error(V, I);
[q_ave_e q_ave_abs] = q_ave_error(V, I);

h(1,1) = refpropm('H','T',T_bf(1,1)+273.15,'P',p(1,1),coolant);
HL = 0.47 * (mean(data(1,18:39)) - T_amb)/L;
T_w_ext(:,1) = data(1,18:39);

for j=1:22

    k = k_i600(T_w_ext(j,1));
    T_w_int(j,1) = T_w_ext(j,1);
    eps=0.2;

     while abs (eps) > 0.1

        Q_loc(j,1) =( I^2 * rho_i600( (T_w_ext(j,1) + T_w_int(j,1))/2 )
/ Acr - HL );
        Q_vol(j,1) = Q_loc(j,1)/Acr;
        T_w_int(j,1) = T_w_ext(j,1) + Q_vol(j,1) / (4*k) * (D^2 -
D_in^2)/4 - Q_vol(j,1) / (2*k)*(D/2)^2*log(D/D_in);
        k_new = k_i600( (T_w_ext(j,1) + T_w_int(j,1))/2 );
        eps = k - k_new;
        k = k_new;

    end;

end;
```

```
j=1;
dTw = zeros(22,1);
dTb = zeros(22,1);
out2 = zeros(22,10);

p_grav=0;
p_acc=0;
p_f=0;
k=1; % PDT counter

hbe = sqrt( hbe^2 + POW_e^2 + (G_e^2 - (2.5e-5)^2) + 1.96*10^-6);
%calculational error in hb

for i=2:2209

    h(i,1) = h(i-1,1) + Q_loc(j,1)*10^-3/m_fr;
    T_bf(i,1) = refpropm('T','h',h(i,1),'P',p(i-1,1),coolant);

    rho_out = refpropm('D','T',T_bf(i,1),'p',p(i-1,1),coolant);
    rho_in = refpropm('D','T',T_bf(i-1,1)+273.15,'P',p(i-1,1),coolant);

    dp_grav = (rho_in+rho_out)/2*9.81/10^6;
    p_grav = p_grav + dp_grav;
    dp_acc = G^2*(1/rho_out - 1/rho_in)/10^3;
    p_acc = p_acc + dp_acc;
    p(i,1) = p(i-1,1) -  dp_grav - dp_acc;
    T_bf(i,1) = T_bf(i,1) - 273.15;

    if ismember(i,TC_loc)

        tbe = T_b_calc_error(p(i,1),h(i,1), hbe);

        dTb(j,1) = tbe*T_bf(i,1);
        dTw(j,1) = T_w_int(j,1)*T_w_int_error2 (T_w_ext(j,1), T_amb,
I);
        twb = ( dTw(j,1)^2 + dTb(j,1)^2 ) / (T_w_int(j,1) -
T_bf(i,1))^2;

        HTC_error(j,1) = sqrt ( q_ave_e^2 + twb );
        HTC_error(j,1) = r2sd2 (HTC_error(j,1), 3);

        out2(j,1) = j+1;
        out2(j,2) = (TC_loc(j)-1)/10;
        out2(j,3) = T_bf(i,1);
        out2(j,4) = tbe;
        out2(j,5) = h(i,1)/1000;
        out2(j,6) = T_w_int(j,1);
        out2(j,7) = T_w_int_error2 (T_w_ext(j,1), T_amb, I);
        out2(j,8) = T_w_int(j,1) - dTw(j,1) - dTb(j,1) - T_bf(i,1);
        out2(j,9) = Q_loc(j,1) / (T_w_int(j,1) -
T_bf(i,1))/(pi*D_in)/1000;
        out2(j,10) = HTC_error(j,1);
        out2(j,11) = G_e;
```

```
    end

    if i>TC_loc(j,1)+TC_loc_l(j,1)/2
        j=j+1;
    end;

    if ismember(i,PDT_loc)

        PDT_data(k+1,5) = p_grav;
        PDT_data(k+1,6) = p_acc;
        PDT_data(k+1,7) = PDT_data(k+1,3) - p_grav - p_acc;
        PDT_data(k+1,8) = T_bf(i,1);
        p_grav=0;
        p_acc=0;
        k=k+1;
    end

end

PDT_data(1,8) = T_bf(2171,1);
PDT_data(1,9) = T_w_int(22,1) + (T_w_int(22,1) - T_w_int(21,1))*14/100;
PDT_data(2,9) = T_w_int(6,1) + (T_w_int(7,1) - T_w_int(6,1))*6/100;
PDT_data(3,9) = T_w_int(11,1) + (T_w_int(12,1) - T_w_int(11,1))*42/100;
PDT_data(4,9) = T_w_int(16,1) + (T_w_int(17,1) - T_w_int(16,1))*78/100;
PDT_data(5,9) = PDT_data(1,9);

%format the name of the output excel file
q_ave = POW_TS / (pi*D_in*L);
fout=num2str(excel_n);
fout=strcat(fout,'-','T8-');
add=num2str(r2sd2(p(1,1),3));
fout=strcat(fout,add);
add=num2str(r2sd2(G,2));
if length(add) == 3
    add=strcat('0',add)
end
fout=strcat(fout,'-',add);
add=num2str(r2sd2(q_ave/1000,2));
if ismember('.',add)
    add=num2str(r2sd2(q_ave/1000,1));
end;
if length (add) == 2
    add = strcat('0',add)
end
fout=strcat(fout,'-',add);
add=num2str(r2sd2(T_bf(1,1),2));
if length (add) == 1
    add = strcat('0',add)
end
fout=strcat(fout,'-',add);
%fout=strcat(fout,'-',add,'-RED');
%formatting output excel file

out1(1:4,1) = [p(1,1)/1000; G; q_ave/1000; T_bf(1,1)];
xlswrite(fout,{strcat(num2str(ki),' lines')},'D1:D1');
```

```
%write average inlet parameters: P, G, q'', T_in
xlswrite(fout,out1,'D5:D8');
%write location of TC, Tb, Tw, HTC and respective errors, etc.
xlswrite(fout,out2,'A13:K34');
%write location of PDTs, and their readings, etc.
xlswrite(fout,PDT_data,'M13:U17');
%write the labels in cells
xlswrite(fout,{'Date & Time'; 'Shape'; 'Raw Data'; 'Test Conditions';
'Inlet Pres.'; 'Mass Flux'; 'Heat Flux'; 'Inlet Temp.'},'A1:A8');
xlswrite(fout,rundate,'B1:B1');
xlswrite(fout,runtime,'C1:C1');
xlswrite(fout,{runid},'C3:C3')
xlswrite(fout,{'TB8.058'; 'SCCO2_ILPHTC'; 'unit'; 'MPa'; 'kg/m2s';
'kW/m2'; 'C'}, 'B2:B8');
xlswrite(fout,{'No', 'Dist.', 'Tb', 'Tb_e', 'hb', 'Tw', 'Tw_e', 'Tw-Tb-
abs_error', 'HTC', 'HTC_e', 'G_e'; '', 'cm', 'C', '', 'kJ/kg', 'C', '',
'C', 'kW/m2K','',''},'A11:K12');
xlswrite(fout,{'No of PDT', 'PDT_loc', 'PD', 'PDT_e', 'p_grav',
'p_acc', 'p_fr', 'Tb', 'Tw'; '(Total PD, PDT110, PDT111, PDT112,
PDT113)','cn','kPa','','kPa','kPa','kPa','C','C'},'M11:U12');

[num, b, runid_c] =
xlsread(fin,strcat('B',num2str(pos+ki),':B',num2str(pos+ki)));
runid=runid_c;
excel_n = excel_n + 1;
pos = pos + ki-1;
end
toc


function [ PDT_e ] = PDT_error( dp, span )
%UNTITLED Summary of this function goes here
%   Detailed explanation goes here

ai = 5.12* (2.5e-4*5.12/4*span);
ad = 5.12/8192/4*span;
PDT_e = sqrt( ((0.005*span)^2 + ai^2 + ad^2)/dp^2 + 1e-6);
PDT_e = r2sd2(PDT_e,3);

End


function [P_in_e] = P_in_error(P_in);

     P_in_e = sqrt ( ( (10)^2 + (3.2)^2 + (1.56)^2 ) / P_in^2 + (10)^-
6);
     P_in_e = r2sd2(P_in_e, 3);

End


% calculate the uncertainty in T_bulk_inlet and H_b_inlet.  These would
be
% the input to the function calculating uncertainty in T_b at any other
% point along the test-section
```

```
function [Tb_in_e Hb_in_e] = T_b_in_error (Tb_in, P_in);

    fluid = 'co2';
    dt = 273.15;
    %Tb_in_e = sqrt ( ( (0.3)^2 + (0.12)^2 + (0.03)^2 ) / Tb_in^2 );
    Tb_in_e = sqrt ( (  (0.5)^2 + (0.53)^2 + (0.06)^2 + (0.03)^2 +
(0.02)^2 ) / Tb_in^2 );
    Tb_in_e = r2sd2(Tb_in_e, 2);

    if Tb_in > 100.0
        Tb_in_e = r2sd2 ( 2.2 / Tb_in, 2);
    end

    P_in_e = P_in_error(P_in);

    Hb =     refpropm('H','T',Tb_in+dt,'P',P_in,fluid);
    Hb_min = refpropm('H','T',Tb_in*(1-
Tb_in_e)+dt,'P',P_in*(1+P_in_e),fluid);
    Hb_max = refpropm('H','T',Tb_in*(1+Tb_in_e)+dt,'P',P_in*(1-
P_in_e),fluid);
    delta_Hb(1) = abs (Hb - Hb_min);
    delta_Hb(2) = abs (Hb_max - Hb);

    delta_Hb_max = max(delta_Hb);

    %Hb_in_e = sqrt ( Tb_in_e^2 + P_in_e^2 + 6.25*10^-4); forgot what
the
    %last numerical term is for!!!
    Hb_in_e = delta_Hb_max/Hb^2;
    Hb_in_e = r2sd2 (Hb_in_e, 3);

end


function [G_e] = G_error (dp, P_in, Tb_in);

    fluid = 'co2';
    dt = 273.15;

    P_in_e = P_in_error(P_in);
    Tb_in_e = sqrt ( (  (0.5)^2 + (0.53)^2 + (0.06)^2 + (0.03)^2 +
(0.02)^2 ) / Tb_in^2 );
    Tb_in_e = r2sd2(Tb_in_e, 2); %assumed that T_in cannot be higher
than 100degC

% Afl_e is assumed to be equal to 0.50 percent

    rho =     refpropm('D','T',Tb_in+dt,'P',P_in,fluid);
    rho_min = refpropm('D','T',Tb_in*(1+Tb_in_e)+dt,'P',P_in*(1-
P_in_e),fluid);
    rho_max = refpropm('D','T',Tb_in*(1-
Tb_in_e)+dt,'P',P_in*(1+P_in_e),fluid);
    delta_rho(1) = abs (rho - rho_min);
```

```
    delta_rho(2) = abs (rho_max - rho);

    delta_rho_max = max(delta_rho);

    rho_e = sqrt(2.5e-7+ (delta_rho_max/rho)^2);
    %rho_e = sqrt(2.5e-7 + 2.5e-3);

    dp_e = sqrt ( ( (0.185)^2 + (0.01184)^2 + (0.0058)^2 )/dp^2 + 1e-6
);

    m_e = sqrt ( 6.4e-7 + (0.5*rho_e)^2 + (0.5*dp_e)^2);
    m_e = r2sd2(m_e, 3);

    G_e = sqrt(m_e^2 + 2.5e-5);
    G_e = r2sd2(G_e, 3);

end


%Find relative and absolute error in total test-section power
measurement.
%Analyzed data are from SCCO2 experiments held by Dr. Pioro at MR-1
(Chalk
%River) in 2003;  Script is written by Eugene Saltanov in July 2013.
Send
%stones, comments and critique to eugene.saltanov@uoit.ca
function [POW_e, POW_abs] = POW_TS_error(V,I)

    POW_e = sqrt( 6.250e-6 + 4.0e-8 + 1.0e-6 + 8.1e-7 + (0.5/I)^2 +
(0.04/V)^2 );
    POW_e = r2sd2(POW_e,3);
    POW_abs = POW_e * I*V;

End


% for this specific case
function [q_ave_e q_ave_abs] = q_ave_error(V, I);

    [POW_e POW_abs] = POW_TS_error(V,I);

    q_ave_e = sqrt(POW_e^2 + 0.0014^2);
    q_ave_e = r2sd2(q_ave_e, 3);

    q_ave_abs = q_ave_e * V*I / 55.8954;
    q_ave_abs = r2sd2(q_ave_abs,3);

end


% This function calculates thermal conductivity of the Inconel alloy
600
```

```
% based on a correlation published in Pioro and Duffey (2007) book on
Heat
% Transfer and Hydraulic Resistance.  The data for k were used from the
Data Information Sheet
% of the Special Metals Corporation (2002)
% Temeprature must be entered in deg C.
function [result] = k_i600(T);

 result = 14.2214329176 + 0.0162450563 * T;

end


% This function calculates electrical resistivity of the Inconel alloy
600
% based on a correlation published in Pioro and Duffey (2007) book on
Heat
% Transfer and Hydraulic Resistance.  The data for k were used from the
Data Information Sheet
% of the Special Metals Corporation (2002)
% Temeprature must be entered in deg C.
function [result] = rho_i600(T);

 result = (10^-8)*(103.1289703317 - 5.4963164982*(10^-4)*T +
6.4711351326*(10^-5)*T^2 - 6.111698975*(10^-8)*T^3);

end


%I needed to do the calculations of error according to metrological
rules
%and was lazy to register at MathWorks site. r2sd = 'round to required
%significant digits'
%If you have comments, please send them to eugene.saltanov@uoit.ca
function [result] = r2sdv2(x, NSD) % x - value to be rounded to the
required number of significant digits

a=round(NSD+1);
b=NSD-1;
fmt1=strcat('%',num2str(a),'.',num2str(b),'e');
c=num2str(x,fmt1);
result=str2num(c);

end


function [Tw_int_e] = T_w_int_error2 (Tw_ext, T_amb, I);

    a = ( (0.3)^2 + (0.16)^2 + (0.03)^2 ) / Tw_ext^2 ;
    if Tw_ext > 100.0
        a = (2.2 / Tw_ext)^2 ;
    end;

    dTw_ext = sqrt(a)*Tw_ext;
```

```
    T_amb_e = ( (0.3)^2 + (0.16)^2 + (0.03)^2 ) / T_amb^2 ;
    if T_amb > 100.0
        T_amb_e = (2.2 / T_amb)^2 ;
    end;

    dT_amb = sqrt(T_amb_e)*T_amb;

    q_vol_e = (6.250e-6 + 4.0e-8 + 1.0e-6 + 8.1e-7 + (0.5/I)^2) +
(0.6e-2)^2 + (5.245e-2)^2 + (dTw_ext^2 + dT_amb^2)/(Tw_ext - T_amb)^2 +
(2.623e-2)^2;

    b = (q_vol_e^2 + (6.25)*10^-4 + (1.036e-2)^2);



    c = (q_vol_e^2 + (6.25)*10^-4 + 8.0*10^-6 +(1.036e-2)^2) ;

    Tw_int_e = sqrt ( a+b+c );
    Tw_int_e = r2sd2 (Tw_int_e, 3);

End


% Here the calculational error for T_bulk and H_bulk is calculated.
The
% required input are the relative errors of the T_bulk and H_bulk at
the
% inlet from T_b_in_error funtion

function [Tb_calc_e Hb_calc_e] = T_b_calc_error (P_in, Hb, Hb_e);

    P_in_e = P_in_error(P_in);

    fluid = 'co2';
    dt = 273.15;

    Tb_calc =     refpropm('T','H',Hb,'P',P_in,fluid);
    Tb_calc_min = refpropm('T','H',Hb*(1-Hb_e),'P',P_in*(1-
P_in_e),fluid);
    Tb_calc_max =
refpropm('T','H',Hb*(1+Hb_e),'P',P_in*(1+P_in_e),fluid);
    delta_Tb_calc(1) = abs (Tb_calc - Tb_calc_min);
    delta_Tb_calc(2) = abs (Tb_calc_max - Tb_calc);

    delta_Tb_calc_max = max(delta_Tb_calc);

    Tb_calc_e = delta_Tb_calc_max / (Tb_calc);

    %thermocouples are calibrated for positive deg C scale
    %Tb_calc_e = sqrt ( Pin_e^2 + Hb_e^2);

    %m_e = sqrt (G_e^2 - (2.5e-5)^2)
```

```
    %Hb_calc_e = sqrt( Hb_e^2 + q_ave_e^2 + (G_e^2 - (2.5e-5)^2) +
6.25*10^-4);

end
```

Appendix B. Non-Dimensional Analysis

The general equations of continuity, motion and energy balance for the unsteady flow of viscous Newtonian fluid with variable thermal properties are presented below in Cartesian system of coordinates (Petukhov et al., 1974).

Continuity equation:

$$\frac{\partial \rho}{\partial t} + \frac{\partial (\rho w_x)}{\partial x} + \frac{\partial (\rho w_y)}{\partial y} + \frac{\partial (\rho w_z)}{\partial z} = 0, \qquad \text{(B.1)}$$

where t – time, and w_i – components of velocity in x, y, and z directions.

Equation of motion:

$$\rho \frac{\partial w_x}{\partial t} = \rho F_x - \frac{\partial p}{\partial x} + \frac{\partial}{\partial x}\left[\mu\left(2\frac{\partial w_x}{\partial x} - \frac{2}{3}\mathrm{div}\vec{w}\right)\right] + \frac{\partial}{\partial y}\left[\mu\left(\frac{\partial w_x}{\partial y} + \frac{\partial w_y}{\partial x}\right)\right] + \frac{\partial}{\partial z}\left[\mu\left(\frac{\partial w_x}{\partial z} + \frac{\partial w_z}{\partial x}\right)\right];$$
$$\rho \frac{\partial w_y}{\partial t} = \rho F_y - \frac{\partial p}{\partial y} + \frac{\partial}{\partial y}\left[\mu\left(2\frac{\partial w_y}{\partial y} - \frac{2}{3}\mathrm{div}\vec{w}\right)\right] + \frac{\partial}{\partial z}\left[\mu\left(\frac{\partial w_y}{\partial z} + \frac{\partial w_z}{\partial y}\right)\right] + \frac{\partial}{\partial x}\left[\mu\left(\frac{\partial w_y}{\partial x} + \frac{\partial w_x}{\partial y}\right)\right];$$
$$\rho \frac{\partial w_z}{\partial t} = \rho F_z - \frac{\partial p}{\partial z} + \frac{\partial}{\partial z}\left[\mu\left(2\frac{\partial w_z}{\partial z} - \frac{2}{3}\mathrm{div}\vec{w}\right)\right] + \frac{\partial}{\partial z}\left[\mu\left(\frac{\partial w_z}{\partial x} + \frac{\partial w_x}{\partial z}\right)\right] + \frac{\partial}{\partial y}\left[\mu\left(\frac{\partial w_z}{\partial y} + \frac{\partial w_y}{\partial z}\right)\right],$$

(B.2)

where p – pressure, and F_i – components of the body forces. The set of Eq. (B.2) is also as the Navier-Stokes equations.

Energy balance equation:

$$\rho c_p \frac{DT}{Dt} = \mathrm{div}(k \cdot \mathrm{grad}T) + q_{vol} + \frac{Dp}{Dt} + \mu\Phi, \qquad \text{(B.3)}$$

where q_{vol} – volumetric internal heat generation rate, $\frac{D}{Dt} = \frac{d}{dt} + w_x \frac{\partial}{\partial w_x} + w_y \frac{\partial}{\partial w_y} + w_z \frac{\partial}{\partial w_z}$ – material (or substantial) derivative, and Φ - dissipative function expressed as:

$$\Phi = 2\left[\left(\frac{\partial w_x}{\partial x}\right)^2 + \left(\frac{\partial w_y}{\partial y}\right)^2 + \left(\frac{\partial w_z}{\partial z}\right)^2\right] + \left(\frac{\partial w_x}{\partial y} + \frac{\partial w_y}{\partial x}\right)^2 + \left(\frac{\partial w_x}{\partial z} + \frac{\partial w_z}{\partial x}\right)^2 + \left(\frac{\partial w_y}{\partial z} + \frac{\partial w_z}{\partial y}\right)^2 - \frac{2}{3}\left(\mathrm{div}\vec{w}\right)^2 \tag{B.4}$$

The governing equations (B.1) – (B.3) are differential non-linear equations, which can be simplified and resolved only for a limited number of situations under several assumptions. For example, for the flow with constant properties, these equations can be simplified to the following form:

$$\begin{aligned}
&\mathrm{div}\vec{w} = 0;\\
&\frac{\partial w_x}{\partial t} + \left(\vec{w}\cdot\mathrm{grad}\right)w_x = F_x - \frac{1}{\rho}\frac{\partial p}{\partial x} + \frac{\mu}{\rho}\nabla^2 w_x;\\
&\frac{\partial w_y}{\partial t} + \left(\vec{w}\cdot\mathrm{grad}\right)w_y = F_y - \frac{1}{\rho}\frac{\partial p}{\partial y} + \frac{\mu}{\rho}\nabla^2 w_y;\\
&\frac{\partial w_z}{\partial t} + \left(\vec{w}\cdot\mathrm{grad}\right)w_z = F_z - \frac{1}{\rho}\frac{\partial p}{\partial z} + \frac{\mu}{\rho}\nabla^2 w_z;\\
&\frac{\partial T}{\partial t} + \left(\vec{w}\cdot\mathrm{grad}\right)T = \frac{1}{\rho c_p}\left(k\nabla^2 T + q_{vol} + \mu\Phi\right).
\end{aligned} \tag{B.5}$$

Although (B.5) is a simplified form of the Eqs. (B.1) – (B.3) it allows to deduce certain regularities of the heat transfer processes.

There are many engineering applications for forced convection flows with no thermal energy generation and for which body forces are negligible. Appreciation of processes occurring in the boundary layer may be obtained by using further simplifications to Eqs. (B.5), known as boundary approximations (Incropera and DeWitt, 2002; Bergman et al., 2011):

$$
\begin{aligned}
& w_x >> w_y; \\
& \frac{\partial w_x}{\partial y} >> \frac{\partial w_x}{\partial x}, \frac{\partial w_y}{\partial y}, \frac{\partial w_y}{\partial x}; \\
& \frac{\partial T}{\partial y} >> \frac{\partial T}{\partial x}; \\
& \frac{\partial p}{\partial y} = 0.
\end{aligned}
\tag{B.6}
$$

The first three equations from the set (B.6) are based on the experimental observations that the boundary layer thicknesses are typically very small, the velocity component along the surface is much larger than that normal to the surface, and gradients of temperature and *x*-component of velocity are the highest in the normal direction to the surface. The last approximation is obtained from the order-of-magnitude analysis (Incropera and DeWitt, 2002). Restricting our attention to a two-dimensional flow, the governing equations can be simplified as follows:

$$
\begin{aligned}
& \frac{\partial w_x}{\partial x} + \frac{\partial w_y}{\partial y} = 0; \\
& w_x \frac{\partial w_x}{\partial x} + w_y \frac{\partial w_x}{\partial y} = -\frac{1}{\rho}\frac{\partial p}{\partial x} + \frac{\mu}{\rho}\frac{\partial^2 w_x}{\partial y^2}; \\
& w_x \frac{\partial T}{\partial x} + w_y \frac{\partial T}{\partial y} = \frac{1}{\rho c_p}\left(k\frac{\partial^2 T}{\partial y^2} + \mu\left(\frac{\partial u}{\partial y}\right)^2 \right).
\end{aligned}
\tag{B.7}
$$

The set of equations (B.7) can be brought to a non-dimensional form by normalizing basic variables entering it to some reference values. These reference values are usually the following: 1) characteristic length *L*; 2) free stream velocity *V*; and 3) characteristic temperature $T^* = \frac{T - T_w}{T_\infty - T_w}$, where T_∞ - free stream temperature. After doing all the necessary transformations of variables, the following set of non-dimensional equations is obtained:

$$
\begin{aligned}
w_x^* \frac{\partial w_x^*}{\partial x^*} + w_y^* \frac{\partial w_x^*}{\partial y^*} &= -\frac{dp^*}{dx^*} + \frac{\mu}{\rho VL} \frac{\partial^2 w_y^*}{\partial y^{*2}}; \\
w_x^* \frac{\partial T^*}{\partial x^*} + w_y^* \frac{\partial T^*}{\partial y^*} &= \frac{k}{\rho c_p VL} \frac{\partial^2 T^*}{\partial y^{*2}} + \frac{\mu V}{\rho c_p L\left(T_\infty - T_w\right)} \left(\frac{\partial w_y^*}{\partial y^*} \right)^2,
\end{aligned}
\tag{B.8}
$$

where non-dimensional pressure is defined as $p/\rho V^2$.

In the first equation **Re** appears in the form of term $\frac{\mu}{\rho VL}$, and reciprocals of both **Re** and **Pr** appear in the second equation in the form of term $\frac{k}{\rho c_p VL} \equiv \frac{\mu}{\rho VL} \cdot \frac{k}{\mu c_p}$

Thus, it follows from (B.8) that non-dimensional temperature is a function characteristic length, pressure gradient, **Re**, and **Pr**

$$
T^* = f\left(x^*, y^*, \frac{dp^*}{dx^*}, \mathbf{Re}, \mathbf{Pr} \right) \tag{B.9}
$$

Since at the solid-fluid interface heat flux be defined by both Newton's cooling law and Fourier's law, HTC can be expressed as follows:

$$
HTC = -k \frac{\left.\frac{\partial T}{\partial y}\right|_{y=0}}{T_w - T_\infty} = k \frac{\left.\frac{\partial T^*}{\partial y^*}\right|_{y^*=0}}{L} \Rightarrow \frac{HTC \cdot L}{k} = \left.\frac{\partial T^*}{\partial y^*}\right|_{y^*=0} \tag{B.10}
$$

Thus, non-dimensional-temperature gradient can be defined as **Nu**.

Therefore, with a number of simplification, the governing equations for flow (with all the original independent vairables) can be reduced to a functional form relating the following non-dimensional numbers:

$$
\mathbf{Nu} = f\left(\mathbf{Re}, \mathbf{Pr}\right) \tag{B.11}
$$

Appendix C. Sensitivity of Calculations to the Convergence Criteria

C.1. Criterion based on the wall temperature

As discussed in Chapter 2, the majority of the existing correlations involve parameters that depend on wall temperature. In the design calculations, wall temperature is one of the unknowns, which should be resolved through the Newton's cooling law:

$$T_w = T_b + \frac{q}{HTC}, \tag{C.1}$$

While HTC value should be obtained from the **Nu**, which is obtained from the correlation:

$$HTC = \frac{\mathbf{Nu}(T_w)k}{D} \tag{C.2}$$

Nu is an implicit function of the wall temperature. Thus, resolving (C.1) and (C.2) requires iterations. The basic approach is to set the convergence criteria base on the wall temperature. That is, iterations are stopped when the difference between the two successive iterated valued of wall temperatures becomes less than the convergence criteria. From the practical point of view, the smallest reasonable criterion is 0.1 K. It was, however, interesting to check how the performance of the correlation changes if this criterion is either relaxed or made more stringent. Four different values for the criterion were chosen (0.5 K, 0.3 K, 0.05 K, and 0.01 K) and compared with the 0.1 K criterion. Correlations Eqs. (7.7) and (7.11) were tested against the AECL NHT and IHT data (2209 points). For both correlation the starting T_w value was chosen as the one exceeding T_b by 10 K. The summary of the tests is presented in Table C.1.

Table C.1. Sensitivity of the correlations to the convergence criterion based on the wall temperature.

Criterion/Statistics		HTC RMS, %	T_w RMS, %	HTC spread, %	T_w spread, %	Average iterations per point
Eq. (7.7) (recommended)	0.5 K	16.7	3.2	–124.1 - +38.2	–17.6 - +14.2	10.6
	0.3 K	16.7	3.2	–123.9 - +38.6	–17.7 - +14.2	11.7
	0.05 K	16.6	3.2	–123.7 - +38.7	–17.8 - +14.2	15.8
	0.01 K	16.6	3.2	–123.7 - +38.7	–17.8 - +14.2	19.4
	0.1 K	16.6	3.2	–123.8 - +38.6	–17.8 - +14.2	14.2
Eq. (7.11) (binned)	0.5 K	9.7	1.7	–41.2 - +30.1	–9.4 - +5.8	11.6
	0.3 K	9.7	1.7	–40.6 - +30.7	–9.5 - +5.8	12.9
	0.05 K	9.7	1.8	–39.6 - +31.0	–9.5 - +5.7	17.4
	0.01 K	9.7	1.8	–39.4 - +31.1	–9.5 - +5.7	21.4
	0.1 K	9.7	1.7	–39.8 - +30.9	–9.5 - +5.8	15.7

The binned correlation Eq. (7.11) had a relaxed convergence criteria, if after 50 attempts it was not able to converge. One or two points depending on the convergence criteria where within 0.5 K from the actual T_w. As it is seen from Table C.1 varying the convergence criteria form 0.01 K to 0.5 K has almost no effect on RMS and maximal spread of HTC and T_w. Therefore, 0.5 K can be safely used as a convergence criterion for the conventional correlation Eq. (7.7). Obviously, the more the criterion is relaxed, the less iterations per point it requires. The same is true for the binned correlation Eq. (7.11). Although this approach requires 1 – 2 more iterations per point, it results in a much narrower spread of predicted data than the conventional approach.

It should be mentioned that, typically, the convergence criterion is not presented when the correlation results are shown and discussed. This is probably caused by a low sensitivity of the predictions to the criterion within a wide range of values that are within reasonable experimental accuracy of temperature measurements.

C.2. Criterion based on the heat transfer coefficient

No mentioning of the convergence criterion based on the heat transfer coefficient was found in the open literature. Therefore, a decision was made to test sensitivity of calculations for the convergence criterion set as follows:

$$\left| \frac{HTC^{(i+1)}}{HTC^{(i)}} - 1 \right| < eps \qquad \text{(C.3)}$$

The following criteria were tested: *eps* = 0.1, 0.01, and 0,001. The results of the calculations were benchmarked against the conventional wall temperature based convergence criterion of the 0.1 K values. The summary for tests of correlation Eq. (7.7) on the AECL NHT and IHT data (2209) points is presented in Table C.2. The starting HTC value was 40 kW/m^{2}K.

Table C.2. Sensitivity of the correlation Eq. (7.7) to the convergence criterion based on the heat transfer coefficient.

Criterion/Statistics		**HTC RMS, %**	**T_w RMS, %**	**HTC spread, %**	**T_w spread, %**	**Average iterations per point**
Eq. (7.7) (recommended)	0.1	18.7	2.8	–139.4 - +33.7	–11.0 - +16.1	8.8
	0.01	16.7	3.1	–124.8 - +37.9	–16.9 - +14.4	14.1
	0.001	16.6	3.2	–123.8 - +38.6	–17.7 - +14.2	19.3
	0.1 K	16.6	3.2	–123.8 - +38.6	–17.8 - +14.2	14.2

It seen from Table C.2 that the value 0.001 for convergence criterion (C.3) produces almost identical statistics as the conventional convergence criterion with 0.1 K value. The latter, however, requires 5 iterations per point less. Another interesting feature of the (C.3) criterion is that decreasing it changes the bias in prediction: at 0.1 value the temperatures are biased to be under-estimated, at lower values of the criterion the temperatures are biases to be over-predicted. Also, the T_w RMS increases with the decrease in tolerance, while

HTC RMS, on the contrary, increases. This inconsistency is caused due to using the bisection method, while the true value may be lying closer to the last iterated value of HTC.

The numerical instability is briefly discussed in Appendix D.

C.3. Comparison of the T- and Q-approaches.

As it was pointed out in the works by Kurganov et al. (2011) and Kurganov et al. (2013a,b), the performance of correlations can be assessed, in general, based on either the "T-approach" or "Q-approach". HTC is calculated based on the experimental T_w and heat flux (q) in the T-approach. However in the design, T_w is not known beforehand, therefore HTC is calculated based on the knowledge of only q. This is called the Q-approach.

It is very important to emphasize what approach is used, whenever the statistics for the correlation are presented. Q-approach always produced wider spread in the predictions that the T-approach. For example, see Figure C.1 and Table C.3 which compare the performance of the binned correlation (7.11) based on T- and Q-approaches.

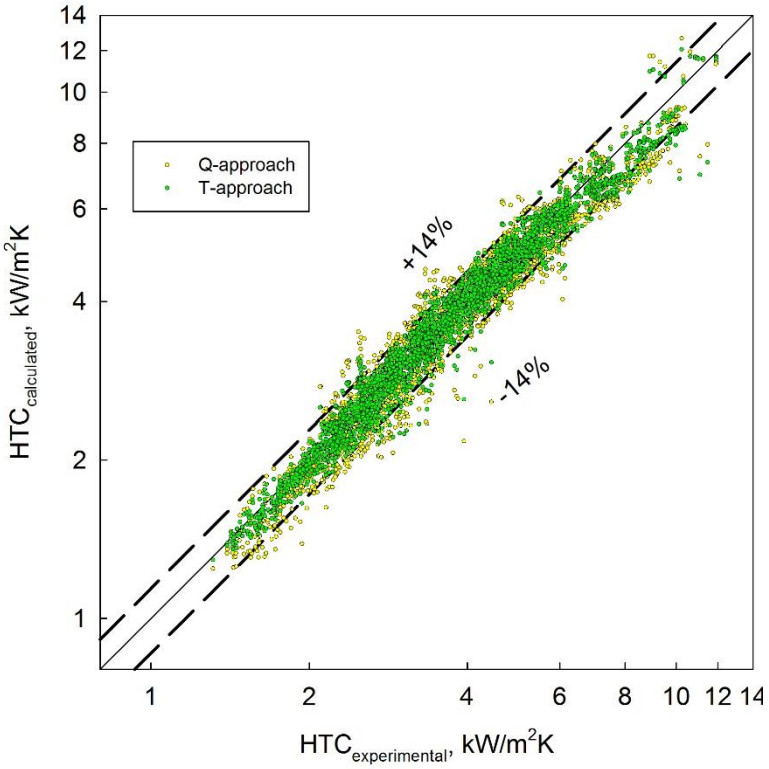

Figure C.1. Comparison of the performance of the binned correlation based on the T- and Q-approaches.

The 14% band corresponds to the 2σ-level for the predicted values based on the T-approach.

Table C.3. Comparison of the performance of the binned correlation based on the T- and Q-approaches.

Approach	HTC RMS, %	T_w RMS, %	HTC spread, %	T_w spread, %
T	6.8	0	–25.7 - +37.2	0
Q	10.0	2.0	–41.2 - +44.9	–12.4 - +8.6

Table C.3 clearly shows that the predictions by the T-approach are significantly more optimistic than those by the Q-approach. Therefore, it is the Q-approach that should be used as a basis for a fair comparison of the correlations.

Appendix D. Numerical Instability of Heat Transfer Correlations

As discussed in Appendix C, conventionally, the convergence criterion in calculating HTC is based on the wall temperature T_w. Heat transfer correlations are non-linear, and often they include terms depending on T_w. HTC, however, is assumed to be inversely proportional to T_w, according to the Newton's cooling law.

A visual example of how the solution is obtained is presented in Figure D.1 by plotting T_w calculated from Newton's cooling law and from Mokry et al. (2009) correlation Eq. (3.36). The tested experimental point was taken from Kirillov's test 38_07, 2 m along the heated test section. The summary of the experimental parameters is in the Table D.1.

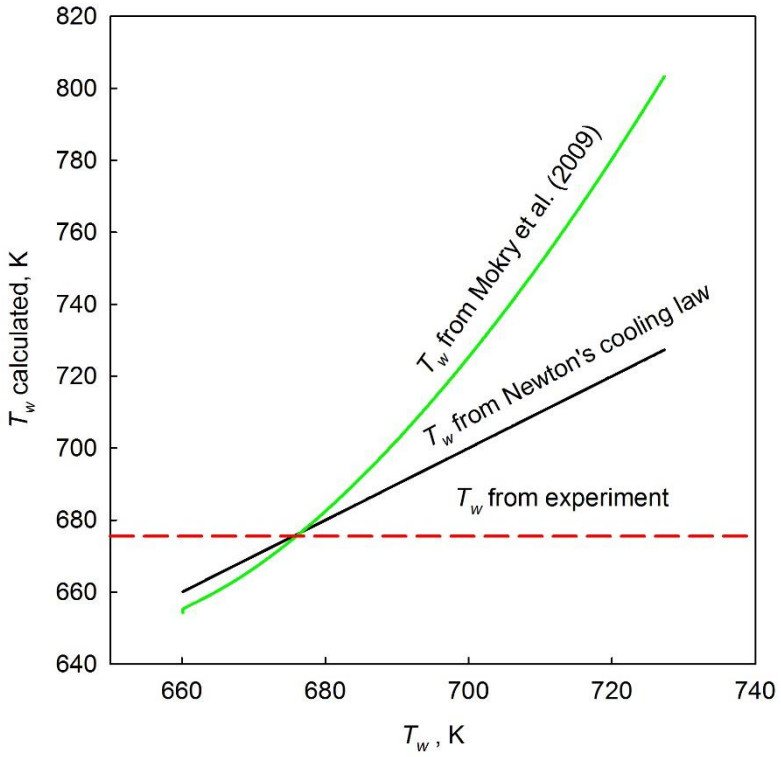

Figure D.1. Graphical solution of the correlation.

Table D.1. Experimental parameters of the point from Test 38_07.

x, m	T_w, K	T_b, °C	q, kW/m^2	P, MPa	G, kg/m^{2}s	D, mm
2	675.55	653.28	483.737	24.057	1002	10

As discussed in Chapter 2, HTC is non-linear for fluids at SC state. Thus, Newton's cooling law may be considered as a principle, which breaks down for heat transfer problems involving fluids at SC state. Still, no better relation between the difference of the wall and bulk-fluid temperatures and heat flux at the surface was proposed.

Thus, it is important to investigate the limitations of the current iterative approach.

As mentioned in Chapter 4, inclusion into a correlation a term containing ratios of specific heats and making convergence criterion very low may cause the iterations to run in an infinite loop, for the points with T_w close to T_{pc}. Apparently, Griem (1996) had a similar problem. He found a potential numerical instability in the obtaining values of HTCs from his correlations. Therefore Griem (1996) proposed to use "biased" successive iteration values for T_w in calculations to overcome the instability. The bias from the bisectional method of iterations was the following:

$$T_{w,6th} = \frac{T_{w,6th} + 2T_{w,5th}}{3} \tag{D.1}$$

$$T_{w,14th} = \frac{T_{w,14th} + 4T_{w,13th}}{5} \tag{D.2}$$

It seems, however, that what he called instability was not the occurrence of unstable solution, but rather correlation running in an infinite iterative loop. The correction he proposed may be useful for the correlations Eqs. (7.7) – (7.9) for the following reason. It was noticed that in a pair of iterations, one of the T_w may be very close to the solution, while averaging with the next iteration, shifts the former away from the solution by at least double the convergence tolerance.

The topic of instability was also touched by Cheng et al. (2009). One of the requirements for the new correlation they were developing is to exclude all terms depending on T_w to avoid any potential numerical instability.

Churkin and Deev (201) conducted a thorough investigation of the actual instability of the correlations and ambiguity of their solutions. They have introduced a non-dimensional parameter **B** to connect mass and heat fluxes in the form:

$$\mathbf{B} = q \cdot 10^3 / \left(G\left(h_{cr} - h_b \right) \right), \tag{D.3}$$

where h_{cr} – specific enthalpy at critical point.

In fact, in such form the non-dimensional parameter proposed by Churkin and Deev (2013) can be viewed as a modified Stanton number **St**:

$$\mathbf{St} = \frac{HTC}{\rho w c_p} \tag{D.4}$$

Churkin and Deev (2011) tested the correlations by Swenson et al. (1965) (see Eq. (3.20)), Jackson and Hall (1979a) (see Eq. (3.27)), and Mokry et al. (2009) (see Eq. (3.36)). All of these correlations were found to have two stable solutions for the rest of the fixed parameters. Churkin and Deev (2011) showed that in coordinates (T_b, T_w, **B**), the correlation by Jackson and Hall (1979a) had the smallest ambiguity region. All the correlations produced ambiguous results within the experimental conditions close to those at which DHT occurs. Thus, instability in solutions occurred at the conditions for which the correlations where not developed. Still, Churkin and Deev (2013) suggested that the ambiguity regions of calculated T_w should be considered when using or developing correlations.

Unfortunately, Churkin and Deev (2013) did not provide the actual value of h_{cr} which they used in their calculations. Thus, it is hard to verify their results.

Finally, in very rare instances, the correlation may not converge at all, when T_w increases to thousands of K. Changing the starting point for iterations and the convergence criterion could help avoiding this.

Appendix E. Relevance of DHT to the Current Canadian SCWR Concept

Generation IV Annual Report (2013) (briefly: *GIF*, 2013) identified thermal-hydraulics and safety as one of the four critical-path Research and Development (R&D) projects in the SCWR System Research Plan. The Thermal-Hydraulics and Safety project is specified in *GIF* (2013) as follows: "Gaps exist in the heat transfer and critical flow databases for the SCWR. Data at prototypical SCWR conditions are needed validating thermal-hydraulic codes. The design-basis accidents for a SCWR have some similarities with conventional water reactors, but the difference in thermal-hydraulic behavior and large changes in fluid properties around the critical point compared to water at lower temperatures and pressures need to be better understood". Thus, understanding the conditions for intensive and stable heat transfer to SuperCritical Water (SCW) is one of the crucial problems in the design of SCWRs.

Acknowledging the importance of resolving the problem of accurate prediction of heat transfer to SCW, International Atomic Energy Agency (IAEA) established a Coordinated Research Project (CRP) "Heat Transfer Behaviour and Thermal-Hydraulics Code Testing for Super-Critical Water-cooled Reactors". The first step of this project was to "establish a base of accurate data for heat transfer, pressure drop, blowdown, natural circulation, and stability for conditions relevant to super-critical fluids" (Cleveland et al., 2007). The CRP was finished in 2012 and its results were presented and summarized in IAEA-TECDOC-1746 (2014). However, the Section 6 "Development of New Correlations for Heat Transfer to Supercritical Pressure Fluids" of IAEA-TECDOC-1746 (2014) ends with the following discussion: "The work reported in this section represents a <u>useful start</u> on the problem of developing new and improved correlations for heat transfer to fluids at supercritical pressures and has exposed some important issues that remain to be addressed. It is clear, however, that more work needs to be done on assessing correlation equations if we are to reach a stage where thermal analysis for high pressure, water cooled nuclear reactors can be performed with the high degree of confidence needed in the case of such plant". Thus, not a single correlation proved to be reliable in predicting heat transfer in all regimes, known in the literature as Normal Heat Transfer (NHT), Deteriorated Heat Transfer (DHT), and Improved Heat Transfer (IHT).

DHT is typically characterized as a regime at which wall temperature T_w goes through a sudden increase due to much lower values of Heat Transfer Coefficients (HTC) than those observed at subcritical cases. Therefore, DHT should be avoided in the core of SCWR (Kurganov et al., 2011; Anglart, 2009). However, Palko and Anglart (2009) and Anglart (2009) having analyzed a wide set of experimental data concluded that the DHT is very likely to occur in the European design of SCWR (commonly referred to in the literature as a High Pressure Light Water Reactor (HPLWR)), unless certain design changes are made. No similar analysis for a Canadian SCWR concept was found in the open literature.

The most recent Canadian SCWR concept was described in the papers by Yetisir et al. (2013), Pencer et al. (2013), and Dominguez et al. (2013). A fuel channel design called a High-Efficiency Channel (HEC) is used in the current concept. The new channel utilizes annular flow: the coolant enters the fuel channel on top through the central tube, changes flow direction at the bottom, and flows upward through the annulus where the fuel rods are located. Each fuel channel consists of a pressure tube of 181 mm Outer Diameter (OD), which is in direct contact with the moderator. A ceramic insulator is used between the fuel bundle and the pressure tube. The geometric specifications of the current fuel bundle design are presented in Table E.1. The major characteristics of the core of the current Canadian SCWR concept are presented in Table E.2.

Table E.1. Geometric specifications of the 62-element fuel bundle (based on Dominguez et al., 2013).

Component	Dimensions
Central flow tube ID*/OD, cm	8.9 / 9.1
Inner fuel pin diameter, cm	0.83
# of inner fuel pins	31
Outer fuel pin diameter, cm	0.93
# of outer fuel pins	31
Fuel pin cladding thickness, cm	0.06
Liner tube ID/OD, cm	14.4 / 14.5
Insulator ID/OD, cm	14.5 / 15.6
Outer liner ID/OD, cm	15.6 / 15.7
Pressure tube ID/OD, cm	15.7 / 18.1
Fuel bundle heated length	500 cm

* ID – Internal Diameter

Table E.2. Major core characteristics (based on Yetisir et al., 2013).

Characteristic	Value
Core thermal power, MW	2540
Inlet/outlet temperature, °C	350 / 625
Inlet pressure, MPa	25
Number of fuel channels	336
Average thermal power per channel, MW	7.56
Fuel channel length, m	5
Core radial power profile factor	1.28

The parameters pertaining to the preliminary thermal-hydraulic calculations can be estimated based on the values presented in Tables E.1 and E.2. These parameters are presented in Table E.3.

Table E.3. Parameters of the 62-element fuel bundle pertaining to the preliminary thermal-hydraulic calculations.

Parameter	Value
Central tube flow area, cm^2	19.80π
Annulus flow area, cm^2	15.60π
Annulus wetted perimeter, cm	85.5π
Hydraulic diameter, mm	7.30
Total mass-flow rate, kg/s	1307.5
Mass-low rate per channel, kg/s	3.89
Heated area, m^2	3.10π
Average heat flux, kW/m^2	776.3
Mass flux in the annulus, kg/m^2s	793.7

Using the values from Table E.3 it is possible to calculate a heat loading factor, defined as the ratio of heat flux q to mass flux G:

$$\frac{q}{G} = 0.978 \text{ kJ/kg} \tag{E.1}$$

It is this parameter that is widely used as a preliminary criterion for the onset of DHT.

The most recent criterion for the onset of DHT in SCW was proposed by Mokry et al. (2011) (see Eq. (3.7)).

According to this criterion, average heat flux in the current Canadian SCWR concept is 1.46 times higher (776.3 / 532.4) than the heat flux at which deterioration occurs in a bare tube, not accounting for the core radial profile factor.

It was shown by Bae and Kim (2009) that the annular flow is less susceptible to DHT than the flow in a bare tube. Furthermore, it may be speculated that the bundles and appendages will turbulize the flow.

However, recent heat transfer experiments with rod bundles in SCW (Razumovskiy et al., 2013) and in SC Freon (Richards et al., 2012) showed that DHT occurs in the bundles.

Therefore, the current Canadian SCWR concept may be susceptible to DHT.

Appendix F. Graphical Representation of AECL MR-1 Loop Data

Figures F.1 – F.42 show the comparison of all AECL HTC data based on the non-dimensional coordinate $\mathbf{X} = \frac{h_b - h_{pc}}{q / G}$. This approach of representing data proved to be helpful in identifying patterns and general trends within the data for fixed D_{hy} (see Chapter 7).

Note that the data below are presented with actual uncertainty. This shows the importance of filtering highly uncertain data from those used for developing a correlation.

The data on the Figures below are grouped in the order of ascending heat loading factor q/G. Additionally, two last runs of each figure are repeated as the first two runs in the next figure to assist recognition of patterns of relation between HTC and **X**. The test runs are written in the legend in the following format: T(diameter of the tube in mm)-(pressure in kPa)-(mass flux in kg/m^{2}s)-(heat flux in kW/m^2)-(inlet temperature in °C).

The zero value of **X** corresponds to the bulk-fluid being at exactly pseudocritical temperature. The pseudocritical temperatures that correspond to the three nominal pressures covered in the experiments are summarized in Table F.1.

Table F.1. Pseudocritical temperatures corresponding to the nominal pressures covered at the AECL experiments.

P, MPa	7.6	8.4	8.8
T, °C	32.3	36.9	39.0

Analysis and discussion of data follow Figure F.42.

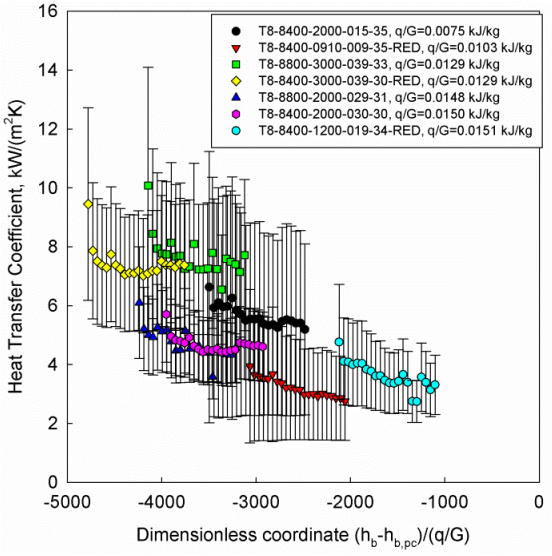

Figure F.1. AECL data – 1 (*q*/*G* = 0.0075 – 0.0151 kJ/kg).

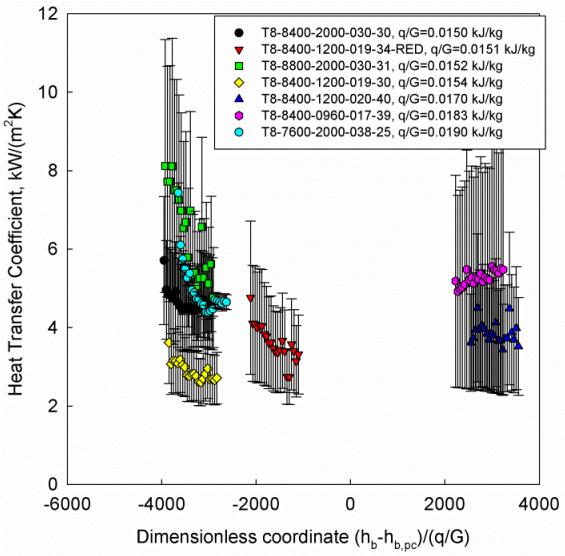

Figure F.2. AECL data – 2 (*q*/*G* = 0.0150 – 0.0190 kJ/kg).

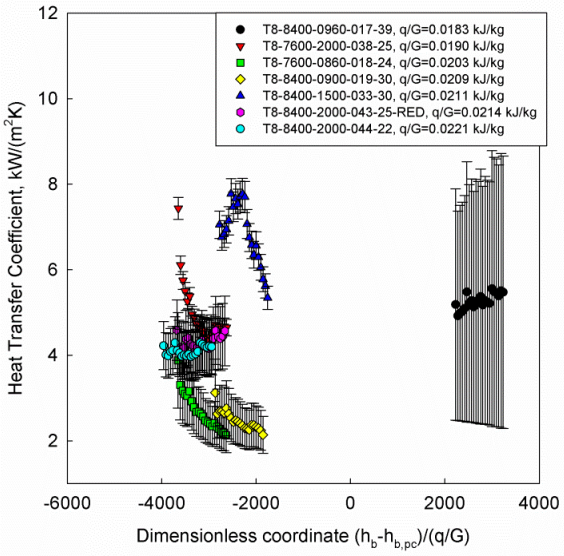

Figure F.3. AECL data – 3 (*q*/*G* = 0.0183 – 0.0221 kJ/kg).

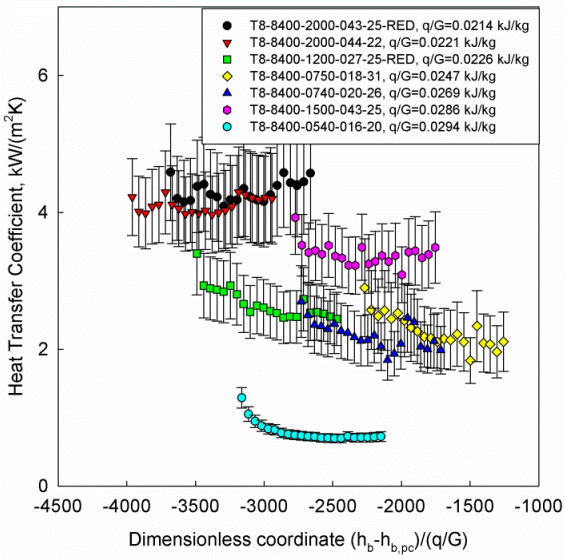

Figure F.4. AECL data – 4 (*q*/*G* = 0.0214 – 0.0294 kJ/kg).

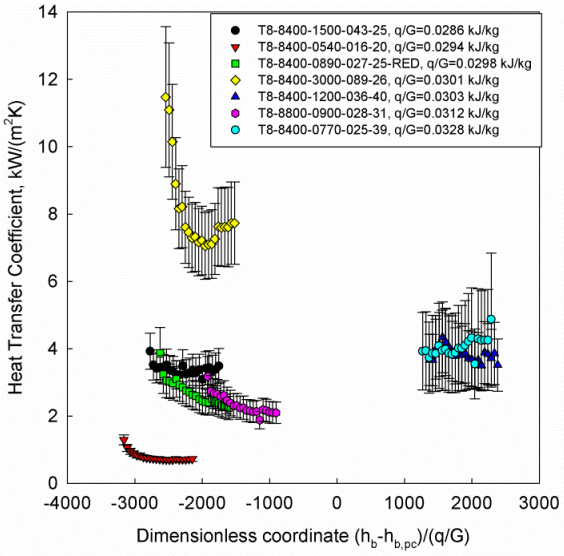

Figure F.5. AECL data – 5 (*q*/*G* = 0.0286 – 0.0328 kJ/kg).

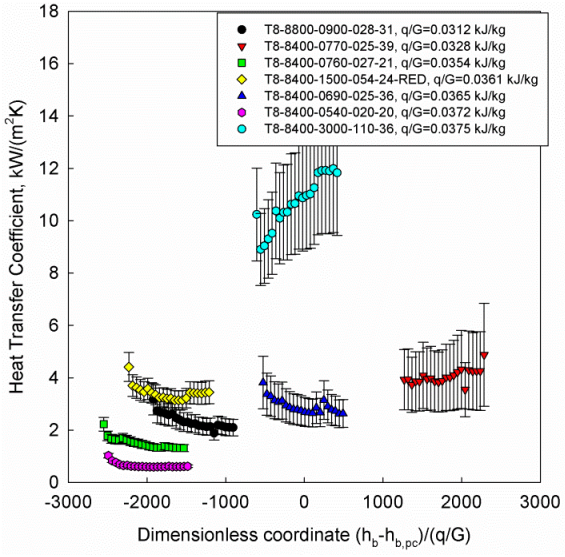

Figure F.6. AECL data – 6 (*q*/*G* = 0.0312 – 0.0375 kJ/kg).

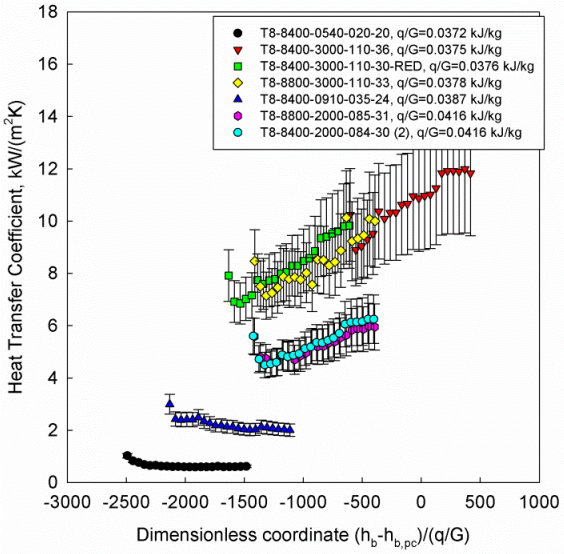

Figure F.7. AECL data – 7 (*q*/*G* = 0.0372 – 0.0416 kJ/kg).

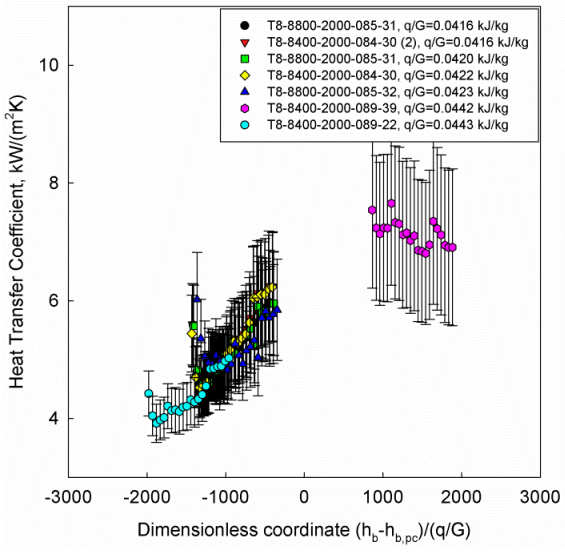

Figure F.8. AECL data – 8 (*q*/*G* = 0.0416 – 0.0443 kJ/kg).

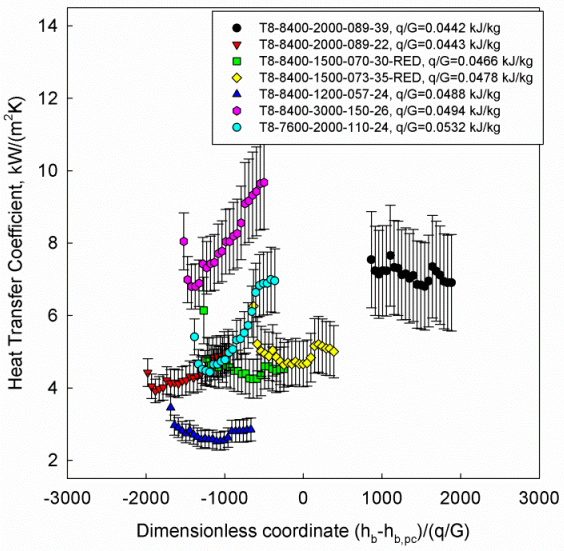

Figure F.9. AECL data – 9 (*q*/*G* = 0.0442 – 0.0532 kJ/kg).

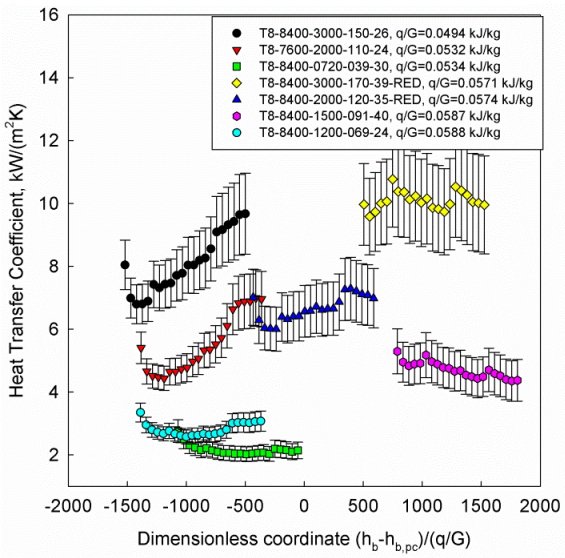

Figure F.10. AECL data – 10 (*q*/*G* = 0.0494 – 0.0588 kJ/kg).

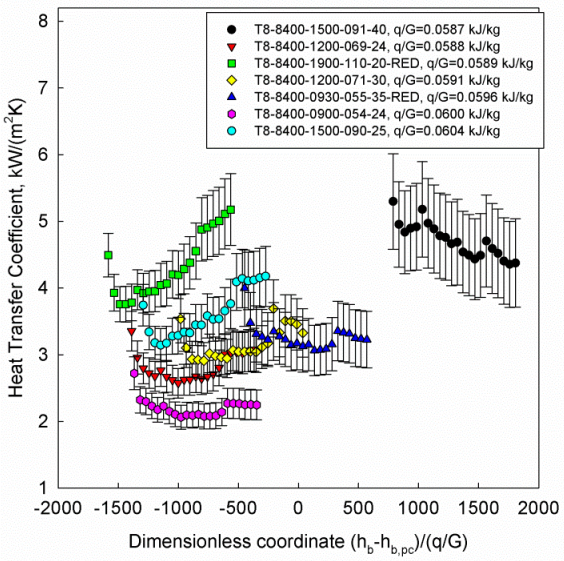

Figure F.11. AECL data – 11 (*q*/*G* = 0.0587 – 0.0604kJ/kg).

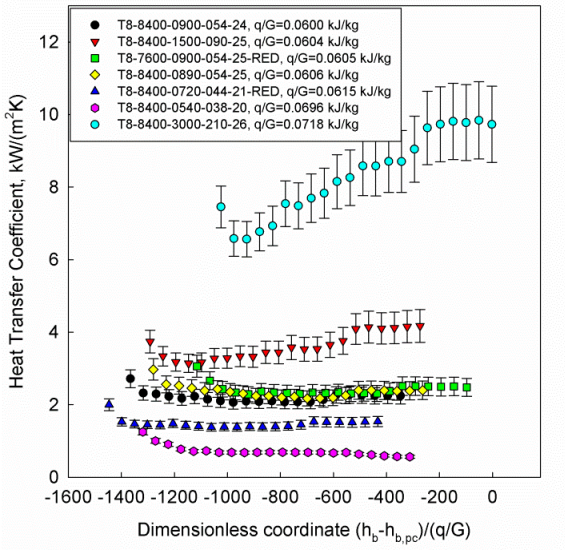

Figure F.12. AECL data – 12 (*q*/*G* = 0.0600 – 0.0718 kJ/kg).

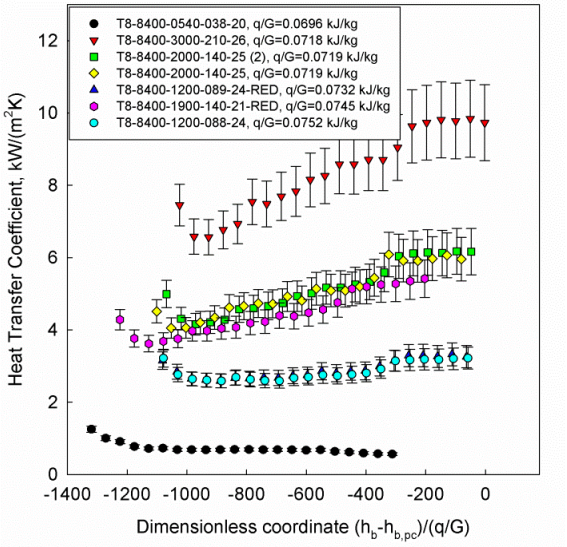

Figure F.13. AECL data – 13 (*q*/*G* = 0.0696 – 0.0752 kJ/kg).

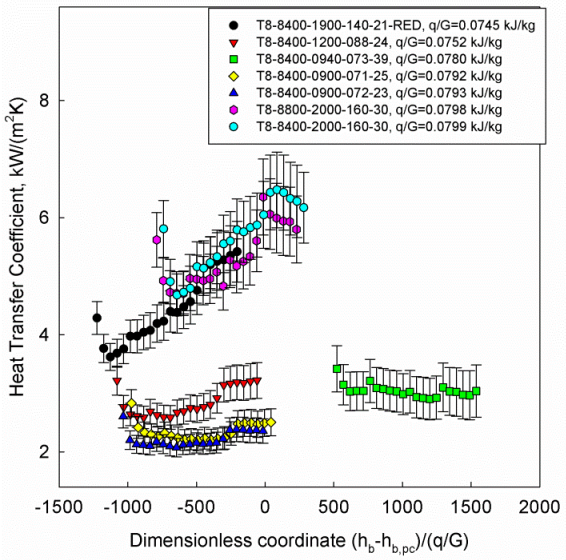

Figure F.14. AECL data – 14 (*q*/*G* = 0.0745 – 0.0799 kJ/kg).

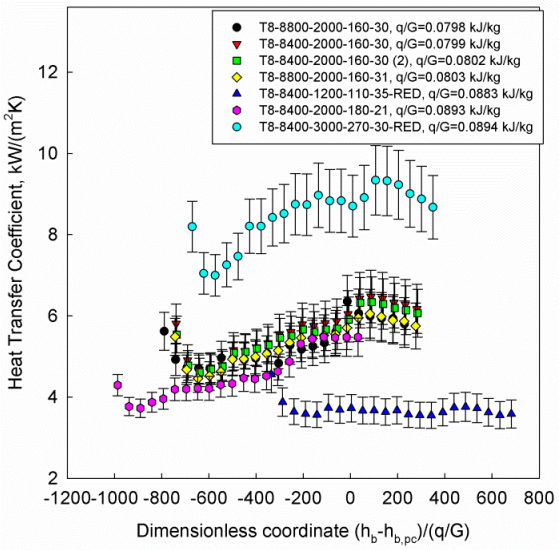

Figure F.15. AECL data – 15 (*q*/*G* = 0.0798 – 0.0894 kJ/kg).

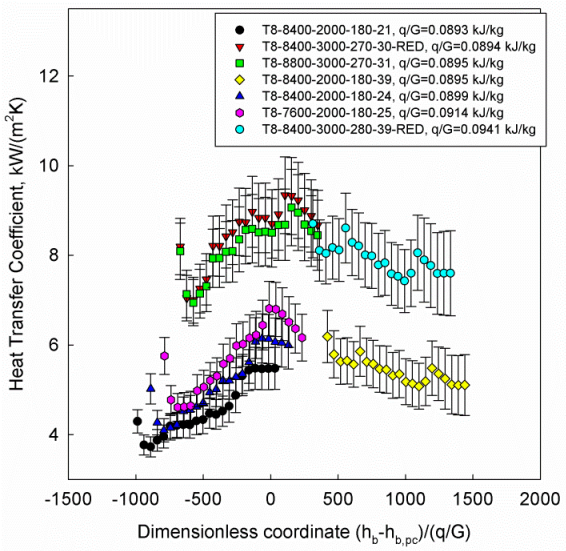

Figure F.16. AECL data – 16 (*q*/*G* = 0.0893 – 0.0941 kJ/kg).

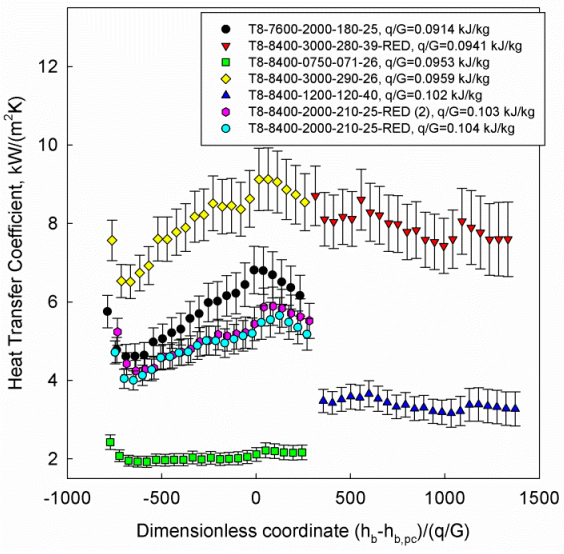

Figure F.17. AECL data – 17 (*q*/*G* = 0.0914 – 0.104 kJ/kg).

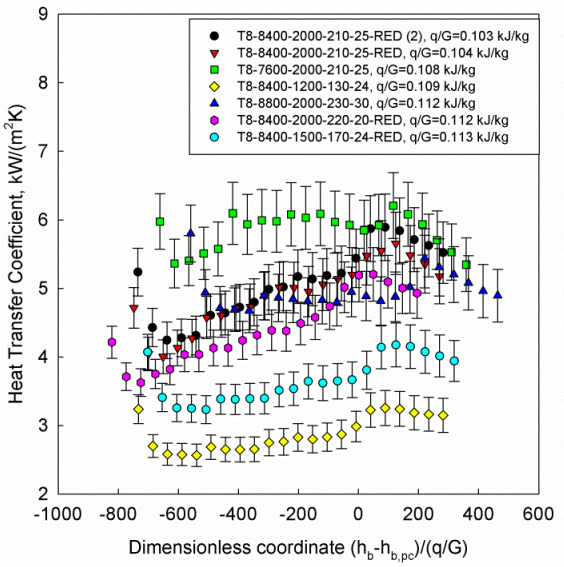

Figure F.18. AECL data – 18 (*q*/*G* = 0.103 – 0.113 kJ/kg).

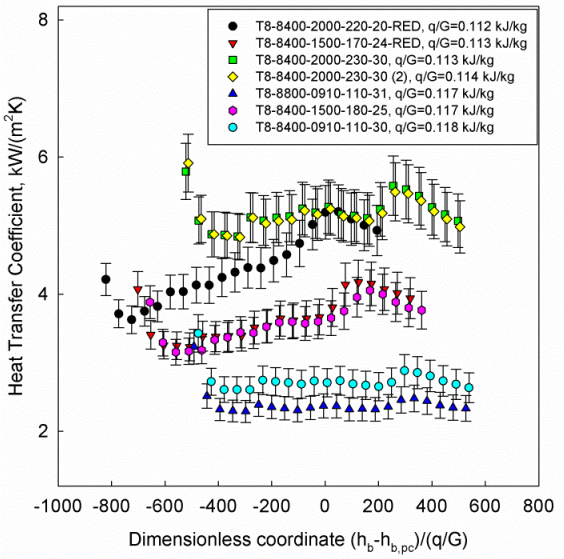

Figure F.19. AECL data – 19 (*q*/*G* = 0.112 – 0.118 kJ/kg).

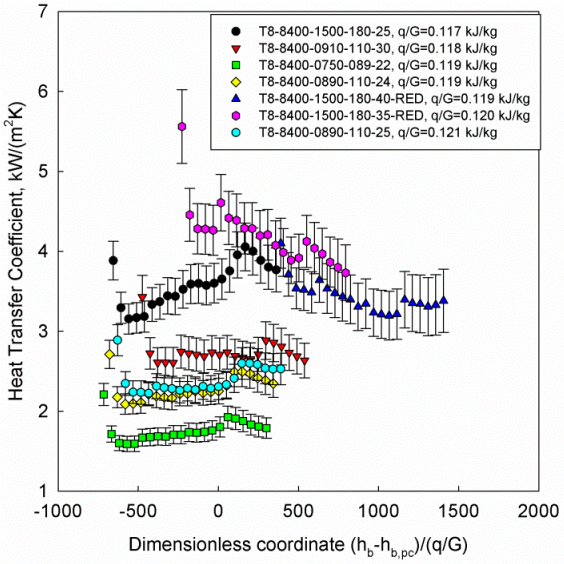

Figure F.20. AECL data – 20 (*q*/*G* = 0.117 – 0.121 kJ/kg).

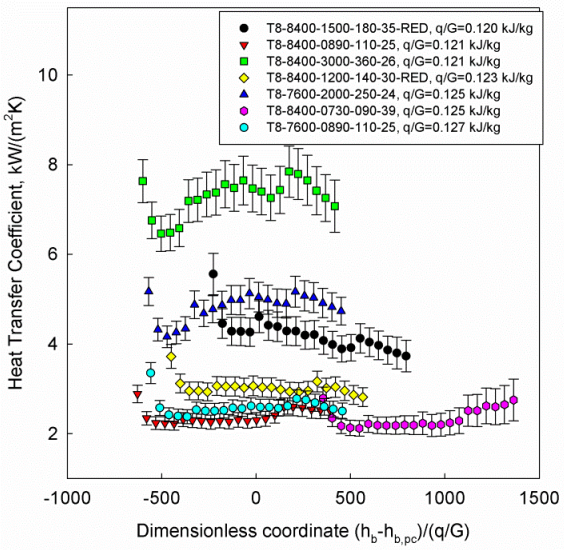

Figure F.21. AECL data – 21 (*q*/*G* = 0.120 – 0.127 kJ/kg).

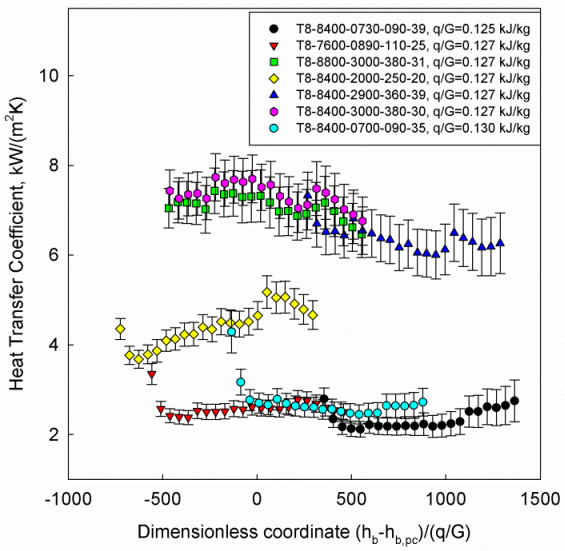

Figure F.22. AECL data – 22 (*q*/*G* = 0.125 – 0.130 kJ/kg).

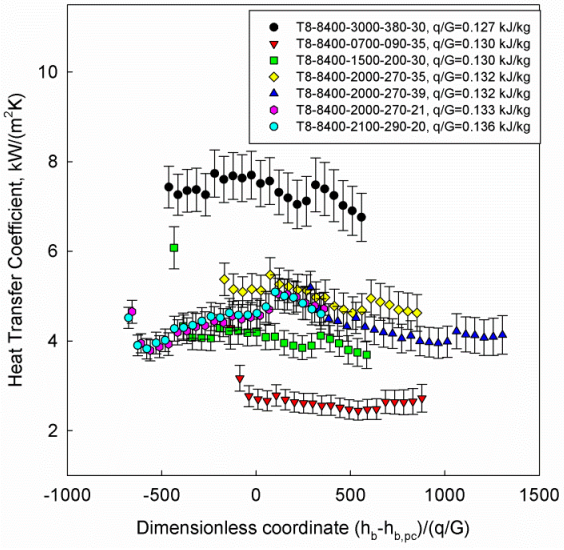

Figure F.23. AECL data – 23 (*q*/*G* = 0.127 – 0.136 kJ/kg).

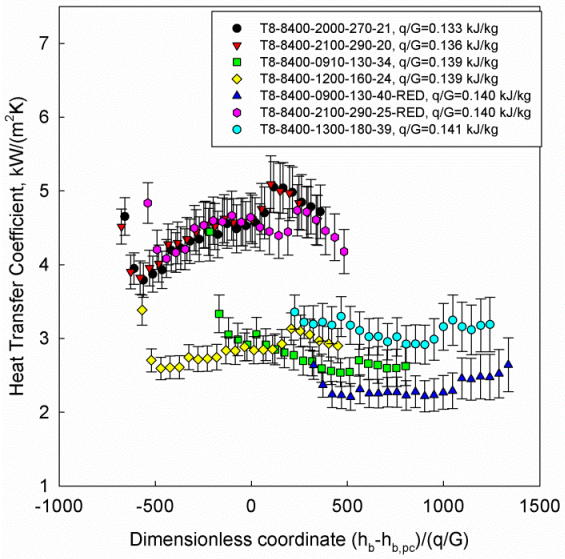

Figure F.24. AECL data – 24 (*q*/*G* = 0.133– 0.141 kJ/kg).

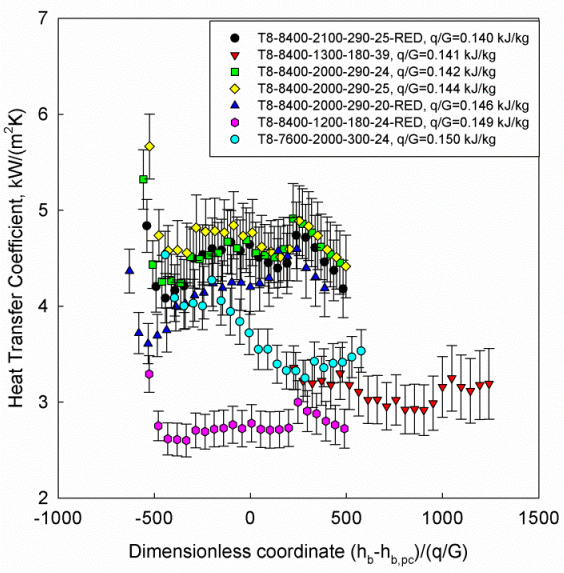

Figure F.25. AECL data – 25 (*q*/*G* = 0.140 – 0.150 kJ/kg).

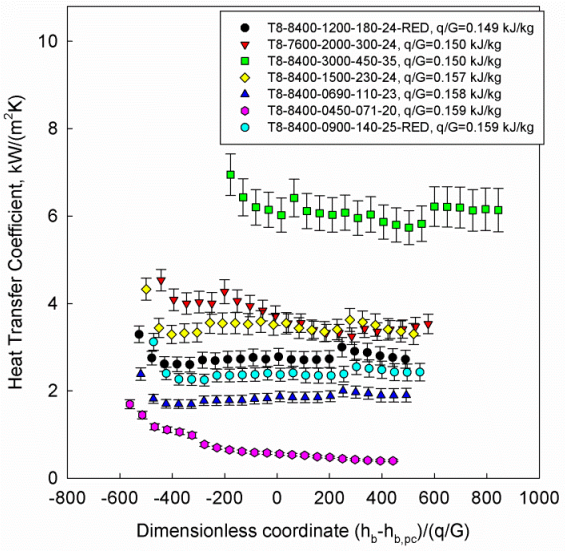

Figure F.26. AECL data – 26 (*q*/*G* = 0.149 – 0.159 kJ/kg).

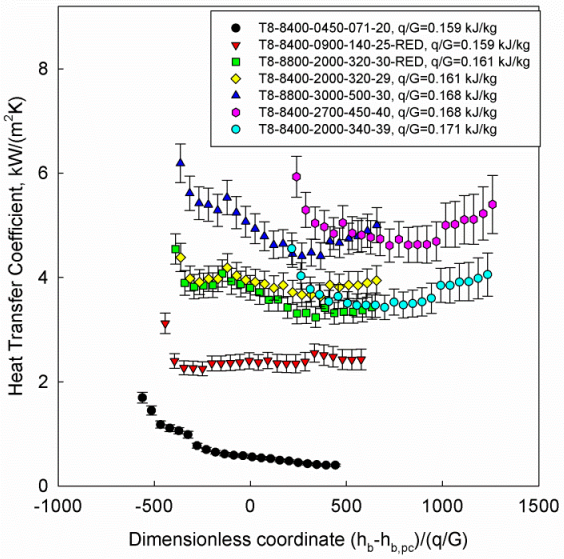

Figure F.27. AECL data – 27 (*q*/*G* = 0.159 – 0.171 kJ/kg).

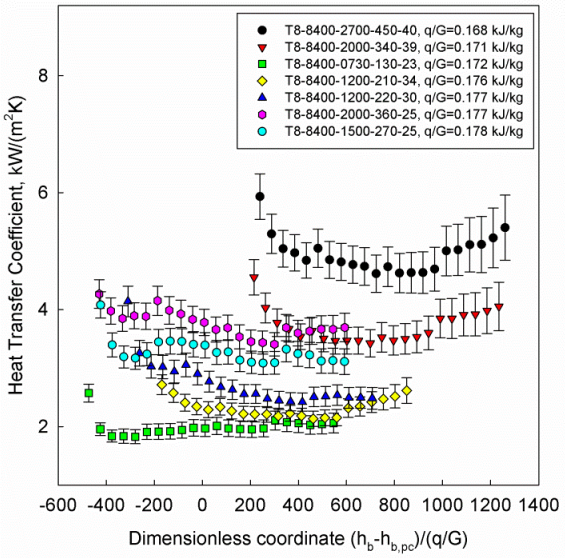

Figure F.28. AECL data – 28 (*q*/*G* = 0.168 – 0.178 kJ/kg).

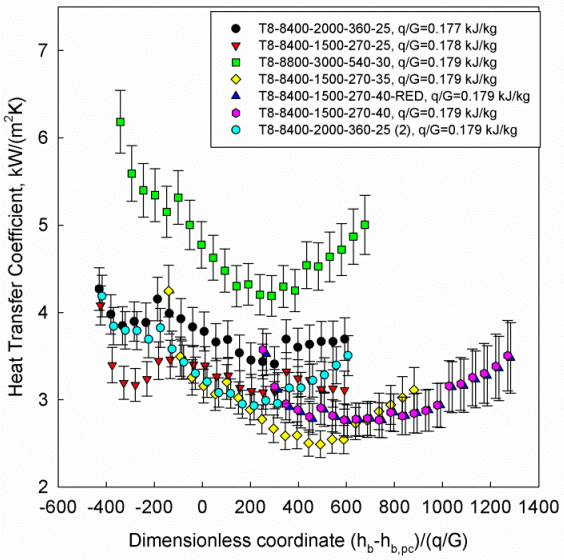

Figure F.29. AECL data – 29 (*q*/*G* = 0.177 – 0.179 kJ/kg).

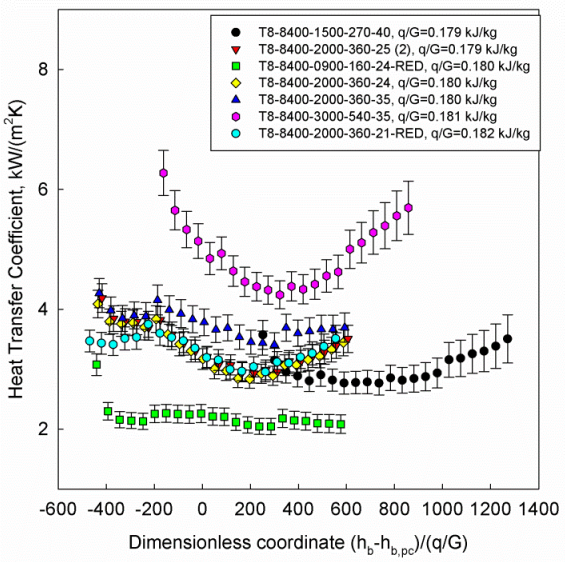

Figure F.30. AECL data – 30 (*q*/*G* = 0.179 – 0.182 kJ/kg).

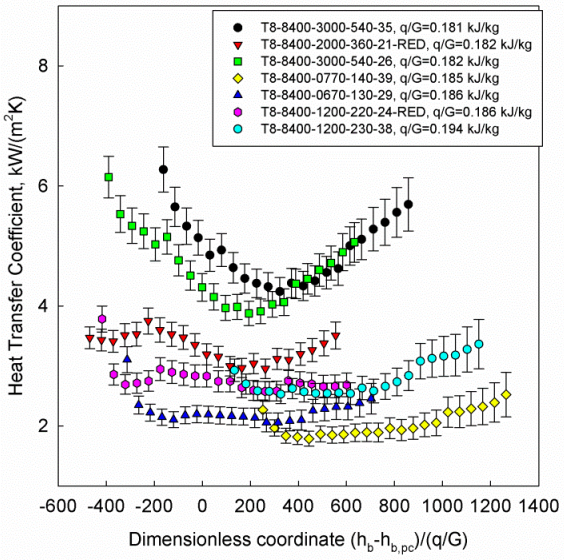

Figure F.31. AECL data – 31 (*q*/*G* = 0.181 – 0.194 kJ/kg).

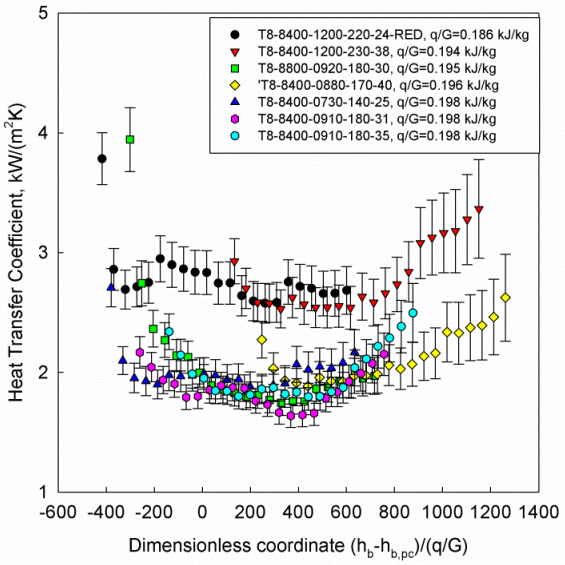

Figure F.32. AECL data – 32 (*q*/*G* = 0.186 – 0.198 kJ/kg).

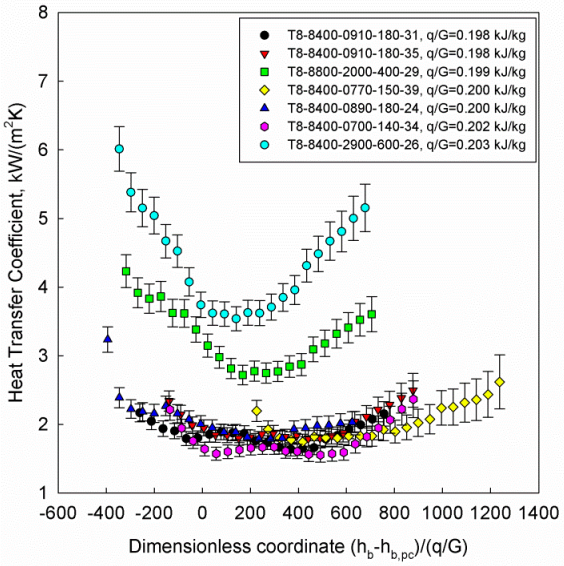

Figure F.33. AECL data – 33 (*q*/*G* = 0.198 – 0.203 kJ/kg).

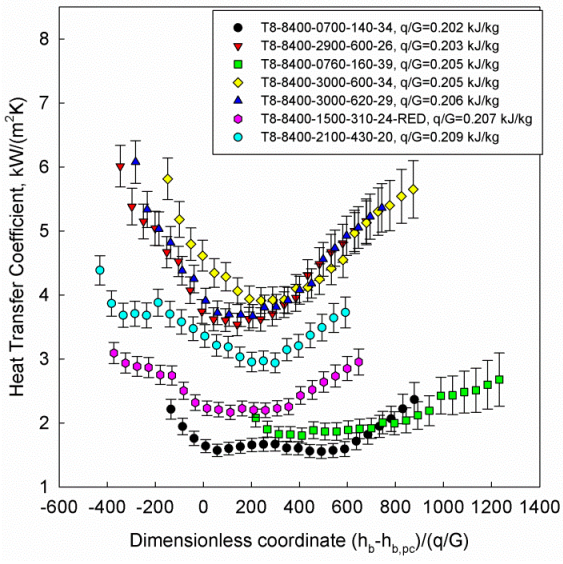

Figure F.34. AECL data – 34 (*q*/*G* = 0.202 – 0.209 kJ/kg).

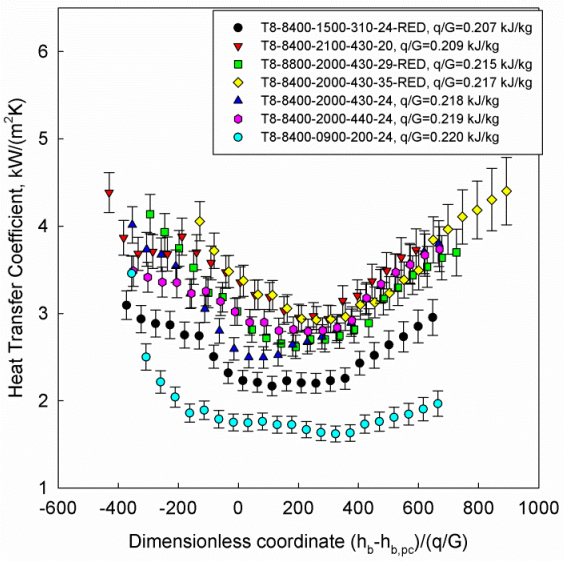

Figure F.35. AECL data – 35 (*q*/*G* = 0.207 – 0.220 kJ/kg).

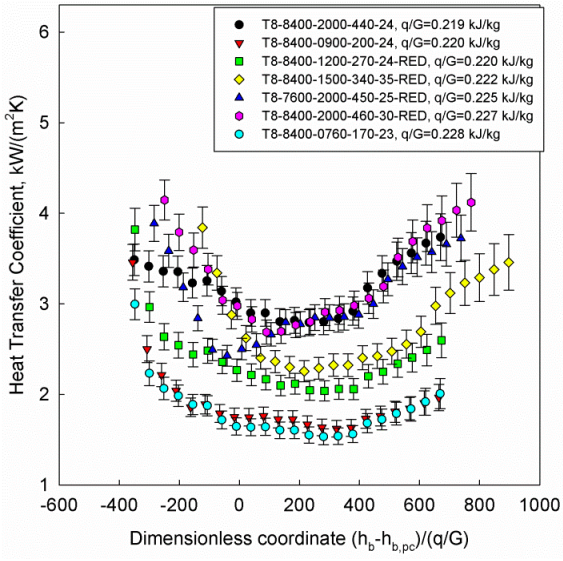

Figure F.36. AECL data – 36 (*q*/*G* = 0.219 – 0.228 kJ/kg).

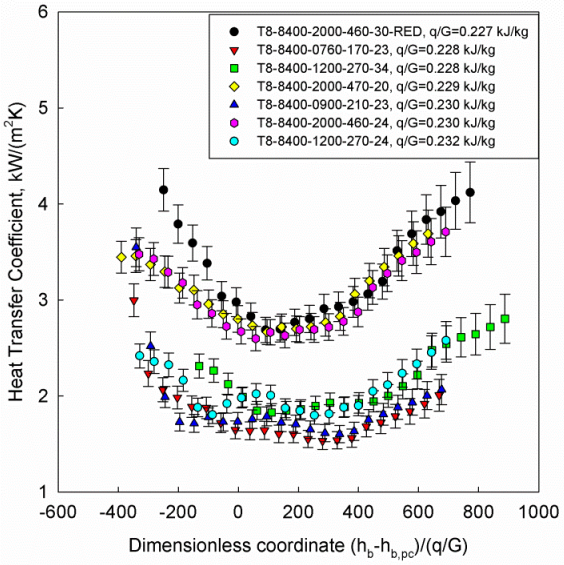

Figure F.37. AECL data – 37 (*q*/*G* = 0.227 – 0.232 kJ/kg).

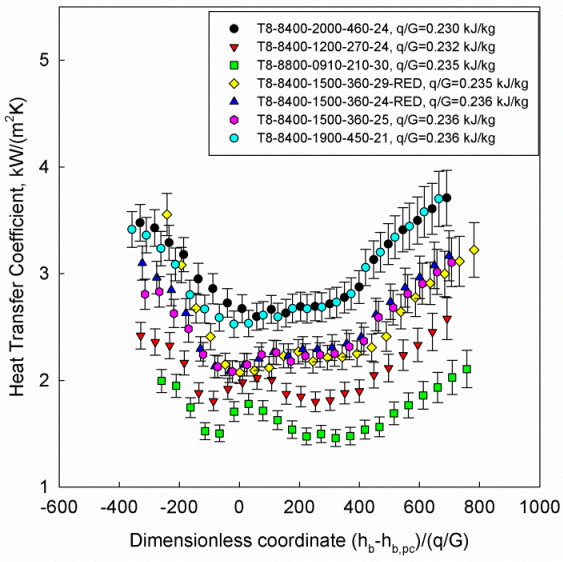

Figure F.38. AECL data – 38 (*q*/*G* = 0.230 – 0.236 kJ/kg).

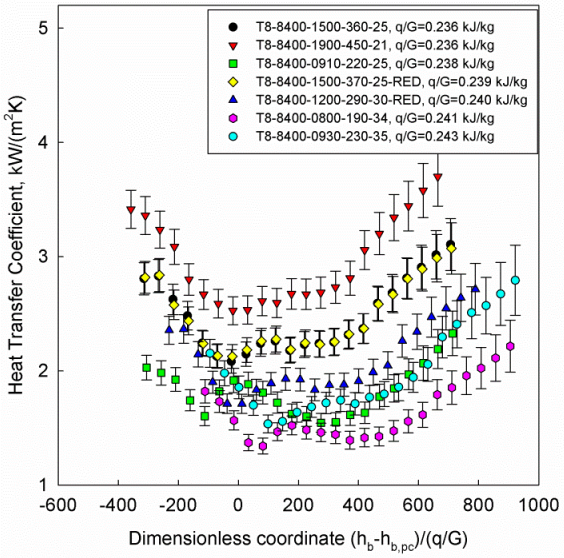

Figure F.39. AECL data – 39 (*q*/*G* = 0.236 – 0.243 kJ/kg).

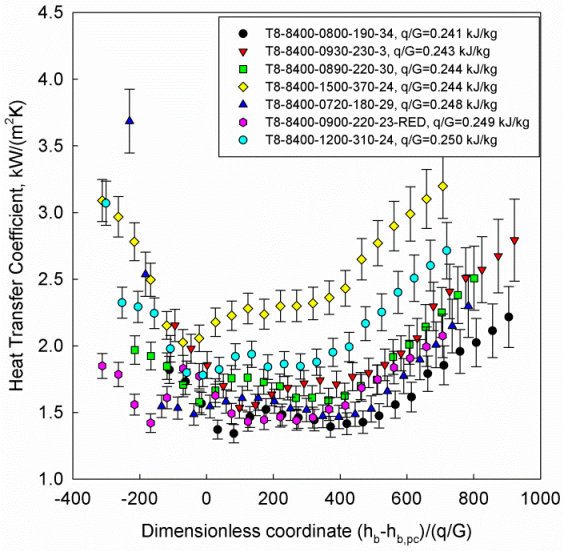

Figure F.40. AECL data – 40 (*q*/*G* = 0.241 – 0.250 kJ/kg).

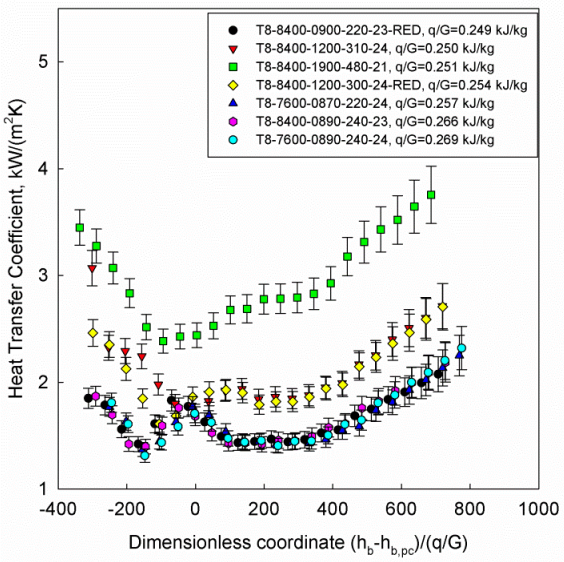

Figure F.41. AECL data – 41 (q/G = 0.249 – 0.269 kJ/kg).

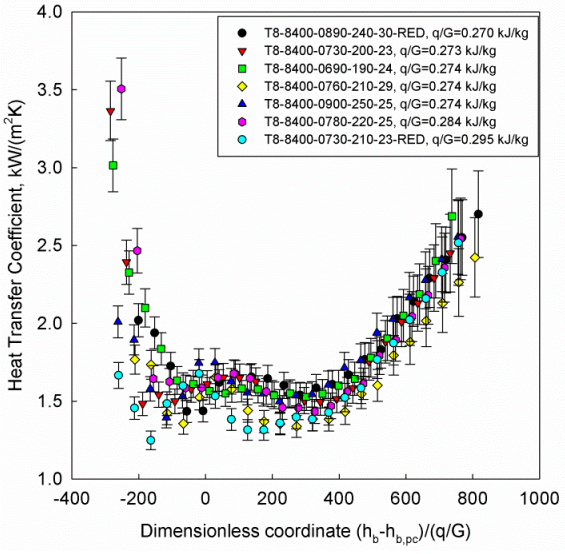

Figure F.42. AECL data – 42 (q/G = 0.270 – 0.295 kJ/kg).

Up until $q/G \cong 0.1$ kJ/kg, the experimental uncertainty is at least 20% throughout the entire test-section. Several exceptions are for the cases of lower q/G ratio and inlet temperature well below the pseudocritical point. With a very few exceptions, all the data exhibit very well pronounced inlet effect of deterioration, independent of inlet temperature. Thus, these data confirm the established fact that deterioration will occur at the inlet as well as within the pseudocritical region. It is, however, hard to distinguish one from another and generalize propagation of this effect. Therefore in further filtering the data of the first three thermocouples were excluded from the data used for the development of NHT correlations.

As discussed in Chapter 4, it is clearly seen that the HTCs jump after the 6th and 17th measurement points. Please note that these points correspond to the readings of the 7th and 18th TCs respectively. This however, comes as no surprise, because PDT -2 and -4 were located very close to those TCs.

An important observation is that the data seem to be overlapping: if the two test runs differ only by inlet temperature, then the temperature distribution will be the same or follow the same trend in the region of overlapping temperatures (entrance effect is neglected) (e.g., see Figures F.7, F.8, F.20, and F.32).

Figure F.7 shows an interesting case for tests T8-8400-3000-110-36 (red data) and T8-8800-3000-110-33 (yellow data): the inlet HTC for yellow data is exactly the same as the HTC for red data at the location of PDT-4. The data for both of the runs coincide beyond this point. I.e., deterioration for the red data is exactly to the level to which the yellow data drops after the turbulence caused by PDT-4 has probably "settled".

Figure F.20 shows a fantastic case when three test runs differ only by inlet bulk-fluid temperature (which is either much lower, near, or higher than the pseudocritical temperature). The three overlapping regions of temperatures gives three almost coinciding (within the uncertainty) regions of HTC. The effect of PDT-4 is especially pronounced here. Since this PDT causes the increase in HTC, the apparent IHT for the test T8-8400-1500-180-25 may be not only due to the thermal properties change, but due to the presence of the PDT. Indeed, the tests displayed on the previous graph (Figure F.19) show that there is only a slight improvement in the pseudocritical region, and this improvement is still within the measurement uncertainty. Figure F.32 represents another case of the overlapping of two tests which differ only by inlet bulk-fluid temperature.

Figures F.18, F.21, F.26, F.28, F.32, and F.35 – F.42 are very clear representation of mass flux effect on HTC (given the same operating conditions, higher values of HTC are reached at higher values of mass flux)

Figures F.21 (tests T8-8400-0890-110-25 and T8-7600-0890-110-25) show that HTCs are higher at lower pressures (given the same operating conditions)

Figure F.24 may mislead, because there appears to be a contradicting trend past the pseudocritical point for the three runs with very similar operating parameters. Purple data (T8-8400-2100-290-25-RED) deteriorate more just upstream of PDT-4, than black (T8-8400-2000-270-21) and red data (T8-8400-2100-290-20). Improvement in HTCs observed for the black and red data is most likely assisted by the presence of PDT-4.

Figure F.27 shows the effect of PDT-4 on the IHT as well. For example, the data for the test T8-8800-3000-500-30 seem to go through deterioration past the pseudocritical point, but instead of the expected stabilization, there is a noticeable IHT because of PDT-4. Also,

the data for T8-8400-0450-071-20 (q/G = 0.16 kJ/kg) signify that the DHT is more pronounced at lower mass fluxes and extends beyond the pseudocritical point. In this case even the presence of PDT-4 had no effect. This trend is also very interesting, because KAERI SPHINX loop data suggest that at such low mass fluxes deterioration occurs at q/G as low as 0.1 kJ/kg rather than 0.18 – 0.20 kJ/kg at high mass fluxes.

Figures starting from F.29 suggest that at higher heat fluxes (q > 270 kW/m^{2}K) there is no IHT, but rather a DHT (a "dip") near the pseudocritical point, although with a recovery. It also appears that the "dip" is shifted towards the lower values of **X** (i.e. recovery of heat-transfer begins earlier) at higher mass fluxes. More specifically, the lowest HTC in the "dip" is always at **X** > 0. E.g., Figure F.30 suggests that it occurs at around **X =** 200 for G = 2000 kg/m^{2}s (P = 8.40 MPa), and at around 330 for G = 3000 kg/m^{2}s (P = 8.40 MPa).

Figure F.31 suggests that the local minimum of HTC in the "dip" is shifted towards the higher values of **X** as the inlet bulk-fluid temperature gets closer to the pseudocritical temperature; but the recovery of heat-transfer still occurs at the same coordinate (i.e. the deteriorated region condenses; compare T8-8400-3000-540-35 (black data) and T8-8400-3000-540-26 (green data)). Figure F.31 also suggests that HTCs beyond pseudocritical region (gas-like state of fluid) will be slightly lower than in the pre-pseudocritical region (liquid-like state of fluid) (compare T8-8400-0670-130-29 (blue data, lower mass flux) and T8-8400-0770-140-39 (yellow data, higher mass flux, but different bulk-fluid temperature at the entrance). Figure F.33 complements this conclusions. The local minimum of HTC in the "dip" is shifted towards the higher values of **X** at lower mass fluxes.

Figures F.31 and F.32 suggest that heat-transfer is almost stable in the pseudocritical region at q/G > 0.185 kJ/kg and G = 670 – 1500 kg/m^{2}s. Here, stable means that the lowest HTC at DHT is either within the experimental uncertainty, or no more than 10% of the stabilized value of HTC at the inlet (3rd measured point). Figures F.38–F.42 suggest that there is a local maximum near the pseudocritical point at these mass fluxes, but at higher heat fluxes (q/G > 0.235 kJ/kg). Moreover, IHT is consistent at G > 1200 kg/m^{2}s (compare T8-8400-1500-370-24 (yellow data) and T8-8400-1200-310-24 (light blue data)). Figure F.41 supports this conclusion: although there is a local maximum in HTCs at lower mass fluxes

(especially pronounced for light blue, purple, and black data), HTCs are still higher at higher mass fluxes, even within the DHT region.

Figures F.35–F.42 show similarity of the HTC patterns with the chosen non-dimensional coordinate **X** at the same inlet bulk-fluid temperatures.

Figure F.36 suggests that the local minimum of HTC in the "dip" is appreciably smaller at lower pressures (compare T8-7600-2000-450-25-RED (blue data) with T8-8400-2000-440-24 (black data) and T8-2000-460-30 (purple data)).

Figure F.39 suggests that HTC is insensitive to the small variations of heat flux with the rest of the parameters being the same, and $q/G \geq 0.236$ kJ/kg (T8-8400-1500-360-25 (black data) coincides with T8-8400-1500-370-25-RED (yellow data), while there is about 3% difference in the heat fluxes between the cases).

To summarize, the following general characteristics were noticed:

1) HTC appears to be higher when the inlet temperature is closer to the pseudocritical temperature (given the rest of the parameters are the same).
2) HTC appears to be higher at higher mass fluxes; the dependence seems to be almost linear at bulk-fluid temperatures lower and higher than the pseudocritical temperature (e.g. see Figure F.15).
3) HTC appears to decrease with an increase in heat flux.
4) HTC appears to be higher at lower pressures and NHT (see Figures F.16 and F.21), given the rest of the parameters are the same. However, HTC appears to deteriorate more at lower pressures (see Figure F.36).
5) HTC appears to be more sensitive to the change in thermal properties within the pseudocritical region at lower pressures and lower mass fluxes.
6) There is a local maximum (oscillation) in the DHT region around the pseudocritical point at $G = 670 – 1500$ kg/m^{2}s and $q/G \cong 0.2$ kJ/kg. However, HTC is still higher at higher mass fluxes, even within the DHT region.

Thus, using **X** as a coordinate for plotting HTC data is potent in distinguishing effects of operating parameters on heat transfer.

Appendix G. A Brief Summary of Thermal and Transport Properties of Prospective Coolants for the Generation IV Nuclear Reactors[13]

The following coolants are proposed for use in the Generation IV reactor systems discussed in Chapter 2:

1. SCW in SCWR.
2. Sodium in a (SFR).
3. Lead or Lead-Bismuth Eutectic (LBE) in a LFR.
4. Fluoride-salt coolant in a MSR.
5. Helium in both GFR and VHTR.

Prior to comparing thermal and transport properties of the coolants, it is reasonable to generally discuss the desired characteristics of reactor coolants. Commonly, the following requirements for nuclear reactor coolants are considered:

1. high specific heat, thermal conductivity and low viscosity;
2. low corrosive and low erosive effects on all the reactor materials;
3. high boiling point and low melting point;
4. high thermal resistance and radiation resistance;
5. low neutron absorption cross-section;
6. explosion-proof, non-combustible, non-toxic;
7. widely available (not rare); and
8. weak activation.

[13] This Appendix is based on author's common paper with Alexey Dragunov (Dragunov et al., 2013b).

SCW is proposed to be used in the SCWR at operating pressure of 25 MPa, and temperature range of 350 °C – 625 °C.

Sodium is proposed to be used in the SFR. Sodium is known to have high thermal conductivity and low neutron-absorption cross-section. The high boiling point (882.8 °C) of sodium allows SFR to operate at low temperature (e.g., 0.1 MPa). Melting point of sodium is approximately 97 °C. Also, as discussed in Chapter 2, sodium reacts chemically with air and water. Therefore, to improve safety, a secondary sodium loop is utilized, which acts as a buffer between the radioactive sodium in the first loop and the steam (or water) in the third loop.

Lead is proposed to for use in the LFR at ambient pressure (~0.1 MPa). Lead has a very high melting point (327.5 °C) which causes specifics of the way the reactor needs to be operated. Overall, lead as a coolant has poor thermal properties

LBE is a eutectic alloy of lead (44.5%) and bismuth (55.5%), which is considered for as an alternative to lead for use in the LFR. One of the main advantages of LBE is a lower melting point (123.5 °C). An intermediate loop of heat removal is not needed compared to the case of SFR, since neither lead nor LBE react readily with water or air. Further technology of LBE application was proven by years of reliable experience in nuclear-powered submarines operated by the Soviet Union since the 1970's.

Very little information is present on molten salt fluorides in the open literature. Generally, molten salt fluorides (which are proposed as coolants for MSR) are known to have promising thermal-hydraulic properties and relatively high boiling temperatures.

Helium coolant is proposed to be used at high outlet temperatures of 850 °C (GFR) and 1,000 °C (VHTR). Such high temperatures allow for very high thermal efficiencies of the plant. Helium has even smaller neutron absorption than sodium. Nevertheless, helium has some requirements, such as cladding surface roughening and high operational pressure.

The investigated region of temperatures covers the operating ranges of the corresponding reactors (see Figure G.1). It is important to note that the properties investigated are presented for a wide range of temperatures (from 250 °C to 1,000 °C), which covers the

range of operating temperatures for Generation IV reactor systems. It is also reasonable to compare the Generation IV reactor systems coolants with current Generation III reactor-system coolants used in the most efficient reactor system (AGR, efficiency up to 42%, coolant – CO_2 under pressure of 4 MPa) and the most common system worldwide (PWR, coolant – water with parameters of 15.5 MPa, T_{in}/T_{out} – 292 °C / 329 °C).

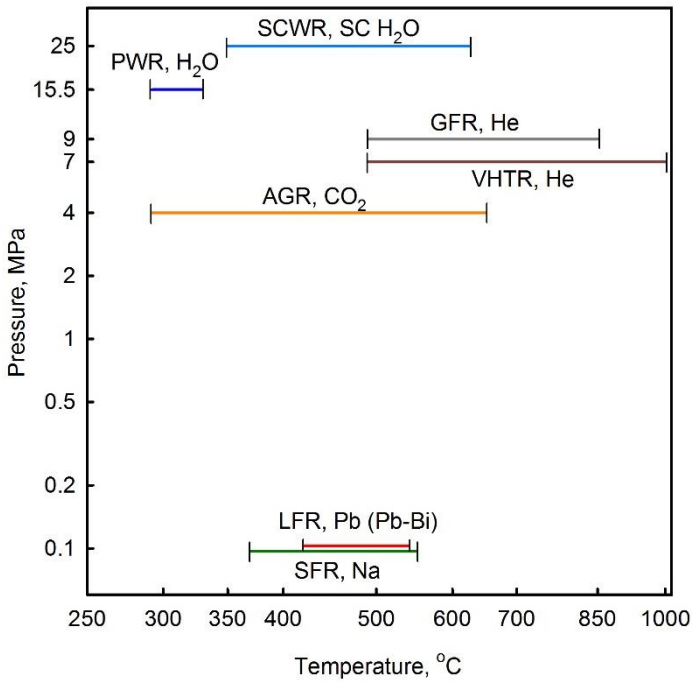

Figure G.1. Pressure – Temperature diagram for PWR, AGR and proposed GEN-IV reactor concepts (pressure drop is not considered).

Properties of SC and subcritical water, CO_2, and helium-4 were obtained from NIST REFPROP software. Properties of sodium were taken from the book by Kirillov et al. (2007). Other properties were calculated using either original correlations presented *in Handbook on Lead-bismuth Eutectic Alloy and Lead Properties, Materials Compatibility, Thermal-hydraulics and Technologies* (2007) or using correlations recommended by authors of this book.

Density drops linearly with the temperature for all the coolants, except SCW (Figure G.2). The density of the gases drops about 1.6 times, however, the density change for liquid metals is insignificant. For SCW the density drops almost 8 times within the pseudocritical region.

Specific heat of He, Na, Pb, and Pb-Bi (Figure G.3) is nearly constant over the whole range of operational parameters. In the case of CO_2, specific heat increases linearly and reaches the same value as for Na at around 750 °C. Specific heat of water goes through a peak (where its value increases almost 8 times) within the pseudocritical region. Specific heats of Pb and LBE are nearly identical and 10 times less than those of Na and CO_2, and almost 40 times less than that of He. At temperatures higher than 450°C, the heat of He is higher than that of SCW

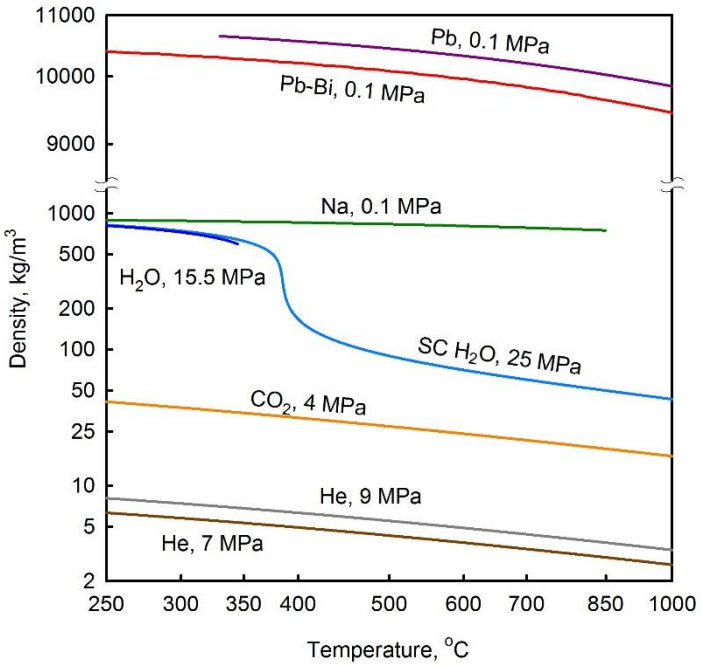

Figure G.2. Density vs. Temperature.

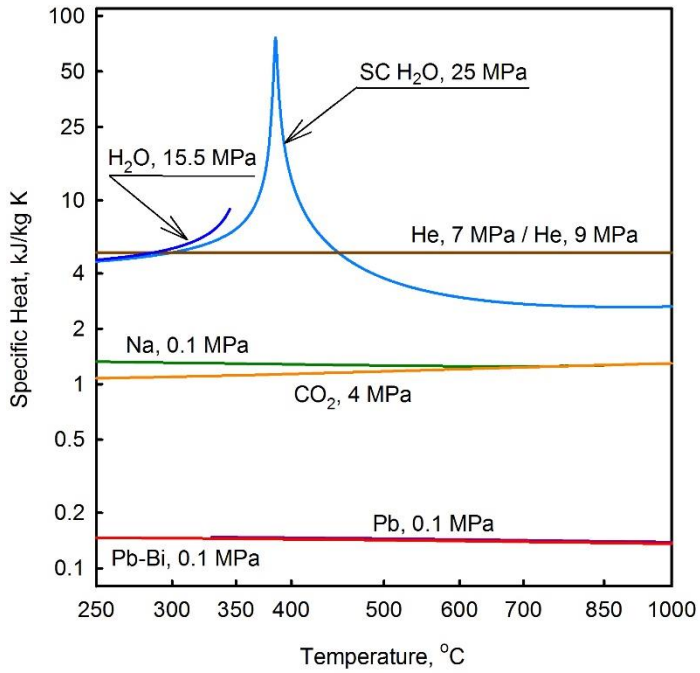

Figure G.3. Specific heat vs. Temperature.

Thermal conductivity of liquid metals is significantly higher than that of gases (50 – 3,000 times, see Figure G.4). Thermal conductivity of Na drops slightly, while that for Pb, LBE, He, and CO_2 increases linearly with the temperature. Thermal conductivity behavior of SCW is peculiar. Thermal conductivity decreases linearly for temperature between 250 – 350 °C, then goes through a small peak in the pseudocritical point, before decreasing smoothly from about 0.4 to 0.1 W/m·K. As the temperature increases above 500°C the thermal conductivity increase linearly to values higher than those of CO_2, but lower than those of He.

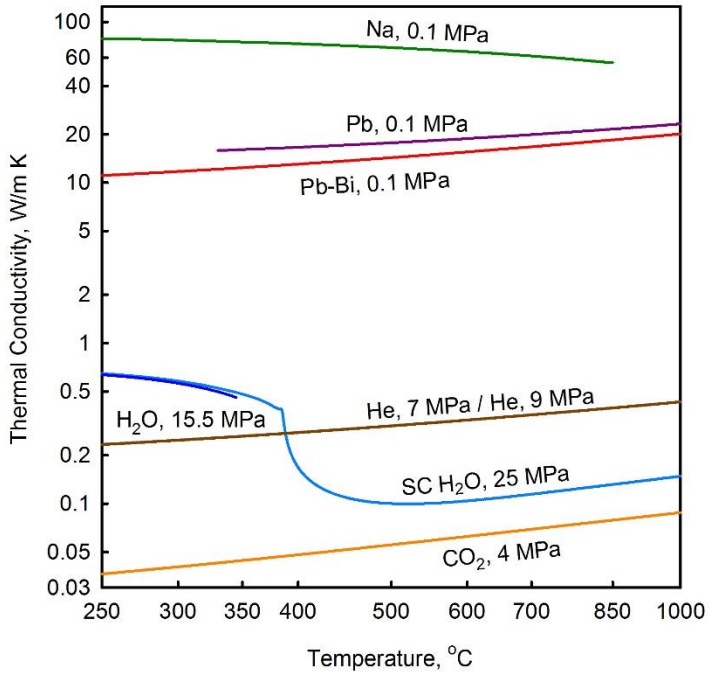

Figure G.4. Thermal conductivity vs. Temperature.

The temperature dependence of the viscosity of liquid metals is opposite to that of gases (Figure G.5). Viscosity of Na and Pb drop linearly over the whole range of temperature, while viscosity of Pb-Bi has a slower linear drop up to 600 °C. Viscosity increases for temperatures between 600 and 1,000 °C, attaining a value close to that measured at 250 °C. Viscosities of gases increase linearly with temperature, and viscosity of SCW at temperatures beyond the pseudocritical range behave in the fashion similar to that of gases. In general, the shape of viscosity-temperature curve for SCW is similar to that of thermal conductivity. However, viscosity does not exhibit a peak in the pseudocritical point.

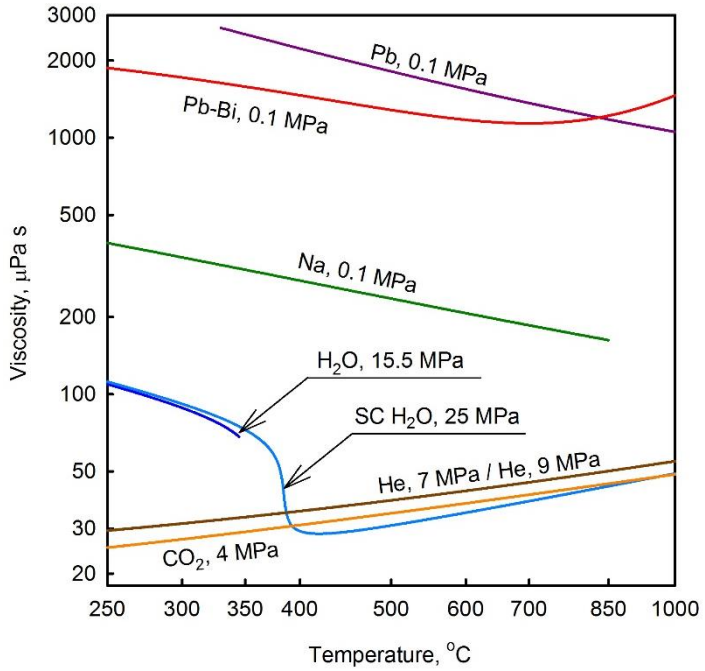

Figure G.5. Viscosity vs. Temperature.

The dependence of the Prandtl number on temperature for different coolants is shown in Figure G.6. As follows from the definition, the shape of **Pr** is governed by the more significantly changing property of the coolant. Therefore, specific heat is nearly constant for all of the considered here coolants, except that of SCW. Therefore, for the rest of the coolants ratio of viscosity to thermal conductivity will affect the shape of the **Pr** vs temperature curve. As we see from Figure G.6, the changes in viscosity and thermal conductivity of gases are such, that they compensate each other, and values of **Pr** for gases are virtually constant over most of the 750 °C temperature span. However, for the liquid metals the viscosity drops more significantly than the thermal conductivity increases. As the result the **Pr** of liquid metals drops almost linearly with temperature. Due to an increase in viscosity of LBE at high temperatures, the corresponding value of Prandtl number also increases. Since specific heat of SCW goes through the most rapid changes compared with its other thermal and transport properties, **Pr** of SCW behaves similar to the specific heat. At high temperatures (> 500 °C), the **Pr** of SCW behaves similar to that of gases.

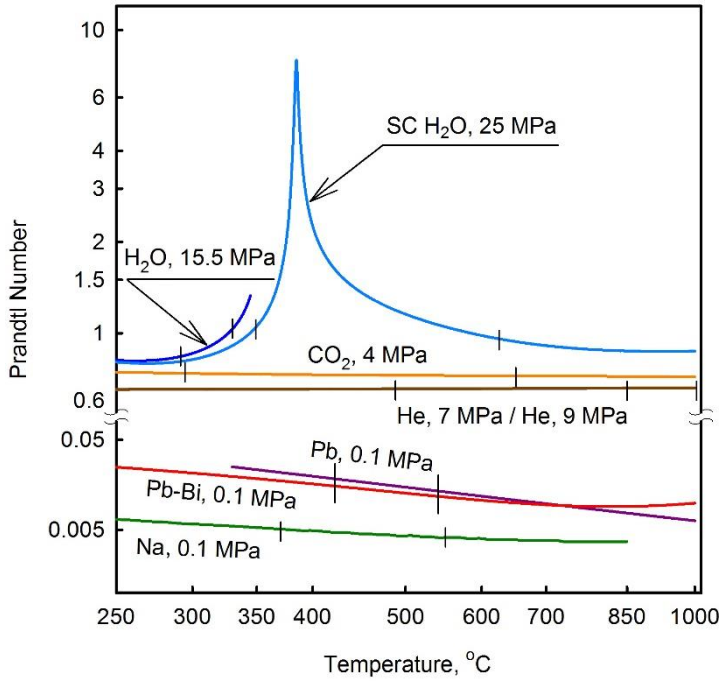

Figure G.6. Prandtl number vs. Temperature.

Volumetric expansivity of liquid metals is much smaller than that of the remaining coolants, and stays almost constant (see Figure G.7).

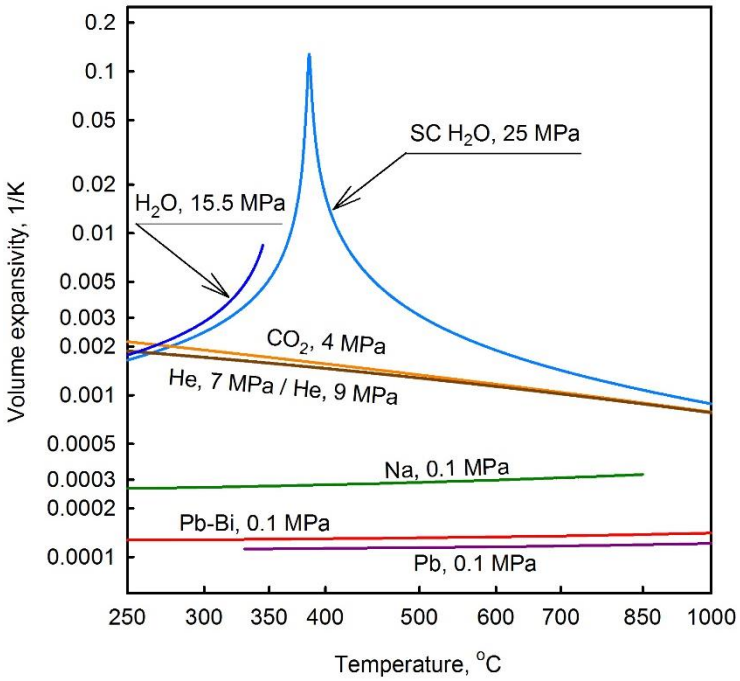

Figure G.7. Volumetric expansivity vs. Temperature.

Volumetric expansivity of gases drops almost twice in a linear fashion, from 250 to 1,000 °C. Remarkably, values of volumetric expansivity for SCW at temperatures below the pseudocritical point are close to those for gases. Near the pseudocritical point, volumetric expansivity of SCW peaks. At higher temperatures, the volumetric expansivity of SCW gradually reaches values corresponding to those of gases.

To summarize the above, the thermophysical properties of liquid metals and gases experience only minor linear changes with increasing temperature. However, all the properties of water at pseudocritical conditions go through very rapid changes.

Another comparison of coolants can be made based on the power required to circulate coolant to achieve a given temperature. Let the circulation power be *W*, then:

$$W = \frac{\dot{m}}{\rho}\Delta P\,, \tag{G.1}$$

where $\dot{m}$ – mass-flow rate of coolant, kg/s; ρ – density of coolant, kg/m^3; and ΔP – hydraulic resistance of the loop.

The total power, $\dot{Q}$, removed by the coolant from the core, can be expressed as:

$$\dot{Q} = < c_p > \dot{m}\Delta T\,, \tag{G.2}$$

where $< c_p >$ is the average specific heat for the given change of coolant's bulk-fluid temperature ΔT.

From a thermal-hydraulic point of view, the best coolant would be the one, which will remove the largest amount of power from the core for a given circulation power. Therefore, if we fix thermal resistance of the loop and then allowed the temperature of the coolant in the core to increase, the coolants can be compared based on the quantity:

$$a \equiv \frac{\dot{Q}\Delta P}{W\Delta T} = < c_p > \rho \tag{G.3}$$

Consider the temperature range of 350 to 650 °C, which corresponds to the temperature range of a coolant in a generic SCWR.

Table G.1. Comparison of coolants based on circulation power required to sustain given inlet and outlet temperatures of the coolant.

Coolant	$< c_p >$, J/kg·K	ρ, kg/m^3	a, Pa/K	$a_{scw}/a_{coolant}$
SCW	6,713	626	4,202,338	1
He at 7MPa	5,189	5.3	27,502	153
He at 9MPa	5,187	4.6	23,860	176
CO_2	1.2	34.2	41	102
Na	1.4	900	1,260	3.33
Pb	0.16	10,500	1,680	25
Pb-Bi	0.16	10,200	1,632	2.58

As seen from Table G.1, SCW outperforms other coolants greatly within the 350 – 650 °C temperature range. Another immediate conclusion is that CO_2 appears to be the most expensive coolant in terms of circulation power. In any case, such a comparison should be complemented by considering the corrosive properties, sizes and costs of the machinery for the power conversion side of the plant, and the net-plant efficiency.

Typical HTCs for coolant candidates are listed in Table G.2. It shows that sodium has the highest HTC among all proposed coolants, making it more competitive.

Table G.2. Typical heat transfer coefficients for coolant candidates [17, 18].

Coolant	Heat transfer coefficient, kW/m^{2}K
SCW	10 – 25
He (rough surface)	10
CO_2 (high pressure)	2 – 5
Na (forced convection)	55 – 85
Pb (forced convection)	25 – 35
Pb-Bi (forced convection)	20 – 30

In general, liquid metal coolants have high thermal stability, high boiling point, and very low saturated vapor pressure which distinguish them from other types of coolants.

The specific heats of Pb and LBE are nearly identical and 10 times less than those of Na and CO_2, and almost 40 times less than that of He. At the temperatures higher than 450 °C, the specific heat of He is even higher than that of SCW.

As one would expect, the thermal conductivity of liquid metals is significantly higher than that of gases (50 – 3,000 times). The highest thermal conductivity was for sodium (60 – 70 W/m·K).

Volumetric expansivity of liquid metals is much lower than that for the other coolants examined, and stays almost constant.

The thermophysical properties of liquid metals and gases show only minor linear changes with temperature. However, all the properties of water go through very rapid changes at pseudocritical conditions.

Compared with LBE, lead has a smaller (~20,000 times) activity from impurities of polonium-210. The cost of lead is about 10 times less than the cost of bismuth. The availability of bismuth may be a limitation for the use of lead-bismuth eutectic in small power reactors and the use of lead in energy production (Beznosov et al., 2007).

Thermal and transport properties of LBE, except for the thermal conductivity, are close to the average values of those of lead and bismuth.

SCW greatly outperforms other coolants in the 350 – 650 °C range in terms of power required to circulate coolant. Another immediate conclusion is that CO_2 appears to be the most expensive coolant in terms of circulation power.

At high temperatures (more than 500 °C) **Pr** of SCW behaves similar to gases (Pioro, 2012).

One of the least desirable properties of water is its high vapor pressure which increases rapidly with temperature. Its relatively low critical temperature (≈ 374 °C) limits the maximum temperature of the coolant and significantly limits the efficiency of the power conversion cycle.

Specific heat of helium is higher than that of CO_2 and liquid metals. The thermal conductivity of helium is 10 times greater than that of CO_2. This characteristic facilitates heat transfer and reduces the size of heat exchangers. Helium is far more inert than CO_2, does not absorb neutrons, and cannot become radioactive on its own.

Helium has a low density, which leads to much higher power requirements for pumps. In order to improve the heat transfer characteristics and reduce the cost of pumping power, helium is pressurized to 7 – 9 MPa.

Helium has less neutron absorption and moderation than other coolants considered.

A direct power conversion cycle is possible using either helium or water as coolants.

Appendix H. List of Publications by Eugene Saltanov

Publications that were made to disseminate and discuss the ideas and results of the research conducted for this thesis are listed below.

Papers in refereed journals

1. **Saltanov, Eu.**, Pioro, I., Mann, D., Gupta, S., Mokry, S., and Harvel, G., 2015. Study of Specifics of Forced-Convective Heat Transfer in Supercritical Carbon Dioxide, *ASME Journal of Nuclear Engineering and Radiation Science*, No. 1 (to be published).

2. Gupta, S., **Saltanov, Eu.**, Mokry, S.J., Pioro, I., Trevani, L. and McGillivray, D., 2013. Developing Empirical Heat-Transfer Correlations for Supercritical CO_2 Flowing in Vertical Bare Tubes, *Nuclear Engineering and Design,* Vol. 261, pp. 116-131.

Papers published in refereed proceedings of international and national conferences and symposiums

1. Pioro, I., **Saltanov, Eu.** and Dragunov, A., 2015. Applications of Supercritical Fluids in Power Engineering, Proceedings of the 7th International Symposium on Supercritical Water-Cooled Reactors (ISSCWR-7), March 15‑18, Helsinki, Finland, Paper #2081, 11 pages.

2. **Saltanov, Eu.**, Mann, D., Pioro, I., and Harvel, G., 2014. Specifics of Forced-Convective Heat Transfer in Supercritical Carbon Dioxide, Proceedings of the 38th Annual CNS/CNA Student Conference at the 19th Annual Pacific Basin Nuclear Conference (PBNC), August 24-28, Vancouver, BC, Canada, Paper #30, 8 pages.

3. **Saltanov, Eu.**, Pioro, I., Mann, D., Gupta, S., Mokry, S. and Harvel, G., 2014. Study on Specifics of Forced-Convective Heat Transfer in Supercritical Carbon Dioxide, Proceedings of the 22nd International Conference on Nuclear Engineering (ICONE-22), July 7-11, Prague, Czech Republic, Paper #30122, 12 pages.

4. Dragunov, A., **Saltanov, Eu.,** Pioro, I., Kirillov, P., and Duffey, R., 2014. Power Cycles of Generation III and III+ Nuclear Power Plants, Proceedings of the 22nd International Conference on Nuclear Engineering (ICONE-22), July 7-11, Prague, Czech Republic, Paper #30151, 13 pages.

5. Gupta, S., **Saltanov, Eu.,** and Pioro, I., 2014. Uses of Supercritical Fluids and their Characteristics within Deteriorated Heat Transfer Region, Proceedings of the 22nd International Conference on Nuclear Engineering (ICONE-22), July 7-11, Prague, Czech Republic, Paper #30274, 12 pages.

6. Pioro, I., Mokry, S., Gupta, S., **Saltanov, Eu.**, Dragunov, A., Draper, Sh., and Mann, D., 2013. Heat Transfer at Supercritical Pressures in Power-Engineering Applications, Proceedings of the 13th UK Heat Transfer Conference (UKHTC2013), Imperial College London, UK, September 2–3, 8 pages.

7. Dragunov, A., **Saltanov, Eu.**, Pioro, I., Harvel, G. and Ikeda, B., 2013. Study on Primary and Secondary Heat-Transport Systems for Sodium-Cooled Fast Reactor, Proceedings of the 21st International Conference on Nuclear Engineering (ICONE-21), July 29-August 2, Chengdu, China, Paper #16014, 9 pages.

8. **Saltanov, Eu.**, Pioro, I. and Harvel, G., 2013. Preliminary Investigation of Heat-Transfer Correlation for Upward Flow of CO_2 at Supercritical Pressure, Proceedings of the 21st International Conference on Nuclear Engineering (ICONE-21), July 29-August 2, Chengdu, China, Paper #16399, 10 pages.

9. Gupta, S., **Saltanov, Eu.** and Pioro, I., 2013. Heat-Transfer Correlation for Supercritical Carbon Dioxide Flowing in Vertical Bare Tubes, Proceedings of the 21st International Conference on Nuclear Engineering (ICONE-21), July 29-August 2, Chengdu, China, Paper #16453, 12 pages.

10. Dragunov, A., **Saltanov, Eu.**, Higgins, A. and Pioro, A., 2013 Investigation of Different Thermodynamic Cycles for Nuclear Power Plants, Proceedings of the 34th Annual Canadian Nuclear Society Conference and 37th CNS/CNA Student Conference, Toronto, ON, Canada, June 9-12, Paper #51, 5 pages.

11. **Saltanov, Eu.**, Preda, T., Pioro, I., and Harvel, G., 2013. Power-Conversion Cycles for Sodium-Cooled Fast Reactors, Proceedings of the 34th Annual Canadian Nuclear Society Conference and 37th CNS/CNA Student Conference, Toronto, ON, Canada, June 9-12, Paper #23, 5 pages.

12. Gupta, S., **Saltanov, Eu.,** and Pioro, I., 2013. Few Challenges Associated with Developing 1-D HTC Correlations For Supercritical CO_2, Proceedings of the 34th Annual Canadian Nuclear Society Conference and 37th CNS/CNA Student Conference, Toronto, ON, Canada, June 9-12, Paper #68, 5 pages.

13. Pioro, I., Mokry, S., Gupta, S., and **Saltanov, Eu.**, 2012. Heat-transfer for Supercritical Water and CO_2 with Upward Flow in Vertical Bare Tubes, Transactions of the European Nuclear Conference (ENC-2012), Manchester, UK, December 9 – 12, Paper ENC2012-A0202, 11 pages.

14. Dragunov, A., **Saltanov, Eu.**, Bedenko, S. and Pioro, I., 2012. A Feasibility Study on Various Power-Conversion Cycles for a Sodium-Cooled Fast Reactor, Proceedings of the 20th International Conference On Nuclear Engineering (ICONE-20) – ASME 2012 POWER Conference, July 30 - August 3, Anaheim, California, USA, Paper #55130, 9 pages.

15. Preda, T., **Saltanov, Eu.**, Pioro, I. and Gabriel, K., 2012. Development of a Heat Transfer Correlation for Supercritical CO_2 Based on Multiple Data Sets, Proceedings of the 20th International Conference On Nuclear Engineering (ICONE-20), July 30 - August 3, Anaheim, California, USA, Paper #54516, 7 pages.

16. Pioro, I., Mokry, S., Peiman, W., **Saltanov, Eu.** and Grande, L., 2012, Application of Supercritical Fluids in Power Engineering, Proceedings of the 10th International Symposium on Supercritical Fluids (ISSF 2012), San Francisco, CA, USA, May 13-16, Paper L205, 9 pages.

Other publications that were made during PhD and MASc studies are listed below.

Chapters in technical books

1. **Saltanov, Eu.** and Pioro, I., 2011. World Experience in Nuclear Steam Reheat, Chapter in book "Nuclear Power: Operation, Safety and Environment", Editor: P.V. Tsvetkov, INTECH, Rijeka, Croatia, pp. 3-28. Free download from: http://www.intechopen.com/books/nuclear-power-operation-safety-and-environment/world-experience-in-nuclear-steam-reheat.

Papers in refereed journals

1. Dragunov, A., **Saltanov, Eu.,** Pioro, I., Kirillov, P., and Duffey, R., Power Cycles of Generation III and III+ Nuclear Power Plants, *ASME Journal of Nuclear Engineering and Radiation Science*, No. 2, 10 pages.

Papers published in refereed proceedings of international and national conferences and symposiums

1. Kovaltchouk, V., Nichita, E., and **Saltanov, E.**, 2015. Temperature Distribution Inside Fresh-Fuel Pins of Pressure-Tube SCWR, Proceedings of the 7th International Symposium on Supercritical Water-Cooled Reactors (ISSCWR-7), March 15‑18, Helsinki, Finland, Paper #2081, 11 pages.

2. Kovaltchouk, V., Nichita, E., and **Saltanov, E.**, 2015. Axial Power and Coolant-Temperature Profiles for a Non-Re-Entrant PT-SCWR Fuel Channel, Proceedings of the 7th International Symposium on Supercritical Water-Cooled Reactors (ISSCWR-7), March 15‑18, Helsinki, Finland, Paper #2081, 10 pages.

3. Vincze, A., Sidawi, K., Abdullah, R., Baldock, M., **Saltanov, E.**, and Pioro, I., 2014. Investigation of Thermodynamic Cycle for Generic 1200 MW_{el} Pressure Channel Reactor with Nuclear Steam Superheat, Proceedings of the 38th Annual CNS/CNA Student Conference at the 19th Annual Pacific Basin Nuclear Conference (PBNC), August 24-28, Vancouver, BC, Canada, Paper #42, 5 pages.

4. Dragunov, A., **Saltanov, E.**, Ikeda, B., and Pioro, I., 2014. Investigation of Heat-Transfer Coefficient Values for Generation-IV Nuclear Reactors, Proceedings of the 38th Annual CNS/CNA Student Conference at the 19th Annual Pacific Basin Nuclear Conference (PBNC), August 24-28, Vancouver, BC, Canada, Paper #, 7pages.

5. Dragunov, A., **Saltanov, E.**, Ikeda, B., and Pioro, I., 2014. Investigation of Heat-Transfer Coefficient Values for Generation-IV Nuclear Reactors, Proceedings of the 38th Annual CNS/CNA Student Conference at the 19th Annual Pacific Basin Nuclear Conference (PBNC), August 24-28, Vancouver, BC, Canada, Paper #, 7pages.

6. Dragunov, A., **Saltanov, Eu.**, Pioro, I., Ikeda, B., Miletic, M., and Zvorykina, A., 2013. Investigation of Thermophysical and Nuclear Properties of Prospective Coolants for Generation-IV Nuclear Reactors, Proceedings of the 21st International Conference on Nuclear Engineering (ICONE-21), July 29-August 2, Chengdu, China, Paper #16020, 11 pages.

7. Peiman, W., **Saltanov, Eu.**, Pioro, I., and Gabriel, K., 2012. Pressure Drop Analysis in a Pressure-Tube Supercritical Water-cooled Reactor, Transactions of the European Nuclear Conference (ENC-2012), Manchester, UK, December 9 – 12, Paper ENC2012-A0258, 8 pages.

8. **Saltanov, E.**, Pioro, I., and Lang, P., 2012. Three Russian Designs of Small Reactors: UNITHERM, KLT-40S, and SVBR-10, Proceedings of the 2nd International Technical Meeting on Small Reactors, November 7–9, Ottawa, Canada, 3 pages.

9. Peiman, W., **Saltanov, Eu.**, Grande, L., Pioro, I., Rouben, B., and Gabriel, K., 2012. Power Distribution and Fuel Centerline Temperature in a Pressure-Tube Supercritical Water-Cooled Reactor (PT SCWR), Proceedings of the 20th International Conference On Nuclear Engineering (ICONE-20) – ASME 2012 POWER Conference, July 30 - August 3, Anaheim, California, USA, Paper #54596, 12 pages.

10. Miletić, M., Růžičková, M., Fukač, R., Pioro, I. and **Saltanov Eu.**, 2011. Supercritical-Water Experimental Setup for Out-of-Pile Operation, Proceedings of the International Conference "Nuclear Energy for New Europe" (NENE), Bovec, Slovenia, September

12-15, Paper 806, 11 pages.

11. **Saltanov, Eu.**, Peiman, W., Caly, A. and Pioro, I., 2011. Heat-Transfer Calculations of a Re-Entrant Channel for Pressure-Tube SCWRs, Proceedings of the 19th International Conference On Nuclear Engineering (ICONE-19), Makuhari, Japan, May 16-19, Paper 43803, 8 pages.

12. **Saltanov, Eu., Peiman, W., Draper, Sh. and Pioro, I., 2011.** Heat-Transfer Analysis of Supercritical-Water and Superheated-Steam-Cooled Channels of SCWR, Proceedings of the 5th International Symposium on SCWR (ISSCWR-5), Vancouver, BC, Canada, March 13-16, Paper P65, 11 pages.

13. Pioro, I., Mokry, S., Peiman, W., Grande, L. and **Saltanov, Eu.**, 2010. Supercritical Water-Cooled Nuclear Reactors: NPP Layouts and Thermal Design Options of Pressure Channels, Proceedings of the 17th Pacific Basin Nuclear Conference (PBNC-2010), Cancun, Mexico, October 24-30, 31 pages.

14. **Saltanov, Eu.**, Peiman, W., Farah, A., King, K., Naidin, M. and Pioro, I., 2010. Steam-Reheat Options for Pressure-Tube SCWRs, Proceedings of the 18th International Conference On Nuclear Engineering (ICONE-18), Xi'an, China, May 17-21, Paper 29972, 12 pages.
15. Pioro, I., Naidin, M., Mokry, S., **Saltanov, Eu.**, Peiman, W., King, K., Farah, A. and Thind, H., 2010. General Layouts of Supercritical-Water NPPs, Proceedings of the 18th International Conference On Nuclear Engineering (ICONE-18), Xi'an, China, May 17-21, Paper 29993, 9 pages.

16. Peiman, W., **Saltanov, Eu.**, Gabriel, K. and Pioro, I., 2010. Heat-Loss Calculations in a SCWR Fuel-Channel, Proceedings of the 18th International Conference On Nuclear Engineering (ICONE-18), Xi'an, China, May 17-21, Paper 30069, 9 pages.

17. **Saltanov, Eu.**, King, K., Farah, A., and Pioro, I., 2010. Nuclear Steam-Reheat Options: World Experience, Proceedings of the 31st Annual Conference of Canadian Nuclear Society and 34th CNS/CNA Student Conference, Montreal, QC, Canada, May 24−27, 8 pages.

18. Pioro, I., Mokry, S., Peiman, W., **Saltanov, Eu.**, Thind, H., Grande, L., Samuel, J. and Harvel, G., 2010. Supercritical Water-Cooled Nuclear Reactors: Thermodynamic-Cycles Plant Layouts and Thermal Aspects of Pressure-Channel Design, Transactions of the European Nuclear Conference (ENC 2010) (http://www.euronuclear.org/events/enc/enc2010/transactions.htm), Barcelona, Spain, May 30 − June 2, 11pages.

19. **Saltanov, Eu.**, King, K., Farah, A., and Pioro, I., 2010. Nuclear Steam-Reheat Options: Russian Experience, Proceedings of the 2nd Canada-China Joint Workshop on Supercritical Water-Cooled Reactors (CCSC-2010), Toronto, Ontario, Canada, April 25-28, Paper No. 72, 8 pages.

20. **Saltanov, Eu.**, Monichan, R., Tchernyavskaya E. and Pioro, I., 2009. Steam-Reheat Option for SCWRs, Proceedings of the 17th International Conference On Nuclear Engineering (ICONE-17), Brussels, Belgium, July 12-16, Paper #76061, 10 pages.

Technical Reports

1. **Saltanov, Eu.**, Pioro, I., Gupta, S., Jouvin, J.C., Abdullah, R., and Sidawi, Kh., 2014. Specifics of Forced-Convective Heat Transfer to Supercritical CO_2 Flowing Upward in Vertical Bare Tubes, Technical Report for Applied Computational Fluid Dynamics Analysis (ACFDA) Inc., under NSERC ENGAGE Grant, November, UOIT, Oshawa, ON, Canada, 143 pages

2. **Saltanov, Eu.**, Dragunov, A., Pioro, I. and Lang, P., 2013. Cermet Fuels, Technical Report for FEDDEV Applied Research and Commercialization Initiative "UNITHERM Nuclear Reactor Design and Technology Evaluation Project", Ver. 1, UOIT, Oshawa, ON, Canada, March-April, 20 pages.

3. **Saltanov, Eu.**, Pioro, I. and Lang, P., 2012. Russian Designs of Small Modular Reactors, Technical Report for FEDDEV Applied Research and Commercialization

Initiative “UNITHERM Nuclear Reactor Design and Technology Evaluation Project”, Ver. 1, UOIT, Oshawa, ON, Canada, July-August, 43 pages.

4. Pioro, I., **Saltanov, Eu.**, Naidin, M., King, K., Farah, A., Peiman, W., Mokry, S., Grande, L., Thind, H., Samuel, J. and Harvel, G., 2010. Steam-Reheat Option in SCWRs and Experimental BWRs, Report for NSERC/NRCan/AECL Generation IV Energy Technologies Program (NNAPJ) entitled “Alternative Fuel-Channel Design for SCWR” with Atomic Energy of Canada Ltd., Version 1, UOIT, Oshawa, ON, Canada, March, 128 pages.

Appendix I. List of Awards Received by Eugene Saltanov

1. 2015 CNS R.E. Jervis Award Nuclear Society R.E. Jervis Award, for outstanding academic accomplishments in nuclear science and technology and contributions to the Canadian research on Generation IV nuclear-reactor concepts**.**
2. Certificate of Appreciation from the ICONE-22 Organizing Committee to Eu. Saltanov, S. Gupta, D. Mann, S. Mokry, G. Harvel and I. Pioro, Paper #30122 "Study on Specifics of Forced-Convective Heat Transfer in Supercritical Carbon Dioxide"; as Winners in the ICONE-22 Student Best Paper Competition at the 22nd International Conference On Nuclear Engineering, Prague, Czech Republic, July 7 – 11, 2014.

3. Certificate of Appreciation from the ICONE-22 Organizing Committee to S. Gupta, Eu. Saltanov and I. Pioro, Paper #30274 "Uses of Supercritical Fluids and their Characteristics within Deteriorated Heat Transfer Region"; as Winners in the ICONE-22 Student Best Poster Competition at the 22nd International Conference On Nuclear Engineering, Prague, Czech Republic, July 7 – 11, 2014

4. Chinese NS S. Qian Best Paper Award for the paper " Preliminary Investigation of Heat-transfer Correlation for Upward Flow of CO2 at Subcritical Pressure" presented at the 21th International Conference on Nuclear Engineering (ICONE21), July 30 – August 3, 2013, Chengdu, China.

5. Certificate of Appreciation to Dragunov, A., Saltanov, Eu., Bedenko, S., and Pioro, I. as Winners in the ICONE20 – POWER2012 Student Best Paper Competition (Paper# 55130) "A Feasibility Study on Various Power–Conversion Cycles for a Sodium–Cooled Fast Reactor" and for participation in the Student Program of the 20th International Conference On Nuclear Engineering (ICONE–20), July 30 – August 3, Anaheim, California, USA).

6. Certificate of Recognition to Saltanov, Eu., Peiman, W., Caly, A. and Pioro, I. as Winners in the ICONE–19 North American and European Student Best Poster Competition (Paper #43803 “Heat–Transfer Calculations of a Re–Entrant Channel for Pressure–Tube SCWRs” and for participation in the Student Program of the 19th International Conference On Nuclear Engineering (ICONE–19), October 24–25, Osaka, Japan).
7. Certificate of Contribution to Preda, T., Saltanov, Eu., Ajorli, K., Pioro, I., and Gabriel, K. for poster "Evaluation of CO2 as Coolant and Modelling Fluid in SCWR applications" presented at Student Research Showcase 2011 held in University of Ontario Institute of Technology (UOIT), August 17, 2011, Oshawa, Canada.

8. Certificate of Recognition to Saltanov, Eu., Peiman, W., Farah, A., King, K., Naidin, M. and Pioro I. as Winners in the ICONE–18 Student Best Poster Competition (Paper #29972 “Steam–Reheat Options for Pressure–Tube SCWRs” and for participation in the Student Program of the 18th International Conference On Nuclear Engineering (ICONE–18), May 17–21, Xi’an, China).

9. Certificate of Recognition to Peiman, W., Saltanov, Eu., Gabriel, K. and Pioro I. as Winners in the ICONE–18 Student Best Poster Competition (Paper #30069 “Heat–Loss Calculations in a SCWR Fuel–Channel” and for participation in the Student Program of the 18th International Conference On Nuclear Engineering (ICONE–18), May 17–21, Xi’an, China)